

Technische Universität München
Lehrstuhl für Kommunikationsnetze

Connectivity and Decentralized QoS Provisioning in Vehicular Networks

Dipl.-Ing. Univ. Robert Nagel

Vollständiger Abdruck der von der Fakultät Elektrotechnik und Informationstechnik der Technischen Universität München zur Erlangung des akademischen Grades eines

Doktor-Ingenieurs (Dr.-Ing.)

genehmigten Dissertation.

Vorsitzender: Univ.-Prof. Dr.-Ing. Andreas Jossen
Prüfer der Dissertation: 1. Univ.-Prof. Dr.-Ing. Jörg Eberspächer
2. Univ.-Prof. Dr.-Ing. Sandra Hirche

Die Dissertation wurde am 16. Dezember 2010 bei der Technischen Universität München eingereicht und durch die Fakultät für Elektrotechnik und Informationstechnik am 17. Mai 2011 angenommen.

Abstract

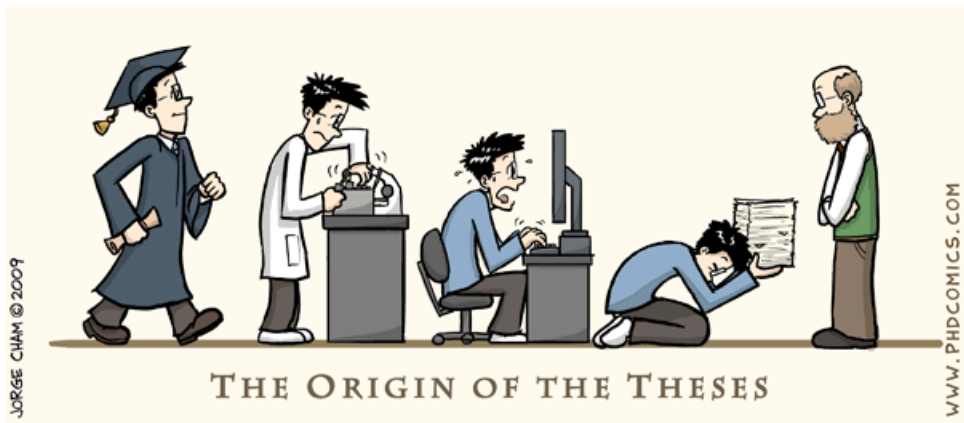
The introduction of wireless ad-hoc networks in vehicles will significantly enhance safety and comfort of driving in the future. However, as of today, we find many important issues regarding the choice of an appropriate networking technology and concerning application design unanswered. This thesis presents an open mathematical framework that allows for a holistic analysis of network performance in arbitrary road traffic situations, so that relevant parameters can be identified and optimized. Based on this analysis, a novel QoS algorithm for distributed wireless networks is introduced that guarantees a defined service level and allows the adaptation of applications to networking conditions at runtime. It is shown how the algorithm can be complemented by future network topology prediction, and discussed how applications can benefit from this information. Finally, a prototypical integration of wireless networking in an existing software architecture for cognitive vehicles is introduced.

Kurzfassung

Die Einführung drahtloser Kommunikation zwischen Fahrzeugen wird die Sicherheit und den Komfort des Reisens deutlich steigern. Jedoch sind noch viele Fragen bezüglich der Auswahl einer geeigneten Kommunikationstechnologie und des Entwurfs von Anwendungen offen. In dieser Arbeit wird ein mathematisches Rahmenwerk vorgestellt, das die ganzheitliche Analyse der Leistungsfähigkeit drahtloser Netze in beliebigen Strassenverkehrsszenarien ermöglicht. Dadurch können relevante Parameter identifiziert und für den Einsatz optimiert werden. Basierend auf der vorhergegangenen Analyse der Anforderungen und verfügbaren Technologien wird ein neuartiger QoS Mechanismus für drahtlose Netze vorgestellt, der es ermöglicht, sowohl anwendungsseitig eine definierte Dienstgüte zu garantieren als auch die netzrelevanten Parameter von Anwendungen zur Laufzeit an den Zustand des Netzes anzupassen. Der Mechanismus wird um ein Verfahren zur Vorhersage zukünftiger möglicher Netztopologien ergänzt. Es wird gezeigt, wie diese Information gewinnbringend an Anwendungen zurückgeführt werden kann. Abschließend wird eine prototypische Integration drahtloser Kommunikation in einer existierenden Softwarearchitektur für kognitive Fahrzeuge vorgestellt.

IN LOVING MEMORY OF MY FATHER,
FRIEDRICH ERIK

DEDICATED TO MY FAMILY



THE ORIGIN OF THE THESES

JORGE CHAM © 2009

WWW.PHDCOMICS.COM

Preface

Foremost, I would like to express my gratitude to my advisor Professor Dr. Jörg Eberspächer, for literally being what is called a “doctoral father” in German. He gave me the necessary liberty to freely pursue my research and the right impulses at the right times. I always appreciated his counsel and his reliable support in challenging and turbulent situations. In his dedication to people and scientific work, he has become a role model to me.

My doctoral family at the Institute of Communication Networks (LKN) at Technische Universität München has provided me with a pleasant, productive, and inspiring environment. For their encouragement, the invaluable discussions, and – of course – for the good times we had and the friendships that have developed during my five years at LKN, I would like to thank Michael Eichhorn, Dr. Stephan Eichler, Dr. Moritz Kiese, Dr. Gerald Kunzmann, Silke Meister, Christian Merkle, my officemate Bernd Müller-Rathgeber, Martin Pfannenstein, Dr. Robert Prinz, Matthias Scheffel, Christoph Spleiß, Dr. Robert Vilzmann, Dr. Hans-Martin Zimmermann, and Dr. Stefan Zöls.

Dr. Martin Maier, our administrative genie, master of the thousand windows, and Red Baron to be, deserves my gratitude for making practically everything possible and simply for being a good pal. Many thanks go to our secretary and good fairy, Sabine Strauss, for her open ears and consolation in times of need. I owe Thomas “Willy” Kurzhals for his support with technical issues and for teaching me the mysteries of offside situations. As the curator of our institution’s museum of telephony, it was a pleasure for me to work with Helmut “R-Relay” Edlinger, who deeply impressed me with his passion for antiquated telephone exchanges and taught me the beauty of simplicity.

Among numerous students, I would like to especially thank Stefan Morscher for his valuable contribution to my scientific work.

Last but not least, I would like to express my deepest gratitude to my family and especially my loving partner Martin for their endless support and understanding. I owe you a lot.

Contents

1. Introduction	1
1.1. Motivation	3
1.2. Contributions	3
1.3. Organization	4
2. Cooperation Between Vehicles: Scenarios and Requirements	7
2.1. Cooperative Applications	8
2.1.1. Cooperative Perception	8
2.1.2. Cooperative Behavior	11
2.1.3. Other forms of cooperation	12
2.2. Wireless Communication Technologies	12
2.2.1. IEEE 802.11 Wireless Local Area Network (WLAN)	13
2.2.2. IEEE 802.11p and the WAVE DSRC Stack	14
2.2.3. Cellular Networks	16
2.2.4. Other Technologies	17
2.3. Conclusion	17
3. Connectivity in Vehicular Ad-Hoc Networks	19
3.1. Related Work	19
3.2. Channel Models	20
3.2.1. Path Loss	22
3.2.2. Large-Scale (Shadow) Fading	25
3.2.3. Small-Scale (Multipath) Fading	26
3.2.4. Vehicular Channel Models in the Literature	29
3.3. Spatial Node Distribution and Mobility Models	30
3.3.1. The Random Direction Model	31
3.3.2. Vehicular Mobility Models	32
3.4. Node Degree	38
3.4.1. Geometry	38
3.4.2. Distance Headways	41
3.4.3. Discussion	43
3.5. Link Lifetime	51
3.5.1. Geometry	52
3.5.2. Velocity Distributions	52
3.5.3. Discussion	53
3.6. Link Generation and Link Break Rate	61
3.6.1. Geometry	64
3.6.2. Discussion	66
3.7. Conclusion	69
4. QoS Analysis and Provisioning in Vehicular Ad-Hoc Networks	71

4.1. Related Work	71
4.2. Network Model	73
4.2.1. Connectivity Matrix	73
4.2.2. Traffic Vector	74
4.3. Medium Access Protocols	76
4.3.1. Collision Recovery Protocols	79
4.3.2. Collision Avoidance Protocols	80
4.3.3. 802.11(e) Distributed Coordination Function (DCF) and Enhanced Dis- tributed Channel Access (EDCA)	81
4.3.4. Reservation-Based Protocols	82
4.3.5. Discussion	83
4.4. Providing Quality of Service (QoS) in Contention-Based Networks	86
4.4.1. Global Traffic Limits Determination	86
4.4.2. Distributed Traffic Limits Determination	87
4.4.3. Admitted traffic and load distribution	88
4.4.4. Stub nodes	93
4.4.5. Fairness	95
4.5. Application Selection and Parameterization	98
4.6. Conclusion	99
5. Predictive QoS Provisioning in Vehicular Ad-Hoc Networks	101
5.1. Related Work	102
5.2. Problem Statement	104
5.3. Mobility Prediction	105
5.3.1. Concept	105
5.3.2. Speed Prediction	106
5.3.3. Distance Calculation	109
5.3.4. Position Prediction	110
5.3.5. Simulative Evaluation of Speed and Position Prediction Accuracy	111
5.4. Channel Parameter Estimation and Prediction	118
5.5. Connectivity Prediction	124
5.6. Conclusions and Outlook	125
6. A System Architecture for Cooperative Cognitive Technical Systems	129
6.1. A Lightweight Network Layer Protocol	129
6.1.1. Radio As A Sensor	130
6.1.2. Timing Measurement	131
6.1.3. Identification	132
6.2. The Communication Manager	132
6.2.1. Network Topology Information	132
6.2.2. Time-triggered Communication	133
6.2.3. Event-triggered Applications	136
6.2.4. System Integration	138
6.3. Conclusion	139
7. Conclusion and Outlook	141
7.1. Results and Contributions	141
7.2. Outlook	142

A. A Spline-Shaped Road Model	143
A.1. Definition of a Spline	143
A.2. Shape Generation	144
A.3. Length of a Spline	145
A.3.1. Numerical Integration	146
A.3.2. Parameter lookup	147
A.4. Fitting	147
B. Physical Layer Parameters	149
C. Analysis Workflow	151
C.1. Networking Parameters	151
C.2. QoS Analysis	151
List of Figures	153
List of Tables	157
Abbreviations	159
Mathematical Notations	161
Bibliography	165

1. Introduction

German road traffic statistics reveal that the number of casualties has remained more or less constant over the last 60 years. The number of fatalities, however, has decreased significantly, especially since the late 1970s (see Figure 1.1), although the number of vehicles — and consequently the number of accidents — has significantly increased in the same period. One can conclude that driving has become much safer over time, an observation that becomes more obvious when the numbers are related to the years of when governmental regulations were enacted. The figures also suggest that the introduction of new (active and passive) technologies of vehicular safety significantly contributed to that process.

In 2002, the eSafety Working Group of leading traffic experts published their final report on improving road safety in Europe by means of Information and Communication Technologies (ICT) [The02]. Among the 28 recommendations of the report, the working group demanded that “the accelerated standardisation of emerging communications protocols” shall be promoted “for vehicle-vehicle and vehicle-infrastructure communications”. Consequently, in 2003 the European Commission (EC) set the goal to further reduce the number of road fatalities by 50% until 2010 [Com03] and stated that the eSafety report concluded that “the greatest potential [...] in solving road transport safety problems is offered by the Intelligent Vehicle Safety Systems”, emphasizing the need for cooperative technologies based on Vehicle-to-Vehicle (V2V) and Vehicle-to-Infrastructure (V2I) communication.

At the time the report was published, using wireless communications between vehicles was not an entirely new idea — as early as 1989, Takada et al [TTIF89] proposed the first V2I communications system that would enable advanced services, such as positioning, navigation based on real-time traffic information, tolling, vehicle identification, and individual communication. Also, the issue of market penetration was raised and the expenditures for installing the necessary infrastructure were analyzed; questions that are still important and mostly unanswered today. At about the same time, researchers with the U.S. PATH¹ project began experimenting with automatic longitudinal control (platooning) of two vehicles [CLD⁺91], which was successfully extended to four vehicles and demonstrated in 1994. Concluding, the authors pointed out that “when a large number of vehicles is used in a platoon, the complexity of the communication scheme increases”. Also in 1994, Collier and Weiland, impressed by the positive response of navigation system field trials, drafted a vision of future intelligent vehicles [CW94] that encompassed not only navigation, but also aspects of traffic management and cooperative driving. Consequently, they argued that in the future, vehicles would be equipped with some kind of radio technology, enabling V2I and V2V communications. An extensive amount of research has subsequently been put into the field of Inter-Vehicle Communication (IVC), in terms of applications, protocols, hardware, etc.; a very comprehensive survey can be found in [WTM09].

EC’s eSafety Initiative has spawned many research projects related to IVC, both pan-european as well as on national levels, and one can expect that with the dawn of new, more elaborate and — most importantly — *networked* driver assistance systems and safety equipment,

¹California Partners for Advanced Transit and Highways (PATH). For a detailed history, see [Shl07].

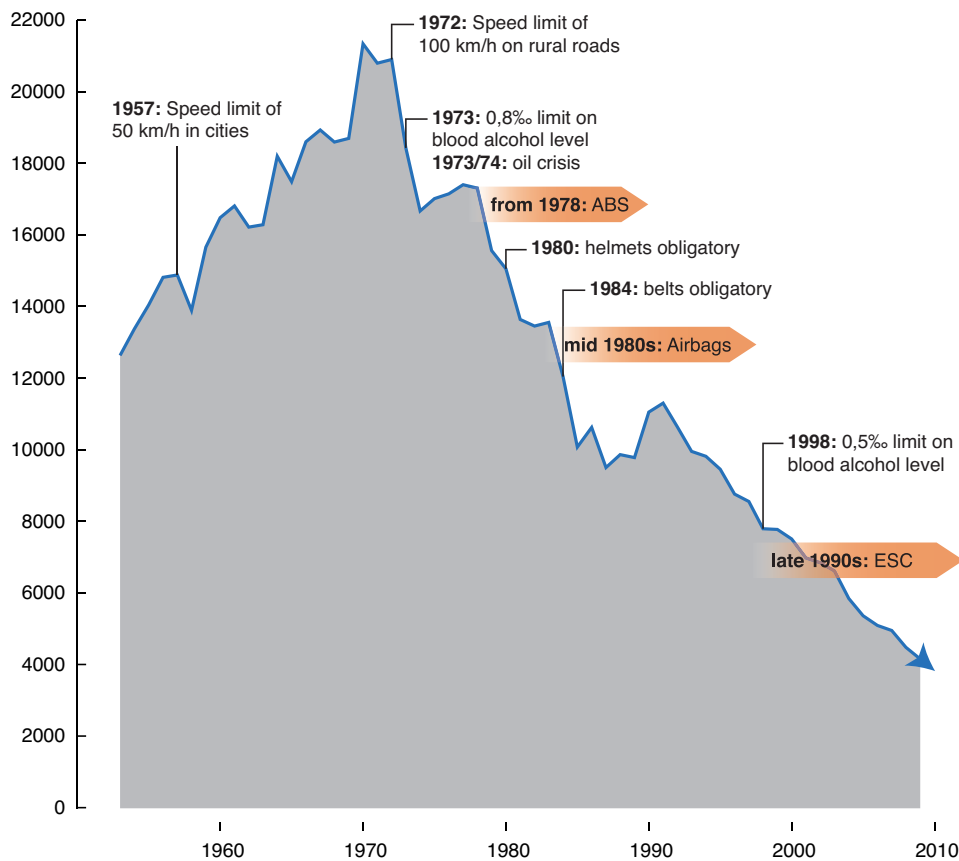


Figure 1.1.: Traffic-related fatalities in Germany [Bun09].

we will soon see another dramatic decrease of casualties and fatalities. The most prominent examples among the research projects are Cooperative Vehicle Infrastructure Systems (CVIS), Global System for Telematics (GST), PReVENTive and Active Safety Applications (PReVENT), Secure Vehicular Communication (SeVeCom), FleetNet or Network on Wheels (NoW) and, recently launched, the german "Sichere Intelligente Mobilität – Testfeld Deutschland (SIM-TD)" which provides researchers and industry with a state-wide testbed for vehicular networking. Other worldwide research project are the Vehicle Safety Communication Consortium (VSC) and the Vehicle Infrastructure Integration Initiative (VII) in the U.S., the Advanced Safety Vehicle (ASV) project as well as the InternetITS Consortium in Japan.

Today, common efforts are taken to promote worldwide standards specifically for the vehicular environment; a radio platform is being defined by the IEEE 802.11p working group, protocols and an architecture has been specified by the IEEE 1609 "WAVE" working group. In 1999, the Federal Communications Commission (FCC) has allocated 75 MHz of spectrum in the 5.9 GHz range for Dedicated Short Range Communication (DSRC). Very recently, the European Commission has allocated 50 MHz of spectrum in the 5.9 GHz band for "Smart Vehicle Communication Systems", a decision that is mainly attributed to the dedicated work of the Car-to-Car Communication Consortium (C2CCC), a task force that has been inaugurated by research institutions and industry to enforce the development of IVC technology and standards. Vehicle manufacturers and component suppliers are developing strategies and business models to widely introduce communication and are actively supporting the C2CCC. In

2008, the harmonization of technologies and standards was demonstrated [ETS09], showing the interoperability of applications from different vehicle manufacturers and also the interoperability of communication units from different suppliers.

1.1. Motivation

The “KogniMobil” project², which sets the context for this thesis, aims at the research of cognitive, cooperative vehicles. These vehicles are capable of perceiving and understanding their environment and of generating an appropriate strategy to fulfill a certain mission, e.g., driving from one location to another via a list of roads. Of course, they must adhere to common rules of traffic, avoid collisions with any other objects in the environment, and act like an inerrant human driver. Consequently, a (visionary) perfect cognitive vehicle represents the *superset of all possible driver assistance systems*. As such, it can be expected that the number of traffic fatalities would decrease significantly with an increasing fraction of vehicles being cognitive.

Through the introduction of wireless communication in cognitive vehicles, the aspect of cooperation between vehicles can be realized: they may exchange their sensor data, allowing the extension of perception beyond the range of individual sensors. Also, they may coordinate maneuvers so as to avoid collisions, overtake safely, increase traffic flow, and thus conserve energy. A large variety of these *cooperative applications* can be thought of.

It is understood that the technologies and protocols available today are not capable of handling the communication requirements of cooperative cognitive vehicles. This necessitates a novel, specifically designed communication solution able to meet these requirements. Supplemental to that, we wish to raise the attention of the application designers to consider certain specific characteristics and inevitable imperfections inherent to wireless transmissions. Clearly, only a close mutual co-design of both the cooperative application and the communication layer will yield the desired results when building reliable, dependable, and safe cooperative systems.

1.2. Contributions

From this perspective, the contributions of this thesis can be briefly summarized:

Connectivity modeling and analysis of vehicular networks: By combining aspects of vehicular traffic flow theory and the characteristics of the wireless communication medium, we formulate a novel open mathematical framework that allows for a comprehensive analysis of vehicular networking in arbitrary static and dynamic traffic scenarios. We demonstrate by means of representative examples how this formulation can be extended to incorporate any given channel model and vehicular flow model. The insights gained from the analysis can effectively be used for the dimensioning of a wireless vehicular networking solution at design time.

Decentralized, proactive QoS provisioning: Based on the results from connectivity analysis, we discuss data traffic engineering issues and present a framework that allows for

²“Kognitive Automobile”, Sonderforschungsbereich Transregio (Transregional Collaborative Research Centre) 28, sponsored by the Deutsche Forschungsgemeinschaft (DFG)

the analysis of QoS abilities of vehicular networks in any arbitrary traffic scenario, and with special respect to the chosen Medium Access Control (MAC) protocol. Again, the formulation of the MAC model is open so that it can easily be extended to any given protocol.

Built on this foundation, we describe a novel resource sharing algorithm that allows for vehicular network nodes to equally share the wireless channel so that a pre-defined QoS level can be guaranteed to the applications that shall be deployed using the network. The presented algorithm is novel in that it is completely decentralized, deterministic and fast and requires only minimal information about the network's current topology. Its specific properties, such as traffic assignment fairness and attained optimality, are analyzed and discussed in detail.

The approach is finally extended through the prediction of future vehicle positions and channel states so as to allow for a statistical forecast of the future network topology. This information can then be fed back to the resource sharing algorithm, supporting applications with an estimate of their expected future share of the wireless channel. Thus, we can provide applications with an aid for the decision of future actions that may depend on the availability of certain communication relations, of a minimum necessary data rate, etc.

System integration and protocol provisioning: In the context of the KogniMobil project, a prototypical software architecture for cognitive vehicles was developed. We present how this solution can be augmented to provide applications with means of networking and discuss how the QoS concepts developed earlier can be integrated in the architecture. We also present a networking protocol that has been tailored to service the specific needs of cognitive vehicles.

1.3. Organization

The thesis is structured as follows: each chapter will give a short introduction as well as an outline and discussion of previous work related to the chapter. Then, the respective contributions are presented. Each chapter closes with a short conclusion. See Figure 1.2 for a graphical representation of the thematic organization.

Chapter 2 gives an overview of the vision of cognitive autonomous vehicles, their general architecture and the specific requirements imposed upon the communication layer. Cooperative applications are presented and the communication relations necessary to the individual applications are discussed. The range of current wireless IVC technologies available to the system designer today are presented and their individual advantages and shortcomings are discussed.

Chapter 3 introduces the term connectivity and describes how the state of "being connected" is related to the physical location of the respective radios on the one hand and the condition of the wireless channel between these locations on the other hand. Relevant channel properties and appropriate models are presented, along with a literature survey of contemporary vehicular channel models. The fundamental relations between traffic flow theory and radio mobility are established and networking parameters such as the distribution of node degrees, communication durations and a measure for the fluctuation of a vehicular network's topology are discussed in detail, based on analysis and simulation. This chapter presents the pre-

determined physical layer factors relevant to a V2V network's performance, i.e., factors that are dictated by the environment and are thus only subject to limited control at design time.

Based on the connectivity properties derived before, Chapter 4 introduces the concept of how a time-variant network topology (i.e., connectivity on the scale of a network) in conjunction with the choice of a specific MAC protocol influences the level of QoS that can be provided to individual applications. A decentralized, distributed algorithm is designed for wireless applications that allows radio network nodes to share the available resources in a fair manner while at the same time ensuring that a defined level of QoS is always attained. We use this information to select and parametrize applications, effectively optimizing the global benefit for the networked vehicles. The results and implications that can be derived from the algorithm's formulation are discussed in detail.

An algorithm that facilitates the connectivity prediction in vehicular networks is presented in Chapter 5. A method for increasing the precision of position prediction by using digital maps information is introduced. By applying an adaptive filter, the positions of the involved vehicles can be predicted for a certain amount of time with a certain accuracy. The choice of parameters and the resulting accuracy are then discussed in detail. We present and discuss a channel parameter estimation based on a particle filter. By fusing the positions predictions and forecasting the estimated channel parameters over the desired time interval, we show how a statistical predication about the future topology of the network can be attained. Using this information, it is then possible to improve the selection and parameterization of applications that perform tasks that take a certain time to complete and require a minimum QoS during runtime. Also, prediction can help to decide whether an application should actually be started, given its networking requirements.

Founded on the previously discussed mechanisms and algorithms, a novel communication solution is presented in Chapter 6. The prototypical integration with an information-based processing architecture for cognitive vehicles is demonstrated. A prototypical, lightweight cross-layer networking protocol is introduced that supports QoS provisioning for cooperative perception and driving applications.

Chapter 7 concludes and summarizes the results of this thesis and gives an outlook on possible future research issues.

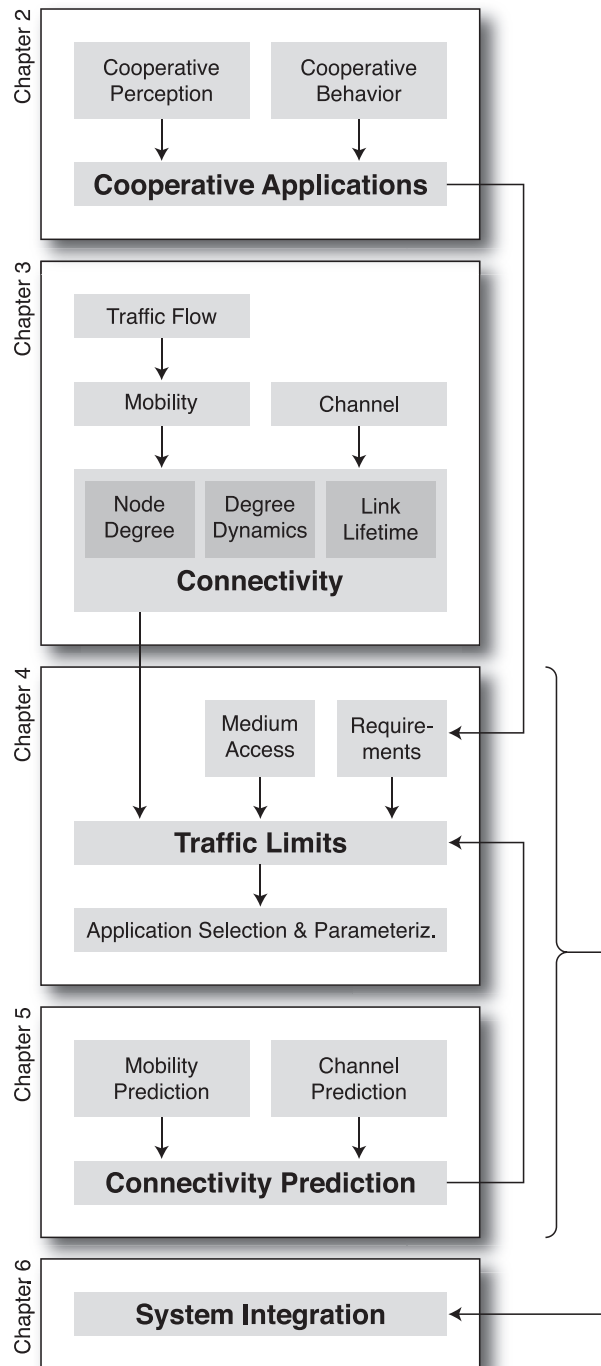


Figure 1.2.: The thematic organization of this thesis

2. Cooperation Between Vehicles: Scenarios and Requirements

Cognition in a human context comprehends the processes of perception, thinking and insight. In the domain of technical systems, cognition characterizes the capability of a machine to perceive itself and its environment by means of appropriate sensorial devices, and to process and rearrange this information — possibly against the background of already acquired knowledge — in a way that allows the machine to interact with its environment in a sensible way and according to its mission. Cooperation between cognitive machines postulates the machines' capability to communicate with each other to exchange sensorial information and knowledge, and to coordinate their individual actions so that a coherent cooperative action can be attained.

One objective of the Transregional Collaborative Research Centre (TCRC) 28 “Cognitive Automobiles” — the context from which this thesis originated — was to investigate cooperative cognitive behavior among autonomous vehicles. Sticking to the above definition of cognitive systems, cognitive behavior of a *singular vehicle* implies an understanding of the perceived environment and the ability to generate strategies to successfully navigate within this environment [SFK07, GAB⁺08]. The internal structure of such a vehicle is arranged as depicted in Figure 2.1: the environment of the vehicle (such as obstacles, pedestrians, other vehicles, etc.) and the vehicle therein (i.e., its position, speed, etc.) is perceived through appropriate sensors, such as positioning systems, odometry, video cameras, laser scanners, etc. This information is then interpreted by identifying (and potentially tracking) environmental objects; drivable lanes are determined, and a scene representation of the environment is established. Based on the scene interpretation, the mission of the vehicle, and knowledge such as traffic rules, a decision about the desired direction and velocity of motion is made and a trajectory for driving is planned. This decision is passed on to a control module, which, through appropriate actuators, guides the vehicles along the planned trajectory.

Through wireless communication, aspects of cooperation between cognitive vehicles become feasible. For instance, vehicles could expand their range of perception beyond the horizon of their own sensors (denoted as *cooperative perception* in the following), allowing a vehicle to react to environmental factors before they can be registered by the vehicle itself. Another example could be the mutual validation or falsification of uncertain sensor data: if an object is registered by more than one vehicle, its probability of existence increases. Furthermore, vehicles could constitute cooperative groups of vehicles and act as such groups [FBB08], in terms of conducting coordinated maneuvers such as, for instance, platooning or avoiding collisions (denoted as *cooperative behavior* in the following). The benefits are obvious: while the former will increase the efficiency of traffic in terms of both travel times and use of energy, the latter helps in avoiding casualties and potentially life-threatening injuries.

During the last years, V2V Communication has been in the focus of many research groups all around the world ([c2c, gst, now], to name a few). Very recently, the European Commission has allocated 50 MHz of spectrum in the 5.9 GHz band for “Smart Vehicle Communication Systems”. These systems are mainly geared towards advanced driver assistance systems

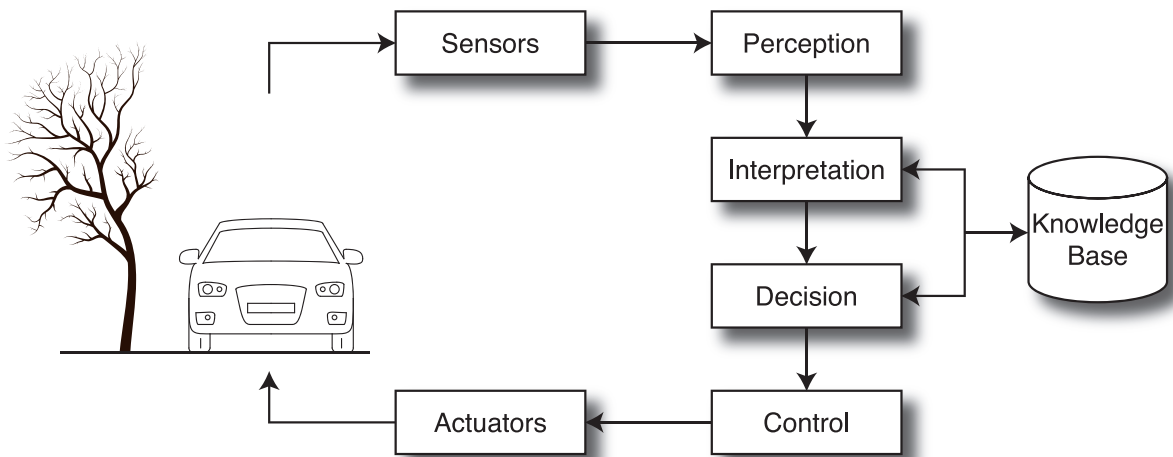


Figure 2.1.: Internal structure of a cognitive vehicle.

such as obstacle warning, red-light information, emergency systems, or infotainment applications [KBSS01, BKK⁺03, SN09]. The communication requirements of cooperative cognitive vehicles, however, by far exceed those of the aforementioned infotainment and driver assistance systems in terms of both real-time requirements and data rates.

2.1. Cooperative Applications

In the discussion of cooperative applications, a distinction regarding the objective of cooperation has to be made: On the one hand side, we wish to employ communication to enable cooperative perception. On the other hand side, cooperative behavior shall be implemented to allow for concerted maneuvers. The specific requirements of these two applications are diverse; not only in terms of required bandwidth and tolerable delays but also in terms of specific communication relations needed to fulfill a certain task.

In the following, we shall regard perfect cooperative cognitive vehicles as the superset of all possible cooperative driver assistance systems. Consequently, the requirements of cooperative cognitive applications set the scope for these systems.

2.1.1. Cooperative Perception

Due to the inherent range limitation of local sensor systems, these means of perception produce a restricted view of a vehicle's environment. Through the exchange of sensorial data between vehicles and subsequent adequate data fusion, the horizon of perception can be extended significantly. Furthermore, the level of detail could be enhanced significantly if data can be exchanged between vehicles that are equipped with different types of sensors. Assume, for instance, that one vehicle may be provided with a video camera that is capable of determining the color of an obstacle and another vehicle that possesses a laser scanner is capable of determining the 3D position of the obstacle within its environment. By merging the information gathered from the two different sensor types, both vehicles are capable of perceiving,

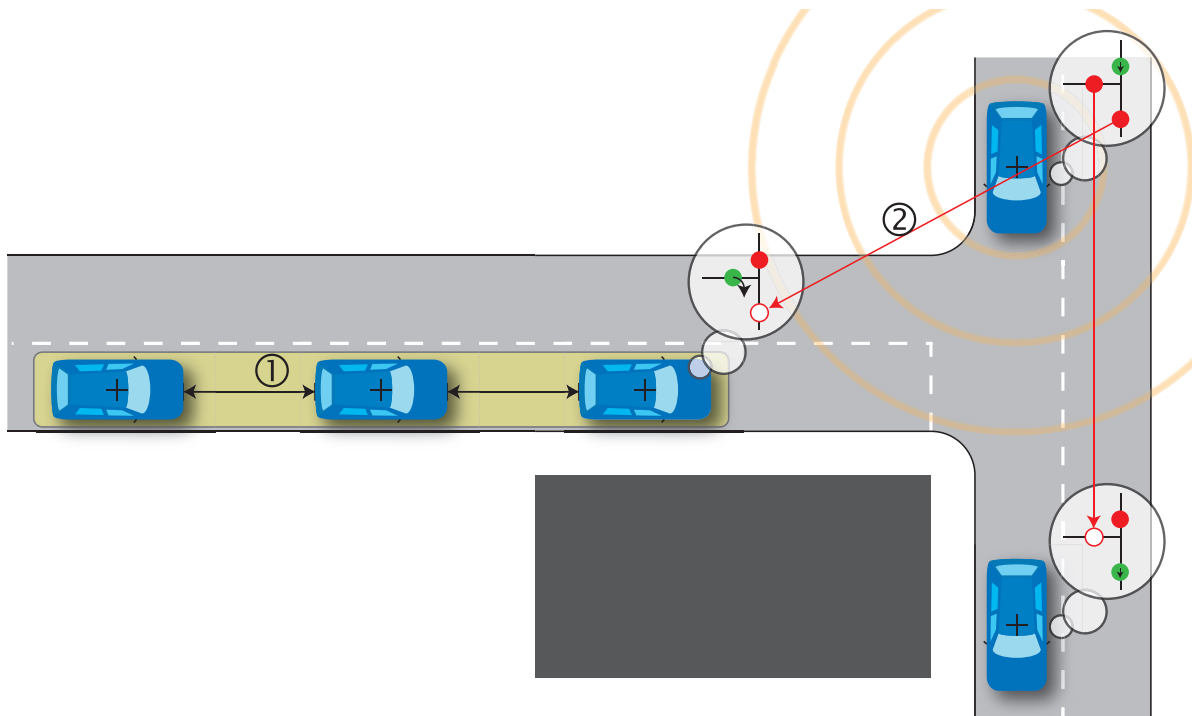


Figure 2.2.: Cooperation of vehicles: Platooning (1) and perception (2) “around the corner”.

for instance, a red obstacle placed at the center of an intersection. Cooperative perception applications can generally be understood as means of generating a rich virtual representation of vehicles’ surroundings from a number of sensorial devices, local and remote, through sensor data fusion. All applications at the interpretation and decision layer that require this information will be able to profit thereof, especially the strategy generation applications. Other applications related to cooperative perceptions are approaching emergency vehicle warning, in-vehicle signing, rollover warning, probe data collection and general emergency warning systems.

A typical scenario with cooperative perception is depicted in Figure 2.2: the first vehicle of the platoon approaches an intersection. Due to a building that obstruct the vision to the vehicle’s right, its sensors are not capable of registering the position and velocity of the vehicle that drives right next to the building. Both vehicles, however, are clearly visible from the top-right vehicle, which has unobstructed sight. Through the combination of positioning and/or sensor data and exchanging this information, all three vehicles are now aware of each others positions and velocities and the former vehicle can compute a strategy of whether it is safe to turn right at the intersection or if it has to slow down.

In Figure 2.1, communication in the context of cooperative perception can be understood as supplemental to the “perception” and “interpretation” layers, enabling these layers to share their information with other vehicles. The temporal conditions for cooperative perception can be derived from the cycle times of the sensors that constitute the input data of the applications running at the perception and interpretation layers (see Figure 2.3). We can therefore assume tolerable delays between 10 ms up to 100 ms, with a data rate volume from a few bytes to some kilobytes per cycle.

2.1. Cooperative Applications

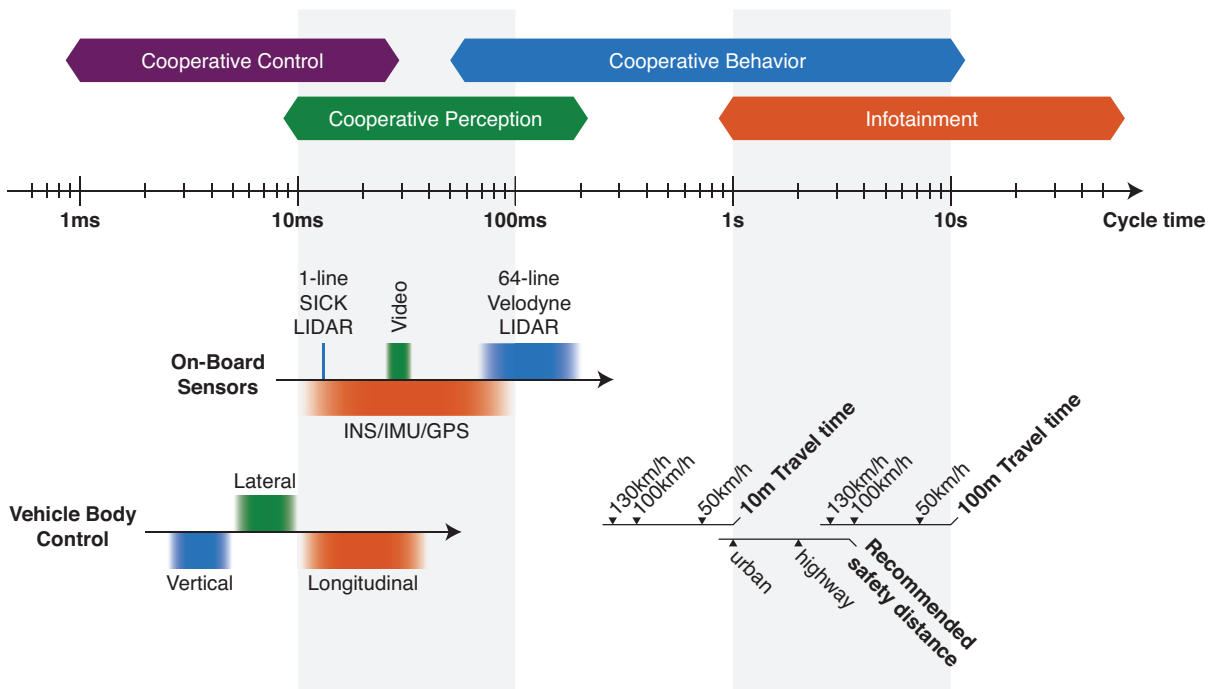


Figure 2.3.: Cycle times of sensors, controllers and cooperative tasks.

It is remarkable that since each piece of sensor information is a gain of knowledge and further details a vehicle's perception of its environment, receiving another vehicle's sensor data results in an immediate benefit for every vehicle. Since a receiver's benefit is also a function of its distance to the sender, i.e., its distance to the point where the sensor data was generated [ESKS06], we constitute that unprocessed sensor data shall be broadcasted (connectionless) and thus be disseminated only one hop from its source. Thus, the problem of coordinating a multi-hop communication has been moved into the application: if it is desirable or the application demands to do so, it is possible to aggregate received sensor data, maybe fuse it with local sensor information and then re-broadcast it to other vehicles in the proximity (effectively forwarding the information over multiple hops). Apart from a reduced complexity of the communication layer, the number of (re-)transmitted messages and thus the network load can be significantly decreased [EMS06].

In the course of this thesis, we will describe that the time-variant and highly density-variant network topology imposes significant restrictions on the available data rate for exchanging sensorial information. As data from sensors may be voluminous, we advise that applications for cooperative perception be scalable and adaptable to the situation, a paradigm that has also been recently backed by the authors of [vEWKH09, vEKH10]. We will show that available data rate has a certain correlation to the traffic situation vehicles find themselves in, especially that significant rate limitation can be found in congested traffic situations, i.e., in situations where the temporal entropy of sensor data is low. It is clear that this fact should be exploited at the design time of cooperative perception applications.

2.1.2. Cooperative Behavior

As mentioned before, communication can also be used to enable cooperative behavior of a group of vehicles. By exchanging information about vehicles' missions, their planned (short-term) trajectories, or — in the most simple cast — their positions, applications such as collisions avoidance, concerted evasive maneuvers, etc. can be realized. Also, cooperative lateral and/or longitudinal control has been studied and their beneficial impact, especially in terms of fuel efficiency, has been demonstrated [vAvDV06, LPvA09]. Other cooperative driving applications include intersection collision avoidance, transit or emergency vehicle priority.

In Figure 2.1, communication supplemental to the “interpretation” and “decision” layer enables cooperative behavior of vehicles. By allowing the interpretation and decision layers to exchange their information, vehicles can generate a common strategy for the situation they find themselves in. The temporal conditions for cooperative behavior generation can not easily be derived. As an example, let us assume that a certain situation demands a group of vehicles to find a common solution for avoiding a collision. The shortest distance between two vehicles is 10 m and the vehicles move at a speed of 50 km/h; consequently, the time until collision is 720 ms. Without considering the time necessary to actually guide the vehicles on their individual collision-free trajectory, the decision for these trajectories has to be found within the time until collision. Figure 2.3 shows the times it takes to cover a certain distance for various common speeds and the recommended safety distances. We can therefore sensibly assume that these applications need a communication solution that allows them to reach a safe decision (possibly after some iterations, a number that should be bounded above and known at design time) within some 100 ms up to 10 s.

From a technical standpoint, based on the current operative situation picture, cooperative groups of several vehicles form up. Within these groups, the necessary pieces of information are exchanged and finally a maneuver is agreed upon by the participating vehicles. For instance, an evasive maneuver could imply that a vehicle traveling on the fast lane reduces its speed to let another vehicle that is yielding an obstacle change its lane. Another example is shown in Figure 2.2, where three vehicles (to the left, highlighted) have teamed up and formed a platoon of vehicles. The leading vehicle sets the direction and velocity and as long as the vehicles' missions coincide regarding the lane they drive on, they use exchanged positioning and velocity information to drive safely and efficiently, potentially with high velocities and reduced headways, increasing the throughput of the lane.

From a networking point of view, vehicles within a cooperative group form an enclosed multicast group, potentially spreading over a large portion of the network necessitating multi-hop routing capabilities. Group communication in our concept is provided by a mechanism called “channels”, in which every cooperative group uses its own channel. Communications over a channel may be authenticated or even encrypted, if necessary. The formation of groups itself is done on the application level, supported by the extended operative situation picture as provided by the cooperative perception applications and by using a special “paging” channel that can be used to forward information to vehicles in a certain geographical area.

When designing safety-critical applications that may potentially impose a threat to life in the case of failure, it must be clear that these applications have to be built in a way that makes them resilient to failures of the communication layer. Wireless channels are inherently unreliable and may be disrupted due to unavoidable external influences. It is absolutely crucial that these applications generate a “plan B” for the case that communications fail during a cooperative

maneuver and to implement recurrent checkpointing for error detection while a maneuver is performed.

2.1.3. Other forms of cooperation

Another form of cooperation is sharing more static knowledge among cars in a peer-to-peer fashion, such as information about long-term environment conditions, traffic rules, newly learned objects, etc. For instance, floating car data (FCD) that is collected by individual vehicles may be aggregated, disseminated and forwarded to a traffic center in a decentralized fashion. This information can for instance be used for dynamic diversion if a part of the planned route is jammed.

Other applications that are based on the cooperation between vehicles and/or between vehicles and road-side equipment — such as traffic signs, signals, warning beacons etc. — are geared towards increased road safety, efficiency, and comfort. They include, but are not limited to, intersection assistance, black spot warning, curve warning, optimal speed advisory, or tolling applications. These application can be categorized as cooperative perception applications, yet the temporal span of the validity of exchanged information is usually much longer than in true cooperative perception applications.

While the mentioned applications employ communications as a means of exchanging their knowledge that is being used by the “interpretation” and “decision” layer, they have rather long time horizons regarding the validity of their information. We may, however, possibly see the extension of the vehicle-guiding algorithms’ control loops beyond the scope of isolated vehicles, if the strong temporal requirements can be fulfilled by the networking technology (see Figure 2.3). Cooperation at the “control” layer could, for instance, allow for better cooperative cruise control systems or enhanced cooperative collision mitigation.

2.2. Wireless Communication Technologies

Sensitive services that potentially pose threats on lives can only be realized through reliable communication connections. The question of connectivity is of primary interest and plays a constitutional rule: if the networks capacity drops under a certain critical bound in situations where vehicle densities (and, consequently, connectivity) is high, such as heavy congestion, insufficient resources may be available for the individual services to function correctly. On the other hand side, highways with free-flow traffic reveal vehicle densities so low that the probability of a vehicle being disconnected, effectively rendering its communication equipment useless, is significant.

Especially the problem of insufficient connectivity could be solved by using static roadside network nodes that constitute a communications infrastructure, potentially even providing a dedicated backbone network that interlinks the individual infrastructure nodes. Also, infrastructure may be helpful in overload scenarios, as a central entity managing the flow of messages. Shortcuts through the infrastructure backbone networks could also be used to effectively send messages to distant regions of the network. However, the use of infrastructure poses an elementary problem: regarding the costly deployment, infrastructure may not be available everywhere where communication is desired. Especially in remote rural regions, it is very unlikely that the necessary equipment is to be deployed promptly. Even worse, a

failure of the infrastructure equipment may significantly reduce the benefit or even disable all communications in the covered area. Therefore, we require that all functionality of the communications layer is completely decentralized and that the network is fully operational without any infrastructure and without any central entity. The term *ad-hoc network* is commonly used for wireless, decentralized, self-configuring, and potentially time-variant networks.

The term QoS refers to the effort of provisioning communications relations over a given network with a certain performance level, regarding data rate, packet loss probability, and delays. Depending on the configuration of the network, especially the Medium Access Control (MAC) used, as well as the actual in-situ connectivity, the individual performance numbers vary significantly and, mostly, it is not trivial to guarantee a certain service level. The influential factors will be discussed later and we will demonstrate how, based on a statistical description of the environment, a probabilistic estimation of the expected service level can be made and QoS can even be guaranteed. However, it is most important to keep in mind that wireless networks are inherently unreliable and that the overall behavior will be highly undeterministic.

A comprehensive overview of MAC protocols for general ad-hoc networks can be found in [GL00], where the authors outline design challenges and present a classification of protocols. Performance issues and application domains are also discussed. In [JLB10] design guidelines for ad-hoc networks are presented and a large number of different protocols is studied and classified. With a focus on vehicular ad-hoc networks, an overview on selected protocols (802.11 and ADHOC MAC [BCCF03]) as well as a qualitative comparison can be found in [MFL06]. A comprehensive survey on the whole vehicular networking stack and simulation models can be found in [SK08]. In [WTM09], a taxonomy for vehicular applications is presented and the relevance of communication protocols for various applications is established.

Although a large number of communication technologies have been suggested and studied in great detail in the literature, we shall present only those that are established and actually available for deployment in this section.

2.2.1. IEEE 802.11 WLAN

The first commercially relevant standard that allowed wireless interconnection and interoperability among a group of equipped computers was the IEEE 802.11 standard [IEE07a], today commonly denoted as “WLAN” (wireless local area network) or more recently as “WiFi”. It was originally approved and published by the Institute of Electrical and Electronics Engineers (IEEE) in 1997. In its first version, 802.11 supported a variety of physical layer interfaces, such as infrared and 2.4 GHz radio using frequency hopping (FHSS) or direct sequence (DSSS) spread spectrum, and data rates of up to 2 Mbit/s. It also introduced the ability of operating the network using infrastructure (so-called access points) and without infrastructure (ad-hoc mode). While transmission coordination may be controlled by the Access Point (AP) in infrastructure mode using Point Coordination Function (PCF), it is inherently self-organizing in ad-hoc mode, using the Distributed Coordination Function (DCF). The radio channel itself is shared among the participating nodes using the contention-based Carrier Sense Multiple Access with Collision Avoidance (CSMA/CA) MAC scheme, with optional RTS/CTS flow control for point-to-point connections.

Over the years, the standard saw many amendments, mostly providing improved PHY specifications that allowed higher data rates - such as 1999’s 11b amendment that allowed that data

rates of up to 11 Mbit/s in the 2.4 GHz ISM band and, widely adopted by equipment manufacturers and customers, made the standard a commercial success. At the same time, the 11a amendment — not so well known in Europe as it was originally not admitted due to frequency band licensing issues — even allowed data rates of up to 54 Mbit/s in the 5 GHz U-NII band, using the novel *Orthogonal Frequency Division Multiplex (OFDM)* modulation scheme. The OFDM modulation and coding scheme used in 11a was later adopted in 2003 for the 2.4 GHz band under the 11g revision. The latest addition to the standard was the 11n amendment, approved in 2009, that introduced MIMO techniques and specifies channel bandwidths up to 40 MHz, allowing for data rates of up to 600 Mbit/s.

Apart of the constant increase in available data rate, the 11e amendment provided the basis for differentiated prioritization of individual services and thus a fundament for the realization of QoS over 802.11-based wireless networks. The WiFi-Alliance, founded by equipment manufacturers, certified compliant devices and coined the term *Wireless Multimedia Extensions (WME)* or *Wi-Fi Multimedia (WMM)* for QoS-enabled equipment. With a clear emphasis on the support of wireless multimedia applications, 11e offered the possibility to assign four different traffic classes to each packet, effectively altering the time before channel access is granted (the so-called Contention Window (CW)) through a modified coordination function, the EDCA. The actual effect of prioritization, however, strongly depends on a careful choice of traffic classes for individual applications, and an incorrect assignment can result in significant performance degradation.

Due to the complex, non-deterministic, contention-based MAC scheme and its dependency on a large number of parameters, determining an expected throughput or packet loss probability is not trivial and only statistical measures can be derived; several publications exist that cover the topic through analysis and simulation. It is worth noting that even if the 11e QoS extension is implemented, it is not possible to guarantee a certain service level (see also Chapter 4).

However, 802.11a/b/g/n+e is the only readily-available standard today, with low prices for high-quality equipment. Its specific properties have been studied by many researchers and it has been (and still is) implemented in almost all V2V scenarios. In the context of the “Cognitive Automobiles” research project, we have specified and successfully used 802.11a/g+e as the communication basis for tested cooperative applications.

2.2.2. IEEE 802.11p and the WAVE DSRC Stack

Due to several shortcomings of the IEEE 802.11 standards and the advent of novel applications for networked vehicles, various new requirements have arisen demanding that the communications solution is able to:

- support longer ranges of operation (up to 1000 m),
- handle high relative speeds of vehicles (up to 500 km/h),
- cope with extreme multipath environments such as urban scenarios where the wireless signal experiences many reflections with long delays of up to 5 μ s maximum excess,
- operate in a dedicated portion of the frequency spectrum,
- provide multiple overlapping ad-hoc networks with extremely high quality of service,
- tightly support automotive applications and their communication requirements (such as for instance reliable broadcast).

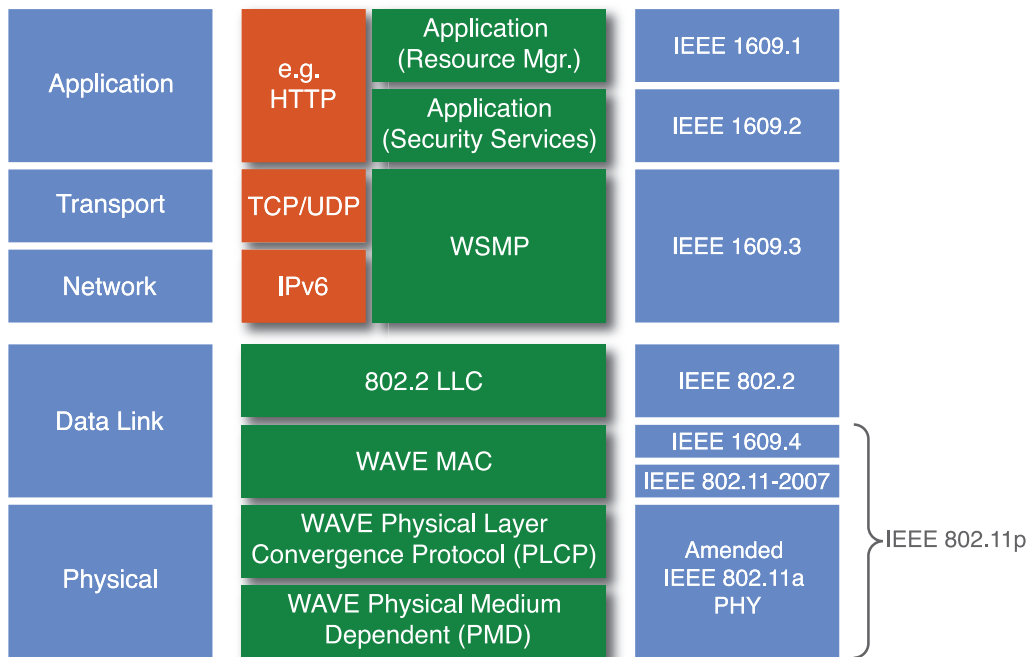


Figure 2.4.: The WAVE communication stack.

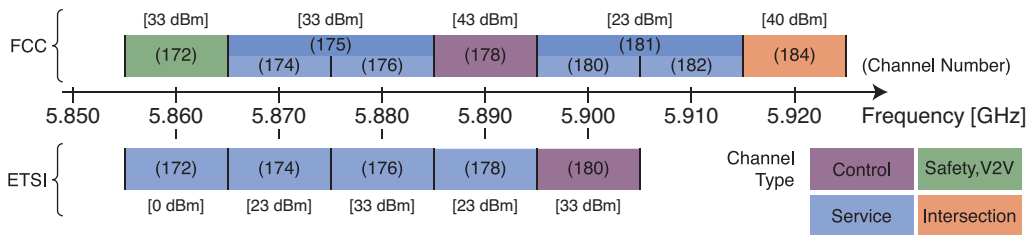


Figure 2.5.: The WAVE frequency assignment.

Given these requirements, the IEEE has defined a new standards suite for vehicular networks, commonly denoted as the Wireless Access in Vehicular Environments (WAVE) standards family (Figure 2.4): there are the IEEE 1609 standards that describe multi-channel MAC layer functionality (IEEE 1609.4 [IEE06a]), security (IEEE 1609.2 [IEE06c]), resource management (IEEE 1609.1 [IEE06b]), as well as addressing and routing (IEEE 1609.3 [IEE07b]). These standards have been designed to be implemented in conjunction with the IEEE 802.11p physical layer standard [IEE10], that basically consists of an 11a radio interface (working in the dedicated and licensed 5.9 GHz frequency band) complemented with slightly adapted 11e QoS extensions. Note that in contrast to the existing WLAN standards, the DSRC standards define a complete protocol stack.

To ensure that vehicular communications are not disturbed by other wireless appliances, the FCC in the U.S. allocated 75 MHz of dedicated, licensed spectrum in the 5.9 GHz band in October 1999. In August 2008, ETSI accepted C2CCC’s proposal and assigned 50 MHz of licensed spectrum to vehicular communications. The frequency assignments, along with power limits and channel types, are depicted in Figure 2.5.

Although the WAVE standards and 11p are specifically targeted at vehicular applications, some criticism has arisen that the proposed solution is not able to cope with requirements typical to vehicular applications. Quite early, [Eic07] argued that the EDCA introduced in 11p through 11e is not sufficient to guarantee QoS. Specifically, the parameter set used for prioritization leads to a complete squeeze-out of lower-priority messages as the number of high-priority messages increases, which presents a critical issue especially in scenarios with high node densities. The author suggests that only a very careful assignment of messages to priorities (at design time) can avoid this effect. In [WCL⁺08], the authors point out that the channel switching scheme used by the WAVE standard, which requires switching to the control channel every 100 ms, causes additional unnecessary overhead as data frames are transmitted without specific alignment. They denoted this effect meaningfully as “bandwidth wastage” problem.

The authors in [BUSB09] argue that 11p is not able to support real-time applications. The decisive issue — inherent to all the 802.11 standards — is that the employed MAC protocol can cause unbounded delays, which practically makes it impossible to guarantee adherence to message deadlines. The authors conclude that using a deterministic MAC protocol that provides for finite channel access delays is inevitable for the realization of safety-critical V2V applications and suggest that a decentralized, self-organizing TDMA protocol could meet these requirements.

2.2.3. Cellular Networks

Using cellular networks has little been discussed in the literature, mostly with a focus on V2I applications. While their consideration in this scope may be sensible (see, for instance, [BVP⁺10]), these technologies do not qualify well as candidates for V2V communication. The main issue here is that the information about spatial proximity of vehicles, which is inherently available to short-range communication systems as the ones presented above and an important prerequisite for cooperative applications, is not directly available in cellular networks without additional technology.

As of today, the round-trip delays experienced in cellular HSPA networks can be expected around 100 ms [Rys09], not including processing and routing overhead at the base station. The authors of [SGSSA08] present a unified V2V and V2I system based on a peer-to-peer approach that creates a location-based group communications infrastructure and have evaluated the delays experienced over a UMTS network at around 850 ms. This delay may be short enough for warning messages, but could pose significant restrictions on other cooperative applications.

The introduction of LTE can be expected to further bring down the experienced delays and their eligibility should be re-evaluated when these technologies become available. Another drawback of cellular networks, however, is the fact that their coverage is usually limited and that their availability is rather limited, especially in rural environments. Furthermore, while the density of installed base stations in cities may be sufficient to cope with the additional data traffic caused by vehicular applications, the network capacity in weakly equipped environments may be quickly exhausted. Additionally, it is very hard to forecast the development of other applications that impose additional load on these networks: for instance, the installed capacity of UMTS networks was expected sufficient before smart phones were introduced that nowadays utilize most of the network capacity and even overload the networks intermittently.

Is it questionable whether the providers would like to see their networks become congested by vehicular applications.

2.2.4. Other Technologies

Over the time, a variety of alternative technologies have been suggested for deployment in vehicular networks. In [LHSR01], the authors suggest an adapted UTRA-TDD Physical Layer (PHY) and MAC mechanism and argue that the time-division properties of the properties allow for relatively simple QoS provisioning. The suitability of Bluetooth for V2V networks has been discussed in great detail in [SD05]. Also, ultra-wideband (UWB) and ZigBee technologies have been suggested for vehicular networks [NHB05]. However, none of the technologies have actually gained any significance and shall therefore not be discussed here.

Relatively new approaches geared towards directed point-to-point connections between vehicles comprise free-space optical technologies [AL10] and data transmission using OFDM modulated radar [SZW09] (which can be expected to be available in a wide range of future vehicles). Solutions geared towards wide-area information dissemination into vehicles through unidirectional broadcast (traffic information, etc.) have been discussed being based on technologies such as DRM, RDS, and DVB (see [BVP⁺10]).

While the former technologies are potential candidates for the cooperative applications presented above (and their performance may actually be studied using the presented methods), the latter are very specialized and applicable mostly to point-to-point and wide-area broadcast. The reader shall be referred to the references for further information.

2.3. Conclusion

In this section, we have classified cooperative applications into the two main categories: cooperative perception and cooperative behavior. We have discussed exemplary applications and their requirements. In the second part, contemporary and readily available communication technologies are presented and their adequacy for cooperative vehicles has been discussed.

For obvious reasons, we do not give any recommendations regarding the choice of a specific communication technology here, as the requirements of actually deployed applications may vary greatly and this choice has to be made with respect to these requirements. In the next chapters, we will present analytical tools that can be used to analyze communication technologies, given an application and a deployment scenario, and that are ultimately to support this choice.

We have argued above that, when designing cooperative applications, it is absolutely crucial that:

- applications are built in a way that allows them to scale and adapt to a varying communication situation,
- applications cope with inherent and unavoidable shortcomings of the wireless medium, especially connections breaking down unexpectedly (have a plan “B” ready).

	Cooperative Perception	Cooperative Behavior
Cycle Time	10 ms . . . 100 ms	100 ms . . . 10s
Data Volume	some kbit	some bit
Communication Relation	broadcast	group-based
Communication Range	neighboring vehicles	cooperative group (some m . . . km)
Triggered Through	sensor cycle, time	event, decision
Design Issues	scalability	fail-safe

Table 2.1.: Typical requirements of cooperative applications.

3. Connectivity in Vehicular Ad-Hoc Networks

This chapter studies the implications of the specific mobility of vehicles traveling on streets on the networking aspects of wireless vehicular ad-hoc networks.

We will first elaborate on the fundamental interdependence of nodes' spatial proximity and the probability that these nodes can exchange messages through means of wireless transmission, commonly termed as "connectivity". We present and discuss several channel models, which can be ultimately interpreted as the tie between spatial properties of the network and consequent connection probability. These spatial properties of wireless vehicular networks are evidently determined by the physical properties of vehicular traffic flow. As such, we introduce and discuss various parameters of (vehicular) traffic modeling, which — in conjunction with appropriate channel models — constitutes the basis for subsequent analysis.

On the basis of the derived framework that integrates channel and mobility models, we shall analyze fundamental properties of connectivity in vehicular networks. As a first step, we make the connection between the node degree (i.e. the number of communication partners) and the distance distribution of vehicles. Then, we investigate the distribution of connection times as a result of the velocity distribution of vehicles. Finally, we combine the node degree and the connection times and obtain the rate at which the connections between vehicles change as a measure of the dynamic of vehicular networks. We derive all necessary formulas that characterize network properties, introduce representative scenarios and discuss the results on their basis.

The main contribution of this chapter is a comprehensive mathematical formulation of number of relevant factors that determine the static and dynamic connectivity of a vehicular network. All results in this chapter are abstract of the radio technology used to actually form the network; instead, they are universally valid theoretical considerations and reasonings about connectivity that contribute to the state of art as a guideline to the design of a physical layer in vehicular networks. Furthermore, these considerations form the basis for the development of dedicated teletraffic engineering mechanisms in the next chapter. Some of the material in this chapter has been published in [NE08, Nag10b].

To avoid ambiguity, the term "traffic" in this chapter refers to the movement and interaction of vehicles on roads.

3.1. Related Work

Connectivity in MANETs and one-dimensional networks has been thoroughly studied through simulation and analysis [MA06, DTH02]. The main part of these contributions address the problem of connectivity in the context of static networks and are thus more applicable to sensor networks. The impact of mobility and the consequences for connectivity is extensively studied in [Bet04], but the studied mobility models are not applicable to vehicular ad-hoc networks as they are not capable of reflecting the specific properties of vehicular traffic flows. Fur-

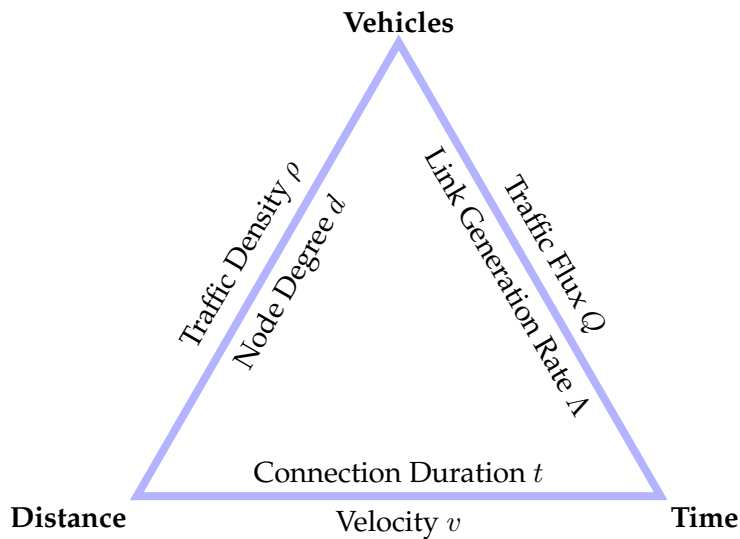


Figure 3.1.: The fundamental relations between number of vehicles, distance, and time in terms of traffic flow theory (outer text) and networking parameters (inner text).

thermore, the studied models are geared towards the analysis of (spatially) two-dimensional networks, whereas vehicular networks are usually modeled in one dimension.

The effect of traffic parameters such as density, velocities and transmission range on connectivity is studied in [ARP04, APR05] through simulation. Link lifetimes have been studied in [Wan04]. An interesting approach is outlined in [YAEAF08], studying the impact of speed distribution and traffic flow on connectivity and connectivity distance. However, there is no model that analytically and comprehensively addresses all three aspects of connectivity, node degree, communication duration and topology change rates in the context of the different traffic density regimes, free-flow and congestion.

Other related work will be addressed in the appropriate places throughout the chapter.

3.2. Channel Models

In communication networks, we denote two network nodes as *connected* if a means of data transportation exists between them so that these nodes can exchange messages. In wireless (i.e. radio) networks, the signal P_r at the receiving node is required to exceed a certain threshold P_s (called the receiver sensitivity) so that the transmitted message can successfully be detected and decoded. In other words, two nodes are connected if, at the receiver, $P_r \geq P_s$ holds true¹.

We assume that both nodes use isotropic antennas and let P_t denote the transmitted power. The attenuation β (in dB)² of the signal between the transmitting and the receiving node is

¹Note that the receiver sensitivity is a function of the data rate and the channel bandwidth. For instance, the 802.11 standard [IEE07a] requires a minimum sensitivity of -82 dBm (≈ 6.3 pW) at a data rate of 6 Mbit/s over a 20 MHz channel.

²Instead of linear dimensions, we will — unless denoted otherwise — use the logarithmic unit dB throughout this thesis. When necessary, we will superscript variables with ^(dB) or ^(lin) to avoid ambiguity.

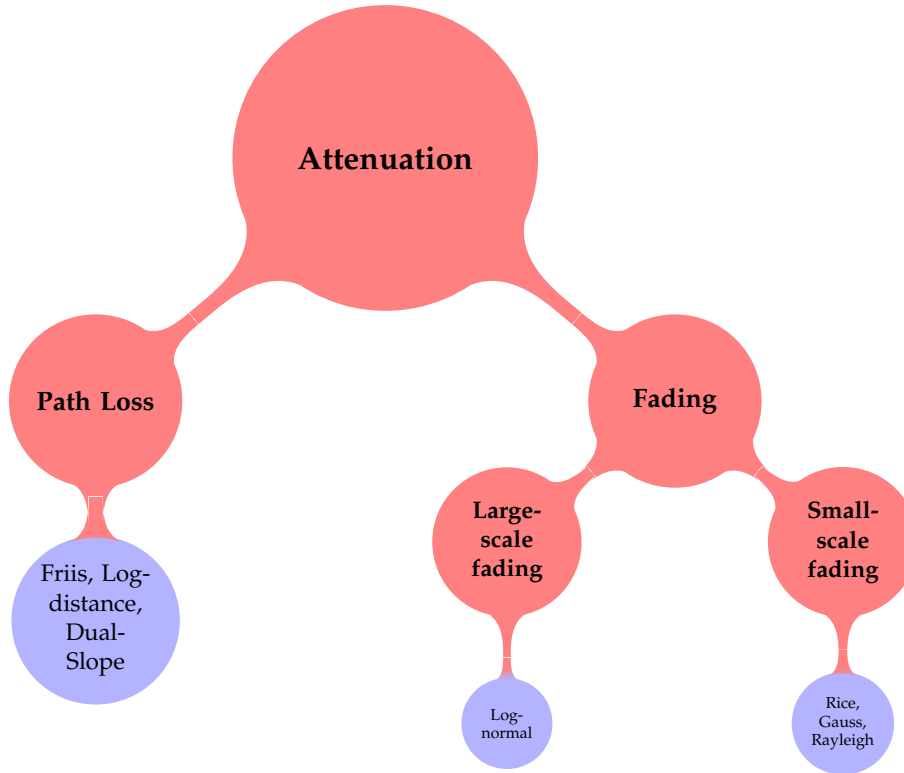


Figure 3.2.: Classification of attenuation effects (red) and their distributions (blue).

then given by:

$$\beta^{(\text{dB})} = 10 \log_{10} \left(\frac{P_t^{(\text{lin})}}{P_r^{(\text{lin})}} \right) = 10 \log_{10} \left(P_t^{(\text{lin})} \right) - 10 \log_{10} \left(P_r^{(\text{lin})} \right) \quad (3.1)$$

$$= P_t^{(\text{dB})} - P_r^{(\text{dB})} \quad (3.2)$$

Attenuation is a result of the propagation of the electromagnetic wave through space and the associated physical effects that reduce the power density of the wave. It is therefore a function of both the environment and the positions of the transmitter $\underline{x}_a(t)$ and a receiver $\underline{x}_b(t)$ therein.

In the literature, a variety of *channel models* exists which — to a certain extent — describe one or more aspects of this relation (Figure 3.2); a very good and comprehensive survey of propagation models can be found in [SJK⁺03]. Beside the (commonly used) statistical channel models, ray-tracing methods [Mau05] have become popular over the last years as a consequence of increased computational power. Ray-tracing can give extremely realistic results; however, very good knowledge and precise modeling of the environment is required, a prerequisite that cannot always be taken for granted. A very thorough survey on V2V propagation channels, especially measured characteristics and parameters, can be found in [MTKM09].

We denote the maximum possible attenuation β_{max} as the margin between transmitted power P_t and the receiver sensitivity P_s (Equation (3.2)):

$$\beta_{max} = P_t - P_s \quad (3.3)$$

In the following, we will discuss formulas for the probability that two nodes A and B placed at distinct positions \mathbf{x}_a and \mathbf{x}_b are connected, i.e. the probability that the attenuation between the nodes is below β_{max} , and formulate the channel model as a function of nodes' physical positions:

$$\chi(\mathbf{x}_a, \mathbf{x}_b) \triangleq P(\beta(\mathbf{x}_a, \mathbf{x}_b) \leq \beta_{max}) \quad (3.4)$$

More precisely, let us define $\chi(\mathbf{x}_a, \mathbf{x}_b)$ to be the probability that node A can transmit messages to node B. If the channel is reciprocal,

$$\chi(\mathbf{x}_a, \mathbf{x}_b) = \chi(\mathbf{x}_b, \mathbf{x}_a) \quad (3.5)$$

3.2.1. Path Loss

The most obvious effect of attenuation is a result of the expansion of the wave front in space, resembling the shape of a growing sphere. This effect is generally denoted as *path loss*, relating attenuation to the distance $d = \|\mathbf{x}_a - \mathbf{x}_b\|$ between transmitter and receiver.

Friis Path Loss

The simplest form of path loss can be given for a free-space environment in which the wave can expand freely in all three dimensions. It has been originally proposed [Fri46] that the received power decays quadratically with the distance d :

$$\beta_f(d) = 20 \log_{10} \frac{4\pi d}{\lambda} \quad (3.6)$$

The parameter λ represents the wavelength. Note however that Equation (3.6) is only valid for distances d in the far-field of the transmitting antenna and is related to the largest linear dimension of the antenna aperture D :

$$d \gg \frac{2D^2}{\lambda} \vee d \gg D \vee d \gg \lambda \quad (3.7)$$

Log-Distance Path Loss

To account for environments in which parts of the wave front are reflected or absorbed, Equation (3.6) has been extended through the introduction of the *path loss exponent* α :

$$\beta_p(d) = \beta_r(d_0) + 10\alpha \log_{10} \frac{d}{d_0} \quad (3.8)$$

$$= 20 \log_{10} \frac{4\pi d_0}{\lambda} + 10\alpha \log_{10} \frac{d}{d_0} \quad (3.9)$$

Equation (3.6) and Equation (3.9) are homologous for $\alpha = 2$. In environments in which parts of the wave front are reflected or absorbed, higher values of α are used; for example, urban environments that include buildings and other obstacles are commonly modeled by letting $\alpha = 3 \dots 6$ [Rap96]. On the other hand, tunnels or undercrossings may act as waveguides, so that $\alpha < 2$.

The distance d_0 at which the reference path loss $\beta_r(d_0)$ is measured or calculated (using Equation (3.6)) must obey the far-field constraints of Equation (3.7). It can safely be chosen as $d_0 = 1$ m for the radio technologies discussed in this thesis.

We can now determine the distance r for the maximum possible attenuation β_{max} so that the received signal is just greater or equal to the receiver sensitivity (Equation (3.3)). This distance is commonly denoted as the *radio range*:

$$r = d_0 \left(\left(\frac{\lambda}{4\pi d_0} \right)^2 10^{0.1\beta_{max}} \right)^{1/\alpha} \quad (3.10)$$

For the log-distance path loss model, r is independent of the actual positions of transmitter and receiver and thus the radius of a disc-shaped area centered at the transmitter. The probability that two nodes at $\underline{\mathbf{x}}_a$ and $\underline{\mathbf{x}}_b$ are connected is thus

$$\chi(\underline{\mathbf{x}}_a, \underline{\mathbf{x}}_b) = \begin{cases} 1 & \text{if } \|\underline{\mathbf{x}}_a - \underline{\mathbf{x}}_b\| \leq r \\ 0 & \text{otherwise} \end{cases} \quad (3.11)$$

Dual-Slope Path Loss

In [NE08], we have proposed the application of a dual slope model for the computation of more realistic path loss. It is based on the consideration of static objects (such as buildings) in the environment whose properties (position, shape, etc.) are *known*: given the positions of the transmitter and the receiver, as well as the position of objects, we can determine the segment $d_l \leq d$ that the wave travels without hitting an object, i.e. the Line-Of-Sight (LOS) distance. The segment $d_n = d - d_l$ is assumed to be Non-Line-Of-Sight (NLOS). The path loss exponent α_l is used for computing the path loss on d_l , while α_n is used for the path loss on d_n (hence the term *dual slope*):

$$\beta_p(d) = 20 \log_{10} \frac{4\pi d_0}{\lambda} + 10\alpha_l \log_{10} \frac{d_l}{d_0} + 10\alpha_n \log_{10} \frac{d}{d_l} \quad (3.12)$$

The dual slope model has originally been proposed to model attenuation in cellular systems (900 MHz up to 1900 MHz) and is predominantly used in this context [FBR⁺94], although its applicability has been demonstrated for other areas, such as ultra-wideband (UWB) [CWM02, DAA⁺04]. Various methods for the prediction of the breakpoint distance (d_l) are investigated in [PWR99]. Chia et al. [CS92], however, related the dual-slope breakpoint distance to “the approximate distance at which the LOS path is lost” and showed that the dual-slope model performed significantly better in urban and highway scenarios than the single-slope log-distance model. Recent studies [CHBS08b] have shown that vehicle-to-vehicle channels can be successfully modeled by the dual slope model.

The radio range $r(d_l)$ is a function of the length d_l of the LOS segment. It is therefore not necessarily disc-shaped, but depends on the properties of the static objects surrounding the transmitter:

$$r(d_l) = d_l \left(\left(\frac{\lambda}{4\pi d_0} \right)^2 \left(\frac{d_0}{d_l} \right)^{\alpha_l} 10^{0.1\beta_{max}} \right)^{1/\alpha_n} \quad (3.13)$$

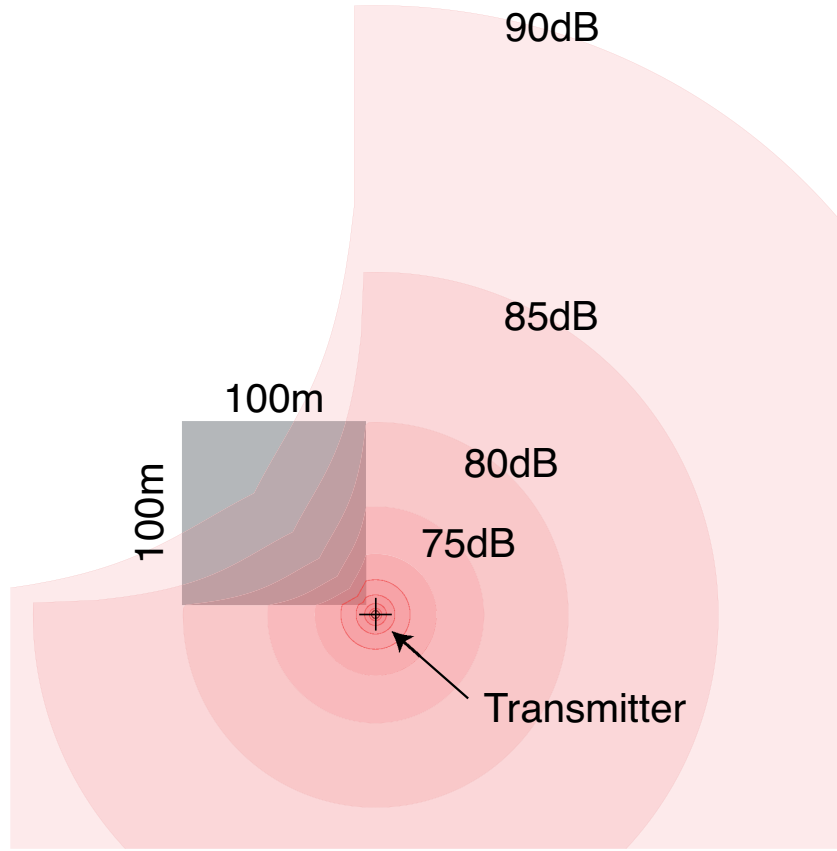


Figure 3.3.: Attenuation for Log-Distance (non-obstructed part) and Dual-Slope path loss models ($\alpha_l = 2$, $\alpha_n = 3$). The obstacle (grey box) significantly influences the attenuation.

The probability that two nodes at \underline{x}_a and \underline{x}_b are connected is thus (with d_l as the distance between the sending node and the closest obstacle along the path from \underline{x}_a to \underline{x}_b):

$$\chi(\underline{x}_a, \underline{x}_b) = \begin{cases} 1 & \text{if } \|\underline{x}_a - \underline{x}_b\| \leq r(d_l) \\ 0 & \text{otherwise} \end{cases} \quad (3.14)$$

Example

Take a sender transmitting with a power of 20 mW (13 dBm). We assume that, for a data rate of 6 Mbit/s, the receiver has a minimum sensitivity of -82 dBm. Without any further losses, the maximum possible attenuation β_{max} is thus -102 dB. At a frequency of 2.4 GHz (or a wavelength λ of 0.125 m) and free space conditions, the radio range r amounts to ≈ 1250 m. For a path loss exponent α of 3, the radio range r is only ≈ 115 m (according to Equation (3.10)).

In another scenario, the wave first propagates under free-space conditions d_l for 30 m, then hits an object that has a path loss exponent of 3. The maximum distance $d_{max}(d_l)$ is then ≈ 360 m (Equation (3.13)). Notice (in Figure 3.4) how, at a distance of 30 m, the slope of the received power changes with the path loss exponent.

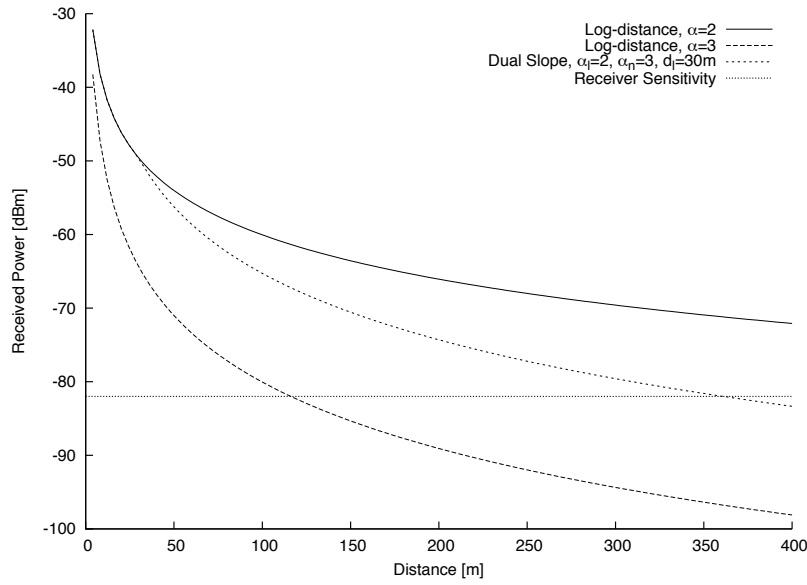


Figure 3.4.: Received power P_r over distance d for Log-distance and Dual-slope path loss models.

3.2.2. Large-Scale (Shadow) Fading

Realistic environments contain a number of dynamic and static objects (such as vehicles, pedestrians, etc.) whose properties (position, shape, etc.) are *unknown*. Consequently, receivers placed at different positions but at a constant distance to the receiver experience different attenuation $\beta(\underline{x})$. Also, due to movement of objects in the environment, a receiver placed at a constant position experiences an attenuation varying over time $\beta(t)$. To account for these effects, the additional stochastic parameter β_s is introduced:

$$\beta_{ps}(d) = \beta_p(d) + \beta_s \quad (3.15)$$

The log-normal shadowing [GW98] model assumes that the propagating wave experiences numerous attenuation effects along its path. Mathematically, their contribution to the attenuation is multiplicative — or, in the logarithmic domain, additive. Under the assumption that the attenuation effects are uncorrelated, the central limit theorem states that the sum of their logarithms is normally distributed³ with variance σ^2 :

$$f_{\beta_s}(\beta_s) = \frac{1}{\sqrt{2\pi}\sigma} \exp\left(-\frac{\beta_s^2}{2\sigma^2}\right) \quad (3.16)$$

The probability that two nodes at \underline{x}_a and \underline{x}_b are connected is thus determined by the probability that $\beta_s \leq \beta_{max} - \beta_p(d)$ (i.e. the margin between the attenuation caused by path loss and

³...or, in the non-logarithmic domain, log-normally distributed; hence termed *log-normal* shadowing.

the maximum possible attenuation)⁴:

$$\chi(\mathbf{x}_a, \mathbf{x}_b) = \int_{-\infty}^{\beta_{max} - \beta_p(\|\mathbf{x}_a - \mathbf{x}_b\|)} f_{\beta_s}(\beta_s) d\beta_s \quad (3.17)$$

$$= \frac{1}{2} + \frac{1}{2} \operatorname{erf} \left(\frac{\beta_{max} - \beta_p(\|\mathbf{x}_a - \mathbf{x}_b\|)}{\sqrt{2}\sigma} \right) \quad (3.18)$$

Note that at the border of the radio range r ($\beta_{max} = \beta_p(r)$), the probability that $\beta_s \leq 0$ is 0.5. As a consequence, the previously well-defined borderline of the radio range should — under shadow fading conditions — rather be regarded as a set of borderlines, with individual connection probabilities.

Example

In the previous example, we have calculated a radio range r of 115 m for a path loss exponent of 3. According to Equation (3.18), this is the border of the area in which the connection probability is at least 0.5. Assume that the standard deviation of the shadow fading process σ is 8 dB. We wish to determine the radius of the area in which the connection probability is greater than 0.95. The shadow fading must then be:

$$\beta_s \leq \sqrt{2}\sigma \cdot \operatorname{erf}^{-1}(1 - 2 \cdot \chi(\mathbf{x}_a, \mathbf{x}_b)) \quad (3.19)$$

i.e. $\beta_s \leq -13.16$ dB. The equivalent radio range $r_{0.95}$ can thus be determined through Equation (3.10):

$$r_{0.95} = r(102 \text{ dB} - 13.16 \text{ dB}) \approx 42 \text{ m} \quad (3.20)$$

3.2.3. Small-Scale (Multipath) Fading

Multipath propagation occurs if objects in the environment reflect, diffract or scatter the propagating wave. The distances covered by the individual propagation paths have different lengths, therefore their phase at the receiver is not equal so that interference — and, as a consequence, attenuation — occurs. The sum of the individual paths changes significantly if the receiver moves by very small distances (one-half the wavelength).

Due to the delays τ caused by the individual path lengths, inter-symbol interference may occur. ISI's frequency domain dual, the *coherence bandwidth* B_C (as a function of the *rms delay spread* σ_τ) is defined as the bandwidth over which the frequency correlation (i.e., the bandwidth over which all spectral components have equal gain and linear phase) is above a certain threshold. The channel is frequency-flat if the symbol duration $T_s > \sigma_\tau$ and the transmission's bandwidth $B_S < B_C$. Otherwise, the channel is called frequency-selective.

Moving terminals experience *Doppler shift* on the various propagation paths, depending on their direction of movement. The sum of the shifts results in a widening of the signals spectrum, commonly denoted as *Doppler spread* B_D . Its time domain dual, denoted as *coherence time* T_C , is a measure of the time period in which the channels fading intensity is almost constant. It is usually utilized to distinguish between *slow and fast fading*: if the symbol duration $T_S < T_C$ and the transmission's bandwidth $B_S > B_D$, the fading is called slow. Otherwise, the fading is called fast.

⁴erf denotes the error function, defined as $\operatorname{erf}(x) = \frac{2}{\sqrt{\pi}} \int_0^x e^{-t^2} dt$.

Recent channel measurement campaigns in both the 2.4 GHz [ATI04] and 5 GHz [MFW02, MSXY05, PKC⁺07] ISM bands as well as in the dedicated 5.9 GHz [CHBS08a, CHC⁺08] DSRC band have revealed maximum Root Mean Square (RMS) delay spreads of less than 1 μ s and medium RMS delay spreads around 0.1 μ s. These delay spreads correspond to propagation path length deviations of 300 m and 30 m, respectively, and appear reasonable in vehicle-to-vehicle communication scenarios. Under the requirement that the frequency correlation is above 0.5, the resulting coherence bandwidth B_C is between 200 kHz and 2 MHz. The IEEE 802.11 standard's OFDM PHY specification for 10 MHz channels, as used in the 802.11p vehicle-to-vehicle amendment, dictates sub-carriers bandwidths of 156.25 kHz, therefore the channel can be considered frequency-flat for these radios.

The Doppler shift f_m is determined from the relative velocity v between transmitter and receiver and the wavelength used for the transmission. Considering PHY operation in the 5.9 GHz DSRC band and vehicles moving with a relative velocity of $v = 30$ m/s, the doppler spread B_D is 590 Hz and the coherence time for a required frequency correlation of 0.5 is $T_C \approx 1$ ms. With a symbol duration of 8 μ s, we can transmit up to ≈ 125 symbols — or 375 B in the 3 Mbit/s data rate mode — under the condition that the channel fades slowly during the transmission.

Rice, Rayleigh and Gaussian Fading

The amplitude envelope x of a received frequency-flat fading signal in a multipath environment is commonly modeled by the Ricean distribution⁵:

$$f_X(x) = \frac{x}{\sigma^2} \exp\left(-\frac{x^2 + \nu^2}{2\sigma^2}\right) I_0\left(\frac{x\nu}{\sigma^2}\right) \quad (3.21)$$

The local-mean of scattered power is denoted as σ^2 and the dominant, non-fading component's power is identified as $\frac{1}{2}\nu^2$. The ratio of the dominant component's power to scattered power is called *Rician K-Factor*, $K = \frac{\nu^2}{2\sigma^2}$. The distribution of the attenuation β_f can be derived from the amplitude distribution as a non-central chi-square distribution with two degrees of freedom and non-centrality parameter ν^2 .

In a scenario with weak or non-existent LOS path (small or zero ν), the distribution becomes Rayleigh [Rap96]. In case of a dominant, very strong LOS path, the distribution becomes Gaussian [AS64, GW98].

Nakagami Fading

Unfortunately, usage of Equation (3.21) is mathematically cumbersome, especially due to the necessary evaluation of the Bessel function. Due to good fit to empirical results, several authors have suggested to use the Nakagami m-distribution [Nak60] for modeling fading channels [TJM⁺04, MSX06, CHS⁺07]. The amplitude envelope is parameterized by a shape parameter m that represents the fading intensity (which is dependent on the environment and the distance to the sender) and a spread parameter Ω (the average received power at a specific

⁵ $I_0(x)$ denotes the Bessel function of the first kind with zeroth order, defined as $I_0(x) = \sum_{m=0}^{\infty} \frac{1}{m!\Gamma(m+1)} \left(\frac{x}{2}\right)^{2m}$.

distance). Its distribution is given by⁶:

$$f_X(x, m, \Omega) = \frac{2m^m}{\Gamma(m)\Omega^m} x^{2m-1} \exp\left(-\frac{m}{\Omega} x^2\right) \quad (3.22)$$

The Nakagami model is a generalization of the Rayleigh model and is equivalent to Equation (3.21) ($\nu = 0$) if $m = 1$. Due to its analytical simplicity it is also widely used as an approximation for Ricean fading channels. Although both fading models behave almost equivalently near their mean value, some authors argue that Nakagami's practical utility appears questionable [Ste87] because it does not provide a good approximation in the near-zero region — i.e. a model's deep fade behavior — which is crucial for the analysis of outage probabilities: the Nakagami model yields excessively optimistic deep fade probabilities.

Influence on Connectivity

The actual influence of small-scale fading effects in vehicular networks is strongly dependent on the environment. In a highway scenarios with low vehicle density, we will mostly find LOS conditions between the transmitter and receiving nodes; a scenario in which the received signal's LOS power can be expected to be much stronger than the scattered power (large Ricean K) thus rendering the influence of small-scale fading negligible. As the vehicle density increases, the scattered power may become stronger due to reflections on other vehicles. Depending on the speed of movement of one or more nodes involved in a transmission, the attenuation of the signal due to small-scale fading changes very quickly. The intensity of the fluctuations may also be very strong, and fluctuation of several tens of dB are likely to be seen. Two paths of equal power may even interfere complete destructive, giving a zero amplitude at the receiver.

Fortunately, modern receivers can resort to advanced techniques that help mitigate these unwanted effects: OFDM modulation uses several carriers that are spaced densely, yet sufficiently far apart to experience independent fading (frequency diversity). If only some carriers are impacted, only some of the bits in the received bitstream will be defective; using an appropriate channel coding scheme may help to correct the errors. Spatial diversity, i.e., several antennas spaced at least half a wavelength apart, is widely employed: if the signal undergoes a deep fade at one antenna, it may still be strong enough at another. If the signals from the antennas are brought together effectively, for instance through Maximal Ratio Combining [Kah54, Cox83], fading can be compensated for.

From a connectivity point-of-view, the influence of small-scale fading needs further discussion. While the positive effect of large-scale fading on connectivity has been demonstrated by several authors [BH05, Mio08], recent work [ZDJ08] has shown that while small-scale fading reduces local connectivity, beneficial influences on global connectivity are revealed at the same time.

In our opinion, connectivity reflects the ability to exchange messages between involved nodes for a period of time longer than that of a potential drop-out due to small-scale fading, i.e., a period longer than the coherence time. In contrast to large-scale fading, which does directly determine connectivity, small-scale fading is rather a statistical factor that reflects the probability that despite the fact that two nodes are actually connected, the link between them is

⁶ $\Gamma(x)$ denotes the Gamma function, defined as $\Gamma(x) = (x - 1)!$, $x \in \mathbb{Z}$.

not available for a very short time. If relevant, this drop-out probability can be determined, depending on various parameters, and accounted for at design time. The simulations and analyses in this thesis, however, will not consider small-scale fading effects.

3.2.4. Vehicular Channel Models in the Literature

In the context of V2V communications, there is not yet [PKC⁺09] a widely accepted channel model. A common approach for characterizing a channel is to work out a theoretical channel model and then validate it against some appropriate measurements. Channel models are usually classified into stochastic and deterministic channel models, where deterministic channel models use ray tracing and similar techniques based on topological information about the environment in order to resolve the Multi-Path Component (MPC) and derive a precise channel characterization for a specific realization. Stochastic channel models, on the contrary, try to depict the statistics of the propagation channel in a more general sense that is not so much focussed on a particular situation. An intermittent approach is taken by geometry based channel models (as presented in [CBS09]) that do use ray tracing; however, instead of using realistic modeling the calculations are based upon randomly placed objects. This section gives an overview of current work and may be a good starting point for the reader.

A large amount of research has been dedicated to the wireless channel in cellular networks. However, looking at the specifics of a vehicular channel, especially in the V2V case it soon becomes clear that its characteristics differ significantly from those of a cellular channel. On the one hand, antennas of both sender and receiver are mounted close to the ground in V2V communications, where with cellular systems usually one of them is mounted high above. This tremendously influences the propagation path of the signals and thus the channel characteristics in terms of diffraction and reflection. On the other hand, communications between vehicles commonly use the 5.9 GHz band which behaves significantly different than the 700-2100 MHz signals used in cellular systems in terms of attenuation and diffraction. Most importantly though, sender and receiver are moving at relatively high speeds in V2V scenarios, which invalidates the assumption of stationarity of the channel characteristics that is commonplace in channel models of cellular systems. That refers not only to a changing impulse response but also to a change of its statistical properties (fading distribution, PDP and Doppler spectrum) [MTKM09]. According to [MFSW04], Doppler shift and Doppler spread characterize the time-variant behavior of the V2V channel mostly due to movement of the communicating vehicles and the adjacent vehicles.

In [MSX06], the authors describe a statistical V2V channel model that is restricted to small scale fading. It uses a tapped delay line model, each tap representing a multi path components received with a certain delay. Each tap has an on/off switching process modeled by a first order Markov chain allowing for persistence parameterization. In general, taps with longer delays have less probability of being on due to their lower energy. Tap amplitudes are modeled using the Weibull distribution where different parameters are proposed for different taps, based on some measurements. The authors differentiate between different scenarios, in some of which the Weibull parameters are “worse than Rayleigh” ($\beta < 2$), a phenomenon that is often called severe fading.

Maurer et al. present a geometry based IVC channel model in [MFSW04]. They first try to model the dynamic road traffic and the environment adjacent to the road and then try to evaluate multi-path wave propagation through means of ray tracing. The road traffic model is

based on the so called Wiedemann model and uses results from the authors previous works. As it seems very difficult to obtain real data with the necessary level of detail and the coverage, a stochastic model is utilized in order to place objects in the surroundings of the road. Different morphographic classes are defined for urban, suburban and highway scenarios that are assigned specific probabilities for different types of objects (trees, buildings, cars, bridges, traffic signs, etc.). Multi-path components are represented by rays, each of which can experience several propagation phenomena like diffraction or reflection. By calculating consecutive snapshots, a time-series of channel impulse responses can be obtained that classifies the channel for the current surrounding. The authors present measurements that validate the channel model with a standard deviation of less than 3 dB in both LOS and NLOS scenarios.

[PKC⁺09] presents some measurements of V2V propagation in suburban driving conditions using Global Positioning System (GPS) receivers. The authors on the one hand derive both a single slope and a dual slope path loss model from their results where the better dual slope model achieves deviations between 2.6 and 5.6 dB compared to the measured path loss. However, they find that received power is significantly less if no LOS propagation is possible. Fading on the other hand is modeled using a Nakagami distribution with variable parameters as already proposed in other works. While the distribution is Rician $\beta > 2$ as long as a LOS component is present, it turns out that fading can be “worse than Rayleigh” $\beta < 2$ once the LOS connection is lost intermittently at large distances between transmitter and receiver. Furthermore, the authors propose that the Doppler spread is dependent on the effective speed and the distance between transmitter and receiver. The dependance on distance is explained by the increasing number of scatterers at larger distances. Using this dependence, the authors present the speed-separation diagram that can help predict the expected Doppler spread and thus small scale fading characteristics at a certain distance.

In [MTKM09], the authors provide a survey on V2V channel models and measurements based on a variety of previous works on the subjects, some of which have already been discussed here. We recommend this paper as an introductory reading on the subject as it introduces important factors for channel characterization and includes a table that summarizes important parameters gathered from multiple measurement campaigns. Important aspects like environment characterization and antenna placements are also discussed that we omit here. One important result from the evaluated measurements is that at least path loss coefficients in V2V communication channels are rather similar to well-known cellular systems as long as a LOS connection is given. In terms of small-scale fading and Doppler spread, the results go alongside those presented in [PKC⁺09]. The authors finally conclude that the amount of comparable measurements carried out on V2V channels is too insignificant in order to allow the formulation of a channel model that resembles the real-world V2V channel and important aspects such as antenna placement and shadowing by adjacent vehicles have not yet been sufficiently explored.

3.3. Spatial Node Distribution and Mobility Models

In the previous section, we have described how channel models relate the physical positions of communicating nodes to their connectivity. If we wish to analyze the connectivity properties of a system of communicating nodes, we also need to model how the nodes are placed on the playground and how their positions change over time. Generally, one can classify these so-called *mobility models* in *microscopic* and *macroscopic* models.

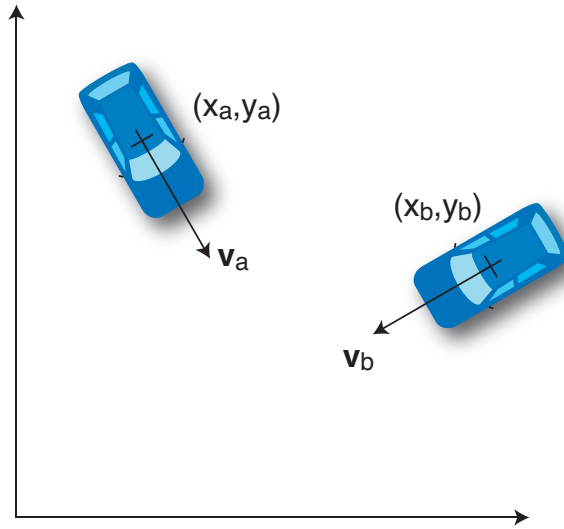


Figure 3.5.: Position $\underline{x} = (x, y)^T$ and velocity \underline{v} as descriptive states of two communicating nodes a and b.

Microscopic models describe the state, i.e., position \underline{x} , velocity \underline{v} and possibly the acceleration \underline{a} of mobile nodes (users, vehicles, etc., see Figure 3.5) as functions of time⁷ and/or previous state(s) of the node (and possibly also of other nodes, if node interaction is accounted for):

$$(\underline{x}_n, \underline{v}_n, \underline{a}_n) = f(n, \underline{x}_{n-1}, \underline{v}_{n-1}, \underline{a}_{n-1}, \dots), n \in \mathbb{N} \quad (3.23)$$

A complete description encompasses not only $f(\dots)$, but also a (presumably random) initial node state $(\underline{x}_0, \underline{v}_0, \underline{a}_0)$. Using a simulator, the spatial positions of moving nodes can then be evaluated for each time step.

Macroscopic models describe the node states through their stochastic properties, such as probability distributions and related identifying properties. If stochastic properties of a network related to mobility shall be studied, using macroscopic models is mathematically more convenient. In some cases it is possible to directly deduce a macroscopic representation from a model's microscopic description, however the effort to do so analytically may be much greater than to simulate a model and then find a stochastic approximation of the simulation results. In the course of this chapter, we will use macroscopic models for the analytical derivation of relevant network parameters.

3.3.1. The Random Direction Model

The Random Direction (RD) mobility model has first been described in [Gue87] and thoroughly studied in [Bet04]. Nodes are initially placed randomly and uniformly on the playground A . For M movement phases of negative-exponentially distributed duration t_m , the associated movement vector's (v_m) direction is chosen uniformly $\gamma \in [0 \dots 2\pi]$, with a velocity

⁷in this context, discrete time n . Of course, time-continuous notation is also possible. The wide-spread use of time-discrete simulators, however, spawns discrete notations.

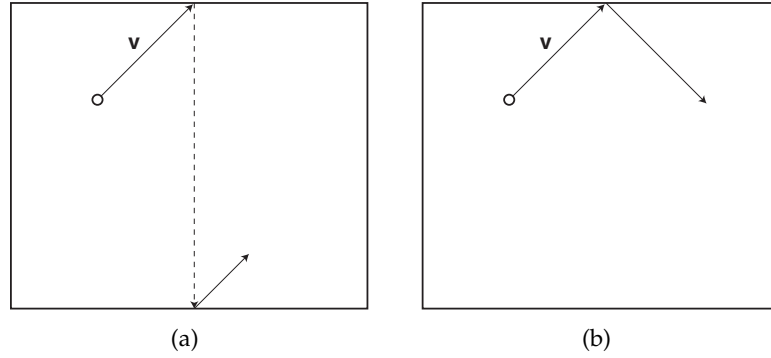


Figure 3.6.: Border strategies for random direction mobility.

of v ⁸. During a phase m , where $\sum_{i=0}^{m-1} t_i < n \leq \sum_{i=0}^m t_i$, the law of movement is:

$$\underline{\mathbf{x}}_n = \underline{\mathbf{x}}_{n-1} + \underline{\mathbf{v}}_m$$

If the playground A is bounded, the number of nodes on A decreases as time advances and nodes move out of the playground. Therefore, a border behavior needs to be carefully defined. To conserve a uniform node distribution, two schemes have proven adequate: Using the “wrap-around” approach (Figure 3.6(a)), nodes that hit the boundary of the playground are mirrored to the opposite boundary and continue their movement from the new position. The “bounce-back” solution (Figure 3.6(b)) horizontally and/or vertically mirrors the velocity vector of a respective node as that node hits the boundary. It can be shown that the resulting steady state Probability Density Functions (PDFs) for node positions $\underline{\mathbf{x}}$ and velocities $\underline{\mathbf{v}}$ are:

$$f_{\underline{\mathbf{x}}_0}(\underline{\mathbf{x}}_0) = \begin{cases} \frac{1}{|A|} & \text{if } \underline{\mathbf{x}}_0 \in A \\ 0 & \text{otherwise} \end{cases}$$

$$\forall m : f_{\underline{\mathbf{v}}_m}(\underline{\mathbf{v}}_m) = \begin{cases} \frac{1}{2\pi} & \text{if } |\underline{\mathbf{v}}_m| = v \\ 0 & \text{otherwise} \end{cases}$$

The RD mobility model is a generalization of the Random Waypoint (RWP) model (first described in [JM96] and thoroughly studied in [BHPC02]): instead of randomly choosing a direction vector at the end of a movement phase, a new random waypoint on the playground is chosen and the velocity vector is adjusted accordingly so that the waypoint is reached within in the next period of movement. Despite its popularity in ad-hoc networks research, RWP has been shown to yield a spatial node distribution that concentrates nodes in the middle of the playground. Even worse, it can be shown that — without further precautions — the average node velocity decreases over time.

3.3.2. Vehicular Mobility Models

The random direction model can be used to model the mobility of nodes that can move freely on a two-dimensional playground, for instance on an (idealized) parking lot or in open-area

⁸Note that there are modified versions of the random direction model that choose v according to a distribution function. Also, some implementations support pause times during which the velocity $v = 0$.

off-road scenarios. Usually, however, vehicles are bound to driving on one-dimensional roads and to preventing collisions with obstacles, especially other cars. This chapter is devoted to the macroscopic study of traffic flow properties. For a comprehensive survey of vehicular mobility models, we recommend [HFB09] for reading. Regarding microscopic models, cellular automata have been studied in [Wol99] and the Intelligent Driver Model was introduced in [THH00]. A joint discussion of micro- and macroscopic simulation results can be found in [HHST02].

Density, Velocity, and Flow

From a macroscopic point of view, the flow of traffic along the lanes of a street can be modeled as a flow of (interacting) particles along a one-dimensional structure. Let the *density* of vehicles (number of vehicles per lane unit) on a lane i at position x and time t be $\rho_i(x, t)$. The sum of the individual lane densities on a road with I lanes is called the *total density* $\rho_t(x, t)$, their arithmetic average is denoted as the *average density* of vehicles $\rho(x, t)$:

$$\rho_t(x, t) = \sum_i \rho_i(x, t) = I \cdot \rho(x, t) \quad (3.24)$$

$$\rho(x, t) = \frac{1}{I} \sum_i \rho_i(x, t) = \frac{1}{I} \cdot \rho_t(x, t) \quad (3.25)$$

Let us assume that vehicles on a lane i travel with a certain *velocity* $v_i(x, t)$. Let us behold a lane section of length Δx that is long enough so that it comprises enough vehicles to deduce a good measure of the density $\rho_i(x, t)$, but short enough so that the vehicles' density and velocity is approximately constant over the segment's length⁹. The number of vehicles contained in this section is thus $n = \Delta x \cdot \rho_i(x, t)$. Let all vehicles of the segment pass by an observer at a fixed position beneath the lane within the time interval $\Delta t = \Delta x / v_i(x, t)$. The *flow* of vehicles $Q_i(x, t)$, i.e., the number of vehicles that the observer sees per time interval, is then

$$Q_i(x, t) = \frac{n}{\Delta t} = \frac{\Delta x \cdot \rho_i(x, t)}{\Delta t} = \rho_i(x, t) \cdot v_i(x, t) \quad (3.26)$$

This relation is often denoted as the *flow-density relation*. The sum of individual lane flows is called the *total flow* $Q_t(x, t)$, their arithmetic average gives the *average flow* $Q(x, t)$:

$$Q_t(x, t) = \sum_i Q_i(x, t) = I \cdot Q(x, t) \quad (3.27)$$

$$Q(x, t) = \frac{1}{I} \sum_i Q_i(x, t) = \frac{1}{I} \cdot Q_t(x, t) \quad (3.28)$$

Finally, if we define the *average velocity* $v(x, t)$ as the arithmetic average of the individual lane velocities weighted with the relative densities:

$$v(x, t) = \sum_i \frac{\rho_i(x, t)}{\rho_t(x, t)} \cdot v_i(x, t) \quad (3.29)$$

we get the rule of *hydrodynamic flow*:

$$Q(x, t) = \rho(x, t) \cdot v(x, t) \quad (3.30)$$

$$Q_t(x, t) = \rho_t(x, t) \cdot v(x, t) \quad (3.31)$$

⁹Both constraints are usually met for $\Delta x = 100$ m.

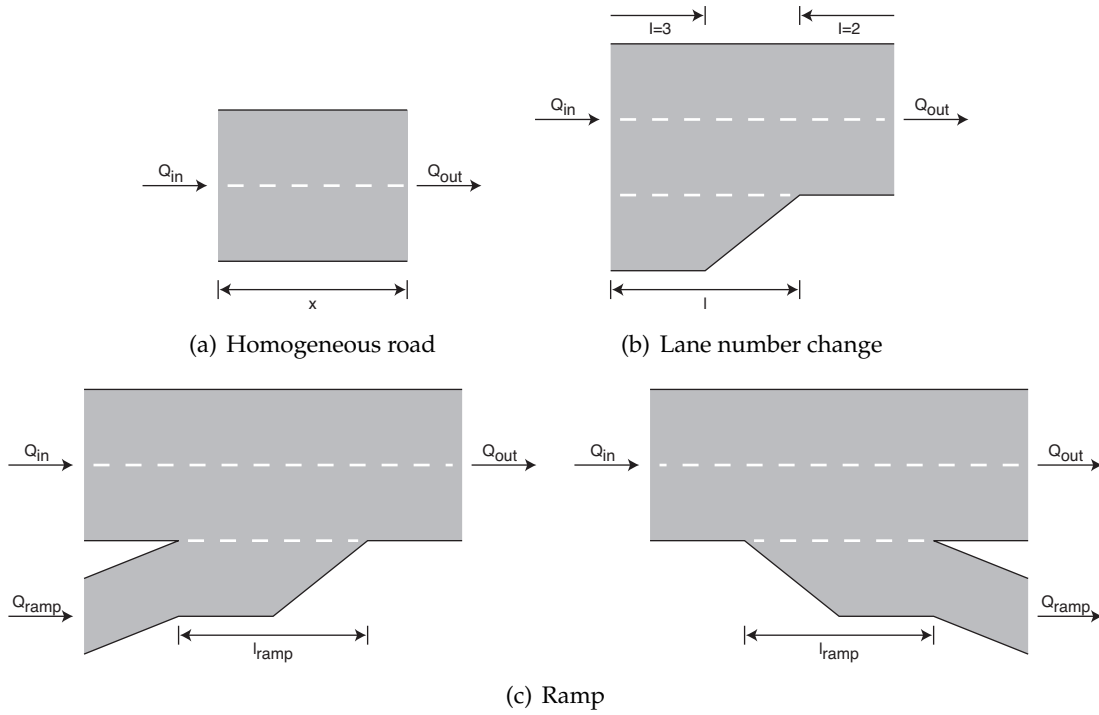


Figure 3.7.: Traffic flow continuity in fundamental road scenarios.

Continuity

Again, let us assume that all studied lane segments obey the length constraints mentioned above. Under the constraint that no vehicles are “lost” and no vehicles are “generated” on a self-contained homogenous lane segment, it is evident that the density of vehicles on that segment (Figure 3.7(a)) is constant over time if the flow of vehicles Q_{in} into that segment is equal to the flow Q_{out} out of the segment. If the inflow is greater than the outflow, the density increases, otherwise the density decreases. Consequently and in analogy to the continuity equation known from fluid dynamics, we can state that the density of vehicles increases over time if the flow decreases over the segment’s length:¹⁰

$$\frac{\partial \rho}{\partial t} + \frac{\partial Q}{\partial x} = 0 \quad (3.32)$$

Let us assume that the number of lanes I changes on a road segment (Figure 3.7(b)), for instance due to constructional reasons or because of the presence of an obstacle on a lane. This change is not a discrete incident, but rather a continuous process between two positions x_0 and $x_1 = x_0 + l$ along the road: Usually, a neck is announced by an appropriate road sign (typically $l = 200 \text{ m} \dots 1000 \text{ m}$). After that sign, drivers start merging from the closing lane to the remaining lane(s). After a broadening, the new lane is used very quickly, typically within $l = \text{some } 100 \text{ m}$.

Let us define the number of lanes as a continuous function over the position along the road, $I(x)$. Consequently, a value of $I(x) = 1.5$ indicates that, in case of a neck (i.e., a $2 \rightarrow 1$ lane

¹⁰In the following, we shall neglect the spatial and temporal dependency terms (x,t) for the sake of readability.

transition), half of the vehicles have changed from the closing to the remaining lane at x . In case of a broadening (i.e., a $1 \rightarrow 2$ lane transition), half of the vehicles have changed to the new lane at x .

Equation (3.32) is valid both for the average as well as for the total density and flow numbers. With continuous $I(x)$, we can rewrite Equation (3.32) for $\rho_t(x, t) = I(x)\rho(x, t)$ (Equation (3.24)) and $Q_t(x, t) = I(x)Q(x, t)$ (Equation (3.27)):

$$\begin{aligned} \frac{\partial(I \cdot \rho)}{\partial t} + \frac{\partial(I \cdot Q)}{\partial x} &= 0 \\ I \frac{\partial \rho}{\partial t} + Q \frac{\partial I}{\partial t} + I \frac{\partial Q}{\partial t} &= 0 \\ \frac{\partial \rho}{\partial t} + \frac{\partial Q}{\partial x} &= -\frac{Q}{I} \frac{\partial I}{\partial x} \end{aligned} \quad (3.33)$$

The right-hand side term in Equation (3.33) corresponds to a “source” term that represents the flow either from the closing lane to the remaining lanes or from the lanes available as yet to the new lane, respectively. Consequently, if $I(x)$ increases (broadening), the source term is negative and the density decreases and vice versa.

Next, we examine locations where roads join and traffic flows merge or split (Figure 3.7(c)). Under the assumption that the inflow ($Q_{ramp} > 0$) respectively the outflow ($Q_{ramp} < 0$) is distributed equally along the length of the ramp l , there is an additional flow gradient $\phi_{ramp}(x, t)$ in the area of the ramp and Equation (3.32) becomes:

$$\begin{aligned} \phi_{ramp}(x, t) &= \begin{cases} \frac{Q_{ramp}(t)}{I \cdot l} & \text{if } x \text{ on ramp} \\ 0 & \text{otherwise} \end{cases} \\ \frac{\partial \rho}{\partial t} + \frac{\partial Q}{\partial x} &= \phi_{ramp}(x, t) \end{aligned} \quad (3.34)$$

Finally, putting Equations (3.32), (3.33), and (3.34) together and letting $Q = \rho V$ (Equation (3.30)), we get:

$$\frac{\partial \rho}{\partial t} + \frac{\partial Q}{\partial x} = -\frac{Q}{I} \frac{\partial I}{\partial x} + \phi_{ramp}(x, t) \quad (3.35)$$

$$\frac{\partial \rho}{\partial t} + \frac{\partial(\rho v)}{\partial x} = -\frac{\rho v}{I} \frac{\partial I}{\partial x} + \phi_{ramp}(x, t) \quad (3.36)$$

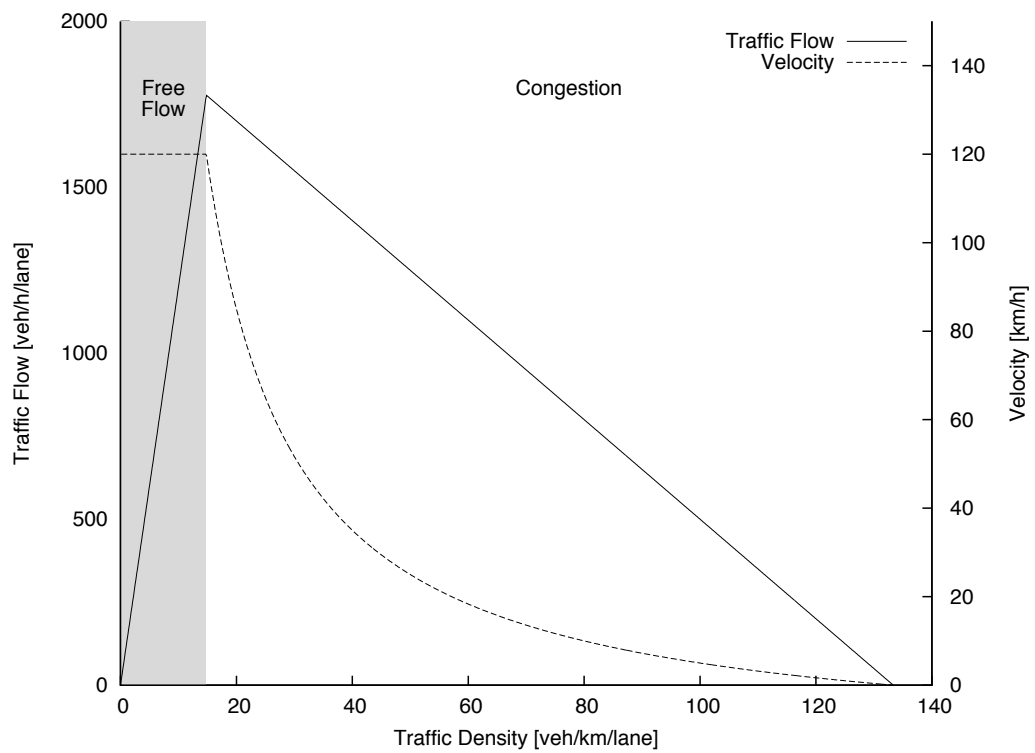
The Fundamental Diagram

Equations (3.35) and (3.36) are partial differential equations in two variables: the density ρ and either flow Q or velocity v . To complete the formal description, an additional equation is required that describes the relation between density and flow or velocity. This gap was closed by Lighthill and Williams, and Richards, respectively, in their 1955/56 milestone papers [LW55a, LW55b, Ric56] through complementing the continuity equation with the assumption that there is a certain — density-dependant — equilibrium velocity V_e (and resulting equilibrium flow Q_e) that solve the continuity equation in case of a homogenous and stationary traffic¹¹:

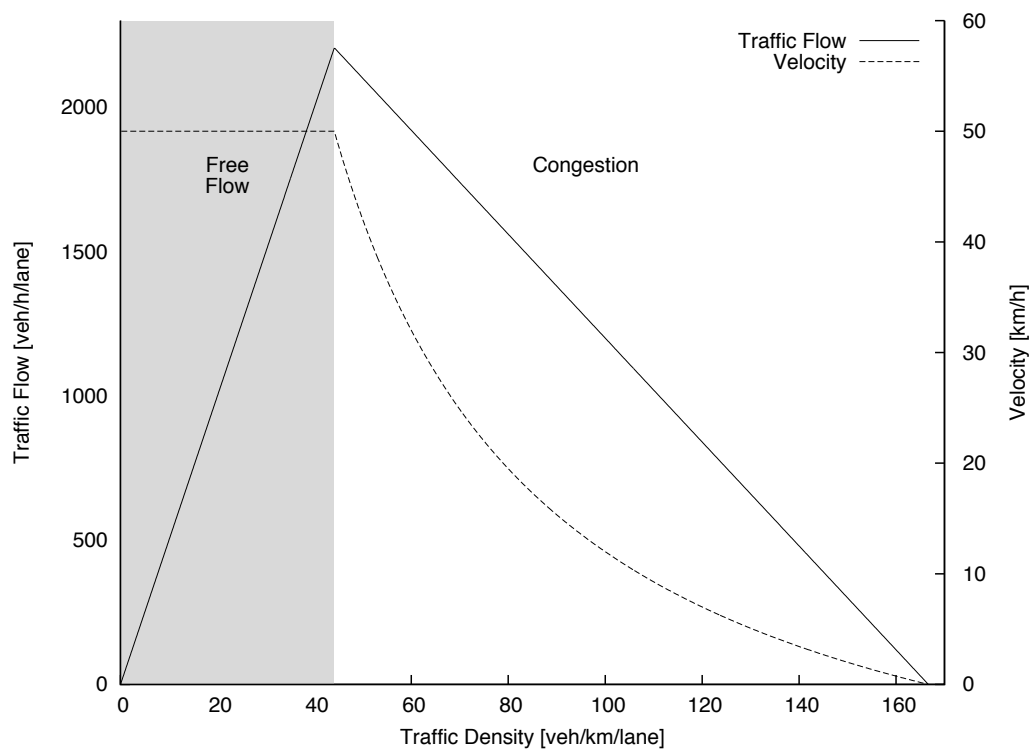
$$Q_e(\rho(x, t)) = \rho(x, t)V_e(\rho(x, t)) \quad (3.37)$$

¹¹Homogenous and stationary traffic means that vehicles travel with the same velocity and distance. Obviously, this is an idealization that can not be observed in reality.

3.3. Spatial Node Distribution and Mobility Models



(a) Highway



(b) City

Figure 3.8.: Fundamental diagrams of (a) highway and (b) city traffic flow.

Parameter		Highway	Urban
v_0	average free velocity	120 km/h	50 km/h
T	average time headway	1.8 s	1.2 s
h_0	minimum vehicle distance (jam distance)	3 m	1.5 m
l	vehicle length	4.5 m	4.5 m
$l_e = h_0 + l$	effective vehicle length	7.5 m	6 m
$\rho_j = 1/l_e$	density inside traffic jams	133.33 km ⁻¹	166.67 km ⁻¹
ρ_c	critical density	14.81 km ⁻¹	44.12 km ⁻¹
C	lane capacity	1967 h ⁻¹	2205 h ⁻¹

Table 3.1.: Parameters of the section-based traffic model.

This function is also called the *fundamental diagram*. Re-writing the basic continuity equation (3.32), we get the formula for the Lighthill-Williams-Richards (LWR) model:

$$\frac{\partial \rho}{\partial t} + \frac{dQ_e(\rho)}{d\rho} \frac{\partial \rho}{\partial x} = 0 \quad (3.38)$$

Note however that as $Q_e(\rho)$ is not a function specified by the LWR model, Equation (3.38) rather defines a *class of models* than a model of its own. As the equilibrium velocity can not be determined from measurements, the fundamental diagram is usually expressed as a fit function for empirical data and, of course, the large variety of data and interpretations has spawned a great number of models. A comprehensive discussion of various models can be found in [Hel01b] and [Ker04]. An example of fluid-dynamic model can be found in [Hel95], gas-kinetic models are described in [Hel96, THH99].

A relatively simple example of such a model is the section-based traffic model, which has been described in [Hel03] and a possible realization is shown in Figure 3.8. The two regions (free flow and congestion) of the fundamental diagram are defined by:

$$Q_e(\rho) = \begin{cases} v_0 \rho & \text{if } \rho \leq \rho_c \\ \frac{1}{T}(1 - \rho l_e) & \text{if } \rho_c < \rho \leq \rho_j \end{cases} \quad (3.39)$$

The critical density ρ_c marking the transition from the free-flow region to the congestion region is defined as the point where the two slopes intersect. This point also represents the maximum lane capacity C .

$$\rho_c = \frac{1}{v_0 T + l_e} \quad (3.40)$$

$$C = \frac{1}{T + \frac{l_e}{v_0}} \quad (3.41)$$

The average velocity resulting from Equations (3.37) and (3.39) (dashed line in Figure 3.8) is defined as:

$$V_e(\rho(x, t)) = \frac{Q_e(\rho(x, t))}{\rho(x, t)} = \begin{cases} v_0 & \text{if } \rho \leq \rho_c \\ \frac{1}{T} \left(\frac{1}{\rho} - l_e \right) & \text{if } \rho_c < \rho \leq \rho_j \end{cases} \quad (3.42)$$

The scenarios relevant in the remainder of this chapter (“highway” or “urban” scenario) and their respective parameters can be retrieved from Table 3.1.

3.4. Node Degree

In the previous sections, we have shown how connectivity between a sender and receivers is defined through the spatial distribution of network nodes in conjunction with a channel model that represents the influence of one or more propagation effects. In this section, we will evaluate the relation between traffic density ρ and node degree d . On the one hand, node degree represents the number of potential communication partners that a vehicle traveling on a road has at a certain time instant; on the other hand, the wireless medium has to be shared among these nodes. We will discuss the trade-off between these sometimes conflictive properties after introducing the underlying theory.

For the analysis of a node's degree, we need to determine the number of nodes that are within that node's transmission range. Knowing the PDF $f_{\underline{\mathbf{x}}}(\underline{\mathbf{x}})$ according to which nodes are placed on the playground (the considered area), the probability to find another node within the transmission range of a node placed at $\underline{\mathbf{x}}$ can be computed through integration of $f_{\underline{\mathbf{x}}}(\underline{\mathbf{x}}')$ over the covered area as defined by the channel model¹² (Equation (3.4)):

$$p_0(\underline{\mathbf{x}}) = \int f_{\underline{\mathbf{x}}}(\underline{\mathbf{x}}') \cdot \chi(\underline{\mathbf{x}}, \underline{\mathbf{x}}') dx' \quad (3.43)$$

If the number of nodes n on the playground is known, we can determine the node degree d as the probability that d out of the remaining $(n - 1)$ nodes are located within the area covered by the considered node at $\underline{\mathbf{x}}$:

$$p(d|\underline{\mathbf{x}}) = \binom{n-1}{d} p_0(\underline{\mathbf{x}})^d (1 - p_0(\underline{\mathbf{x}}))^{n-d-1} \quad (3.44)$$

By integration of $p(d|\underline{\mathbf{x}})$, weighted with the location probability, over all possible node locations, the global statistics of d can be determined:

$$p(d) = \int p(d|\underline{\mathbf{x}}) \cdot f_{\underline{\mathbf{x}}}(\underline{\mathbf{x}}) dx \quad (3.45)$$

The method has been successfully applied to various ad-hoc network configurations and is studied in-depth in [Bet04]. However, it is not applicable for vehicular networks due to some fundamental differences regarding some particular properties:

- The number of nodes placed on the playground is not necessarily known. Instead, the density of vehicles ρ and the corresponding average vehicle distance $D = 1/\rho$ is established.
- The positions of vehicles are not always statistically independent: as mentioned above, vehicles have a limited degree of freedom when it comes to placement. In most cases, we find them located on a lane. Their position thereon shall be identified by the shape of the lane and the distance (along the shape) from the lane's origin.

3.4.1. Geometry

Let the longitudinal (one-dimensional) positions of vehicles s_i on a lane be defined by the variates h_i of a random variable H that models the inter-vehicle distance headway (the "headway

¹²The channel model (i.e., the condition of connectedness) is a class of models; the actual realization depends on the chosen channel model and its respective parameters.

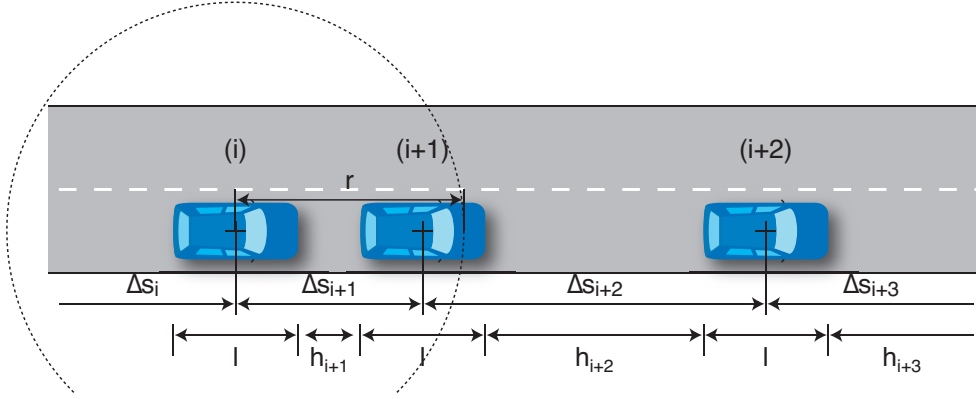


Figure 3.9.: Reference setup for node degree analysis.

process"). Assuming that l is equal for all vehicles, we can compute the total distance Δs_{i+1} between identical points (for instance, the center of gravity) of two vehicles (i) and ($i+1$) (see Figure 3.9):

$$s_{i+1} = s_i + l + h_{i+1} \quad (3.46)$$

$$\Delta s_{i+1} = s_{i+1} - s_i = l + h_{i+1} \quad (3.47)$$

There exists a function $\Phi(\cdot)$ that projects a longitudinal position s_i of a vehicle i on a lane onto a point \mathbf{x}_i in the planar space with the appropriate number of dimensions n as required by the chosen channel model (in most cases, $n \in \{2, 3\}$). Let the lane's shape be modeled as a spline defined by the knot vector \mathbf{k} (see Appendix A):

$$\Phi: \mathbb{R} \rightarrow \mathbb{R}^n \quad (3.48)$$

$$s_i \mapsto \text{proj}(\mathbf{k}, s_i) \quad (3.49)$$

Vehicles Ahead

Given the projection function $\Phi(s_i)$, we can now apply the chosen channel model to compute the probability that two subsequent vehicles at given s_i and s_{i+1} are connected. Let us assume that the additional constraint $s_i < s_{i+1}$ holds true, i.e., for now we only consider vehicles in one direction of the lane. If the PDF of the inter-vehicle distance headway, $f_H(h)$ is known, we can compute the probability that there is at least one vehicle ahead of a vehicle at s_i that is within the coverage area:

$$P(D^+ \geq 1) = \int f_H(h) \cdot \chi(\Phi(s_i), \Phi(s_i + l + h)) dh \quad (3.50)$$

To determine the probability that exactly d nodes are within the coverage area, we need to establish the probabilities of the inter-vehicle distance headway of vehicles spaced n vehicles apart. The distance between n -subsequent vehicles Δs_{i+n} , is the sum of the vehicle lengths and the sum of n independent random variates of H :

$$\Delta s_{i+n} = s_{i+n} - s_i = nl + \sum_{j=1}^n h_{i+j} \quad (3.51)$$

The PDF resulting from the addition of random variables is the convolution¹³ of the individual PDFs. In this case, the PDF of the inter-vehicle distance headway between n -subsequent vehicles corresponds to the recursive convolution of $f_H(h)$:

$$f_H^{(1)}(h) = f_H(h) \quad (3.52)$$

$$f_H^{(n)}(h) = f_H^{(n-1)}(h) * f_H(h) \quad (3.53)$$

Combining the Equations (3.53) and (3.50), we can determine the probability that there are at least d , $d \in \mathbb{N}$ vehicles ahead of a vehicle at s_i that are within the coverage area:

$$P(D^+ \geq d) = \int f_H^{(d)}(h) \cdot \chi(\Phi(s_i), \Phi(s_i + dl + h)) dh \quad (3.54)$$

Consequently, the Probability Mass Function (PMF) of the degree distribution $f_{D^+}(d)$, its Cumulated Density Function (CDF) $F_{D^+}(d)$ and the expected node degree $E\{D^+\}$ are then

$$\begin{aligned} f_{D^+}[d] &= P(D^+ = d) = P(D^+ \geq d) - P(D^+ > d) \\ &= P(D^+ \geq d) - P(D^+ \geq d + 1) \end{aligned} \quad (3.55)$$

$$\begin{aligned} F_{D^+}[d] &= P(D^+ \leq d) = 1 - P(D^+ > d) \\ &= 1 - P(D^+ \geq d + 1) \end{aligned} \quad (3.56)$$

$$E\{D^+\} = \sum_{d=0}^{\infty} d \cdot f_{D^+}[d] \quad (3.57)$$

Multiple Lanes

In the derivation above, we have considered only subsequent vehicles ahead of a vehicle i : $s_i < s_{i+1}$ and retrieved the PMF of the random process D^+ . The degree distribution regarding vehicles in the behind direction D^- is computed likewise. The individual degree distributions are independent; to retrieve the total degree distribution, the discrete convolution¹⁴ of the two (ahead and behind) distributions needs to be calculated:

$$D = D^- + D^+ \quad (3.58)$$

$$f_D[d] = \sum_{i=0}^d f_{D^+}[i] \cdot f_{D^-}[d - i] \quad (3.59)$$

The expected node degree $E\{D\}$ is then the sum of the two individual expected node degrees:

$$E\{D\} = E\{D^+\} + E\{D^-\} \quad (3.60)$$

If more than one lane shall be studied, under the assumption that the distance between adjacent parallel lanes is small compared to the radius of the coverage area, determination of the composite expected node degree can be simplified by adding up the individual expected node degrees. For other geometries, the effective range s_r must be used instead of the $2r$ term (see next section).

¹³The continuous convolution is defined as $(f * g)(t) = \int_{-\infty}^{\infty} f(\tau)g(t - \tau)d\tau$.

¹⁴The discrete convolution is defined as $(f * g)[n] = \sum_{m=-\infty}^{\infty} f[m]g[n - m]$. Because $f_D[d]$ is only defined for $d \in \mathbb{N}^{0+}$, summation borders are $i = 0 \dots d$.

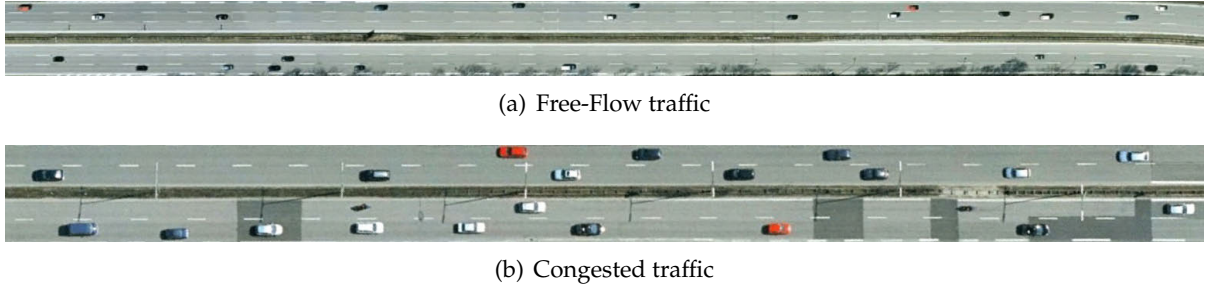


Figure 3.10.: Typical highway traffic patterns.

3.4.2. Distance Headways

As a result of intense research, there are a lot of studies based on empirical data, attempting to model (spatial and temporal) headways. Urban headways are studied in [MLD00] and it is demonstrated how headways may be influenced by external factors, such as (in this case) traffic signs. A lot of attention has been devoted to highway traffic and some specific properties: [NTH03] shows that time gap statistics on highways is related to the traffic density ρ and that higher traffic densities lead to longer time headways; [BWM09] shows how time headways increase with decreasing velocities. Based on highway traffic data, [MK09] argues that the vehicle arrival process under heavy traffic conditions reveals self-similar characteristics and that time headways follow a heavy-tailed distribution. In [TKH07], an approach is constituted that models headways as a function of the local velocity variance (a measure of the inhomogeneity of traffic flows). A number different headway distributions and their respective adequacy under varying traffic conditions is studied in [YLZ⁺09].

Virtually the first theoretical research paper on headway distributions was published in 1975 by Cowan [Cow75]. He developed a set of models of increasing generality and first introduced the notion that headways are a result of two random process: a “free” component and a “tracking” component, a suggestion that was later seized by Krauss et al [KWG96] who suggested and demonstrated different gap distributions for free and congested traffic through analysis and simulation. The modeling approach used in this section has been inspired by the work of Abul-Magd [AM07], who employed superstatistics [BC03] (i.e., the statistics of statistics) to blend two headway distributions, according to the actual traffic state as determined by the density.

Free-Flow Traffic

It has been demonstrated [Bre63, The64] that, at some reasonably large distance from the entry point, cars on a road will be spatially distributed according to a poisson process with a certain intensity (the traffic density ρ). Consequently, the headway process H under free-flow conditions has an exponential distribution:

$$f_{H,f}(h) = \rho \exp(-\rho h) \quad (3.61)$$

$$E\{H_f\} = \frac{1}{\rho} \quad (3.62)$$

Among other assumptions used for the approach, two important conditions demand that:

- Vehicles do not aggregate. This condition only holds true if vehicle may move freely and overtake other vehicles if needed. Clearly, this is only possible if the density of traffic is very low and/or enough lanes are available for overtaking.¹⁵
- The velocities of vehicles are independent of each other and identically distributed. Again, this is only true if vehicles are free to move at their desired speed, without the need to accelerate or decelerate to avoid collisions.

These conditions are usually met if traffic is in the free-flow region of the fundamental diagram (see Equation (3.37), Figure 3.8), where $\rho \leq \rho_c$. A typical traffic situation is shown in Figure 3.10(a).

Through Laplace transformation, we obtain the n-fold convolution form; in this case, the Erlang distribution:

$$\begin{aligned}
 f_{H,f}^{(n)}(h) &= \mathcal{L}^{-1} \{ \mathcal{L} \{ f_H(h) \}^n \} \\
 &= \mathcal{L}^{-1} \left\{ \left(\frac{\rho}{s + \rho} \right)^n \right\} \\
 &= \frac{\rho^n h^{n-1}}{\Gamma(n)} \exp(-\rho h)
 \end{aligned} \tag{3.63}$$

$$\mathbb{E}\{H_f^n\} = \frac{n}{\rho} \tag{3.64}$$

Congested Traffic

When the traffic density grows beyond the critical density $\rho_c \leq \rho$, the conditions postulated above do not hold true any more; overtaking cannot take place as required any more due to the lack of space. As a consequence, vehicles start “synchronizing”, i.e., drivers will adapt their speed to the vehicle ahead. A typical situation is depicted in Figure 3.10(b): the effect of synchronization is clearly visible in the lower left region. This adaptation reduces the average speed of the involved vehicles and effectively leads to a decreasing traffic flow on the road; the effect is illustrated by the congested region of the fundamental diagram Figure 3.8.

Without going into the details of traffic flow theory, it is clear that the critical density ρ_c and the lane capacity C are not fixed numbers; instead, they are time-variant [BRG05] and depend on a number of parameters such as the current weather situation (obviously, the capacity decreases if weather conditions are bad), traffic control activities, the shape (bending, steepness) of the lanes, etc. Consequently, the state transition from free flow to congestion should be regarded as a continuous process that is modulated by the traffic density. This approach has led to the so-called three-phase traffic theory, developed by Kerner [Ker04, KKH07], which has subsequently spawned a lot of discussion [SH09, TKH10].

In their remarkable papers [KS00, Kv03], Krbálek and Šeba, knowing that the spatial distribution of tightly interacting particles in one-dimensional systems can be well described using random-matrix theory, applied this finding to bus arrival time measurements. Usually, these

¹⁵Interestingly, an Indian study [TAK03] revealed that an exponential distribution well approximates headways of urban mixed-traffic that is dominated by small vehicles (such as motor scooters etc.). It is common experience that these vehicles — given experienced, yet sometimes indiscriminate drivers — are usually not bounded by other vehicles in terms of overtaking or speed limitation. It is therefore not surprising that, contrary to the high traffic density, the domination of small vehicles yields a poisson distribution process.

times can be modeled as a poisson process; the data used in their case studies, however, was obtained in a special context: due to certain influences, bus drivers were forced to optimize the inter-arrival times of their buses:

- Autonomously: the drivers know only the temporal distance to the previous bus. Their means of adjustment are acceleration or deceleration.
- As long a time gap as possible: The random arrival process of passengers at the bus stop (which, technically, controls the systems) leads to a growing number of passengers. In order to maximize the income, the bus driver will slow down as much as possible and thus increase the time gap to the preceding bus to take as many passengers as possible.
- As short a time gap as necessary: If the driver slows down too much, he expects to be overtaken by the following bus.

This constitutes a self-organizing system that autonomously adapts the inter-arrival times of the buses to the current demand (the arrival rate of passengers). The resulting inter-vehicle distribution is well modeled using the Gaussian Unitary Ensemble (GUE) of random-matrix theory. The conceptual parallels to dense traffic are obvious: a driver sees the distance to the vehicle he is following, and he will try to adjust that distance to a safe value (as long as possible) while trying to keep up with the preceding vehicle (as short as necessary). Subsequent work has shown that GUE is well suited for modeling inter-vehicle headways in dense traffic (see [AM07] for a summary):

$$f_{H,c}(h) = \frac{32\rho^3}{\pi^2} h^2 \exp\left(-\frac{4\rho^2}{\pi} h^2\right) \quad (3.65)$$

$$E\{H_c\} = \frac{1}{\rho} \quad (3.66)$$

Following the concept of headway components [KWG96], [AM07] argues that using a poissonian process for the free-flow region and the GUE process for the congested region and blending the resulting PDFs using a density-dependent parameter α very well fits the headway processes actually measured on roads. Consequently, we shall regard the actual headway process on an arbitrary road as the weighted combination of the two processes introduced in this section:

$$f_H(h) = \alpha f_{H,f}(h) + (1 - \alpha) f_{H,c}(h) \quad (3.67)$$

The determination of the parameter α is not straightforward as it depends on the actual traffic situation and external parameters (as mentioned above) and thus subject to fitting to actual measured data. It is therefore not possible to directly study the headway distribution in the transition phase. However, studying the two cases $\alpha = \{0, 1\}$ allows us to identify two conditions that represent the two extreme network realizations: The realization of an actual network will be somewhere in between.

3.4.3. Discussion

For the sake of simplicity, let us first model the considered road segment as a straight horizontal line so that $\underline{\Phi}(t) = [t, 0]^T$ (an idealized highway segment). As channel model, we use

the log-distance path loss model (Equation (3.11)) with a maximum coverage area of radius r . Equation (3.54) can then be simplified:

$$P(D^+ \geq d) = \int_0^r f_H^{(d)}(h)dh \quad (3.68)$$

Where appropriate, we shall assume that the traffic density ρ is in the region of free flow, $\rho \leq \rho_c$, so we can use Equation (3.63) and the PMF of the degree distribution (cf. Equation (3.55)) follows the Poisson distribution:

$$f_D[d] = \frac{(2\rho r)^d}{d!} \exp(-2\rho r) \quad (3.69)$$

$$E\{D\} = 2\rho r \quad (3.70)$$

All plots in this discussions show node degrees computed for one lane; the composite node degrees for multi-lane scenarios can be computed by convolution as described above. Where applicable, the composite expected node degree can be determined by multiplication. Note that the expected node degree, $E\{D\}$ depends on the expected headway $E\{h\} = 1/\rho$ — the scaling condition — and is thus independent of the chosen headway distribution.

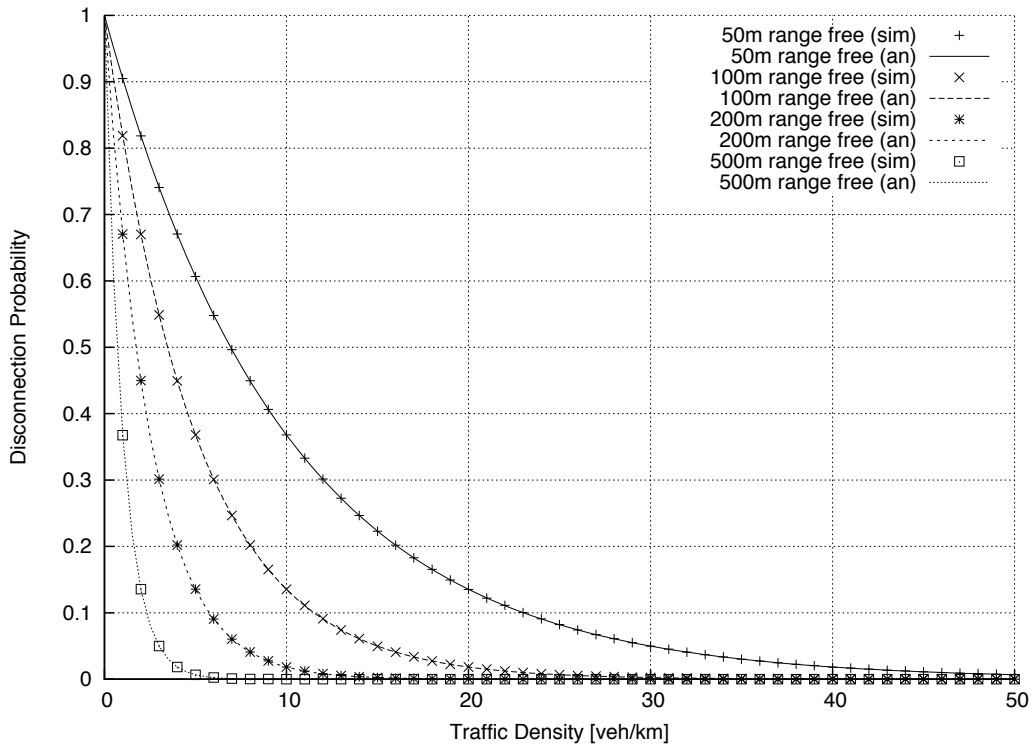
Disconnection and Leafnode Probability

Figures 3.11 and 3.12 depict the probabilities that a node is 0- or 1-connected, depending on the radio range. The choice of an appropriate radio technology and subsequent dimensioning of transmission power is sometimes the only degree of freedom available at the design time of a communication system and, consequently, requires special care. Two important properties that may influence this choice are:

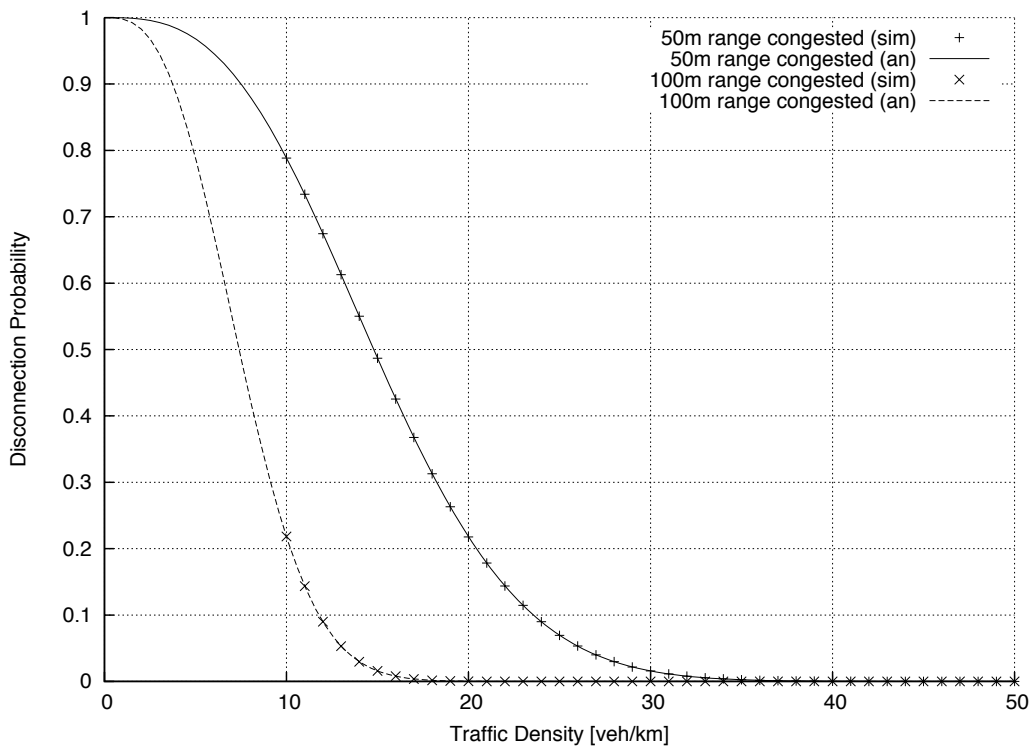
- A node degree of 0 implies that a node is isolated or disconnected, i.e. there is no communication partner available in the surrounding. Thus, it represents the fraction of nodes that will not be able to perform any cooperative tasks or make use of cooperative perception. Figures 3.11(a) and 3.11(b) show the percentage of isolated nodes over traffic density. Although isolation may not be a problem in typical city scenarios, nodes *will* experience isolation on highways with free-flow traffic conditions, i.e., with traffic densities of typically $\rho \leq 16 \text{ km}^{-1}$ (compare Table 3.1).

It is clearly desirable to reduce the probability of isolation as much as possible. As the shown figures imply, the easiest way to do so is to increase the vehicles' radio ranges. This may be done by using higher transmission powers or modulation schemes that require lower Signal-to-Noise-Ratios (SNRs). A major drawback of this, however, is the fact that on the other end of the traffic density scale, i.e., in congested situations where the density is very high, the average node degree resulting from the increased radio range takes very high values. As a result, the per-node data rate goes down because the wireless medium has to be shared between an increasing number of nodes.

If available, power control techniques, should be used to ensure minimum connectivity in sparsely populated scenarios and to limit the radio range yielding a sensible node degree in dense scenarios. Depending on the projected applications, chances are high that it is not even sensible to communicate with vehicles as far as 500 m away in a dense urban setting. An algorithm for deployment in vehicular scenarios is presented in [TMMSH09], along with a thorough survey of other power control techniques.



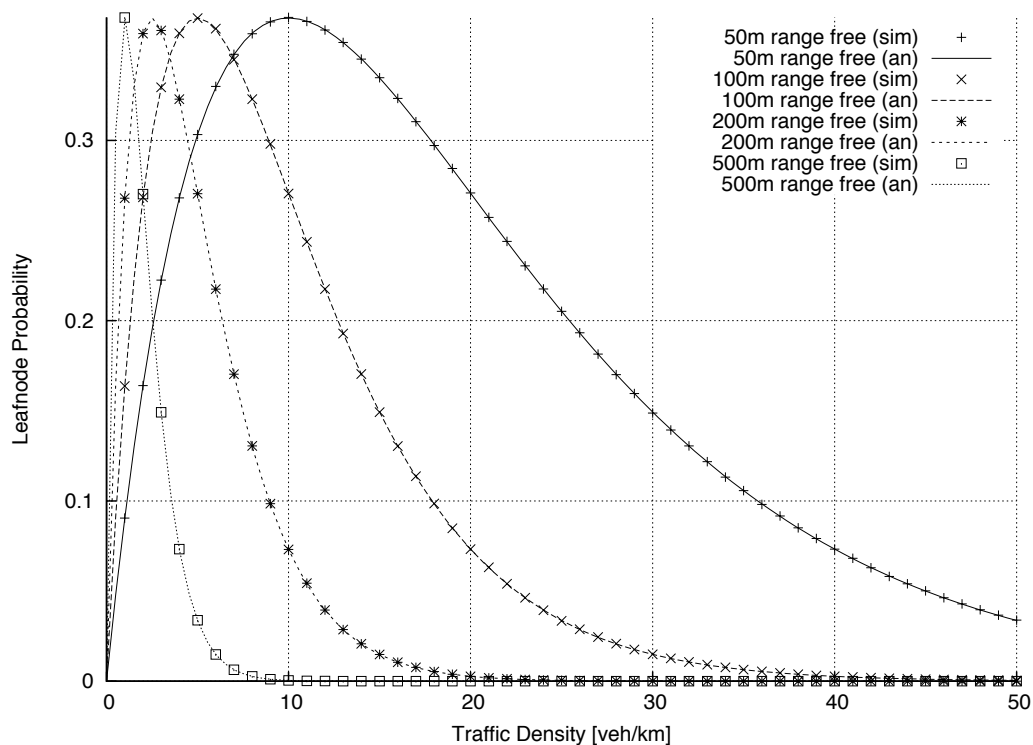
(a) Disconnection probabilities in free-flow traffic



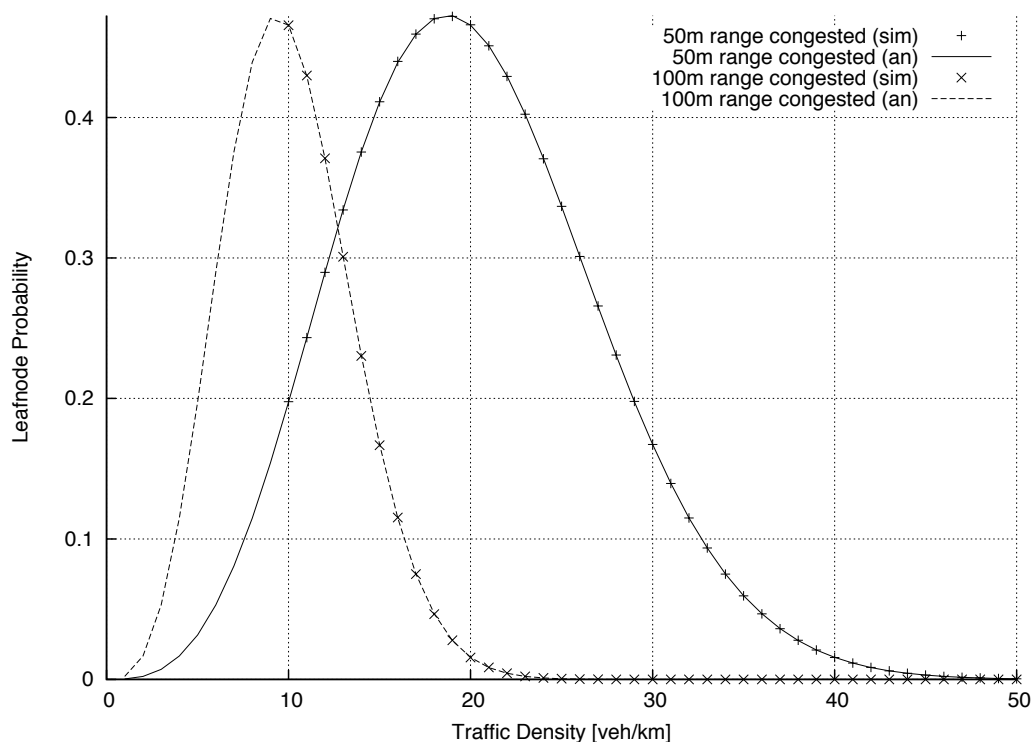
(b) Disconnection probabilities in congested traffic

Figure 3.11.: Disconnection probabilities over traffic density.

3.4. Node Degree



(a) Leafnode probabilities in free-flow traffic



(b) Leafnode probabilities in congested traffic

Figure 3.12.: Leafnode probabilities over traffic density.

- The probability of a node degree of 1 is the probability that a node is a leafnode; the probabilities over traffic density are shown in Figures 3.12(a) and 3.12(b).

From a networking perspective it is an undesired property of a leafnode that, although the node itself is connected, it does not contribute to the connectedness of the network. This is problematic especially in very sparse highway scenarios where the expected node degree is around 2: the vehicles form a string-like network, along which information can propagate. A 1-connected node would break the string and effectively stop the propagation of messages. If applications are desired that rely on messages to be transported over large distances, choosing a large enough radio range and thus avoiding node degree of 1 may be sensible. As with node isolation, this comes at the cost of significantly increased degrees in congested scenarios and the statements made above apply. Another potential strategy in this scenario may be to use a store-and-forward scheme (see [KTH10] for a survey and a proposal), where oncoming vehicles are used as information storage. They carry the information to be disseminated, potentially use their communication partners and ultimately transport the information towards the designated area.

Example

An isolation probability of less than 20% is desired at a traffic density of 10 km^{-1} . A radio range of 100 m is sufficient to fulfill the requirement. If no power control techniques are available, at an urban 2 + 2 lane junction, given a (rather low) traffic density of 50 km^{-1} , the expected node degree will be 20. Assuming an ideal MAC scheme, a typical 6 Mbit/s channel, shared equally among the 20 contending vehicles, yields a maximum data rate of 300 kbit/s per node.

The probability of leafnodes, however, is $\approx 27\%$. If the application asks for a leafnode probability of less than 20% at a traffic density of 10 km^{-1} , a radio range of $\approx 130 \text{ m}$ is sufficient. At the same intersection, the expected node degree will then be 26, and the maximum data rate around 230 kbit/s.

Node Degree and Velocity

Knowing that density ρ and average velocity v are related via the fundamental diagram (Equation (3.37)), we can relate velocity and expected degree $E\{d\}$, as shown in Figure 3.13. The curves are characterized by two distinct regions (that stem from the fundamental diagram):

- Free-flow traffic (constant velocity $v = v_0$, sub-critical densities $\rho \leq \rho_c$): the expected node degree $E\{d\}$ increases linearly with increasing traffic density. Depending on the chosen radio range r , the expected node degree varies in $E\{d\} = [0 \dots 2\rho_c r]$. Due to the fact that the critical density is higher in urban scenarios, the expected limiting node degree is higher than in highway scenarios.
- Congested traffic (adapted velocities $v < v_0$, hyper-critical densities $\rho_c \leq \rho$): further increase in density consequently results in even higher expected node degrees. However, this further increase correlates with decreasing velocities.

We can conclude that the limiting conditions are extremely low traffic densities (and correspondingly high probabilities of node isolation and leafnodes) on the one hand and extremely low data rates due to resource sharing among too many nodes on the other hand. Apart from the necessity to use power control techniques (which has, for instance, the drawback of a reduced one-hop interaction radius), lately the discussion has shifted towards building adaptive applications that are able to adjust their channel usage according to the channel state

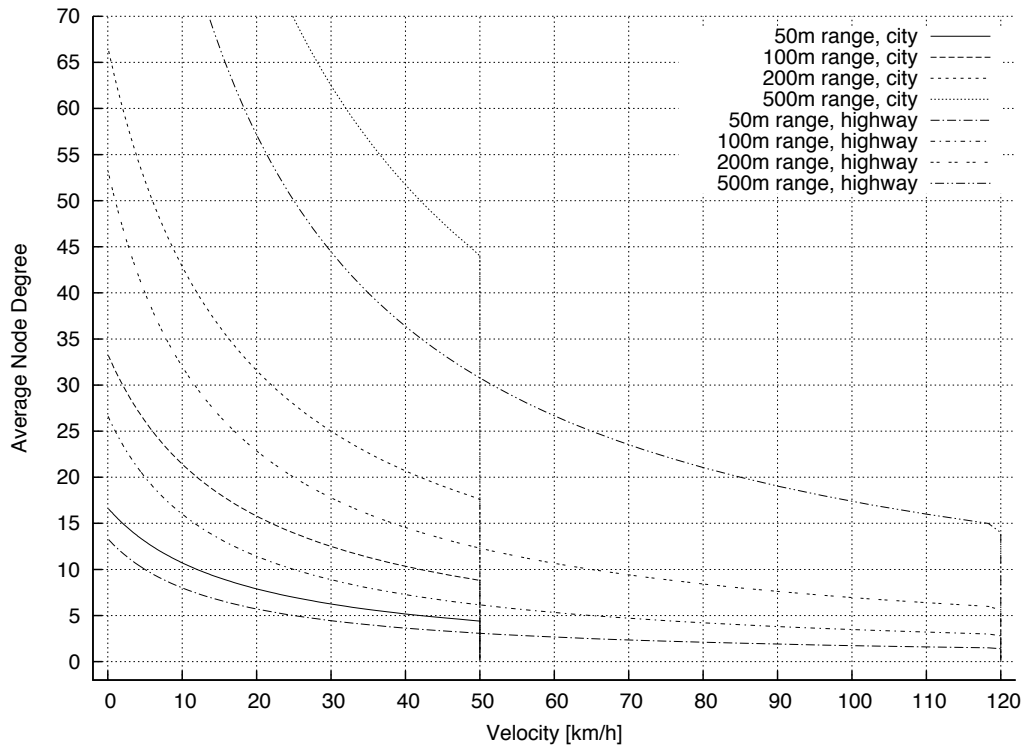


Figure 3.13.: Average node degree over velocity.

and environmental influences. This is an interesting issue in the vehicular context, since the entropy of sensor data may be a function of the temporal and/or spatial variance of the perceived environmental. Since the velocity of movement is related to that variance, there exists a class of applications that could actually make use of this relation and reduce the amount of data rate necessary for their functioning according to the speed at which vehicles are moving and, consequently, the implications of increasing node degrees in the congested region may be compensated for, at least up to a certain amount (see Chapter 4).

Equipment Ratio

The probabilities considered so far assumed that every vehicle is equipped with the necessary radio technology, i.e., that the equipment ratio is $\eta = 100\%$. Especially during the introductory phase of V2V communication, the equipment ratio will be significantly lower. It is clear that low equipment ratios, combined with sparse scenarios, pose significant problems: the node isolation probability may be so high that it could be impossible to actually run applications in these scenarios.

The expected node degrees, considering the equipment ratio η , can be determined as:

$$f_D[d, \eta] = \begin{cases} (1 - \eta) + \eta f_D[d] & \text{if } d = 0 \\ \eta f_D[d] & \text{if } d > 0 \end{cases} \quad (3.71)$$

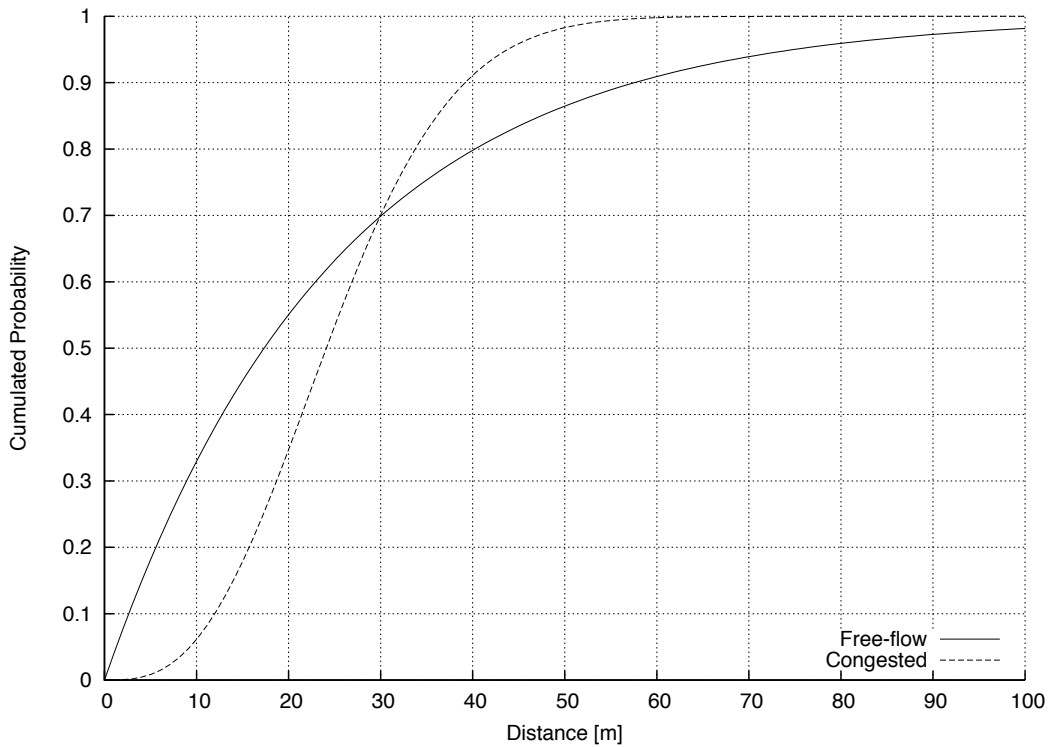


Figure 3.14.: CDFs of free-flow and congested traffic headway distributions for a traffic density of $\rho = 40 \text{ km}^{-1}$.

Regulatory directives allow transmission powers of up to 2 W on dedicated DSRC channels which, under perfect conditions, allows a maximum radio range of approximately 2.3 km at a data rate of 6 Mbit/s. Because for densities $\rho \geq 2 \text{ km}^{-1}$

$$f_D[0] = \exp(-2\rho r) \approx 0 \quad (3.72)$$

the isolation probability of a node is then

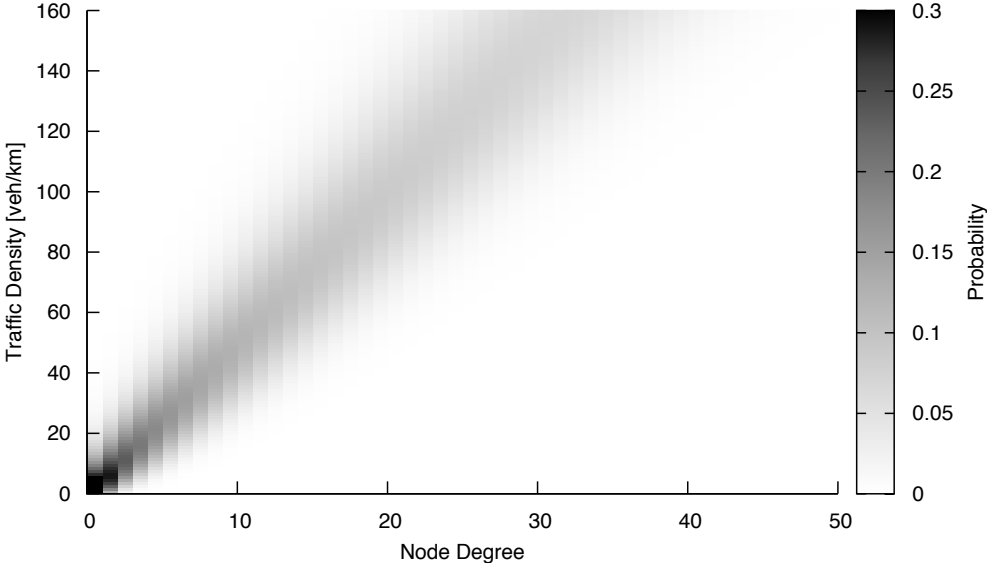
$$f_D[0, \eta] \approx 1 - \eta \quad (3.73)$$

Node Degree Dispersion

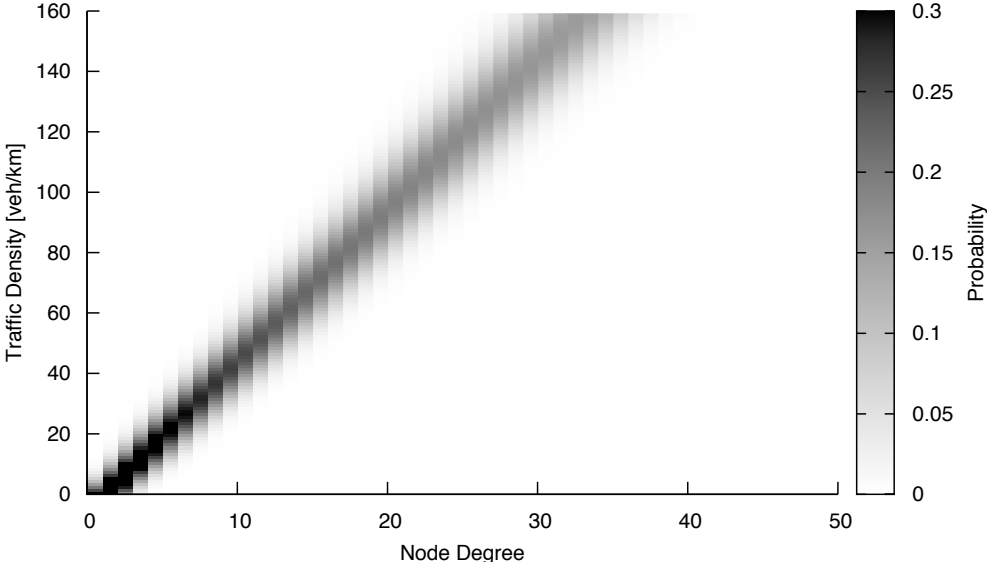
Figure 3.15 shows the probability distributions for both free-flow and congested traffic situations over the range of traffic densities that a vehicle can be expected to actually experience in real-life traffic. It is remarkable that the range in which the degree varies (the degree dispersion) is extremely wide in free-flow traffic, especially when compared to the dispersion in the case of congested traffic condition. Although the average node degree is equal for both traffic conditions (see above), the distribution of node degree under free-flow conditions are characterized by:

- Increased spatial degree inhomogeneity, causing some nodes in the network to experience significantly higher degrees than other (possibly neighboring) nodes. Due to reasons that we will study in the next chapter, this effectively reduces the globally available

3.4. Node Degree



(a) Free-flow traffic



(b) Congested traffic

Figure 3.15.: Dispersion of node degree probabilities over traffic density for (a) freeflow and (b) congested traffic. Radio range is $r = 100$ m.

data rate for applications and, consequently, the experienced QoS. For the same reasons, fairness among nodes regarding the assignment of resources is reduced.

- Increased temporal degree inhomogeneity, necessitating a strong and fast adaptation to intense degree variations over time. The range in which the degree varies over time and the rapidity of these swings correlates with the effort necessary to maintain an updated view on the networks topology.

The reason for the higher degree dispersion of free-flow traffic is the higher variance of the underlying free-flow headway distribution, when compared to the congested traffic's distribution (which is also clearly visible in Figure 3.14):

$$\text{Var}\{H_f\} = \frac{1}{\rho^2} > \text{Var}\{H_c\} = \frac{1}{\rho^2} \left(\frac{3\pi}{8} - 1 \right) \quad (3.74)$$

We have already argued that with increasing traffic densities, the headway distribution changes from free-flow towards that of congested traffic. The highest degree dispersion should consequently be expected at a traffic flow close to the lane capacity whereas at high and low densities, the dispersion will be rather small. This is an important finding since high traffic densities cause high expected degree and thus presents a potentially problematic situation to the application designer: it can be stated that the negative impact of degree inhomogeneity, at least, is not relevant in these scenarios.

3.5. Link Lifetime

Beside a node's degree, the lifetime of the individual communication relations of that node to any other node within its communication range is an important factor that needs to be addressed when studying vehicular networks' properties. In this section, we will discuss how spatial distribution and movement patterns of vehicles, combined with a channel model, determines this lifetime.

In the following, let the dynamic state of a vehicle be described by three vectors (analogous to the formulation used in Section 3.3): the position of the vehicle $\underline{\mathbf{x}}(t)$, its velocity $\underline{\mathbf{v}}(t)$ and its acceleration $\underline{\mathbf{a}}(t)$. From kinematics, the relations between these variables are:

$$\begin{aligned} \underline{\mathbf{a}}(t) &= \frac{\partial}{\partial t} \underline{\mathbf{v}}(t) = \frac{\partial^2}{\partial t^2} \underline{\mathbf{x}}(t) \\ \underline{\mathbf{v}}(t) &= \frac{\partial}{\partial t} \underline{\mathbf{x}}(t) = \underline{\mathbf{v}}_0 + \int_0^t \underline{\mathbf{a}}(\tau) d\tau \\ \underline{\mathbf{x}}(t) &= \underline{\mathbf{x}}_0 + \int_0^t \underline{\mathbf{v}}(\tau) d\tau \\ &= \underline{\mathbf{x}}_0 + \underline{\mathbf{v}}_0 t + \int_0^t \left[\int_0^{\tau} \underline{\mathbf{a}}(\tau') d\tau' \right] d\tau \end{aligned} \quad (3.75)$$

Generally, the expected total time t at which two vehicles A and B are located within each other's covered area as defined by the channel can be computed through integration.¹⁶

$$t = \int \chi(\underline{\mathbf{x}}_a(\tau), \underline{\mathbf{x}}_b(\tau)) d\tau \quad (3.76)$$

¹⁶The integration boundaries should be adjusted so that multiple encounters are avoided.

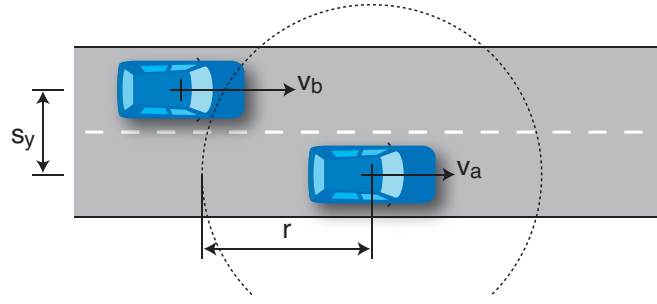


Figure 3.16.: Reference setup for link lifetime analysis.

3.5.1. Geometry

These equations fully describe the free movement of vehicles and may be used for any setup. As in Section 3.4, we wish to study real scenarios where the movement of vehicles is restricted to actual lanes. For two vehicles a and b, let us use the projection function $\underline{\Phi}_{a/b}(\cdot)$ and re-write Equation (3.76):

$$\begin{aligned}\underline{\mathbf{x}}_a(t) &= \underline{\Phi}_a(s_a(t)) \\ \underline{\mathbf{x}}_b(t) &= \underline{\Phi}_b(s_b(t)) \\ t &= \int \chi(\underline{\Phi}_a(s_a(\tau)), \underline{\Phi}_b(s_b(\tau))) d\tau\end{aligned}\quad (3.77)$$

Note the time dependence of the vehicles position. Analogous to Equation (3.75), we can write the vehicle position as:

$$s(t) = s_0 + \int_0^t v(\tau) d\tau \quad (3.78)$$

$$= s_0 + v_0 t + \int_0^t \left[\int_0^\tau a(\tau') d\tau' \right] d\tau \quad (3.79)$$

3.5.2. Velocity Distributions

Velocity is a constitutional dimension of the fundamental diagram. The section-based model, as an exemplary realization thereof, relates vehicles' velocities to the traffic density (Equation (3.42)). For instance, in the free-flow regime, the resulting velocity is equal to the average free velocity v_0 , a parameter to the model. As the traffic density ρ increases beyond the critical density, the average velocity decreases with $1/\rho$.

It is commonly accepted that the distribution of vehicles' velocities under free-flow conditions follows a normal distribution. Recent empirical studies on urban freeway traffic flow [GH08] suggest that this also holds true for denser traffic conditions. A very detailed discussion of this finding can, for instance, be found in [Hel01a].

In the following, let us model the vehicles' velocity distributions with the normal distribution:

$$f_V(v, \bar{v}, \sigma) = \frac{1}{\sqrt{2\pi\sigma^2}} \exp\left(-\frac{1}{2} \frac{(v - \bar{v})^2}{\sigma^2}\right) \quad (3.80)$$

Experimental findings support the intuitive hypothesis that both mean velocity \bar{v} as well as velocity variance σ are rather high in the free-flow regime and then decrease as vehicles start synchronizing. It is clear that as long as vehicles enjoy unlimited overtaking possibilities, velocity variance reflects the individual velocity choices of drivers and the capabilities of their vehicles. The transition to congested traffic, however, leads to a gradual adjustment of differential (i.e., inter-vehicle) velocities until synchronicity is reached [Hel01b].

A similar behavior can be observed studying the differential velocities between vehicles driving on the right (regular) and the left (fast) lane of a highway. Up to a certain density, vehicles on the fast lane travel significantly faster than on the regular lane; also, the variance of the differential velocity is much higher. Vehicles then start changing lanes to maximize their individual velocity, a process that finally leads to equal velocities on both lanes. Consequently, the differential velocities scatter around zero.

Common literature about traffic studies characterize vehicles' velocities by the average velocity \bar{v} and the velocity of the 85 percentile, v_{85} . Assuming a normal distribution, 84.13 % of the variates lie within the interval $[-\infty \dots \bar{v} + \sigma]$. Consequently, the velocity's standard deviation is approximately:

$$\sigma = v_{85} - \bar{v} \quad (3.81)$$

If v_a and v_b of two vehicles A and B are distributed normally, the differential velocity is also distributed normally. Assuming that A and B are traveling at an angle of φ , the resulting expected differential velocity and the differential variance are given by:

$$\bar{v} = \sqrt{\bar{v}_a^2 + \bar{v}_b^2 - 2\bar{v}_a\bar{v}_b \cos \varphi} \quad (3.82)$$

$$\sigma^2 = \sigma_a^2 + \sigma_b^2 \quad (3.83)$$

3.5.3. Discussion

As in Section 3.4, we shall assume a log-distance path loss model (Equation (3.11)) with a maximum coverage area of radius r .¹⁷ Under the condition of unaccelerated movement, let $s_{a/b}$ be the initial positions and $v_{a/b}$ the time-invariant velocities of two vehicles a and b. The inequality holds true for all times τ during which the two vehicles are within each others coverage radius:

$$\forall \tau \in [t_0 \dots t_1] : \|\underline{\Phi}_a(s_a + v_a\tau) - \underline{\Phi}_b(s_b + v_b\tau)\| \leq r \quad (3.84)$$

Consequently, the total link lifetime t is the length of the interval $[t_0 \dots t_1]$. Let the lane segments be straight and have an angle of θ . The resulting projection function is then:

$$\underline{\Phi}(s(t)) = \begin{bmatrix} x_0 \\ y_0 \end{bmatrix} + s(t) \begin{bmatrix} \cos \theta \\ \sin \theta \end{bmatrix} \quad (3.85)$$

In the following, we describe the scenario by the initial distance vector \underline{x} and velocity difference vector \underline{v} . It may be more convenient in some scenarios to use the polar notation of the

¹⁷It is clear that an additional component modeling large-scale fading yields the same results. It is, however, mathematically cumbersome to compute analytically.

velocity difference vector (with length v and angle φ):

$$\begin{aligned}\underline{\mathbf{x}}_a(t) - \underline{\mathbf{x}}_b(t) &= \underline{\Phi}_a(s_a + v_a \cdot t) - \underline{\Phi}_b(s_b + v_b \cdot t) \\ &= \underline{\mathbf{x}} + \underline{\mathbf{v}} \cdot t\end{aligned}\quad (3.86)$$

$$= \underline{\mathbf{x}} + v \cdot t \begin{bmatrix} \cos \varphi \\ \sin \varphi \end{bmatrix}\quad (3.87)$$

where

$$\underline{\mathbf{x}} = \begin{bmatrix} x_a - x_b + s_a \cos \theta_a - s_b \cos \theta_b \\ y_a - y_b + s_a \sin \theta_a - s_b \sin \theta_b \end{bmatrix}\quad (3.88)$$

$$\underline{\mathbf{v}} = \begin{bmatrix} v_a \cos \theta_a + v_b \cos \theta_b \\ v_a \sin \theta_a + v_b \sin \theta_b \end{bmatrix}\quad (3.89)$$

$$v = \|\underline{\mathbf{v}}\| = \sqrt{v_a^2 + v_b^2 - 2v_a v_b \cos(\theta_a - \theta_b)}\quad (3.90)$$

$$\varphi = \angle \underline{\mathbf{v}} = \arctan \left(\frac{v_a \sin \theta_a + v_b \sin \theta_b}{v_a \cos \theta_a + v_b \cos \theta_b} \right)\quad (3.91)$$

The total time that the two vehicles are in each other's range (i.e. the link lifetime) is then:

$$t = 2 \frac{\sqrt{2x_x x_y v_x v_y + v_x^2 (r^2 - x_y^2) + v_y^2 (r^2 - x_x^2)}}{v_x^2 + v_y^2}\quad (3.92)$$

$$= \frac{2}{|v|} \sqrt{r^2 - (x_x \sin \varphi - x_y \cos \varphi)^2}\quad (3.93)$$

Time Distribution

If the distribution of the vehicles' velocities $f_V(v)$ is known, the distribution of link lifetimes $f_T(t)$ can be computed by transforming $f_V(v)$ through Equation (3.76):

$$f_T(t) = f_V(v(t)) \cdot \frac{dv(t)}{dt}\quad (3.94)$$

Due to lane shape constraints, we can assume that the orientation of the differential velocity vector $\underline{\mathbf{v}}$ does not change, i.e., φ is constant. Therefore, we can introduce a geometry-dependent constant, s_r , that represents the distance (in meters) that the two nodes travel, being within each others radio range or simply the *effective range*:

$$s_r = 2 \sqrt{r^2 - (x_x \sin \varphi - x_y \cos \varphi)^2}\quad (3.95)$$

Solving Equation (3.76) for t and subsequent differentiation yields:

$$v = \pm \frac{s_r}{t}\quad (3.96)$$

$$\frac{dv}{dt} = \pm \frac{s_r}{t^2}\quad (3.97)$$

Assuming normally distributed velocities (Equation (3.80)) in Equation (3.94), the link lifetime's PDF as a function of average velocity \bar{v} , velocity variance σ^2 , and the geometry s_r is then:

$$f_T(t, \bar{v}, \sigma, s_r) = \begin{cases} 0 & \text{if } t < 0 \\ \frac{s_r}{t^2} \frac{1}{\sqrt{2\pi\sigma^2}} \left(\exp\left(-\frac{1}{2} \frac{(s_r - \bar{v}t)^2}{\sigma^2 t^2}\right) + \exp\left(-\frac{1}{2} \frac{(s_r + \bar{v}t)^2}{\sigma^2 t^2}\right) \right) & \text{if } t \geq 0 \end{cases} \quad (3.98)$$

The probability that a connection is shorter than a certain time t , i.e., the CDF $F_T(t)$ is:

$$F_T(t, \bar{v}, \sigma, s_r) = \int_0^t f_T(t, \bar{v}, \sigma, s_r) \quad (3.99)$$

$$= 1 - \frac{1}{2} \operatorname{erf}\left(\frac{1}{\sqrt{2}} \frac{s_r - \bar{v}t}{\sigma t}\right) - \frac{1}{2} \operatorname{erf}\left(\frac{1}{\sqrt{2}} \frac{s_r + \bar{v}t}{\sigma t}\right) \quad (3.100)$$

Vehicle-to-Vehicle on Straight, Parallel Lanes

Let us assume that A and B move on two parallel lanes that have a lateral displacement of s_{\perp} . Their initial positions are \mathbf{x}_a and \mathbf{x}_b , traveling in on parallel, straight lines with constant velocities v_a and v_b . The surveyed scenarios and associated parameters used for computation are listed in Table 3.2. The parameters are typical for a highway scenario and have been taken from [Tho93]. The results are shown in Figure 3.17.

It is obvious that for oncoming vehicles, the resulting connection times are short ($t \approx 3$ s for $r = 100$ m) due to the high relative velocities ($\bar{v} = 64.6$ m/s), Figure 3.17(d). The connection duration may be increased significantly if the radio range is increased; however, the drawbacks of increased radio range as discussed in the previous section should be accounted for. The practical usability of connections with oncoming traffic thus depends highly on the desired application and the availability of routed (multihop) connections which, in turn, is subject to isolation or leafnode connectivity and potentially unavailable. It is highly unlikely that cooperative maneuvers can be coordinated and controlled over highly transient connections. On the other hand, the availability time of a connection may be long enough to inform oncoming traffic about obstacles or emergency situations.

For vehicles traveling in the same direction, connection times reveal a completely different nature; this is due to the low relative velocities ($\bar{v} = 3.1$ m/s). For instance, if $r = 100$ m, almost 50% of all connections have a connection time $t \geq 50$ s. The shortest connection is about 8 s. In contrast to the scenario with oncoming traffic, the connection time PDF changes into a heavy-tailed distribution: if \bar{v} is chosen close to zero meters per second and/or σ is sufficiently high so that $f_V(v)$ reveals a significant density around 0 m/s, connection times tend to $t \rightarrow \infty$. From a practical standpoint, this means that there are some vehicles that are (at least, in principle) connected infinitely long, because they follow the leading vehicle (platooning) or two vehicles drive in parallel to each other. Actual vehicles, however, will only travel together for a either certain part of their route (i.e. at least for the length of the current lane until the next ramp) or until the rear vehicle passes by the front vehicle. Driver models, such as the MOBIL model [KTH07], can be used to represent the probability that a vehicle will pass by another vehicle and thus to derive the probability that two vehicles will platoon for a certain time (and consequently limit t).

The discussed results clearly show that the communication durations in the oncoming traffic scenario are mostly determined by the differential velocity of the vehicles which may be rather

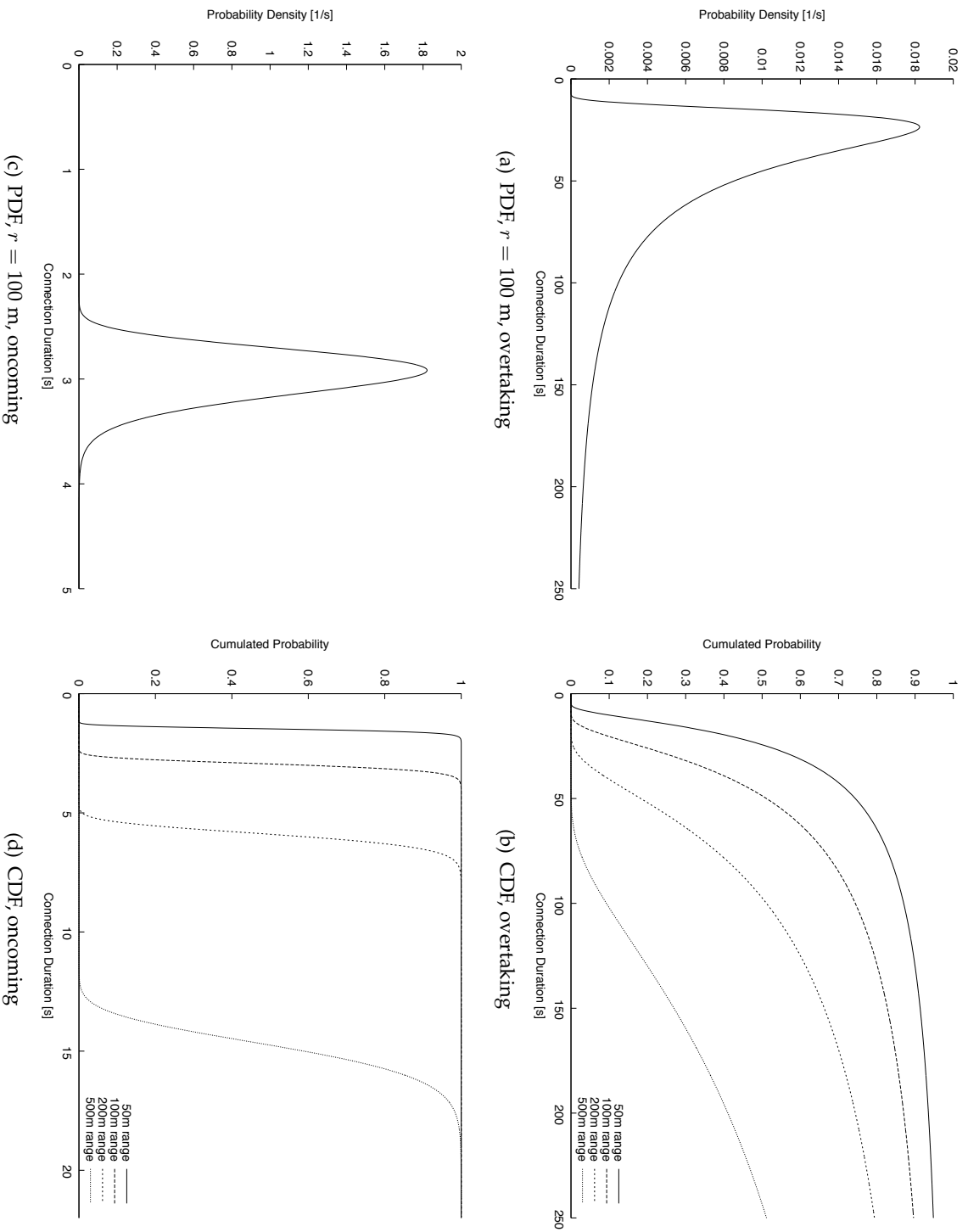


Figure 3.17.: PDF (a), (c) and CDF (b), (d) of communication duration with oncoming and same-direction fast lane vehicles. PDFs shown for a communication range of $r = 100m$.

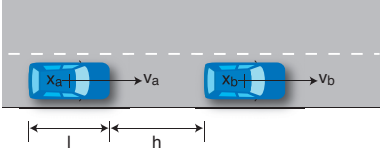
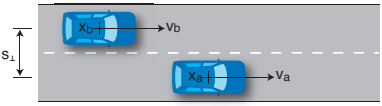
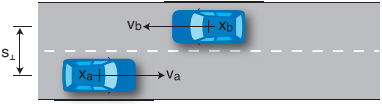
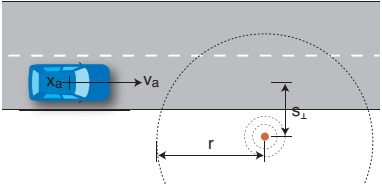
Scenario	Parameter
Following 	$\underline{\mathbf{x}}_0 = \begin{bmatrix} l + h \\ 0 \end{bmatrix}, \underline{\mathbf{v}} = \begin{bmatrix} v_a - v_b \\ 0 \end{bmatrix}, s_r = 2r$
Overtaking (Fig. 3.17(a)) 	$\underline{\mathbf{x}}_0 = \begin{bmatrix} 0 \\ -s_{\perp} \end{bmatrix}, \underline{\mathbf{v}} = \begin{bmatrix} v_a - v_b \\ 0 \end{bmatrix}, s_r = 2\sqrt{r^2 - s_{\perp}^2}$ $\bar{v}_a = 30.8 \text{ m/s}, \bar{v}_b = 33.9 \text{ m/s},$ $\sigma_{v_a} = \sigma_{v_b} = 3.6 \text{ m/s}, s_{\perp} = 3.8 \text{ m}$
Oncoming (Fig. 3.17(c)) 	$\underline{\mathbf{x}}_0 = \begin{bmatrix} 0 \\ -s_{\perp} \end{bmatrix}, \underline{\mathbf{v}} = \begin{bmatrix} v_a + v_b \\ 0 \end{bmatrix}, s_r = 2\sqrt{r^2 - s_{\perp}^2}$ $\bar{v}_a = \bar{v}_b = 33.9 \text{ m/s}, \sigma_{v_a} = \sigma_{v_b} = 3.6 \text{ m/s},$ $s_{\perp} = 7.9 \text{ m}$
Vehicle-to-Infrastructure (Fig. 3.19(a)) 	$\underline{\mathbf{x}}_0 = \begin{bmatrix} 0 \\ -s_{\perp} \end{bmatrix}, \underline{\mathbf{v}} = \begin{bmatrix} v_a \\ 0 \end{bmatrix}, s_r = 2\sqrt{r^2 - s_{\perp}^2}$ $\bar{v}_a = 30.8 \text{ m/s}, \sigma_{v_a} = 3.6 \text{ m/s}$ $s_{\perp} = 3.8 \text{ m}$

Table 3.2.: Vehicle-to-Vehicle on straight, parallel lanes. Scenarios and parameters used for computation.

high, especially on highways. In the overtaking scenario, the differential velocity is low, potentially even close to zero. Consequently, the communication duration is mainly determined by the velocity variance.

Mean Duration and Percentiles

Unfortunately, the link lifetime distribution (Equation (3.98)) does not have a moment generating function. Consequently, it does not have a defined expected value and no defined variance. As mentioned above, there are sets of parameters for which the link lifetime is quite well-defined (for instance, the oncoming traffic scenario) and there are parameters for which the link lifetime may be infinite for some vehicles.

The problem is that the integral for computing the mean does not converge and therefore, no closed form exists:

$$\bar{t} = \int_0^{\infty} \tau f_T(\tau) d\tau \rightarrow \infty \quad (3.101)$$

Looking at the discussed distributions, however, it is clear that the distribution shown in Figure 3.17(c) does have a mean value that could be determined by integrating, for instance, in the range from 2 s to 5 s. The distribution shown in Figure 3.17(a) does not have a well-defined mean, because it has significant densities for $t \rightarrow \infty$. Consequently, it may be possible for some parameters to limit the integration borders to t_- and t_+ and numerically compute the mean:

$$\bar{t} = \int_{t_-}^{t_+} \tau f_T(\tau) d\tau \quad (3.102)$$

The first parameter to choose is the probability interval $[\epsilon \dots 1 - \epsilon]$, that should be accounted for in the computation. This corresponds to limiting the integration borders:

$$\epsilon \leq F_T(t) \leq 1 - \epsilon \quad (3.103)$$

$$t \in [t_- \dots t_+] \quad (3.104)$$

Let us rewrite Equation (3.100), so that:

$$\epsilon = \frac{1}{2} \operatorname{erf} \left(\frac{1}{\sqrt{2}\sigma} \left(\frac{s_r}{t} - \bar{v} \right) \right) + \frac{1}{2} \operatorname{erf} \left(\frac{1}{\sqrt{2}\sigma} \left(\frac{s_r}{t} + \bar{v} \right) \right) \quad (3.105)$$

and assume that the second expression's argument is large (greater than 3 would be sensible). Consequently,

$$\lim_{t \rightarrow \infty} \frac{1}{2} \operatorname{erf} \left(\frac{1}{\sqrt{2}\sigma} \left(\frac{s_r}{t} - \bar{v} \right) \right) = \frac{1}{2} \quad (3.106)$$

from above. The CDF $F_T(t)$ is then dominated by the first expression. Let us denote the first expression's argument as the parameter κ :

$$\kappa = \frac{1}{\sqrt{2}\sigma} \left(\frac{s_r}{t} - \bar{v} \right) = \operatorname{erf}^{-1}(2\epsilon - 1) \quad (3.107)$$

Some typical values of κ have been compiled in Table 3.3. We can now solve for t_- and t_+ and get the desired integration interval:

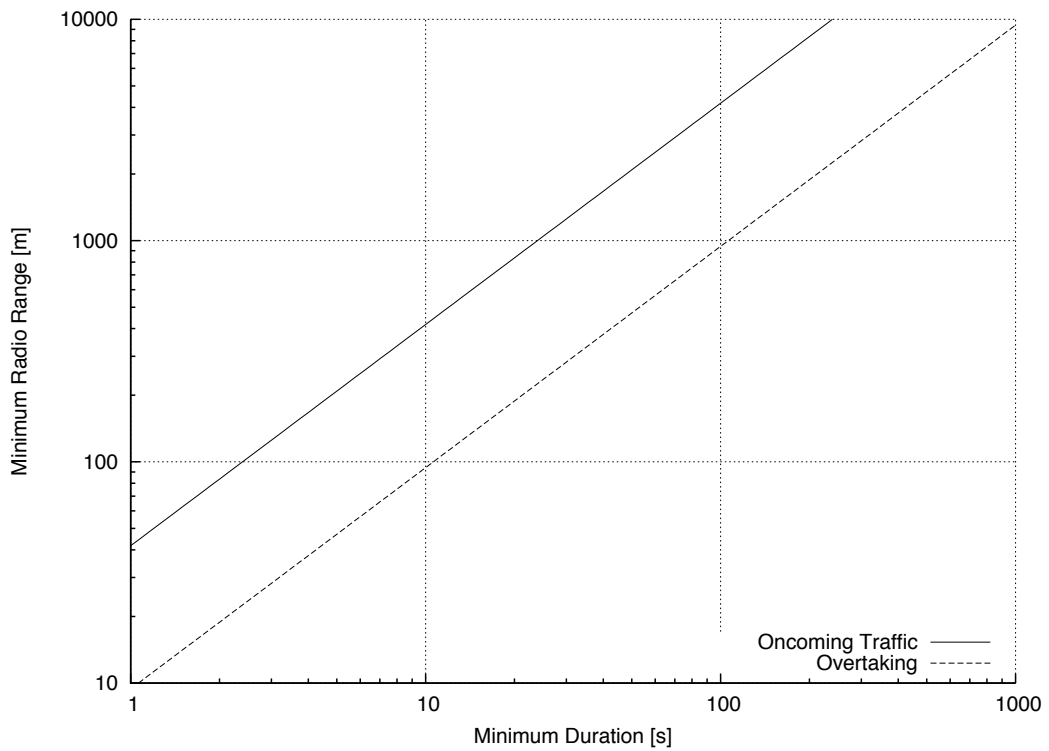
$$t_{\pm} = \frac{s_r}{\bar{v} \pm \sqrt{2}\kappa\sigma} \quad (3.108)$$

Now, how is it possible to determine if a certain parameter set yields a well-defined distribution or not? For a chosen κ (which can be rather large, depending on the tolerable error), the integration boundaries must be positive and finite. Therefore, the denominator of Equation (3.108) must not be negative or zero. Consequently we can approximate the expected value, if

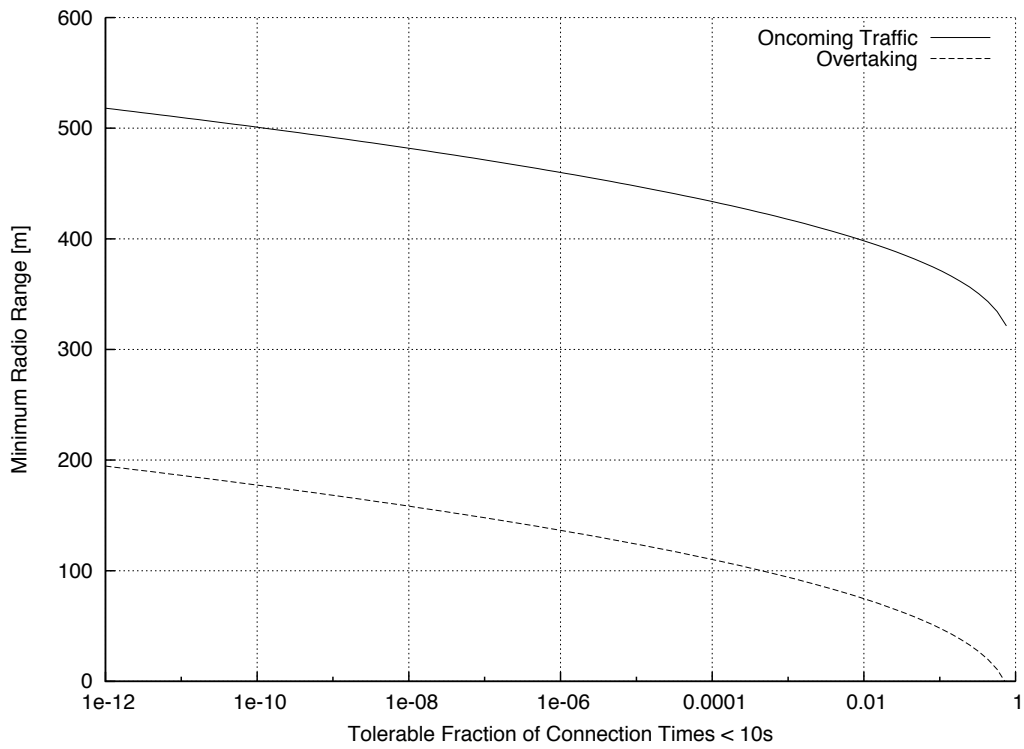
$$\bar{v} \stackrel{!}{>} \sqrt{2}\kappa\sigma \quad (3.109)$$

Note that if we let $\epsilon = 0.5$ ($\kappa = 0$), we obtain the median value \tilde{t} of the connection duration with sufficient accuracy if \bar{v} is reasonably high:

$$\tilde{t} = \frac{s_r}{\bar{v}} \quad (3.110)$$



(a) Range r over time t , $\epsilon = 10^{-3}$.



(b) Range r over fraction ϵ , $t = 10$ s.

Figure 3.18.: Minimum required radio ranges for communication times t (a) and fractions of shorter times, ϵ (b).

ϵ	κ
10^{-1}	-0.9062
10^{-2}	-1.6450
10^{-3}	-2.1851
10^{-4}	-2.6297
10^{-5}	-3.0157
10^{-6}	-3.3612
...	...
10^{-9}	-4.2411
10^{-12}	-4.9741

 Table 3.3.: Some values of κ as a function of ϵ .

Radio Range Adaptation

For all $\kappa \leq \bar{v}/\sqrt{2}\sigma$ and corresponding ϵ , Equation (3.108) yields a valid lower integration boundary, t_- . The integral

$$\epsilon \approx \int_0^{t_-} f_T(\tau) d\tau \quad (3.111)$$

represents the fraction of nodes that have a connection time shorter than t_- .¹⁸ We have argued above that the linear relation of the radio range to the communication duration makes it seem sensible to adjust the range so as to satisfy the demands of the application.

Using a representative set of scenario parameters (\bar{v} , σ), it is possible to calculate the necessary minimum radio range to provide enough (i.e., a fraction of more than ϵ) connections with durations of at least t seconds by solving Equation (3.108) for s_r and consequently solving s_r for r :

$$s_r = t(\bar{v} - \sqrt{2}\kappa\sigma) \quad (3.112)$$

Example

An application may be unavailable with a probability of $\epsilon = 10^{-3}$ (1 ‰) and requires connections with a minimum duration of $t = 10$ s. Given the overtaking and oncoming traffic scenario from Table 3.2, what is the minimum radio range required to meet these demands?

For the desired ϵ , $\kappa = -2.1851$. Solving Equation (3.112) for the overtaking scenario ($\bar{v} = 3.1$ m/s, $\sigma = \sqrt{2} \cdot (3.6 \text{ m/s})^2 = 5.091$ m/s) yields $s_r = 188.32$ m and, consequently,

$$r = \frac{1}{2} \sqrt{s_r^2 + 4s_1^2} \approx 94 \text{ m} \quad (3.113)$$

For the oncoming traffic scenario with much higher relative velocities ($\bar{v} = 67.8$ m/s), the connection durations are much shorter so the necessary radio range can be expected to be much greater than in the overtaking scenario: $s_r = 835.32$ m and, consequently, $r \approx 418$ m.

The minimum required radio ranges over the desired ϵ , given a minimum communication duration of $t = 10$ s are shown for both scenarios in Figure 3.18(b). Conversely, the ranges over the desired minimum communication durations t , given a tolerable fraction of lower durations $\epsilon = 10^{-3}$ are shown in Figure 3.18(a).

¹⁸This approximation stems from the fact that we neglected the second $\text{erf}(\cdot)$ term of Equation (3.100) during the derivation of Equation (3.108).

Vehicle-to-Infrastructure on Straight, Parallel Lanes

In the previous sections, we have considered two communicating vehicles, each moving with an individual velocity v_a and v_b , respectively. Using the same mathematical framework, it is quite easy to analyze the communication durations between a moving vehicle and roadside infrastructure, i.e. a V2I constellation. To do so, we consider only one vehicle, let $v_b = 0$ m/s, and adjust the position vector accordingly — in the demonstrated case, we assume the infrastructure equipment to be mounted with a lateral offset of s_{\perp} relative to the lane's center. The results have been depicted in Figure 3.19.

Of course, the above considerations regarding radio range adjustment are also applicable in the V2I scenario. However, in contrast to the V2V scenario, we can expect not to find infinite connection durations; instead, the mean duration may be assumed rather well defined.

Duration and Traffic Density

Unless we consider a pure V2I scenario, the link duration does not depend on the velocity of a vehicle itself but rather on the differential velocities between vehicles. Therefore, it is not easily possible to make a statement about the link duration based on the average velocity as a function of the traffic density ρ , Equation (3.37). If, however, the fundamental diagrams of the lanes on which two communicating vehicles travel are known, the traffic densities of these lanes are known, and the degree of correlation between the lanes are known, the average link lifetimes could be calculated.

The results shown in Figure 3.20 have been computed assuming that the fundamental diagrams of neighboring lanes A and B are equal and parameterized according to the highway scenario specified in Table 3.1. Under free-flow conditions, the fundamental diagram specifies equal average velocities for vehicles which, in turn, lead to infinite connection durations; hence the white triangle in the lower left corner. It is clear from the diagram that under heavily congested traffic conditions and/or very synchronous traffic (equal densities), connection durations are significantly longer than under conditions in which the densities differ more.

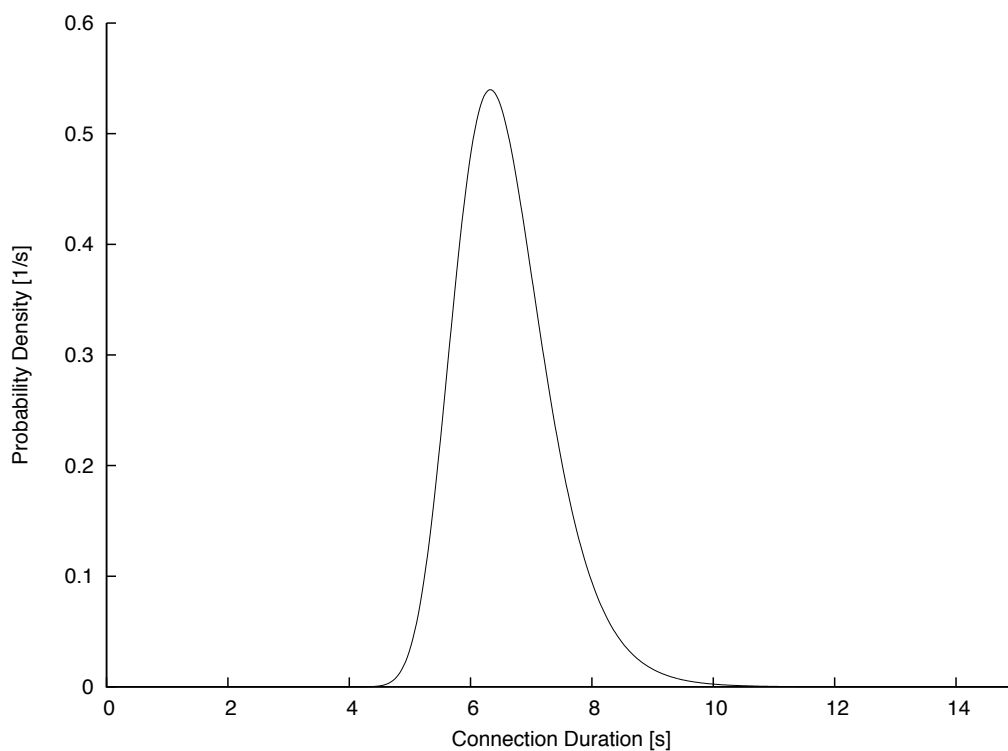
On the contrary, if a pure V2I scenario with fixed infrastructure equipment should be studied, the velocity of vehicles can be easily determined. The resulting median connection duration \tilde{t} is shown in Figure 3.21, assuming the highway scenario as used above.

3.6. Link Generation and Link Break Rate

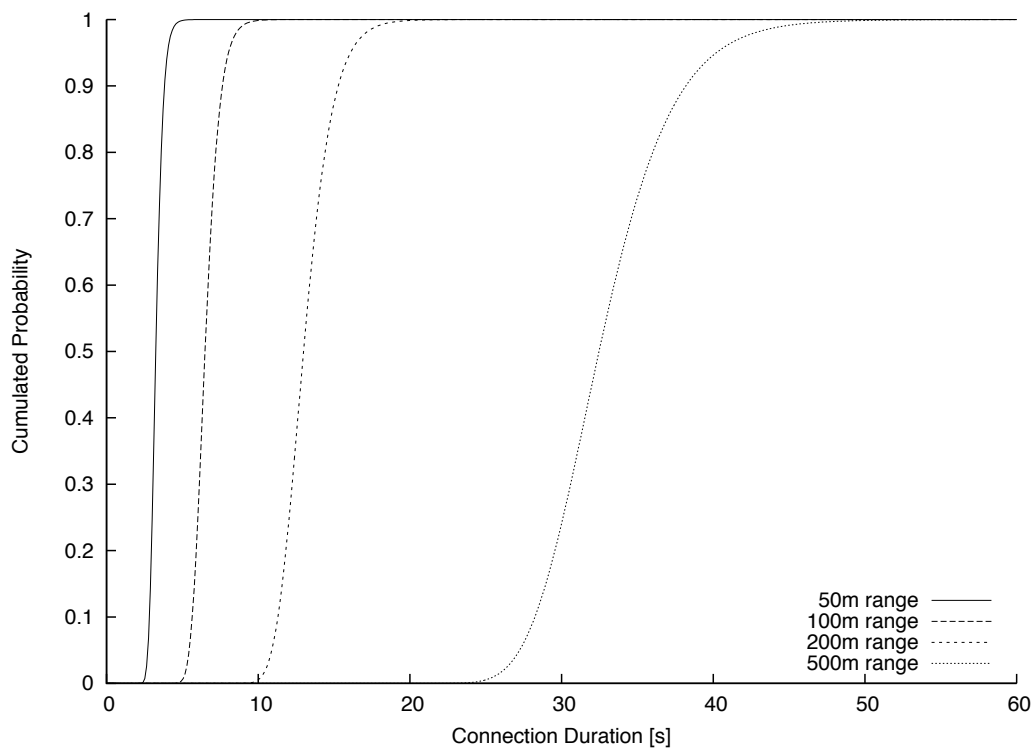
The third relevant dimension of connectivity is the rate at which communication relations change over time. As new vehicles enter a vehicle's range radio, a new link is established. Other vehicles leave the radio range and links break away. The rate at which these events happen, Λ , is relevant because it defines a measure of a network's dynamic. In the previous sections, we have discussed how the node degree d is related to the traffic density ρ and how link lifetimes t are defined by (differential) velocities v . Knowing that traffic density and velocities are related through the measure of traffic flow, Q , this section will discuss how the link generation rate Λ is related to Q .

Little's Law [Lit61], a fundamental law in queueing theory, states that the average number of customers in a shop is the arrival rate of customers multiplied with the average time spent in

3.6. Link Generation and Link Break Rate



(a) PDF, $r = 100$ m, vehicle-to-infrastructure



(b) CDF, vehicle-to-infrastructure

Figure 3.19.: CDF (b) and PDF (a) of communication duration with roadside infrastructure. PDFs shown for a communication range of $r = 100m$.

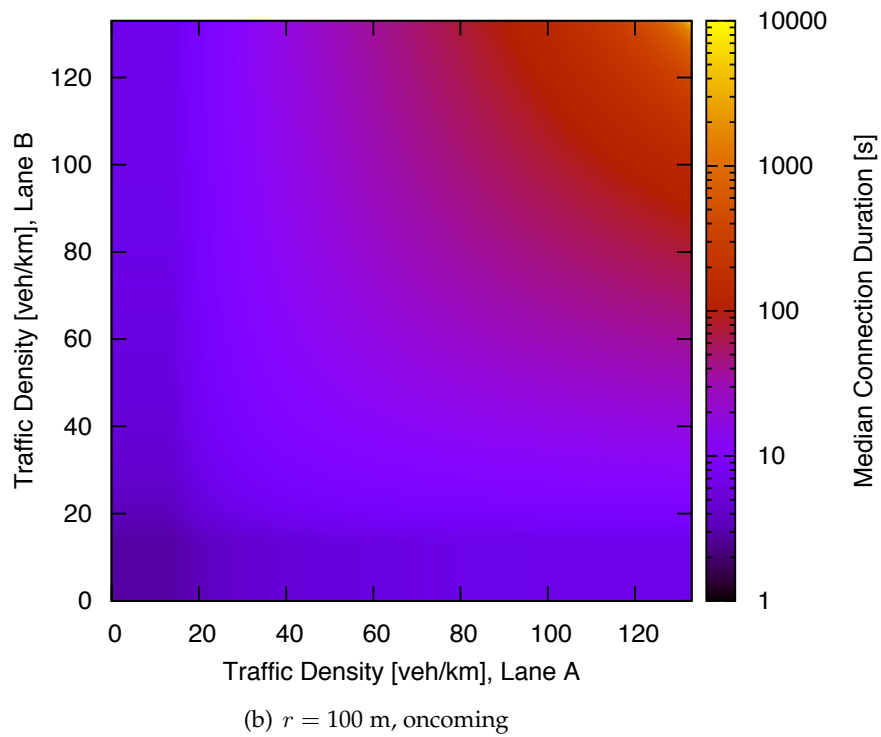
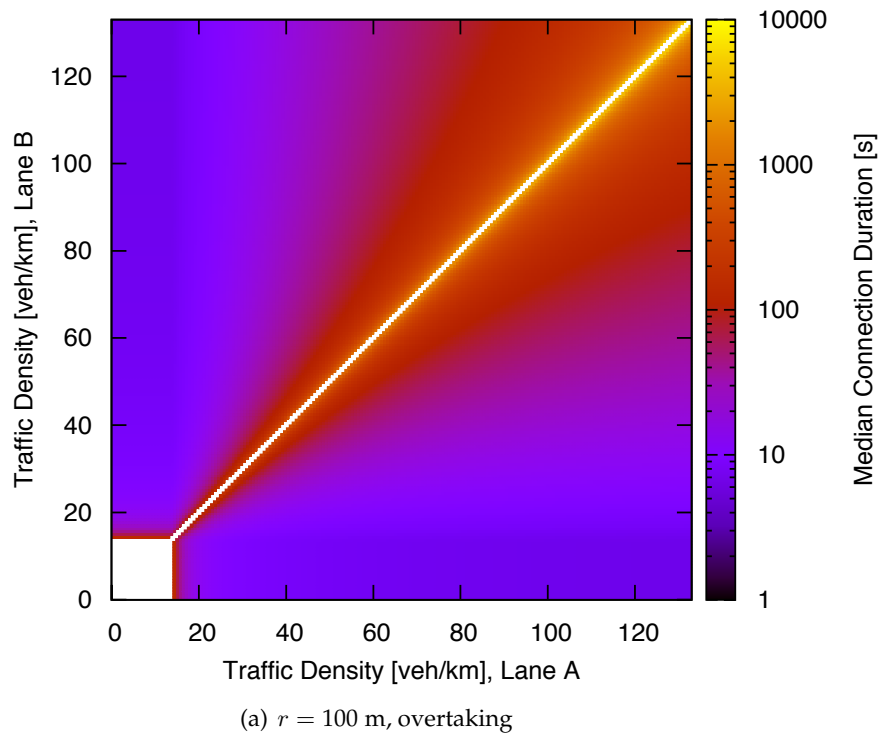


Figure 3.20.: Median connection duration \tilde{t} over traffic densities ρ_A, ρ_B for two lanes.

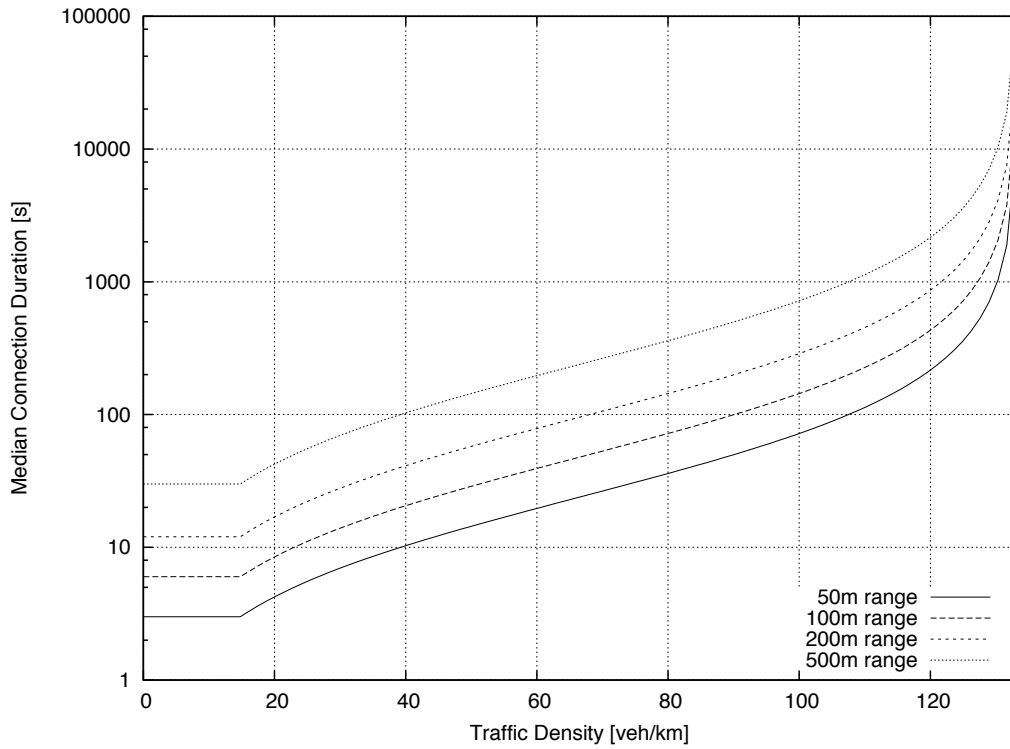


Figure 3.21.: Median connection duration \tilde{t} over traffic density ρ in the V2I scenario.

the shop. As an analogy, let the average number of customers represent the average number d of nodes within the radio range, i.e., $E\{D\}$. The average link lifetime $E\{T\}$ relates to the average time spent in the shop; consequently, the arrival rate relates to the link change rate, Λ . Mathematically,

$$E\{D\} = \Lambda \cdot E\{T\} \quad (3.114)$$

Unfortunately, as we have discussed in the previous section, there exists no closed form of the expected link lifetime $E\{T\}$. It may, however, be computed numerically. If this is not possible (very heavy tail of the differential velocity distribution), we can state that:

$$E\{T\} \geq \frac{s_r}{E\{V\}} \quad (3.115)$$

This approximation is useful, because using the left-hand term of Equation (3.115) represents a “worst-case” link lifetime. Consequently, the highest expected link change rate is:

$$\Lambda = \frac{E\{D\}}{E\{T\}} \leq \frac{E\{D\} \cdot E\{V\}}{s_r} \quad (3.116)$$

3.6.1. Geometry

We shall start the geometrical consideration for the simplified case in which the radio does not change its position, i.e., the V2I case and then extend the findings to a more general formulation. We can assume that unless the traffic density changes, the expected node degree does

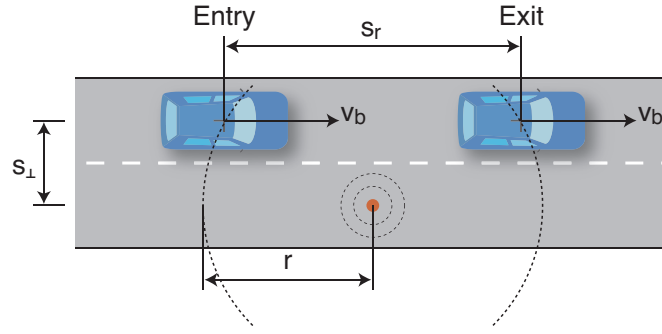


Figure 3.22.: Reference setup for link generation analysis, V2I scenario.

not vary over time. This indicates that the rate at which new links are generated (i.e., the rate at which vehicles pass the “entry” point) is equal to the rate at which links break (the rate at which vehicles pass the “exit” point).

Vehicle-to-Infrastructure

As outlined in Figure 3.22, the rate at which vehicles enter the radio range of the immobile infrastructure shall be determined. Let us consider only one lane with traffic density ρ and vehicles moving with an average differential velocity of $\bar{v}(\rho)$ relative to the infrastructure equipment. According to Equation (3.70)¹⁹ and Equation (3.80), we can write Equation (3.116) as:

$$\Lambda = \rho \cdot \bar{v}(\rho) = Q \quad (3.117)$$

This is sensible as for the static observer, the rate at which vehicles pass by equals the traffic flow. Consequently, the rate at which vehicles enter the radio range, i.e., the link generation rate is equal to the traffic flow at the entry point and the link break rate is equal to the traffic flow at the exit point. Thus, the rates correspond directly to the fundamental diagram (see Figure 3.8) and shall not be repeated here.

It is worth noting that, due to the varying nature of vehicles’ headway process (depending on the traffic density), the points in time when vehicles enter or leave the radio range follows a Poisson process under free-flow traffic conditions. As the traffic density grows, the headway variance decreases significantly and the link generation process becomes more deterministic.

Vehicle-to-Vehicle

Let a vehicle A move on one lane that has a traffic density of ρ_a and another vehicle B move on another lane with a traffic density of ρ_b (Figure 3.23).

The expected node degree of vehicle A regarding lane B and vice versa is (Equation (3.70)):

$$E\{D\}_a = \rho_b \cdot s_r \quad (3.118)$$

$$E\{D\}_b = \rho_a \cdot s_r \quad (3.119)$$

¹⁹In the form as discussed in the previous section, Equation (3.70) does not account for a lateral lane offset. Taking this into account, we need to re-write Equation (3.70) as $E\{D\} = \rho s_r$. Intuitively, it is clear that the range expressions in the nominator and denominator are equal and can thus be cancelled.

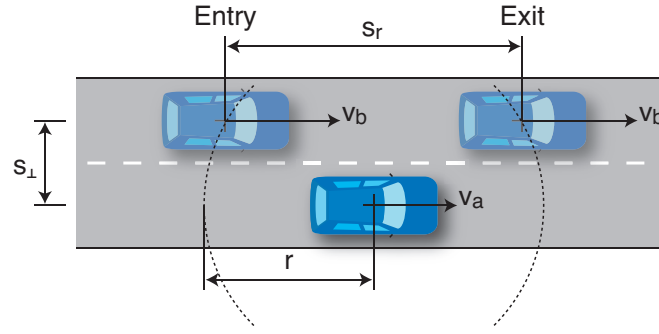


Figure 3.23.: Reference setup for link generation analysis, V2V scenario.

Let \bar{v} be the differential velocity of vehicles, according to Equation (3.82). Letting φ the angle of the differential velocity vector, we can write, considering the dependence on the traffic densities:

$$\bar{v}(\rho_a, \rho_b, \varphi) = \sqrt{\bar{v}(\rho_a)^2 + \bar{v}(\rho_b)^2 - 2\bar{v}(\rho_a)\bar{v}(\rho_b)\cos\varphi} \quad (3.120)$$

The link arrival rate from vehicle A's perspective is the product of the expected node degree regarding lane B with the average differential velocity and vice versa:

$$\Lambda_a = \frac{E\{D\}_a \cdot E\{V\}}{s_r} = \rho_b \cdot \bar{v}(\rho_a, \rho_b, \varphi) \quad (3.121)$$

$$\Lambda_b = \frac{E\{D\}_b \cdot E\{V\}}{s_r} = \rho_a \cdot \bar{v}(\rho_a, \rho_b, \varphi) \quad (3.122)$$

It is clear that vehicles A and B experience different link generation rates: vehicles traveling with high velocities in free-flow conditions that pass a line of congested vehicles will have higher link generation rates because they pass by more vehicles in the same time than the congested vehicles see vehicles passing by.

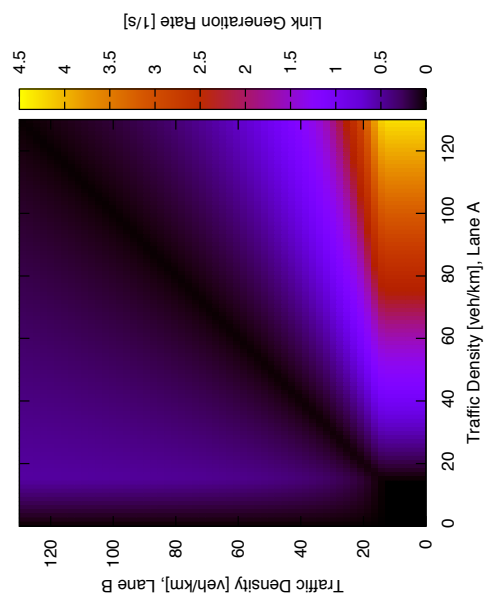
Multiple Lanes

If multiple lanes shall be considered the total link generation rate of a vehicle traveling on lane J can be found by simply summing up the product of the respective differential velocities and node degrees:

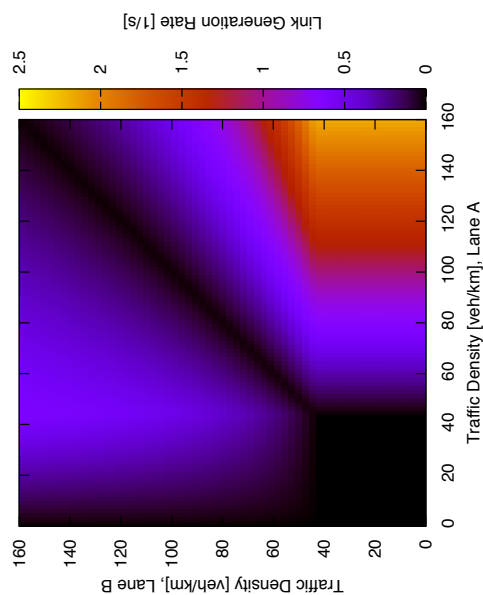
$$\Lambda_j = \sum_{\substack{i=0 \\ i \neq j}}^N \rho_i \cdot \bar{v}(\rho_i, \rho_j, \varphi_{ij}) \quad (3.123)$$

3.6.2. Discussion

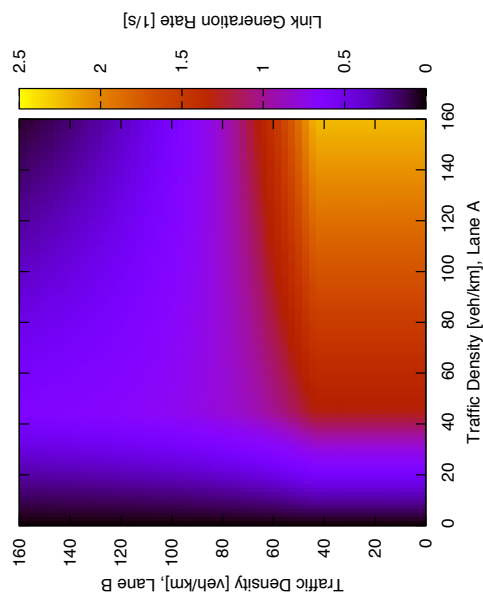
In accordance to the previous section, the results shown in Figure 3.24 have been computed assuming equal fundamental diagrams for the neighboring lanes A and B. The parameters have been chosen according to the highway and city scenario of Table 3.1. The geometry of the traffic situations "overtaking" and "oncoming" can be found in Table 3.2. The link generation rates shown in the figures have been computed for the vehicle moving on lane B, i.e., they



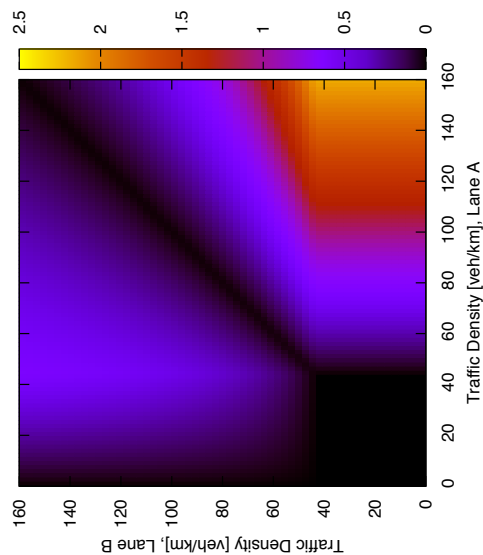
(a) Highway, Oncoming Traffic



(b) Highway, Overtaking



(c) City, Oncoming Traffic



(d) City, Overtaking

Figure 3.24.: Link generation rates Λ_b over traffic densities ρ_A, ρ_B for two lanes.

represent Λ_b . However, reversing the two axes yields the rates for a vehicle moving on lane A, i.e., Λ_a .

Intuitively, one would expect the highest link generation rates in situations where vehicles move with high relative velocities, i.e., in scenarios with oncoming traffic. The results shown in Figures 3.24(a) and 3.24(c), however, show only very moderate rates. At a traffic density of $\rho = 20 \text{ km}^{-1}$, we obtain rates for the highway scenario of $\Lambda_b \approx 0.94 \text{ s}^{-1}$ and for the city scenario of $\Lambda_b \approx 0.6 \text{ s}^{-1}$.

If both vehicles travel in the same direction, their differential velocity will be almost equal if the traffic densities are equal and consequently, the link generation rate is zero. The highest rates are always obtained in situations where one vehicle is stuck in highly congested traffic for the vehicle passing by the congestion, independent of the direction (overtaking or oncoming). It is, however, unlikely to be found in a realistic situation that two equidirectional lanes reveal significant differences regarding their traffic densities.

If the lanes are aligned counterdirectional — such as on a highway — the situation is very likely to be found and needs further consideration. If routing should be implemented in the network, the link generation rate and the link break rate represent the dynamic at which the network's topology changes and consequently correspond to the rate at which routing tables have to be updated. Careful consideration is necessary to decide if routing can sensibly be implemented under all traffic situations.

Example

Let us consider a highway. Lane A is jammed ($\rho_a = 120 \text{ km}^{-1}$), the counterdirection lane B is free ($\rho_b = 10 \text{ km}^{-1}$). The expected differential velocity, assuming the fundamental diagrams parameterized according to Table 3.1, is then $\bar{v} = 33.8 \text{ m/s}$. Consequently, the experienced link generation rates are:

$$\Lambda_a = \rho_b \cdot \bar{v} = 0.338 \text{ s}^{-1} \quad (3.124)$$

$$\Lambda_b = \rho_a \cdot \bar{v} = 4.056 \text{ s}^{-1} \quad (3.125)$$

Let us assume a radio range of $r = 200 \text{ m}$. Consequently, the expected node degrees of a node with respect to lanes A and B can be determined:

$$E\{D\}_a = 2r\rho_a = 48 \quad (3.126)$$

$$E\{D\}_b = 2r\rho_b = 4 \quad (3.127)$$

The protocol specifies that upon every topology change, a routing message shall be transmitted. We have argued above that the topology change rate is the link generation rate plus the link break rate, which are assumed to be equal here. Therefore, a node on lane A will transmit a routing message at a rate of $2\Lambda_a$ and receive $2\Lambda_a \cdot E\{D\}_a$ messages from other vehicles on lane A that are in range. Also, it will receive $2\Lambda_b \cdot E\{D\}_b$ messages from vehicles in range on lane B. The total message rate is then:

$$\lambda = 2\Lambda_a(1 + E\{D\}_a) + 2\Lambda_b \cdot E\{D\}_b \quad (3.128)$$

$$\approx 66 \text{ s}^{-1} \quad (3.129)$$

Depending on the protocol, the routing messages can have various sizes. For simplicity, let us assume that the total message size including all headers is 100 B and the medium offers a data rate of 6 Mbit/s. The total offered traffic from routing messages is thus:

$$g = 66 \text{ s}^{-1} \cdot \frac{100 \text{ B}}{6 \text{ Mbit/s}} \approx 0.01 \quad (3.130)$$

This means that approximately one percent of the channel capacity will be occupied by routing information. The number does not seem very high, but — as we will discuss in the next chapter — it is a significant amount of traffic. Furthermore, we have only considered one lane per direction; the presence of two lanes in each direction (the usual geometry on highways) doubles the traffic.

3.7. Conclusion

In this section, we have discussed various channel models and presented a mathematical formalism that captures the individual properties of these models. We have then introduced the basics of vehicular traffic flow theory and discussed the fundamental diagram and various models thereof. We have discussed how traffic flow Q , traffic density ρ , and vehicle speed v are related.

Using traffic flow theory as a mobility model and combining it with an appropriate channel model, we have presented an analytical framework that relates important parameters of the road traffic to networking parameters. We have outlined the defining states of traffic flow, free-flow and congestion and the transition phase between these two states. Then, we have derived a mathematical framework that allows to relate ρ to the node degree d and its distribution for all traffic states in a rather straight-forward manner. Using some simple scenarios, we have pointed out some issues with node degree, including the isolation and leafnode probability, discussed the impact of equipment ratio and the dispersion of node degrees. Through the fundamental diagram, a relation between the average vehicle speed and the expected node degree has been established and the consequences have been discussed.

We have then presented a geometry-based model that allows for the computation of the distribution of connection durations $f_T(t)$ according to the situation's geometry and velocity distributions. We have discussed typical results for both oncoming traffic and overtaking situations in highway scenarios and consequences for wireless connections. Also, we have discussed mathematical issues related to the connection duration distribution function, especially related to the non-existence of the distribution function's moment generating function. Furthermore, we have discussed how adjusting the radio range could help enabling sensible communication in oncoming traffic scenarios that typically have very short communication durations. Finally, we have extended our considerations from the V2V to the V2I situation. The relation between connection duration and traffic density has been established by means of representative scenarios.

The last section of the chapter discusses the rate Λ at which new links are generated and at which links break and related this rate to the node degree and the connection duration through Little's Law. Starting from the consideration of a V2I scenario in which the relation of Λ to the traffic flow, Q , was established we have generalized the formula to a V2V scenario. In the discussion, we have presented typical rates for highway and urban settings. An exemplary situation has been discussed showing that the topology change rate is the sum of the link generation and the link break rate and we have argued how the topology change rate determines the teletraffic caused by routing messages in the network.

The formulas and numbers derived in this section are suitable to describe the overall connectivity properties of a vehicular network and shall form the basis of the data teletraffic engineering methods that we will introduce in the next chapter. They are summarized in Table 3.4.

Traffic Theory	
Traffic Density	ρ [km ⁻¹]
Average Velocity	$v(\rho)$ [m/s]
Traffic Flow	$Q(\rho) = \rho \cdot v(\rho)$ [s ⁻¹]
<hr/>	
Section-Based Model	
Average Velocity	$V_e(\rho(x, t)) = \frac{Q_e(\rho(x, t))}{\rho(x, t)} = \begin{cases} v_0 & \text{if } \rho \leq \rho_c \\ \frac{1}{T} \left(\frac{1}{\rho} - l_e \right) & \text{if } \rho_c < \rho \leq \rho_j \end{cases}$
<hr/>	
Node Degree	
Headway Process	$f_{H, f}(h) = \rho \exp(-\rho h)$ (free-flow), $f_{H, c}(h) = \frac{32\rho^2}{\pi^2} h^2 \exp\left(-\frac{4\rho^2}{\pi} h^2\right)$ (congestion)
Expected Headway	$E\{H_f\} = \frac{1}{\rho}$, $E\{H_c\} = \frac{1}{\rho}$
Radio Range	r [m]
Expected Node Degree	$E\{D\} = 2\rho r$
<hr/>	
Connection Duration	
Geometry	$s_r = 2\sqrt{r^2 - (x_x \sin \varphi - x_y \cos \varphi)^2}$
Differential Velocity Distribution	$V \sim \mathcal{N}(\bar{v}, \sigma)$
Connection Duration	$f_T(t, \bar{v}, \sigma, s_r) = \begin{cases} 0 & \text{if } t < 0 \\ \frac{s_r}{t^2} \frac{1}{\sqrt{2\pi\sigma^2}} \left(\exp\left(-\frac{1}{2} \frac{(s_r - \bar{v}t)^2}{\sigma^2 t^2}\right) + \exp\left(-\frac{1}{2} \frac{(s_r + \bar{v}t)^2}{\sigma^2 t^2}\right) \right) & \text{if } t \geq 0 \end{cases}$
Median Duration	$\tilde{t} = \frac{s_r}{\bar{v}}$
Radio Range Dimensioning	$s_r = t(\bar{v} - \sqrt{2}\kappa\sigma)$
<hr/>	
Link Generation and Link Break Rate	
Link Generation Rate	$\Lambda = \frac{E\{D\}}{E\{T\}} \leq \frac{E\{D\} \cdot E\{V\}}{s_r}$

Table 3.4.: Relevant formulas derived in this chapter.

4. QoS Analysis and Provisioning in Vehicular Ad-Hoc Networks

In the previous chapter, we have discussed three fundamental connectivity properties of vehicular networks: node degree, connection duration and topology dynamics. These insights have mainly arisen from the consideration of connection probabilities between two nodes. In this chapter, we extend the meaning of connectivity to describe the communication relations between a subset of nodes in a potentially infinitely large network and we shall focus on the particular characteristics of wireless networks.

It has been demonstrated early [Tob74, KL75, KT75] that for all random access MAC schemes, there exists a relation between the teletraffic offered to the medium and the collision (i.e., packet loss) probability. One consequence of an increase of collisions is a decrease of a network's throughput due to packets rendered useless. The other consequence is that if acknowledged transmissions are to be implemented, the delay a packet experiences (caused by — possibly several — necessary re-transmissions) before it is successfully received increases with increasing collisions. Throughput, packet loss and packet delay are today commonly subsumed under the label Quality of Service (QoS).

In this chapter, we will demonstrate how QoS can be attained and even guaranteed in arbitrarily connected networks. In contrast to previous works, we will not try to adapt an existing MAC scheme to our needs or even design a new scheme; instead, we introduce a mechanism that controls the amount of traffic offered to the medium. As a matter of fact, the choice of a particular MAC scheme is not important for our reasonings; rather, we demonstrate how the relevant protocol properties can be described and consequently studied. Although we will make a certain choice of MAC schemes for illustrative reasons, the methods used and mechanisms introduced in this chapter can ultimately be applied to any contention-based scheme¹. We will start our considerations for a situation in which either one central node or all distributed nodes have global knowledge about the network's connectivity. Then, we demonstrate how our QoS algorithm may be implemented in a decentralized manner, with only minimal local connectivity information. Finally, we will discuss how applications can be selected from a set of applications and even parameterized, utilizing cross-layer information from the QoS algorithm. Some of the material in this chapter has been published in [Nag10a].

To avoid ambiguity, the term “traffic” in this chapter refers to data being exchanged between networked nodes.

4.1. Related Work

With the advent of affordable and powerful computers in the seventies, it became necessary to interconnect host computers and remote terminals. Soon it was realized that because of

¹The mechanism is implicitly included in reservation-based schemes.

the bursty data generation process at the terminals as well as that of the host computer, only a fraction of the available data rate of circuit-switched connections is used. Consequently, random access mechanisms were invented in which a number of users share one channel. Due to the multiplexing of a large number of users generating bursty traffic, the resulting combined traffic (in the optimal case) is smoothed. Because of the non-deterministic nature of data generation, collisions on the channel may occur and recovery procedures are necessary to avoid data loss. Consequently, it is not possible for a random access scheme to achieve the maximum throughput of a channel.

General analysis of the throughput of (slotted) ALOHA and CSMA schemes can be found in the pioneering papers [KT75, Abr77], in which the authors study the performance of the protocols in terms of collision (packet loss) probability, resulting throughput and retransmission delays. The concept of “hearing graphs” (i.e., connectivity matrices) was introduced in [Tob74, TK75] to analyze the effect of hidden terminals, but was not applied to traffic dimensioning problems. We will discuss relevant work related to MAC protocols in Section 4.3.

Quite early it was realized that it is desirable to achieve or even guarantee a certain throughput and/or bounded delay to individual users. In [LK75], the authors propose various dynamic control procedures to ensure stable operation of slotted ALOHA systems. It is shown that optimal traffic control policies exist that can maximize the stationary channel throughput and at the same time minimize the average packet delay. However, the proposed procedures require state information about the channel that are not known a priori and must consequently be estimated. To a certain extent, this paper can be regarded as the first work dedicated to QoS provisioning over random access network.

In the following years, a large number of MAC protocols have been presented that could provide users and applications with QoS under certain scenarios, the most prominent example being the relatively new 802.11e standard for wireless local area networks. Other approaches can be found at the network layer, such as IntServ (RSVP) and DiffServ. These extension to the Internet Protocol (IP) control the routing and queueing procedures that guide a packet through the network. As for DiffServ, it provides only a framework to differentiate traffic into various classes; it does not specify how labeled packets should be treated along the path and therefore it is difficult to predict the actual end-to-end behavior of a connection. The idea to have applications differentiate and prioritize their traffic, however, is crucial and prerequisite to all QoS approaches throughout the whole networking stack.

The idea of limiting the rate at which messages are sent to the network is not entirely new. The authors of [Inz04] suggest traffic control mechanism that are based on a number of delay, bandwidth and packet-loss metrics instead of simply fair and/or flexible bandwidth management. The proposed mechanism, however, is based on the channel state and is thus not deterministic. The same holds true for the traffic shaper proposed by the authors of [BKSM06], that uses the current throughput and number of frame retransmissions as inputs. In [WR05], the authors provide a utility-based packet forwarding and congestion control scheme that works on top of the IEEE 802.11 MAC protocol and is focused on non-safety applications. Other authors have argued that this approach needs the road to be segmented into sections for calculating the message utility metric, thus it cannot be used directly in the context of safety applications. In [ZGZC09], the authors suggest a cross-layer design that jointly addresses the problems of rate control, medium access and routing for unidirectional flows in routed networks. Unfortunately, their approach requires its own MAC protocol and is thus not generally applicable.

We will discuss further related work throughout the chapter where appropriate.

4.2. Network Model

Assuming that we have a connected ad-hoc network, let $\mathcal{V} = \{v_1, \dots, v_n\}$ denote the set of nodes (i.e., the set of radios) and let $n = |\mathcal{V}|$ be its cardinality. Let \mathcal{E} be the set of connections between the nodes: a tuple $(v_i, v_j) \in \mathcal{E}$ indicates that the nodes v_i and v_j are connected.

In the previous chapter, we have defined connectivity between two nodes v_i and v_j as a result of the attenuation between them (Equation 3.4). Attenuation itself depends on the physical positions of the two nodes, \mathbf{x}_i and \mathbf{x}_j , as well as on their radio environment, described by means of an appropriate channel model, $\chi(\mathbf{x}_i, \mathbf{x}_j)$.

Note that the channel model determines the probability that a connection exists between two nodes; in this chapter, however, we study the connectivity properties of actual static realizations of a network. Consequently, a pair of nodes is either connected or not; therefore, we define the connection probability obtained from the channel model as the average over an infinite amount of realizations:

$$P((v_i, v_j) \in \mathcal{E}) = \chi(\mathbf{x}_i, \mathbf{x}_j) \quad (4.1)$$

4.2.1. Connectivity Matrix

The network's graph $G := (\mathcal{V}, \mathcal{E})$ can also be described through its *connectivity matrix* $\mathcal{C}(G) = (c_{ij})^2$, where

$$c_{ij} = \begin{cases} 1 & \text{if } (v_i, v_j) \in \mathcal{E} \\ 0 & \text{otherwise} \end{cases} \quad (4.2)$$

In our considerations, we assume that the links in the network are always bidirectional, i.e. that if node v_i is connected to node v_j , node v_j is also connected to node v_i . Because of this assumption, the connectivity matrix is symmetric:

$$c_{ij} = c_{ji} \quad (4.3)$$

Hypergraph Notation

In contrast to a fixed network in which individual links may be technically realized as dedicated links, the broadcast nature of the shared wireless channel causes *one* message to be received by *all* adjacent nodes of the sender *at the same time*. Consequently, when studying wireless networks, we should consider their representation as a hypergraph H , i.e., a generalized graph in which edges are ordered pairs of sets (hyperarcs) rather than tuples: $H := (\mathcal{V}, \mathcal{A})$. A hyperarc a is a pair of a set of senders \mathcal{S} and a set of receivers \mathcal{R} :

$$a = (\mathcal{S}_a, \mathcal{R}_a) \in \mathcal{A} \quad (4.4)$$

$$\mathcal{S}_a \cap \mathcal{R}_a = \emptyset \quad (4.5)$$

The type of relation between the nodes is a one-to-many relation, but there are two perspectives:

²The adjacency matrix of the graph: $\mathcal{C}(G) \in \{0, 1\}^{n \times n}$.

- Every singular sender has a set of receiving nodes, represented by an associated hyperarc from the one sender to the set of receivers. The set of send hyperarcs \mathcal{A} is thus:

$$\forall v_i \in \mathcal{V} : (\{v_i\}, \mathcal{R}_i) \in \mathcal{A} \quad (4.6)$$

- Every receiver has a set of senders that it hears, represented by an associated hyperarc from a set of senders to the one receiver. The set of receive hyperarcs \mathcal{A}' is thus:

$$\forall v_j \in \mathcal{V} : (\mathcal{S}_j, \{v_j\}) \in \mathcal{A}' \quad (4.7)$$

The cardinality of the vertex and edge sets is:

$$|\mathcal{A}| = |\mathcal{A}'| = |\mathcal{V}| \quad (4.8)$$

The traditional network representation $G := (\mathcal{V}, \mathcal{E})$ can be transformed into $H := (\mathcal{V}, \mathcal{A})$:

$$\forall a = (\{v_i\}, \mathcal{R}_i) \in \mathcal{A} : (v_i, v_j) \in \mathcal{E}, \text{ if } v_j \in \mathcal{R}_i \quad (4.9)$$

$$\forall a' = (\mathcal{S}_j, \{v_j\}) \in \mathcal{A}' : (v_i, v_j) \in \mathcal{E}, \text{ if } v_i \in \mathcal{S}_j \quad (4.10)$$

Let i denote the row index and j the column index of the connectivity matrix $\underline{\mathbf{C}}$. According to the definition of connectivity in Chapter 3, c_{ij} is one if v_i can transmit to v_j . Therefore, a one in a row i indicates membership in \mathcal{R}_i ; the rows of the connectivity matrix can thus be understood as a representation of the set of send hyperarcs \mathcal{A} . On the other hand, a one in a column j indicates membership in \mathcal{S}_j ; thus, the columns represent the set of receive hyperarcs \mathcal{A}' .

Because of the link symmetry (Equation (4.3)), we can state that

$$\forall v_i \in \mathcal{V} : (\{v_i\}, \mathcal{R}_i) \in \mathcal{A}, (\mathcal{S}_i, \{v_i\}) \in \mathcal{A}' : \mathcal{R}_i = \mathcal{S}_i \quad (4.11)$$

4.2.2. Traffic Vector

Traffic theory commonly uses the term *offered traffic* as “a measurement for the total number of attempts to seize a group of servers”. In other words, offered traffic measures the amount of traffic that would be carried by the network (the servers, in our context) if the network had unlimited capacity.

In the following, we denote the traffic that is generated by a node v_i and subsequently sent to the network as “(sourced) traffic” s_i . The term refers only to the traffic for which v_i is the actual source. Generally³, let λ be the message generation rate in s^{-1} , l the message length in bit, and R the data rate at which the message is sent, then the sourced traffic s is:

$$s = \lambda \cdot \frac{l}{R} \quad (4.12)$$

The accumulated sourced traffic of the nodes that share a common segment of the medium shall be denoted as “the (cumulated) load” throughout this chapter. We have already stated that wireless networks share a common medium, the wireless channel, among the network’s

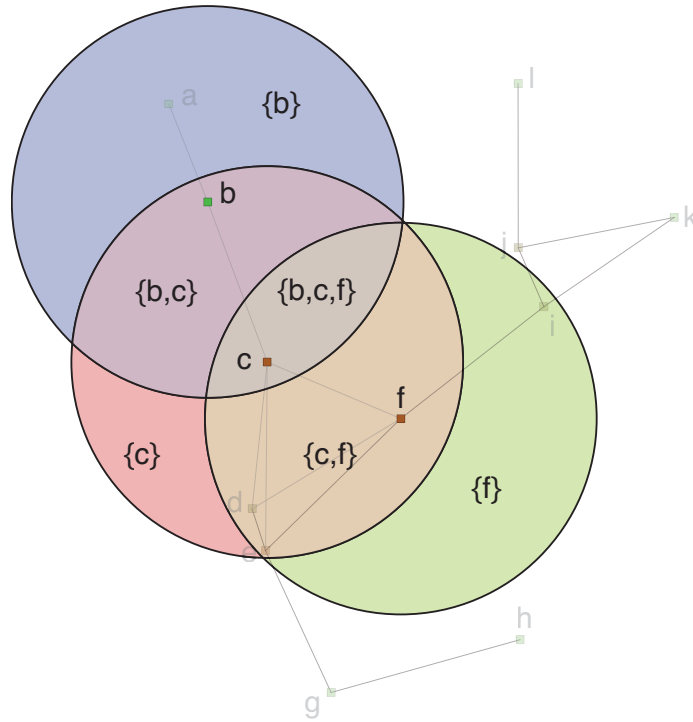


Figure 4.1.: Exemplary network. The radio ranges are indicated for nodes B, C, and F.

nodes. It is, however, relevant to understand that there exists a number of different “segments” of the wireless network that are determined by the network nodes that are in range and actually make use of that network segment.

As a convention, we define network segments according to the set of receive hyperarcs \mathcal{A}' and we shall in the following denote these segments the *collision domains*. At a node $v_j \in \mathcal{V}$, the medium is shared between v_j and the nodes that v_j can hear, i.e. the nodes in the set \mathcal{S}_j .

The cumulated load is then the sum of the traffic for which the nodes in \mathcal{S}_j are sources, plus the traffic for which v_j is the source. We denote the load as u_j :

$$u_j = s_j + \sum_{v_i \in \mathcal{S}_j} s_i \quad (4.13)$$

$$= s_j + \sum_{i=0}^N c_{ij} \cdot g_i \quad (4.14)$$

Let \mathbf{u} denote the load vector where u_i is the cumulated load at node v_i 's collision domain. The vector \mathbf{s} denotes the source traffic vector where s_i is the traffic sourced into the network by node v_i . Then, the vector:

$$\begin{aligned} \mathbf{u} &= \mathbf{C}^T \mathbf{s} + \mathbf{s} \\ &= (\mathbf{C}^T + \mathbf{I}) \mathbf{s} \end{aligned} \quad (4.15)$$

³... and thus omitting the appropriate node indices ...

is the vector that represents the cumulated load (total traffic offered to the medium) at each node's collision domain. We will use this representation throughout the remainder of this chapter.

Example

In Figure 4.1, an exemplary network is shown. The radio ranges of nodes B, C, and F have been highlighted. The network can be described as a hypergraph:

$$\mathcal{V} = \{a, b, c, d, e, f, g, h, i, j, k, l\} \quad (4.16)$$

$$\mathcal{A} = \{(\{a\}, \{b\}), (\{b\}, \{a, c\}), (\{c\}, \{b, d, e, f\}), (\{d, \}, \{c, e, f\}), (\{e\}, \{c, d, f, g\}), \quad (4.17)$$

$$(\{f\}, \{c, d, e, i\}), (\{g\}, \{e, h\}), (\{h\}, \{g\}), (\{i\}, \{f, j, k\}), (\{j\}, \{i, k, l\}), \quad (4.18)$$

$$(\{k\}, \{i, j\}), (\{l\}, \{j\})\} \quad (4.19)$$

$$\mathcal{A}' = \{(\{b\}, \{a\}), (\{\mathbf{a}, \mathbf{c}\}, \{\mathbf{b}\}), (\{\mathbf{b}, \mathbf{d}, \mathbf{e}, \mathbf{f}\}, \{\mathbf{c}\}), (\{\mathbf{c}, \mathbf{e}, \mathbf{f}, \}, \{\mathbf{d}\}), (\{\mathbf{c}, \mathbf{d}, \mathbf{f}, \mathbf{g}\}, \{\mathbf{e}\}), \quad (4.20)$$

$$(\{\mathbf{c}, \mathbf{d}, \mathbf{e}, \mathbf{i}\}, \{\mathbf{f}\}), (\{\mathbf{e}, \mathbf{h}\}, \{\mathbf{g}\}), (\{\mathbf{g}\}, \{\mathbf{h}\}), (\{\mathbf{f}, \mathbf{j}, \mathbf{k}\}, \{\mathbf{i}\}), (\{\mathbf{i}, \mathbf{k}, \mathbf{l}\}, \{\mathbf{j}\}), \quad (4.21)$$

$$(\{\mathbf{i}, \mathbf{j}\}, \{\mathbf{k}\}), (\{\mathbf{j}\}, \{\mathbf{l}\})\} \quad (4.22)$$

The load at the collision domains of node B, C, D, E, and F can be computed by summing up the traffic sourced by the nodes that are senders to them:

$$u_b = s_a + s_b + s_c \quad (4.23)$$

$$u_c = s_b + s_c + s_d + s_e + s_f \quad (4.24)$$

$$u_d = s_c + s_d + s_e + s_f \quad (4.25)$$

$$u_e = s_c + s_d + s_e + s_f + s_g \quad (4.26)$$

$$u_f = s_c + s_d + s_e + s_f + s_i \quad (4.27)$$

$$\quad (4.28)$$

In matrix-vector notation, the load vector \underline{u} can be computed from the connectivity matrix \underline{C} and the source vector \underline{s} :

$$\begin{bmatrix} u_a \\ u_b \\ u_c \\ u_d \\ u_e \\ u_f \\ \vdots \end{bmatrix} = \underbrace{\begin{bmatrix} 1 & 1 & 0 & 0 & 0 & 0 & 0 & \dots & 0 & \dots \\ 1 & 1 & 1 & 0 & 0 & 0 & 0 & \dots & 0 & \dots \\ 0 & 1 & 1 & 1 & 1 & 1 & 0 & \dots & 0 & \dots \\ 0 & 0 & 1 & 1 & 1 & 1 & 0 & \dots & 0 & \dots \\ 0 & 0 & 1 & 1 & 1 & 1 & 1 & \dots & 0 & \dots \\ 0 & 0 & 1 & 1 & 1 & 1 & 0 & \dots & 1 & \dots \\ \vdots & \vdots & \vdots & \vdots & \vdots & \vdots & \vdots & \vdots & \vdots & \vdots \end{bmatrix}}_{(\underline{C}^T + \underline{1})} \cdot \begin{bmatrix} s_a \\ s_b \\ s_c \\ s_d \\ s_e \\ s_f \\ s_g \\ \vdots \\ s_i \\ \vdots \end{bmatrix} \quad (4.29)$$

4.3. Medium Access Protocols

The QoS parameters throughput, packet loss and packet delay are dimensions that depend not only on the physical layer implementation of a wireless technology that basically determines the maximum attainable data rate by means of various modulation schemes, but more so on the Medium Access Control (MAC) layer implementation: The way that wireless nodes actu-

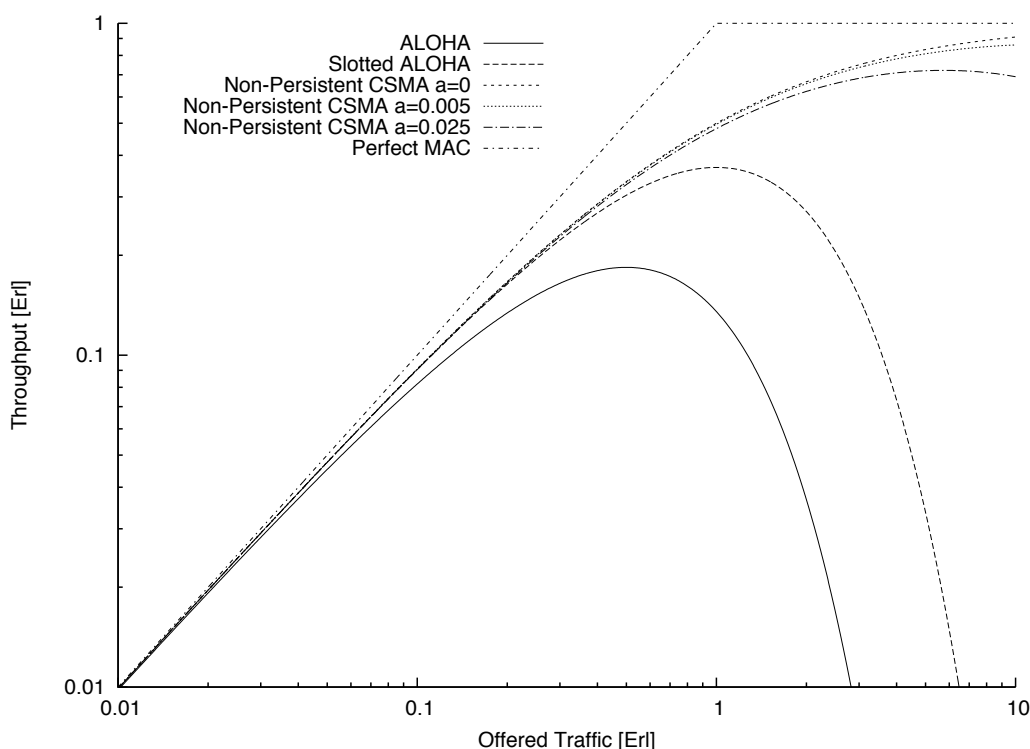


Figure 4.2.: Throughput over offered traffic.

ally access the channel has a significant impact on these parameters. All MAC protocols have to make a tradeoff between maximum throughput, simplicity of implementation, fairness, and so on. The actual performance of a protocol may depend on a number of further parameters such as the number of nodes that share the medium, the message length, message prioritization, resource allocation, susceptibility to interference, etc. It is not the aim of this section to introduce a new MAC protocol but rather to extend the connectivity analysis framework with a means for efficient modeling and consequent analysis of existent protocols.

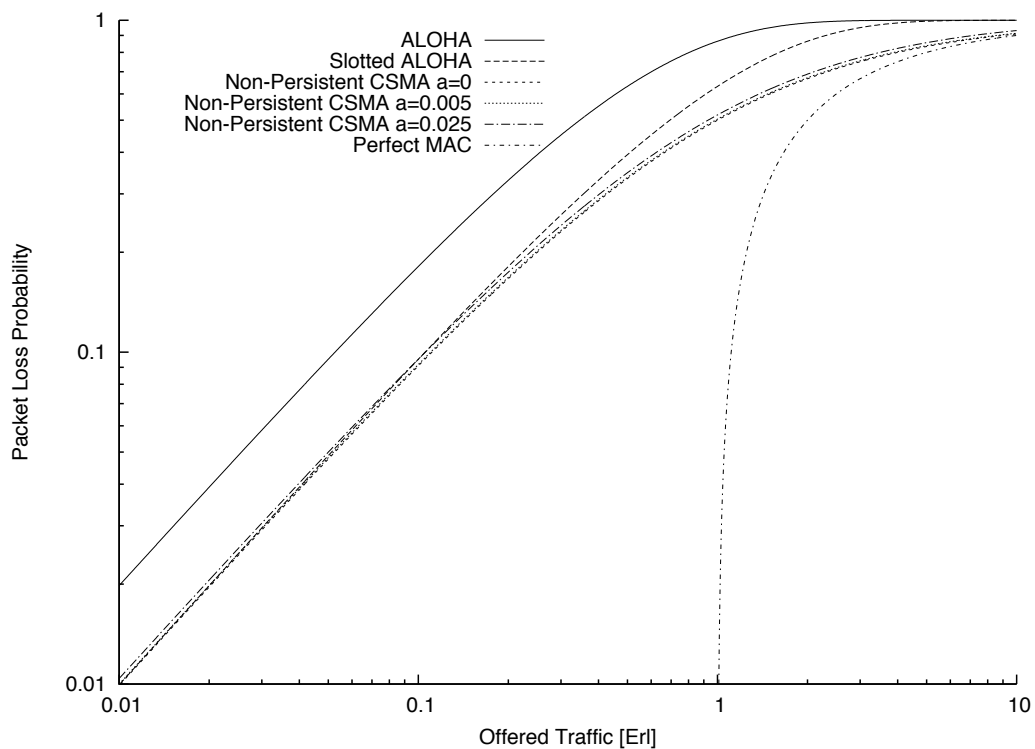
The key factor that determines the performance of a MAC protocol is the probability that a packet is successfully transmitted from the sender to the receiver(s). Aside the — protocol-dependent — parameters mentioned above, the most influential parameter is obviously the cumulated load (i.e., the sum of the individual offered traffic) in a collision domain.

Let us denote the success probability as p_s . A perfect protocol would transport every packet successfully ($p_s = 1$), until the cumulated load u exceeds the capacity $C = 1$ Erl of the wireless channel. The throughput v of the protocol is thus equal to the cumulated load and then remains at the channel capacity:

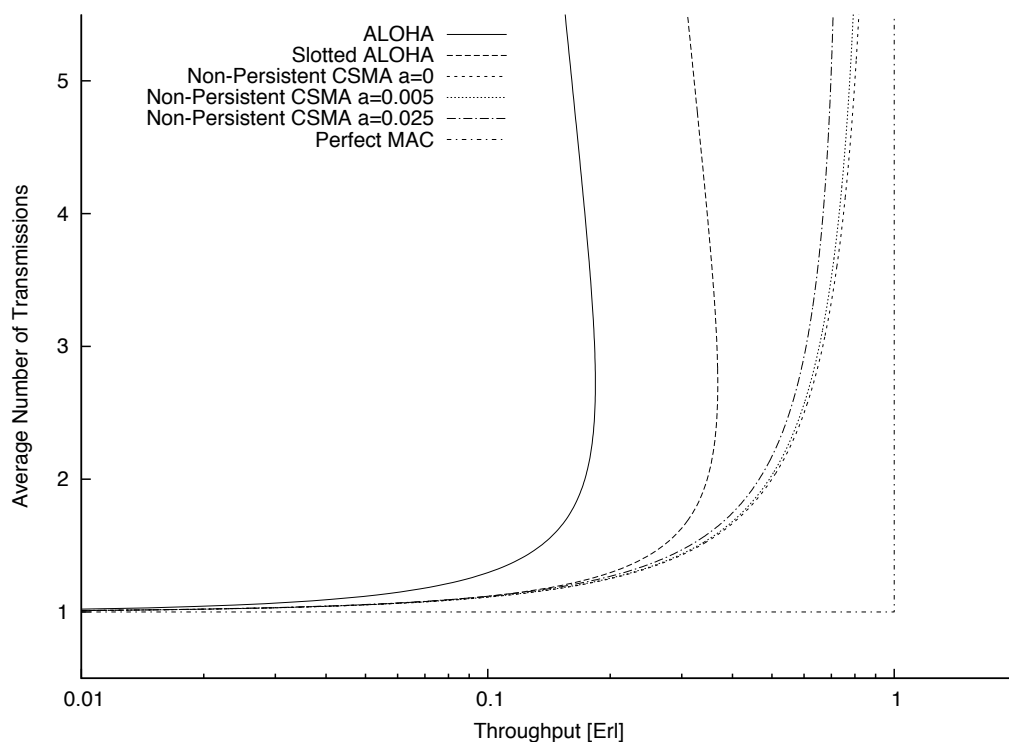
$$v(u) = \begin{cases} u & \text{if } u \leq C \\ C & \text{if } u > C \end{cases} \quad (4.30)$$

The throughput (i.e., the successfully transported traffic) for some of the protocols discussed in the following is shown in Figure 4.2; the perfect MAC performs as expected.

In the following, we require that the throughput as a function of the cumulated load $v(u)$ is known, either analytically or through simulations. Consequently, we can derive the QoS



(a) Packet loss probability



(b) Number of transmissions

Figure 4.3.: Packet loss probability and number of transmissions.

measures:

- The *packet loss probability* $p_l(u)$ is complementary to the success probability $p_s(u)$, see Figure 4.3(a). We can thus write:

$$p_l(u) = 1 - p_s(u) = 1 - \frac{v(u)}{u} \quad (4.31)$$

- The delay that a packet experiences (Figure 4.3(b)) is determined on the one hand by the amount of time that the packet has to queue before the MAC actually gets to access the channel. On the other hand, the number of necessary retransmissions until successful delivery plays an important role. In case that a protocol has a means of detecting that a packet has not been correctly transmitted, it may reschedule the packet and retry⁴. This procedure may be repeated for a number of time, until the transmission was successful or the sender gives up. However, every retry adds to the delay that the packet experiences.

Let us denote the average time until channel access as τ . Then, we can determine the average time T until the transmission is successful:

$$\begin{aligned} T &= p_s \tau + p_s(1 - p_s) \cdot 2\tau + p_s(1 - p_s)^2 \cdot 3\tau + p_s(1 - p_s)^3 \cdot 4\tau + \dots \\ &= \tau p_s \cdot \sum_{n=0}^{\infty} (1 - p_s)^n (n + 1) \\ &= \frac{\tau}{p_s} \end{aligned} \quad (4.32)$$

The *average normalized packet delay*, as a function of the cumulated load, is then:

$$\delta(u) = \frac{u}{v(u)} = \frac{1}{p_s(u)} \quad (4.33)$$

The packet delay variation is commonly denoted as *packet delay jitter*.

Over the years, a large number of MAC protocols have been proposed, and quite some have found their way into a standard. In [GL00], the authors introduce the basic concepts of wireless medium access protocols. A thorough survey, classification and analysis of 34 MAC protocols can be found in [JLB10]. For further reading, the said publications should be considered as starting points.

In this section, we present very selected, fundamental protocols, classify them in three families and discuss their properties relevant for the further considerations. The families of collision recovery protocols and collision avoidance protocols can be grouped together and constitute the class of *contention-based* protocols.

4.3.1. Collision Recovery Protocols

The ALOHA protocol [Abr70] is the simplest collision-based MAC protocol. A station accesses the channel immediately when a packet arrives and transmits the packet. Given the existence of an ideal, collision-free return channel, it awaits an acknowledgement from the receiver.

⁴This is probably not applicable if broadcast applications are to be deployed.

If a certain timeout expires and no acknowledgement was received, the station retries the transmission to *recover* from the collision.

Let us assume that the channel access inter-arrival times follow a poisson process, we can determine the throughput of ALOHA as:

$$v_A(u) = u \cdot \exp(-2u) \quad (4.34)$$

The ALOHA protocol was later improved by adding the rule that the channel may not be accessed at random points in time but only at the beginning of a time slot. Hence, the extended version was called Slotted ALOHA [Rob75, KL75]. The throughput is given by:

$$v_{SA}(u) = u \cdot \exp(-u) \quad (4.35)$$

Figure 4.2 shows that the maximum throughput is attained at an offered traffic of $u = 0.5$ Erl, where the throughput is $v_A(0.5 \text{ Erl}) \approx 0.18$ Erl. The packet loss probability at this point, however, is $\approx 63.2\%$ and the average number of necessary transmissions until success is about 2.72. It is remarkable that through increasing collisions, the throughput actually decreases to zero if the amount of offered traffic is increased beyond 0.5 Erl. This is called the stability criterion. The maximum throughput of Slotted ALOHA is increased to twice that of pure ALOHA (due to the shortened critical time where collisions may occur), at an offered traffic of $u = 1$ Erl: $v_{SA}(1 \text{ Erl}) \approx 0.37$ Erl. The packet loss probability at this point is equal to that of ALOHA at the throughput maximum; consequently, the number of required transmissions is equal.

In the following years, a number of protocols have been developed that build on the foundation of ALOHA, among which the R-ALOHA protocol [CRW⁺73] is most noteworthy: it unites both elements of contention and reservation. Nodes contend for time slots and, upon having successfully transmitted a message in one slot, may keep “their” slot for a certain time thus achieving reservation of a certain resource share. Its performance in terms of throughput, delay and packet loss has been studied in [Lam80]. In [BCCF03], the authors propose RR-ALOHA, a distributed, reliable, reservation-based ALOHA variant for use in mobile applications (sometimes also denoted as ADHOC MAC).

4.3.2. Collision Avoidance Protocols

The large family of Carrier Sense Multiple Access (CSMA) MAC protocols is based on the principle of sensing the medium for the existence of a carrier before starting a transmission, i.e., testing if the channel is already busy with another transmission. If so, the station defers the access to a later point in time, otherwise, it starts its transmission. This way, the protocol tries to *avoid* collisions on the channel. There are numerous different variants and a most comprehensive study (along with performance considerations) can be found in the landmark papers [KT75, TK75, TK76, TK77].

A rough classification can be made by means of the persistence:

- After the channel is found busy, p -persistent protocols continuously check the channel until it is found free. Then, it starts transmitting with a probability of p . A 1-persistent protocol, for instance, starts transmitting immediately after the channel is found unused.

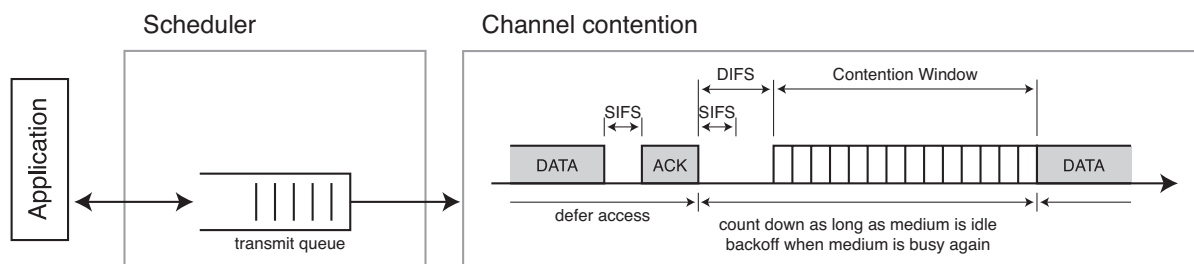


Figure 4.4.: The 802.11 DCF mechanism

- After finding the channel busy, non-persistent protocols wait a random time and then check again. This procedure is repeated until the channel is found free, then the transmission is started.

Figure 4.2 shows the throughput of non-persistent CSMA. Let a be the ratio of propagation delay to packet transmission time, then the throughput is:

$$v_{CSMA}(u, a) = \frac{u \cdot \exp(-au)}{u \cdot (1 + 2a) + \exp(-au)} \quad (4.36)$$

Clearly, CSMA has an advantage over the ALOHA schemes in terms of maximum throughput. However, as the offered traffic increases, packet loss and consequently, the number of necessary transmissions also increases.

4.3.3. 802.11(e) Distributed Coordination Function (DCF) and Enhanced Distributed Channel Access (EDCA)

The widely used 802.11 technology, IEEE's standard for wireless networks [IEE07a], has adopted a modified variant of non-persistent CSMA. Apart from an operating mode that employs a central control instance — a functionality that most devices do not implement and that is not applicable in ad-hoc networks — the standard offers a mechanism denoted as Distributed Coordination Function (DCF) that aims to reduce the percentage of packets lost due to collisions (see Figure 4.4 for illustration). Put simple, upon arrival of a new packet in the transmit queue, a random "backoff" counter is chosen if the stations finds the medium busy. The MAC then defers the access until the medium is free again (after the ACK plus the DIFS) and then decrements the counter with every free time slot; if another stations starts transmitting, the counter is stopped again. When the counter reaches zero, the station transmits the packet. A detailed description of the mechanism can be found in section 9.2.5 of the standard [IEE07a].

There exist innumerable papers on the throughput of the 802.11 MAC, therefore we shall name only some important and initial papers: The first paper to study the performance of the then-emergent standard using a simulative approach was [BFO96], which was later amended in the milestone paper [Bia00]. In this work, Bianchi introduced an analytical approach to the 802.11 DCF using a Markov model; all current analytical studies go back to this publication. However, Ho [HC96] actually first suggested a 2D finite-state Markov chain approach when he analyzed the impact of the DCF extension to CSMA and addressed the issue of hidden terminals. This topic was later taken on in [KKJ98] where the authors found that, depending on the fraction of hidden terminals, the performance of the protocol can drop very significantly.

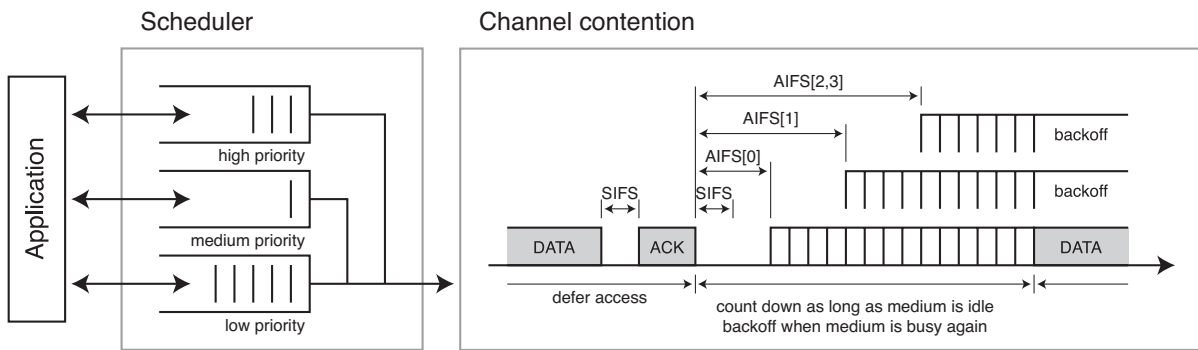


Figure 4.5.: The 802.11 EDCA mechanism

The so-called capture effect, i.e., the ability of a receiver to correctly decode a transmission in the presence of other lower-power transmissions, and the resulting capacity of the 802.11 MAC protocol in multipath-faded channels has initially been studied in [HVS02].

Recently, broadcast services (especially in the context of vehicular networks) have gained more attention and consequently some dedicated studies on the performance of 802.11 in broadcast networks were published. A performance analysis under saturation conditions was published in [MC08], in which the authors point out that the choice of the range from which the backoff counter chooses its value is critical to throughput. The used model was then extended [WAFS09] to also account for non-saturated conditions.

The EDCA of the 802.11e standard offers the possibility to differentiate traffic into four access classes, each with their own priority. To achieve this, the DCF mechanism has been modified such that decreasing the backoff counter is only allowed after variable-length AIFS times have passed. By this means, higher-priority traffic gain privileged channel access so that AC0 is served before AC1, which in turn is served before AC2 and AC3 (see Figure 4.5).

Again, a number of studies on the performance have been published. In [TFM05], the authors analyze the throughput and delay under saturation conditions and show the effectiveness of the prioritization. Using Markov chains, [HD05] presents a unified analytical model for performance analysis. Another analytical model is presented in [PPQ10] and the various model parameters are discussed to facilitate proper design for specific applications. A simulative study of the packet loss probability in vehicular broadcast network using priorities is published in [TMJH04], where the authors analyze the impact of some design parameters and show that prioritization effectively reduces packet delay. Since the EDCA mechanism was adopted for the upcoming 802.11p vehicular radio standard [IEE10], a thorough analysis of EDCA in the control channel can be found in [GMM09]. Some criticism of the EDCA has been expressed in [Eic07], where the author states that a careful choice and assignment of applications to access classes is inevitable to provide the desired QoS characteristics of the 802.11p MAC.

4.3.4. Reservation-Based Protocols

In reservation-based protocols (such as, for example, Time Division Multiple Access (TDMA)), the medium is divided into resource partitions (such as time slot, frequencies, codes, etc.) which are then assigned to the individual network nodes. Let us denote a node's share of the

medium with c (in Erl), then the throughput is:

$$v(u, c) = \begin{cases} u & u \leq c \\ c & u > c \end{cases} \quad (4.37)$$

It is clear that as long as the offered traffic is less or equal to a node's share of the channel, the protocol is ideal. If a *central* instance is available that has global (or, at least, enough) knowledge of a network's topology, it can easily compute and assign the channel shares to the individual network nodes. However, if such a system is to be implemented in a *distributed, decentralized* fashion, significant issues arise. A comprehensive study of the problem of scheduling broadcast transmissions in TDM multihop networks can be found in [ET90], in which the authors also prove that the problem is NP complete. In [You99], a self-organizing TDMA protocol is proposed that caters for bursty traffic as well as for low latency data transport through reserved channels. The authors of [KUHN03] propose an extension to that, increasing the efficiency by dynamically controlling the TDMA frame length. A slot assignment method based on a centralized genetic algorithm and the knowledge of two-hop connectivity has been studied in [NL03].

The resource allocation in reservation-based protocols is basically an edge-coloring problem: throughout the network, all transmitters adjacent to a receiver must use dedicated resources (i.e., the colors) for their transmissions (i.e., the incident edges) so that the transmissions do not collide at the receiver. According to Vizing's Theorem [Viz64], a graph with maximum node degree Δ can be colored using χ' colors (the *chromatic index* of the graph):

$$\Delta \leq \chi' \leq \Delta + 1 \quad (4.38)$$

Vizing's Theorem, however, holds for an optimal coloring of the graph. An overview and discussion of the performance of distributed edge coloring algorithms can be found in [ZHZ⁺07], where the authors state that no current distributed algorithm is capable of obtaining an optimal coloring. For their own algorithm, they assume that $\chi' = 1.25\Delta$ holds true. Consequently, we can state that if the channel's capacity is C , then the individual node shares have a capacity of:

$$c = \frac{C}{\chi'} \quad (4.39)$$

The node degree probabilities for different scenarios can be determined using the formulas described in Chapter 3.

4.3.5. Discussion

The choice of a specific MAC protocol is very much dependent on the requirements of the applications that shall be run over the network. Especially in vehicular networks, throughput may not be the most determining factor. For example, many control algorithms have been shown to function well, even under severe packet loss, as long as delays are bounded.

Some factors that may influence the decision for a certain MAC protocol are listed in Table 4.1 and shall be discussed here:

Collision recovery protocols (such as ALOHA and slotted ALOHA) are rather easy to implement. Especially in the context of vehicular networks, when external timing information such as GPS devices are available, time synchronization is easily achieved. Apart

	Collision Recovery ALOHA, slotted ALOHA	Collision Avoidance CSMA, 802.11	Reservation-Based TDMA
Complexity	Low	Medium	High
Time Synchronization	Not Needed (unslotted) / Mandatory (slotted)	Not Needed	Mandatory
Mobility Support	Good	Good	Problematic
Scalability	Good	Good	Limited
Channel Usage Efficiency	Low – Medium	High	High (depending on application)
Reliability	Low	Medium	High
Susceptible to Hidden Terminals	No	Yes	No
Delay Characteristics	Deterministic	Probabilistic	Deterministic

Table 4.1.: Some characteristics of MAC protocol families.

from that, no further synchronization or interaction with other radios is required. Therefore, these schemes do not require any adaptation to support mobility. The channel usage efficiency, as shown above, is low (≈ 0.18 Erl) to medium (≈ 0.37 Erl) depending on the scheme. The great advantage of (slotted) ALOHA, however, is that it is not susceptible to hidden terminals and that it offers deterministic delays: upon arrival of a new packet, the channel is either immediately accessed or at the beginning of the next slot. The outcome of the transmission, however, is rather unreliable.

Collision avoidance protocols (such as CSMA or 802.11) are more complex than collision recovery protocols, as they require queues and the additional carrier sense mechanism. This very mechanism also makes their performance susceptible to hidden terminals which can reduce their performance significantly, even well below that of slotted ALOHA (see for instance [TK75, KKJ98]). Especially in vehicular scenarios, this effect may be significant and can render the additional complexity pointless. In scenarios with a low percentage of hidden nodes and only a few contending stations, however, the channel usage efficiency can be quite high and the reliability of transmissions is good. The major drawback of this family of protocols, however, is that their delay characteristic is non-deterministic: depending on the back-off strategy, the time between packet generation and the actual transmission may vary greatly. Scalability (to a certain extent) and mobility support, however, are good.

Reservation-based protocols (such as TDMA) are most complex to implement, especially if there is no central entity that assigns the resources to the individual network nodes. For TDMA, time synchronization among nodes is crucial for obvious reasons. The changing network topology, especially in vehicular scenarios, imposes great requirements on the resource distribution mechanism. In the same way, the scalability of these networks is constricted as the administrative effort for resource management increases more than linearly with the number of network nodes. The throughput efficiency is high for continuous traffic and low for bursty traffic; a careful consideration of the suitability of such a protocol should thus be made with respect to the desired applications. Reservation-based protocols, on the other hand, have significant benefits over the other protocols: because contention for resources is not necessary and every node has a guaranteed share of the medium, the reliability of transmission is very high and the delay characteristics are absolutely deterministic.

Special respect should also be paid to the type of communication relations: in case that broadcast applications are to be deployed, ALOHA schemes may have an advantage over CSMA schemes due to infeasible packet-level acknowledgements. Depending on the node degrees in the network and the chosen backoff interval, CSMA schemes will not perform better than ALOHA in terms of packet loss and still reveal non-deterministic delays (see [MC08] for a detailed study of these effects).

The delay distributions of slotted ALOHA and CSMA in unicast scenarios and a comparison of the two schemes can be found in [YY03]. The global throughput of obstacle-free multi-hop network using ALOHA and CSMA has been studied in [MSQT04]. Other interesting conclusions are drawn in a recent study [KJ08], in which the authors conclude that in networks with low densities, ALOHA outperforms CSMA. For higher densities, however, the situation reverses. Knowing the density and the structure of a network, these findings raise the question if a dynamically parameterized MAC layer protocol could be sensible.

Thorough overviews of existing MAC protocols with an explicit emphasis on the deployment

in vehicular networks are presented in [MFL06, SK08], in which the authors review design choices and compare various technologies.

4.4. Providing QoS in Contention-Based Networks

In this section, we assume that a contention-based MAC protocol has been chosen for deployment. In the desire to provide applications with a pre-defined QoS, it is now necessary that the application designer specifies at least one of the following QoS parameters:

- Maximum tolerable average packet loss: Using Equation 4.31, the traffic limit \hat{u} for the candidate MAC mechanism can be determined.
- Maximum tolerable average delay: With Equation 4.33, the traffic limit \hat{u} can be determined.

If the cumulated load \underline{u} in all collision domains is below the determined load limit \hat{u} , the desired QoS is attained. The QoS criterion is thus (Equation (4.15)):

$$\hat{u} \mathbf{1} \leq (\underline{\mathbf{C}}^T + \underline{\mathbf{I}}) \underline{\mathbf{s}} \quad (4.40)$$

As we have described in the previous section, the traffic vector $\underline{\mathbf{s}}$ comprises *all* traffic that is generated by the individual nodes (i.e., unicast, multicast, and broadcast traffic) due to the broadcast nature of the wireless medium.

To fulfill the QoS criterium given the current network connectivity $\underline{\mathbf{C}}$, a control algorithm shall be designed that determines a traffic vector $\underline{\mathbf{s}}$ that (in Equation 4.40):

- guarantees that the load in every collision domain is bounded: $\forall i : u_i \leq \hat{u}$, (R1)
- maximizes the traffic s_i that may be sourced by each node, (R2)
- allocates the amount of traffic sourced so that a fairness criterion among contending nodes is met (R3).

There are several ways of obtaining $\underline{\mathbf{s}}$: either, a central instance with global knowledge of the network could compute a global $\underline{\mathbf{s}}$ and then distribute it to the nodes. Or, the nodes themselves could — through exchanging the appropriate bits of information — compute their own s_i . The dynamically computed s_i shall then be used at the nodes to control their traffic, so that the pre-defined QoS is attained throughout the network.

Obviously, in a purely decentralized ad-hoc scenario, the latter approach is more desirable as infrastructure with global network knowledge is not available. Furthermore, the exchange of messages with a central entity would either introduce additional messaging overhead or require additional communication hardware.

4.4.1. Global Traffic Limits Determination

Although impracticable in a distributed network, a simple iterative global algorithm for benchmarking purposes is outlined in Algorithm 1. Given the vertex set \mathcal{V} and the degree vector $\underline{\mathbf{d}}^5$, the algorithm starts with those nodes that have the highest degree d_i . The QoS criterion

⁵The degree vector $\underline{\mathbf{d}}$ can be determined through:

$$\underline{\mathbf{d}} = \underline{\mathbf{C}}^T \mathbf{1} \quad (4.41)$$

Algorithm 1: Global determination of traffic source vector \underline{s}

Input: Graph's vertex set \mathcal{V} , QoS traffic threshold \hat{u}
Output: Admitted traffic vector \underline{s}

```

1  $\mathcal{V}' \leftarrow \mathcal{V}$  ▷ Copy vertex set
2 forall the  $v_i \in \mathcal{V}'$  do
3   |  $s_i \leftarrow \hat{u}$  ▷ Assign QoS threshold to all nodes
4 end
5 while  $\mathcal{V}' \neq \emptyset$  do
6   | forall the  $v_i \in \mathcal{V}'$ ,  $\max d_i$  do ▷ Select remaining nodes with maximum degree
7     |  $s_i \leftarrow \hat{u}/(d_i + 1)$  ▷ Assign fair share of threshold to these nodes ...
8     | forall the  $v_j \in \mathcal{V}'$ ,  $v_j \sim v_i$ ,  $s_j > s_i$  do ▷ ... and their neighbors
9       |  $s_j \leftarrow s_i$ 
10      | end
11      | remove  $v_i$  from  $\mathcal{V}'$ 
12    | end
13 end
    
```

is fulfilled if the traffic of all neighboring nodes plus that of the node itself does not exceed \hat{u} . Therefore, the algorithm assigns a “fair” maximum traffic of $s_i = \hat{u}/(d_i + 1)$ to the node and all its neighbors. It then continues with untouched nodes until all nodes have an assigned maximum traffic.

This algorithm is guaranteed to satisfy requirements (R1) and (R2). We will discuss the fairness requirement (R3) later.

4.4.2. Distributed Traffic Limits Determination

Let every node v_i maintain a set of direct (1-hop) neighbors, \mathcal{N}_i . This set is updated either upon receiving a message from a neighboring node v_j by adding v_j to \mathcal{N}_i or, if v_j times out (last message from j received more than τ_{out} seconds ago), by removing v_j from \mathcal{N}_i . The cardinality of \mathcal{N}_i thus corresponds to the number of direct neighbors. Sufficient information about the network's topology can now be shared among the nodes through periodically broadcasting the cardinality of the set \mathcal{N}_i so that every neighboring node v_k that receives this information can update its own set of direct neighbors, \mathcal{N}_k , and keep track of the maximum node degree of its neighbors $d_j \forall v_j \in \mathcal{N}_k$.

In short, all the information required by the algorithm is the maximum node degree of a node v_i and of all its neighbors. The idea behind this rule is that if all nodes limit the amount of traffic they source into the network so that the load at the neighbor that has the highest node degree does not exceed \hat{u} , the QoS criterion is fulfilled.

The maximum admissible traffic s_i is computed at each node i using Algorithm 2. Basically, the algorithm first determines the cardinality of the set of direct neighbors \mathcal{N}_i (number of direct neighbors) and then checks if any of the direct neighbors has a greater number of neighbors. Finally, s_i is adjusted so that the traffic threshold \hat{u} is divided by the greatest number of neighbors plus one.

Algorithm 2: Distributed determination of admissible traffic s_i

Input: Set of node's neighbors \mathcal{N}_i , Degrees of neighbors $d_j \forall v_j \in \mathcal{N}_i$

Output: Admitted traffic vector s_i

```

1  $n \leftarrow |\mathcal{N}_i|$                                 ▷ Limit traffic for local number of neighbors
2 forall the  $v_j \in \mathcal{N}_i$  do                       ▷ Go through set of neighbors
3   |  $n \leftarrow \max n, d_j$                        ▷ If neighbor has higher degree, limit traffic to that number
4 end
5  $s_i \leftarrow t_t / (n + 1)$                        ▷ Assign fair share of threshold to node

```

Despite its simplicity, the algorithm proves to be extremely efficient in realistic environments. Its specific advantages are:

- It requires minimal information about the network's topology. Information about the identity of the direct neighbors is usually easily available by monitoring ongoing transmissions. The mandatory requirement of knowing a neighbor's number of neighbors (their identities are not relevant) can easily be achieved by adding information about a node's degree to every transmitted message. This implies minimal additional overhead (some bytes) and ensures correct functioning of the algorithm. A realistic implementation, however, would usually keep track of the two-hop neighborhood topology for routing purposes, which essentially contains the same information plus the identities of two-hop neighbors.
- No negotiation with neighboring nodes is necessary and the valid traffic limit is instantaneously available at every node and with every topology update (i.e., upon receiving a message from a previously unknown node or after a neighboring node has timed out). This information can then be passed on to the higher layers of the communication system. The reliability of the system is significantly increased, since the topology information is updated regularly with every packet; no additional control message exchange is necessary that might compromise the system's performance if messages are lost.

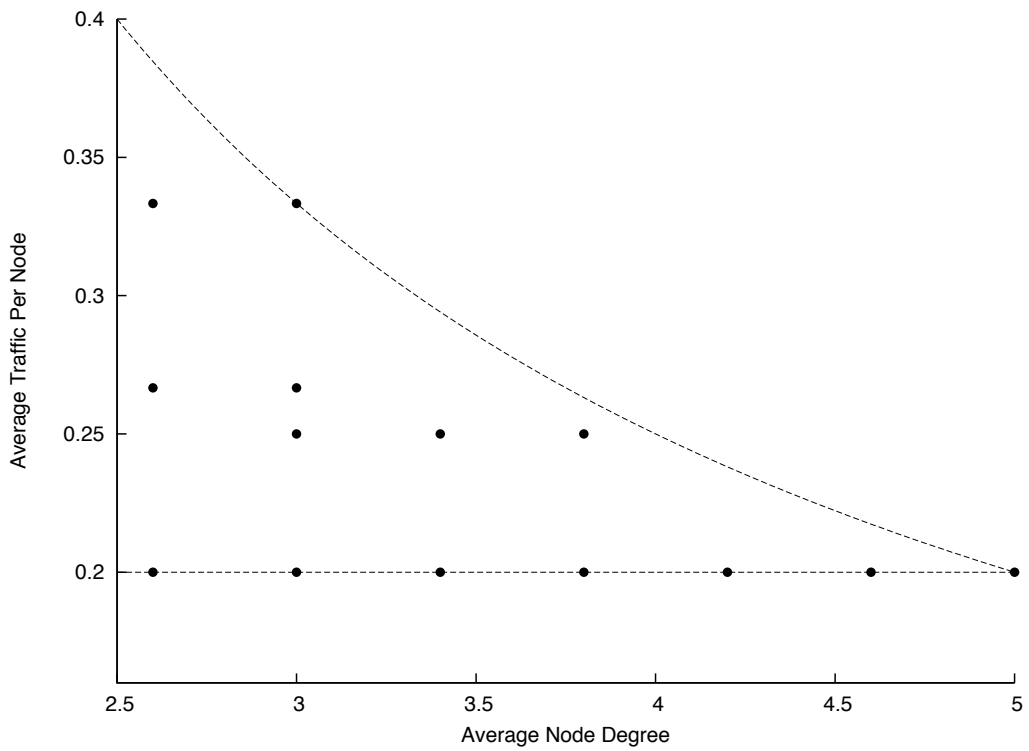
4.4.3. Admitted traffic and load distribution

The admitted traffic and the load distribution has been computed for all possible realizations of connected five- to eight-node networks. For comparison, the baseline shall be the maximum traffic threshold \hat{u} divided by the number of nodes n in the network. This corresponds to the assumption that in the worst case, all nodes are within each others radio range (i.e., the network is fully meshed):

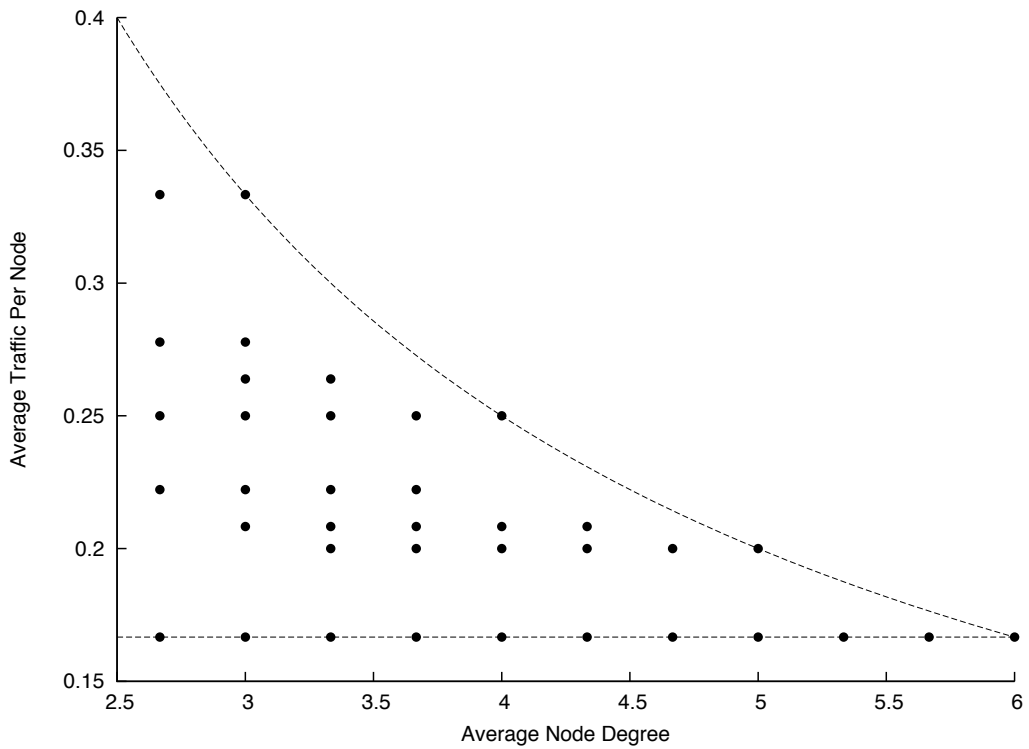
$$s_b = \frac{\hat{u}}{n} \tag{4.42}$$

Figure 4.6 depicts the admitted traffic \bar{s}/\hat{u} for all 21 (112) groups of isomorphic, connected 5-(6-) node network graphs. Note that in this discussion, the average node degree \bar{d} includes not only the number of neighbors d_i of a node i , but also the node itself. Therefore, its degree is $d_i + 1$.⁶ Also, some configurations have equal $(\bar{d}, \bar{s}/\hat{u})$ values, which is why there are only

⁶This comes from the fact that Equation 4.15 can also be written as $\underline{\mathbf{u}} = (\underline{\mathbf{C}}^T + \underline{\mathbf{I}}) \underline{\mathbf{s}}$. Therefore, the node degree corresponds to the number of ones in a node's row or column.



(a) 5-node networks



(b) 6-node networks

Figure 4.6.: Average admitted traffic per node \bar{s} (in units of \hat{u}) over average node degree \bar{d} . Upper and lower bounds are also shown (dashed lines).

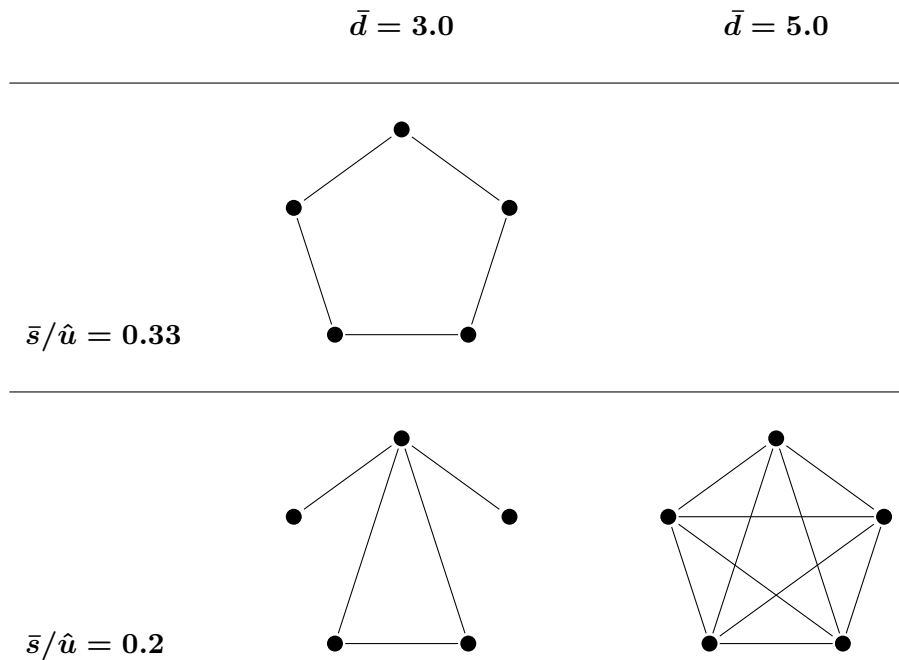


Table 4.2.: Average admitted traffic per node \bar{s} and average node degree \bar{d} for some representative network topologies.

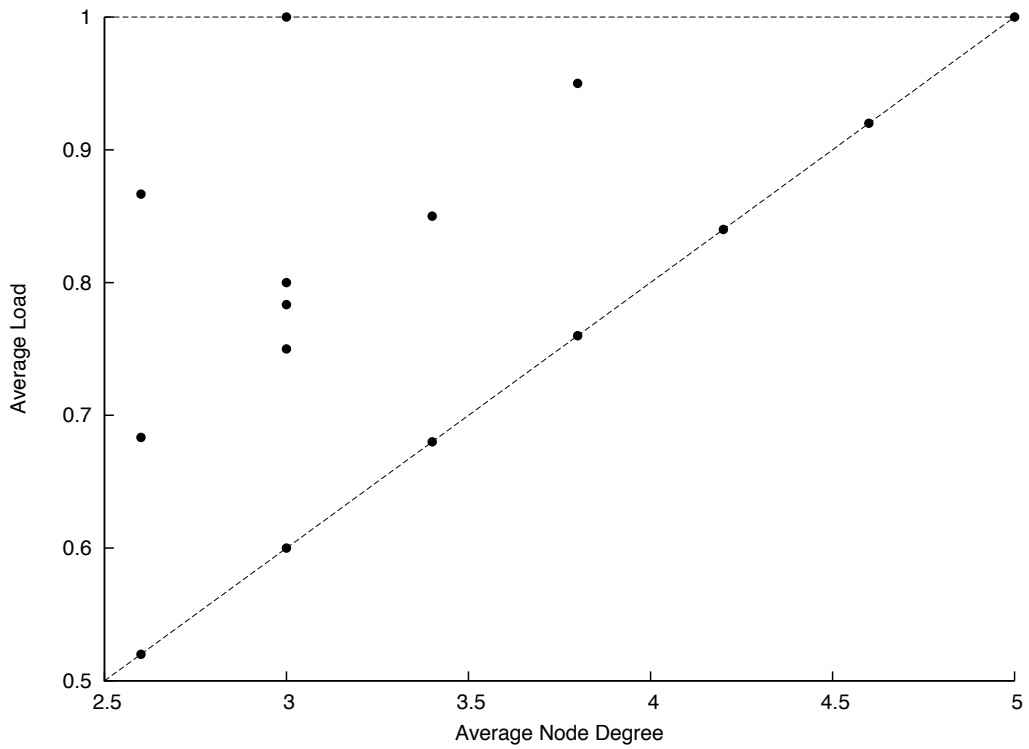
14 (37) visible data points.

The lower dashed line depicts the baseline and corresponds to networks that are either densely meshed (converging towards the fully connected network, to the right) or that have a very unfavorable configuration (to the left). The upper dashed line represents the upper bound of achievable \bar{s} , which, for the 5-node networks, is reached by one configuration. However, most configurations (9 out of 21 possible) are somewhere in between (conforming to requirement R2). This is even more apparent for the 6-node networks.

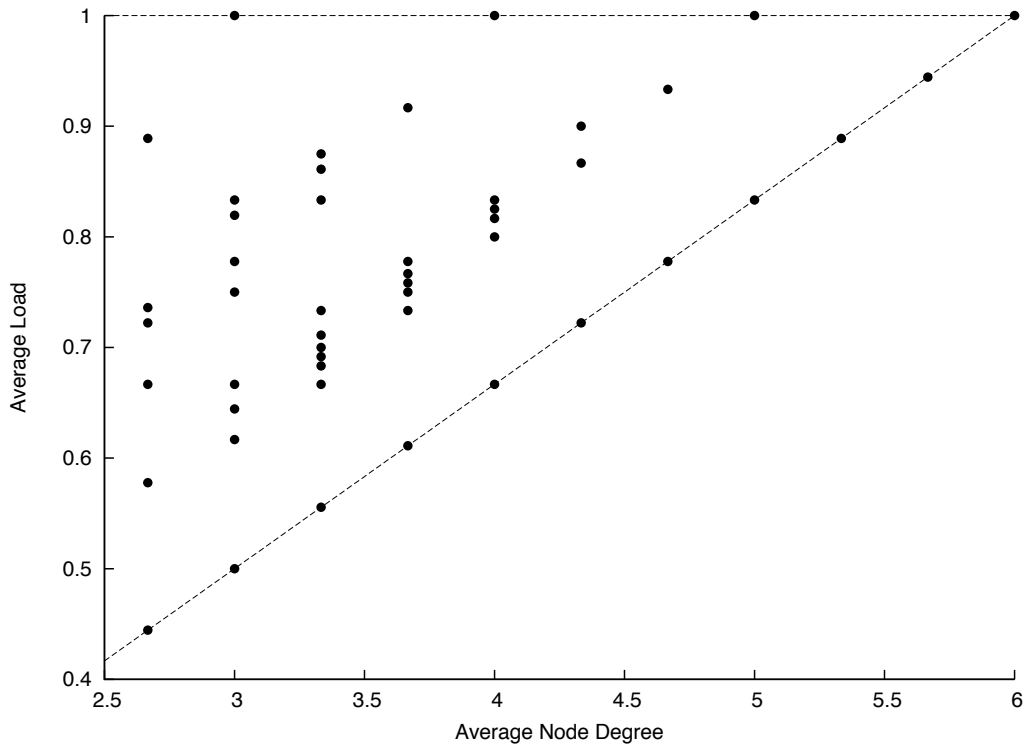
Table 4.2 shows the extreme configurations. The circular network (3.0, 0.33), due to its low and uniform node degree, achieves the “best” traffic assignment and corresponds to the data point on the upper bound. It is worth noting that circular network configurations are the best configurations in *all* n -node networks, as they are the sparsest configurations possible that yield a connected network, an upper-bound s and an upper-bound \bar{u} .⁷ The fully-connected network (5.0, 0.2), as expected, limits the baseline to the right. An interesting case, however, is the third network (3.0, 0.2): due to the fact that there is a “central” node that has connections to all other nodes in the network, this central node limits the s of all other nodes. This opens an interesting perspective: by changing only two vertices of the graph — possibly by means of topology control — the network could be transformed into the (3.0, 0.33) network. The effect is immediate: an increase of two thirds of admitted traffic s for every node.

Figure 4.7 depicts the average load \bar{u} that results from the network configuration and the corresponding source vector \underline{s} . Conforming to requirement (R1), all configurations exhibit a load of maximally \hat{u} . Consequently, \bar{u} is bounded above by \hat{u} (upper dashed line). Similarly, \bar{u} is bounded below (lower dashed line) by the product of the baseline s_b and the average node

⁷Only a circular configuration with one vertex missing (the (2.6, 0.33)-configuration) is sparser but it also has suboptimal \bar{u} .



(a) 5-node networks



(b) 6-node networks

Figure 4.7.: Average load \bar{u} (in units of \hat{u}) over average node degree \bar{d} . Upper and lower bounds are also shown (dashed lines).

network nodes	5	6	7	8
isomorphism groups	21	112	853	11117
baseline admitted average traffic per node	$\hat{u}/5$	$\hat{u}/6$	$\hat{u}/7$	$\hat{u}/8$
fraction of groups with average admitted traffic per node of...				
baseline	52.4%	30.4%	18.2%	9.4%
gain > 0%	47.6%	69.6%	81.8%	90.6%
gain \geq 33%	23.9%	31.3%	43.3%	58.2%
gain \geq 50%	9.5%	25.9%	21.8%	21.5%
gain \geq 100%	–	1.8%	1.3%	1.9%

Table 4.3.: Per-node traffic gains for various network sizes

degree. Again, the circular configuration (3.0, 0.33) shows the highest average load (upper left dot).

Table 4.3 shows the potential gains over baseline for networks of various sizes. For five-node networks, we find that roughly one half of all possible network configurations (52.4%) do not actually benefit from the presented algorithm. As networks increase in size, however, this benefit also grows significantly: for seven-node networks, more than 80% of all possible network configurations exhibit an increase of average admitted traffic, with more than 20% showing an increase of one half or more. The maximum ratio g between the baseline and the best (the circular) configuration of an n -node network is given by

$$g = \frac{n}{3} \quad (4.43)$$

Example

Consider an intersection scenario. The radio parameters have been chosen to yield a range $r = 100$ m. On all four lanes, the traffic density $\rho = 50 \text{ km}^{-1}$. As predicted with Equation 3.70, the expected node degree of vehicles on the intersection is 40 vehicles. The node degree of the vehicles is shown in Figure 4.8.

Consider an application that shall be run using a slotted ALOHA MAC and a PHY supporting a data rate of $R = 10 \text{ Mbit/s}$. The application can tolerate a packet loss of up to $p_l = 10 \%$.

With Equations 4.31 and 4.35, we obtain the QoS load limit \hat{u} :

$$p_l(\hat{u}) = 1 - \frac{v_{SA}(\hat{u})}{\hat{u}} = 1 - \exp(-\hat{u})$$

$$p_l(\hat{u}) \stackrel{!}{=} 0.1 \rightarrow \hat{u} = 0.105 \text{ Erl}$$

The chosen realization implements the presented distributed traffic limiting algorithm. Figure 4.9(a) shows the nodes' shares for the intersection scenario. Intuitively, vehicles in and directly around the area of the highest node degree are assigned the smallest share of the medium: $s = \hat{u}/40 = 0.02625 \text{ Erl}$. What is the data rate that these nodes can attain?

$$D = Rs = 10 \text{ Mbit/s} \cdot 0.02625 \text{ Erl} = 26.25 \text{ kbit/s} \quad (4.44)$$

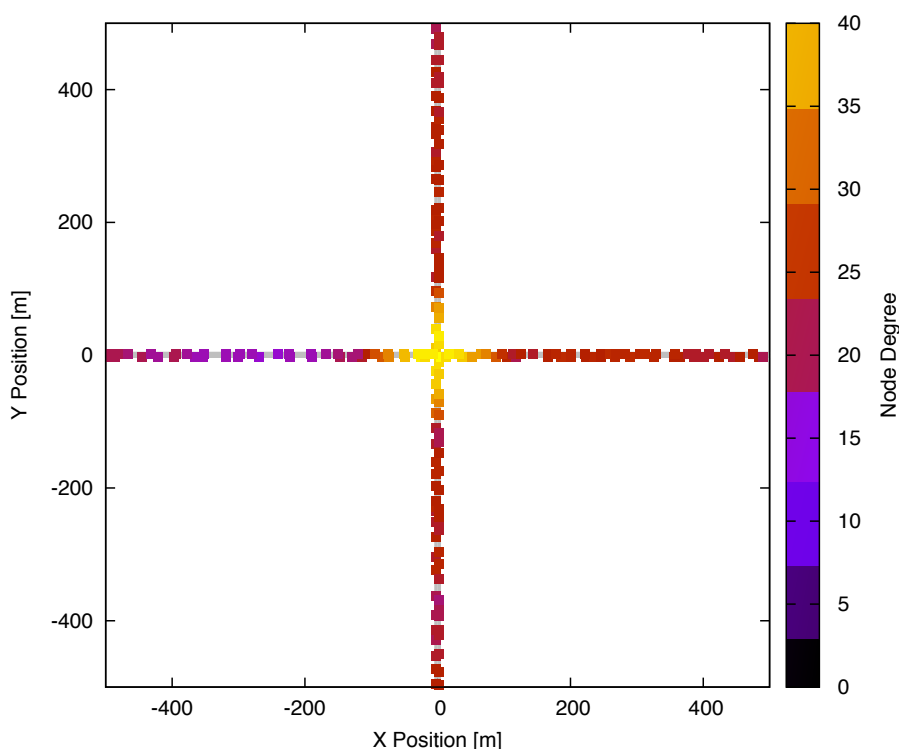


Figure 4.8.: Node degrees for the intersection scenario.

Assuming that the application needs to transmit ten packets per second, the maximum packet size is then (Equation (4.12)):

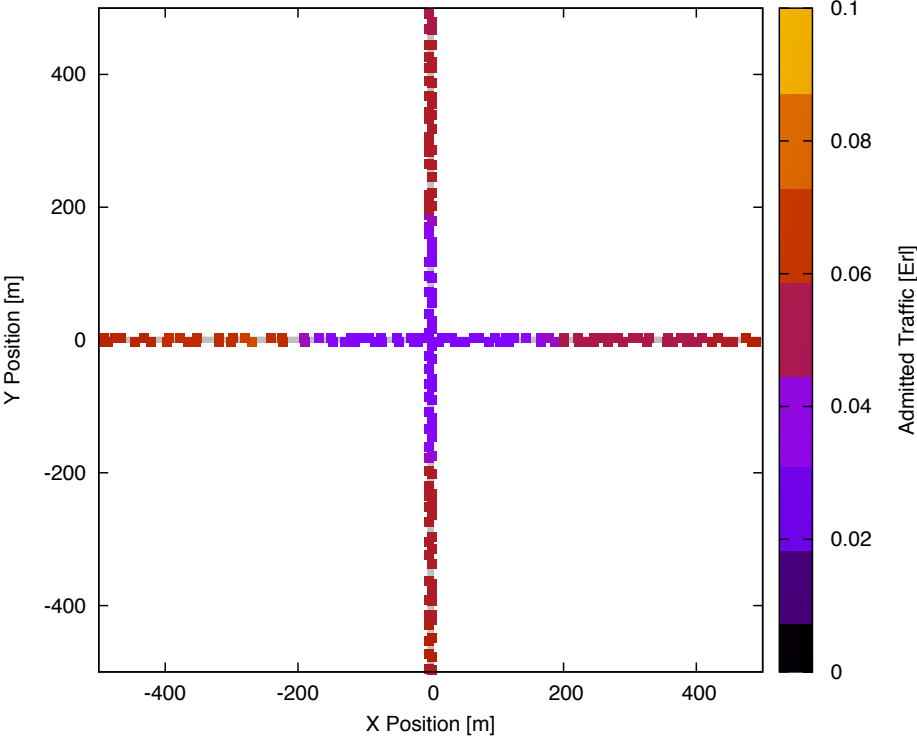
$$l_p = \frac{26.25 \text{ kbit/s}}{10 \text{ s}^{-1}} = 328 \text{ B} \quad (4.45)$$

The tolerable packet loss is now $p_l = 1\%$. Consequently, the QoS load limit is then $\hat{u} = 0.01005$ Erl and the maximum packet size is 31 B. Another choice for this setup may be to use the traffic limit computed above ($\hat{u} = 0.105$ Erl) and transmit every message *twice*. This effectively reduces the packet loss probability to meet the new requirement. On the other hand, the maximum packet size (due to the doubled number of transmissions) only reduces to 164 B. Repeating transmissions may thus be more efficient than reducing the traffic to meet a QoS requirement.

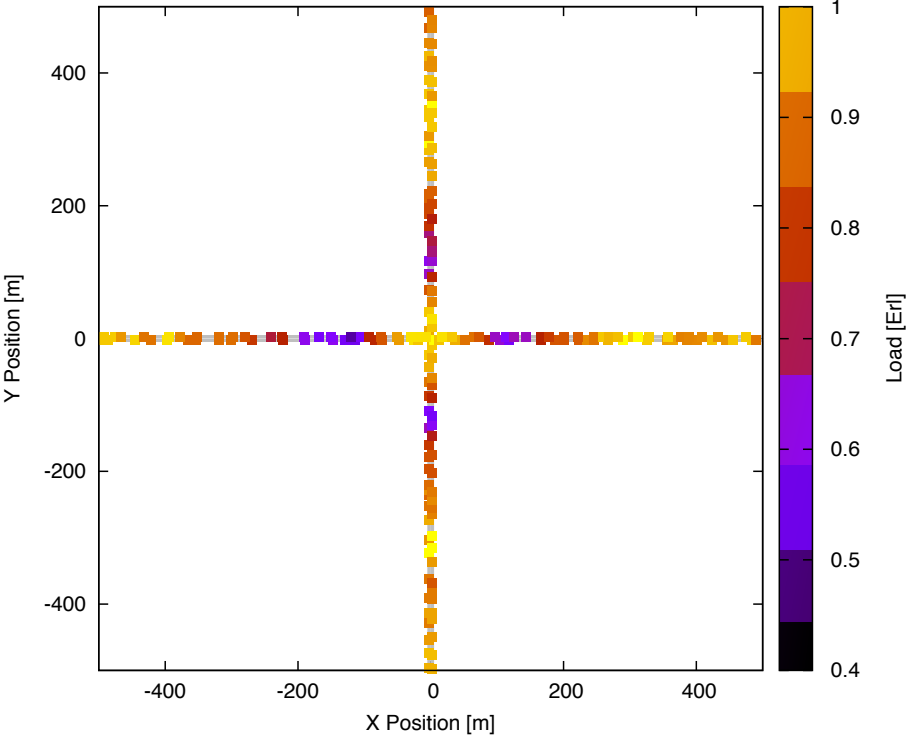
It is interesting to note that the cumulated load goes down significantly in a circular area about 100 m around the intersection (Figure 4.9(b)). This is caused by nodes that are just inside the boundary of the very high density region and thus receive low traffic coming from few nodes close to the center with a low admitted traffic. Also, they receive only a part of the higher-traffic nodes outside the boundary.

4.4.4. Stub nodes

Obviously, the inhomogeneous distribution of node degrees lead to an unbalanced traffic assignment at the nodes. On the one hand side, this yields a benefit in average admitted traffic, as discussed above. On the other hand side, however, neighboring nodes may experience very unequal assignments. Stub nodes of degree 2 will — in the best case — be admitted to source a traffic of $\hat{u}/3$. In the worst case, all other nodes are connected to a central node which a degree



(a)



(b)

Figure 4.9.: Admitted traffic (a) and cumulated load (b) for the intersection scenario.

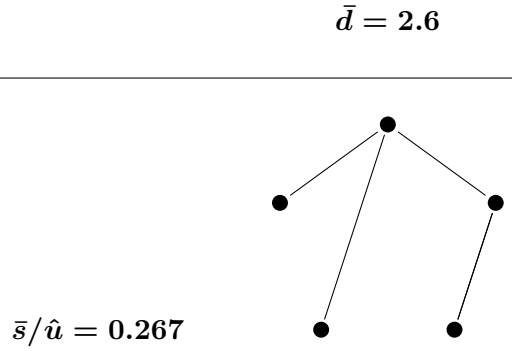


Figure 4.10.: An example for a stub configuration

of $(n - 1)$ and therefore be admitted a traffic of $\hat{u}/(n - 1)$. The maximum ratio r_s between the highest and lowest assigned traffic in a network with n nodes and n_s stub nodes is then

$$r_s = \frac{n - n_s}{3} \quad (4.46)$$

One example for a stub configuration is shown in Figure 4.10. This configuration has one stub node and an $r = 4/3$. In most configurations (like the one shown), stub nodes could even be admitted a higher traffic: in the example shown, the traffic s_s admitted to the stub node could be increased from $1/3$ to $1/2$. For the centralized algorithm, it is very easy to improve stub assignments; for the distributed algorithm, however, the knowledge of the two-hop neighborhood alone is not enough for an optimal stub assignment.

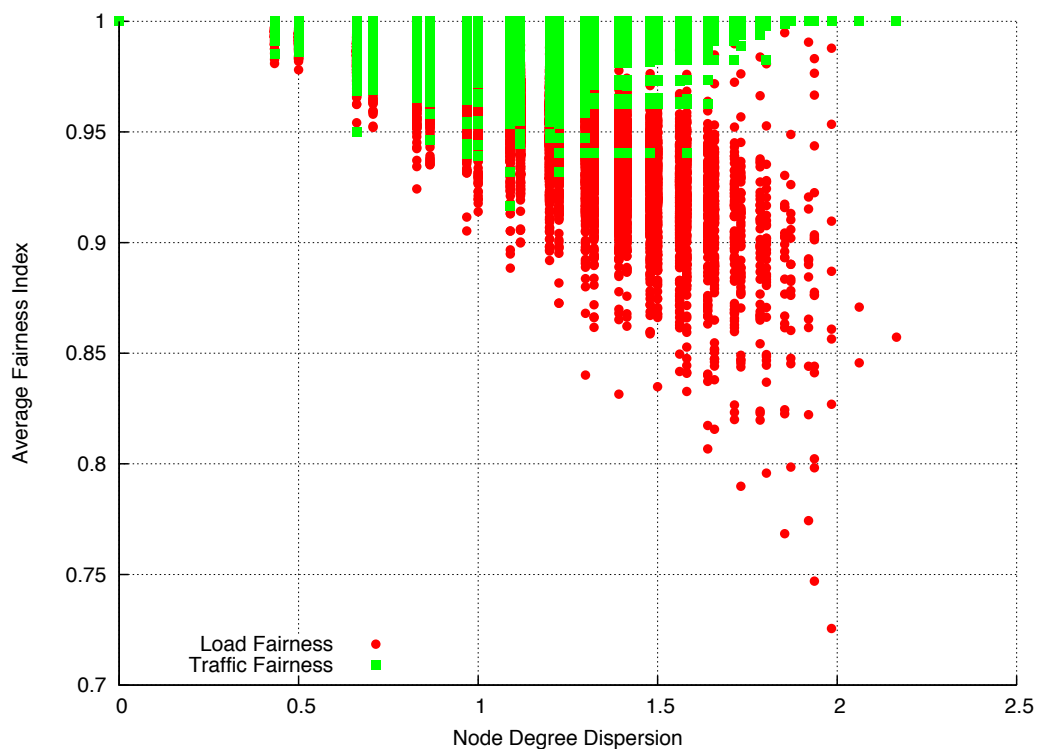
4.4.5. Fairness

A common measure of fairness is Jain's fairness index [JCH84]. The global fairness of the traffic assignment can be determined through:

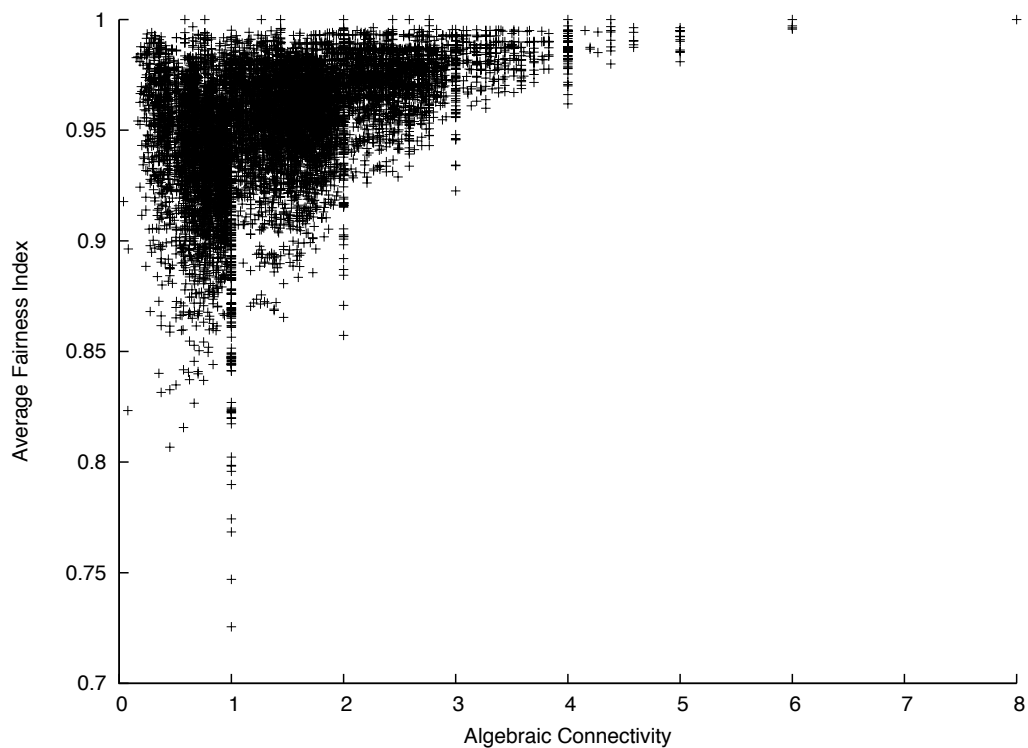
$$\Phi = \frac{\left(\sum_{v_i \in \mathcal{V}} s_i \right)^2}{|\mathcal{V}| \sum_{v_i \in \mathcal{V}} s_i^2} \quad (4.47)$$

For this discussion, however, we wish to determine the fairness of the traffic assignment in the individual collision domains and use this as a criterium for the assessment of the proposed algorithm. Let \mathcal{R}_i denote the set of receive hyperarcs (i.e., the senders transmitting in the collision domain of node v_i), then the average fairness index ϕ is given by the average of all nodes' collision domains' fairness indices:

$$\phi = \frac{1}{|\mathcal{V}|} \sum_{v_i \in \mathcal{V}} \frac{\left(\sum_{v_j \in \mathcal{R}_i} s_j \right)^2}{|\mathcal{R}_i| \sum_{v_j \in \mathcal{R}_i} s_j^2} \quad (4.48)$$



(a) 8-node networks, average fairness over degree dispersion



(b) 8-node networks, average fairness over algebraic connectivity

Figure 4.11.: Average load and per-node traffic fairness over degree dispersion (a) and algebraic connectivity (b).

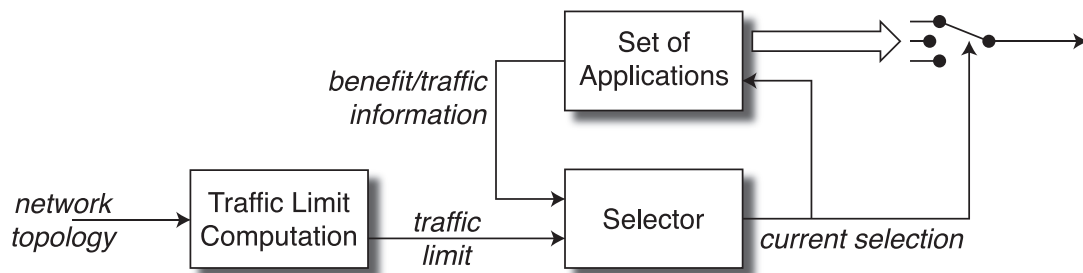


Figure 4.12.: The proposed mechanism for application selection and parameterization

For this discussion, the fairness index has been computed for both the traffic assignment and the resulting load on the nodes (replace s with u in the above formulas). The goal of the algorithm is to attain a traffic assignment that best meets the fairness criterion (R3), which shall be defined as achieving parity between equal, indistinguishable nodes that share one collision domain.

The dependence of the traffic assignment on the network topology is reflected in Figure 4.11, computed for the 11,117 possible isomorphic realizations of 8-node networks. In the upper graph (Figure 4.11(a)), we have used the standard deviation of the node degree as a measure of network imbalance; in the previous chapter, we have denoted this as “node degree dispersion”. It is interesting to see that while the fairness of the traffic assignment is generally rather high and displays some lower levels between $\sigma = 1 \dots 1.5$. The reason for this finding is that networks with low degree dispersion tend to be very evenly meshed, they could be a ring or an (almost) fully meshed network. Networks with very high degree dispersion rather resemble a star, with one central node of high degree and satellite nodes with low degrees. In both cases, the traffic assignment is equal for all nodes and hence considered fair. Medium node degree dispersions relate to networks that have some nodes with high degree and some with very low degree; a typical configuration could be a star with lots of stubs.

At the same time, the cumulated load resulting from the traffic assignment exhibits a more and more unequal distribution over the nodes as the network imbalance increases. Figure 4.11(b) plots the cumulated load over the algebraic connectivity⁸ as a measure of how well the network is connected. Clearly, networks that are “more connected” reveal a more uniform load distribution and hence a higher level of fairness. Networks with a low load fairness usually have most, if not all, nodes connected to a central node that determines the maximum admitted traffic and varying connections between them which cause unequal loads. As the number of connections between these nodes increase (and the connectivity increases), the loads balance and the average fairness goes towards 1.

4.5. Application Selection and Parameterization

A potential implementation of a higher-layer application selector and parameterization is outlined in Figure 4.12: Once a node v_i has computed its traffic limit s_i , the information can be used at higher layers to select a subset of active applications for a set of runnable applications. Also, the selected applications can then be parameterized by assigning them a specific share of the admitted traffic.

Let us assume that the application selector has a specific set of applications \mathcal{P} to choose from. Every application has an associated utility function that accepts as a parameter the application's share of the admitted traffic, s_p :

$$\forall p \in \mathcal{P} : U_p(s_p) \quad (4.50)$$

Selecting the set of active applications $\mathcal{P}^* \subseteq \mathcal{P}$ is then a maximization problem, as described and discussed in [FC05]:

$$\text{maximize } \sum_{p \in \mathcal{P}^*} U_p(s_p) \quad (4.51)$$

$$\text{subject to } \sum_{p \in \mathcal{P}^*} s_p \leq s_i \quad (4.52)$$

where the variables are s_p and \mathcal{P}^* . It should be noted that applications also need to have priorities associated so that during the selection process, safety-critical applications are considered before non-critical applications are assessed.

Feeding back the traffic allocation to the applications could enable them to adapt to the current specific network state and to better select, quantize, and/or reduce the transmitted information and thus increase the overall utility. Some examples of parametrizable applications are:

- Cooperative awareness applications can be parameterized so that for instance the resolution of the transmitted data can be adjusted or the range of the transmitted information is limited. This could be done, for instance, with occupancy maps as well as with images or live video streams. Also, GPS data could be quantified according to the available bandwidth. The global utility may be much greater if more applications can be run at lower data rates (for example, low-resolution video plus low-resolution GPS) than only one application run at a higher data rate.
- Cooperative driving applications could be parameterized so that potentially unsafe situations can be avoided. For instance, a cooperative adaptive cruise control could be adjusted so that the time gap between the controlled vehicle and the leading vehicle is long enough to ensure safe operation of the algorithm, even if the status of the network does not allow very high resolution of communicated sensor data.

Furthermore, the applications should be able to dynamically alter their utility function, depending on the current driving situation. For instance, an intersection assistant has a higher

⁸The algebraic connectivity is commonly defined as the second-smallest eigenvector λ_2 of the Laplacian matrix $\underline{\mathbf{L}}$ of the network's graph [Fie73], where $\underline{\mathbf{C}}$ is the connectivity matrix as defined above:

$$\underline{\mathbf{L}} = \text{diag}(\underline{\mathbf{C}}^T \mathbf{1}) - \underline{\mathbf{C}}^T \quad (4.49)$$

utility when driving in a city than when driving on a highway. At the same time, a collision avoidance application may run at lower data rates with the same utility when driving in heavily congested traffic than in free-flow traffic.

The exact realization of such a solution shall not be discussed here, instead we would like to refer the reader to the works of Eichler [ESKS06] and Zhou [ZGZC09], where these optimization issues are addressed in-depth.

4.6. Conclusion

In this chapter, we have demonstrated a graph-theoretic representation of network connectivity using hypergraphs and connectivity matrices. We have discussed the broadcast nature of the wireless medium and introduced the concept of traffic vectors that we use to describe the traffic in a network and to study the cumulated load as the result of the connectivity and the traffic. Furthermore, we have presented various relevant MAC protocols that qualify for implementation in a vehicular network. By quantifying their specific traffic/packet loss relations, based on their specific offered traffic to throughput relation ($v(u)$), we could infer a method to determine the maximum allowable load, given a desired level of QoS, which may be described by either the maximum allowable packet loss or delay for a specific application. The insights gained from the MAC protocol and network modeling as described here can be used for the performance analysis of MAC protocols, given scenarios described through the means presented in Chapter 3.

These insights can also be used as input parameters for the algorithm presented in the following, that allows for fast computation of the maximum admissible traffic at any node in a given network. We have demonstrated both a centralized algorithm using global knowledge, and a decentralized algorithm that uses two-hop connectivity information to instantaneously compute the admissible traffic at each node. We have shown through complete simulations for five-, six-, seven-, and eight-node networks that both algorithms guarantee that the network is not overloaded and that most nodes achieve the highest possible traffic assignment. We have also discussed exceptions and bounds. Using the presented algorithm, we can ensure that the maximum load chosen at design time is never exceeded at runtime and that, consequently, the desired QoS is attained at all times. The algorithms is thus perfectly suited for implementation in networks as an effective QoS control mechanism.

Further work on this topic should seize on the opportunity to not only compute an optimal \underline{s} for a given connectivity matrix \underline{C} , but also to try to optimize the connectivity matrix itself for a desired traffic. This may be attained through advanced techniques such as power control (as implicitly presented in [TMMSH09]) or smart antennas. Another starting point may also be to study how one node can maintain a set of connectivity matrices for diverse data rates and consequently, since traffic is the quotient of a message's packet size times its generation rate over the data rate at which it is being sent, diverse traffic and cumulated load. This may be desirable since closer nodes could be served at higher data rates (and lower traffic) without disturbing long-haul transmissions that run at lower data rates (and thus cause higher traffic). To do so, it would be necessary to introduce the idea of a receiver sets for certain messages and then choosing optimal \underline{C} s for these transmissions.

Network Model	
Network Graph	$G := (\mathcal{V}, \mathcal{E})$
A Vertex	$v_i \in \mathcal{V}$
An Edge Between Two Vertices i and j	$(v_i, v_j) \in \mathcal{E}$
Relation to the Channel Model	$P((v_i, v_j) \in \mathcal{E}) = \chi(\mathbf{x}_i, \mathbf{x}_j)$
Connectivity Matrix	$\mathbf{C}(G) = (c_{ij}), c_{ij} = \begin{cases} 1 & \text{if } (v_i, v_j) \in \mathcal{E} \\ 0 & \text{otherwise} \end{cases}$ (4.1)
Packet Size	l [B]
Packet Generation Rate	λ [s^{-1}]
Data Rate	R [bit/s]
Offered Traffic	$s = \lambda \cdot \frac{l}{R}$ [Erl]
Traffic Vector	$\underline{\mathbf{s}}$
Cumulated Load Vector	$\underline{\mathbf{u}} = (\mathbf{C}^T + \mathbf{I})\underline{\mathbf{s}}$ (4.15)
Medium Access Protocols	
Throughput	$v(u)$ [Erl]
Packet Loss Probability	$p_l(u) = 1 - p_s(u) = 1 - \frac{v(u)}{u}$ (4.31)
Average Normalized Packet Delay	$\delta(u) = \frac{u}{v(u)} = \frac{1}{p_s(u)}$ (4.33)
ALOHA	$v_A(u) = u \cdot \exp(-2u)$ (4.34)
Slotted ALOHA	$v_{SA}(u) = u \cdot \exp(-u)$ (4.35)
Non-Persistent CSMA	$v_{CSMA}(u, a) = \frac{u \cdot \exp(-au)}{u \cdot (1+2a) + \exp(-au)}$ (4.36)

Table 4.4.: Relevant formulas derived in this chapter.

5. Predictive QoS Provisioning in Vehicular Ad-Hoc Networks

In the previous chapter, we have demonstrated that through controlling the amount of tele-traffic that is injected by the nodes, effective distributed mechanisms can be employed that are, given minimal information about nodes' connectivity, able to provide (and even guarantee) a certain level of QoS. These mechanisms, however, are based on the current connectivity of the network and are effective only at present time. Should an application require a certain amount of QoS over a larger period of time, additional provisions become necessary. Although it is possible to control connectivity in certain boundaries (for instance through power control or adaptive antennas) and at a certain cost, the fundamental physical causes of connectivity themselves (location, mobility, and wireless channel state) cannot be influenced by the application as they are dictated by the user's behavior and the environment. It is, however, possible to anticipate a network's future connectivity — at least for a certain time horizon — and to compute the resulting future QoS. Upon this information, applications, services, and routing protocols could be parameterized accordingly: as an example, if the future QoS of a connection using a certain route is predicted to fall below a necessary level due to a link break, the expected remaining time until the link actually breaks could be used to proactively find and set up a backup route that uses other, potentially more stable links. Also, if a connection was to be set up for a limited time, it may be very helpful to assess if the required QoS can actually be provided by the network for the desired duration before the connection is actually established.

While other work mainly uses mobility prediction in cellular scenarios to estimate hand-over times, or to support ad-hoc routing in random-mobility ad hoc scenarios, this chapter focuses on connectivity prediction in the special case of vehicular networks. Networked vehicular nodes can be assumed to adhere to certain rules that constitute drivers' basic behavior: they move along roads and try to avoid collisions with obstacles, such as buildings and other cars. Founded on the vehicular scenario constraint, we present an algorithm that predicts the location of vehicles based on their current state (position and velocity) and information from digital street maps obtained through the Open Street Map (OSM) project. A filter-based, self-adaptive velocity prediction algorithm is used to model the user-inflicted velocity changes. Using their current positions and the predicted velocities, possible future positions of cars on the street grid and their respective probabilities can be determined. Although the main focus of this chapter is on mobility prediction, we discuss an effective channel parameter estimation technique and propose to predict the network's future connectivity using an adaptive channel model.

It should be noted that the proposed position prediction mechanism does not completely exhaust all opportunities provided by the vehicular scenario. For instance, we assume that vehicles have no information about other vehicles' missions, i.e., the planned route through the road grid. Furthermore, we make no assumptions about other vehicles' capabilities (in terms of maximum acceleration and deceleration, yaw rate, etc.). Also, we do not consider environmental properties, such as weather, street and road traffic conditions, etc. We will, however,

point out and discuss the potential spots where these additional informations could be exploited to further augment the proposed algorithm.

Most of the material in this chapter has been published in [NM11].

5.1. Related Work

One possible way of predicting a network's future connectivity is to use a model that reflects the individual mobility properties of a node. Given the knowledge of the initial position velocity of a node, a future position could be projected by multiplying the velocity vector with the desired time interval. Obviously, this approach does not account for changes in the length and/or direction of the velocity vector. Several more sophisticated approaches have been suggested and today, mobility prediction has become a common research topic in wireless networks.

Due to the distinct characteristics of vehicular ad-hoc networks, especially the high speeds and restricted degree of freedom in the movement of vehicles, most of the work on prediction for ad hoc networks is too general and thus inappropriate for vehicular networks. Nevertheless, some approaches are discussed here because they give an overview of mobility prediction in general. Material specific to mobility prediction in vehicular networks is very rare and the topic is often neglected in works on vehicular ad hoc networks.

[KK10] presents an approach for mobility prediction using neural networks. Although it is not specifically designed for vehicular networks it should perform better than other general approaches as it is independent of the underlying mobility model. A trajectory is calculated for multiple steps in the future using several past positions in quite a similar manner as the adapting Finite Impulse Response (FIR) filter for velocity prediction presented in this work. However, the approach does not use any map material and hence the predicted positions may lie far off the road and may thus be unrealistic. The approach using neural networks could be used for velocity prediction in the constellation presented in this works to substitute the FIR filter, however it is expected to perform in a very similar manner and the FIR filter seems less complex to implement.

A similar approach for mobility prediction using spatial contextual maps and Dempster-Shafer's theory for decision making is formulated in [SK05]. A framework is presented that allows prediction of the users mobility trajectory based on various bits of contextual information from e.g. user profile and map data. The approach is motivated by the fact that contextual information is becoming more common for adapting services towards the users needs and it uses the additional information in order to predict the users mobility. The concept seems feasible for e.g. cell phone users traveling on foot but does not seem appropriate for vehicular networks as the only contextual information possibly available and relevant to the future mobility is the chosen route to the destination. A complex theory to combine evidence into a prediction is not necessary in this case.

[HCY⁺08] suggests a prediction algorithm based on fuzzy logic that aims at the prediction of a possible link break or a congested link which then triggers the construction of an alternate route. Similar to our algorithm, the prediction of a link break is based on the prediction of the future vehicle speed, the basis on which the predicted distance to the vehicle can be determined. This requires the generation of a fuzzy rule base that is then dynamically trained using Particle Swarm optimization (which in our approach is done using the adaptive filter for speed

prediction). The authors use similar ideas in terms of the speed prediction but implements a fundamentally different concept. Furthermore, it is focussed on route break prediction and hence the performance of the isolated velocity prediction compared to our algorithm cannot be easily evaluated.

In [BRP09], the authors present some general thoughts on mobility prediction in vehicular networks and propose a simple prediction algorithm based on movement vectors in order to reduce the frequency of location beacons without introducing a higher mean error in respect to the positions used for routing packets. In [RPB09], the same authors introduce the Network Neighbor Prediction protocol (NNP) that uses the results from their prior works to predict new routes that are going to be available in the near future and to calculate the lifetime of those routes that are currently in use.

Another approach, although developed in the context of a different problem, is described by [ASB10]. The authors compute the set of points that could be reached by vehicles within the prediction times, given the capabilities (minimum and maximum acceleration, yaw rate, etc). of the considered vehicles. The approach is computationally complex and requires a lot of contextual information.

These previous works have demonstrated in their simulation results that mobility prediction is a useful and necessary aspect in vehicular networks and should be researched in greater detail than it currently is. Our approach extends the available mechanisms by complementing the adaptive FIR filter approach with road data from digital maps, which further increases the precision of prediction.

Using the predicted position it should also be possible to predict the future connectivity to a certain extent using an appropriate channel model. Due to the complexity of the V2V channel (see literature survey in Section 3.2.4), an adequate prediction of channel quality seems challenging. Analogous to position prediction, an estimation of channel quality can be seen as a trade-off between computational complexity and prediction accuracy. An approach involving ray-tracing similar to the one presented in [MSX06] on the one hand produces rather adequate results if provided with the necessary extent of details concerning the surrounding environment (including moving and parked vehicles), building geometries, plants and road signs. However, it seems unrealistic and infeasible to supply an on-board connectivity prediction engine with this amount of knowledge. Measurements suggest a dual-slope model for the Path Loss Exponent (PLE) as a simple yet effective approach. Small-scale fading is usually modeled using statistical models with strong dependency upon separation distance which limits the possibilities of a prediction to a qualitative worst case approximation. [PKC⁺09] also identifies significant differences between LOS and NLOS cases in both path loss and fading statistics.

A sophisticated approach to predict the PLE using a particle filter has been proposed in [RC10], based on a log-normal fading channel model in wireless sensor networks. Particles are initialized in a random state with their respective weights being iteratively updated to provide an estimation of the path loss exponent. Weak particles with low weights are periodically replaced to avoid degeneration. The filter is parameterized with the type of the fading distribution and its variance. The authors, too, show that the PLE changes significantly as soon as the LOS is lost.

Our work extends the particle filter approach in that it bases on the dual-slope channel model as presented in Chapter 3. By using digital map information, it is possible to obtain the length of the LOS path and to estimate the channel's LOS and NLOS PLEs. In conjunction with the

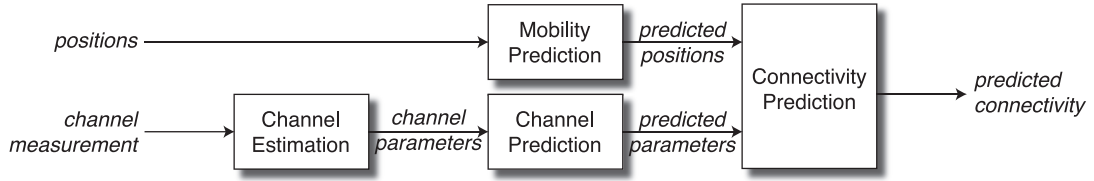


Figure 5.1.: Structure of the connectivity predictor.

predicted positions, the dual-slope channel estimation allows for the consideration of scenarios that contain radio obstacles, such as buildings etc.

5.2. Problem Statement

In the previous chapter, we have outlined how QoS provisioning based on a network's connectivity can be attained. The basis for the computation is the connectivity matrix \mathcal{C} that describes the communication relations between n networked nodes. Let $\chi(\underline{\mathbf{x}}_i, \underline{\mathbf{x}}_j)$ denote the channel function, taking as parameters the physical positions $\underline{\mathbf{x}}_i, \underline{\mathbf{x}}_j$ of two vehicles v_i, v_j in the environment.

The connectivity matrix \mathcal{C} then arises from Equations (3.4) and (4.2). Essentially, two vehicles v_i and v_j are connected if they are located within each others' radio ranges; if they are located further apart, they are not connected. Consequently, the probability that the respective entry in the connectivity matrix is one is determined by the channel function:

$$\mathcal{C} = (c_{ij}), c_{ij} \in \{0, 1\} \quad (5.1)$$

$$P(c_{ij} = 1) = \chi(\underline{\mathbf{x}}_i, \underline{\mathbf{x}}_j) \quad (5.2)$$

Assume that every node v_i is allowed to source teletraffic amounting to s_i into the network. Multiplying the source vector $\underline{\mathbf{s}}$ with the connectivity matrix results in the load vector $\underline{\mathbf{l}}$ (Equation (4.15)):

$$\underline{\mathbf{u}} = (\mathcal{C}^T + \underline{\mathbf{I}})\underline{\mathbf{s}} \quad (5.3)$$

We have shown that the QoS criterion is fulfilled if the injected traffic is dimensioned so that each entry in the load vector u_i does not exceed a certain pre-defined threshold \hat{u} . For more detail, especially on the distributed algorithm, refer to Chapter 4. The issue with this approach, however, is that $\underline{\mathbf{s}}|_{t_0}$ is only valid for the current connectivity matrix $\mathcal{C}|_{t_0}$. In the desire to fulfill the QoS criterion over a certain time Δt , it becomes necessary to predict the future physical positions of the vehicles, estimate the channel function and then deduce the prospective future connectivity matrix.

$$\mathcal{C}|_{t_0+\Delta t} = (c_{ij})|_{t_0+\Delta t} \quad (5.4)$$

$$P(c_{ij} = 1) = \left(\underbrace{\chi|_{t_0+\Delta t}}_{\text{Channel Estimation}} \left(\underbrace{\underline{\mathbf{x}}_i|_{t_0+\Delta t}, \underline{\mathbf{x}}_j|_{t_0+\Delta t}}_{\text{Mobility Prediction}} \right) \right) \quad (5.5)$$

After that, the future source vector can be computed and a decision can be made whether the current demand can be satisfied under the future network conditions and consequently,

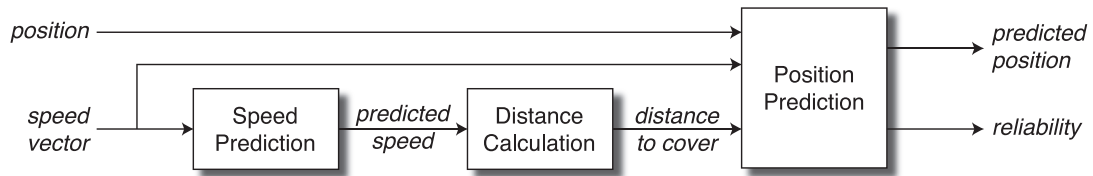


Figure 5.2.: Structure of the mobility predictor.

adequate measures can be taken. The structure of the connectivity predictor is shown in Figure 5.1.

5.3. Mobility Prediction

Generally, the spatial behavior of a vehicle is defined by two factors: On the one hand, speed and direction are controlled by the driver who adapts to the environment and the current situation. On the other hand, movement of a car is restricted to roads so the surrounding road topology is the major limiting factor. This is the key criterion that simplifies location prediction for vehicles compared to regular mobile users. Cars are usually not allowed to travel anywhere, they are bound to a relatively small portion of the world, the lanes. Combined with a small memory of past positions, the current velocity and direction of movement can be calculated. This further limits the amount of available future positions, as cars are usually not expected to u-turn spontaneously and velocity changes are bounded by the maximum deceleration and the maximum acceleration.

5.3.1. Concept

The prerequisite for the prediction is knowledge about a vehicle's current position, direction of movement and the surrounding road topology. The latter is provided by digital street maps (available, for instance, through the OpenStreetMap Project). All of these factors are very stable in terms of prediction. The destination or rather the mission of the car is assumed to be unknown to the algorithm, so at a crossroads basically all directions seem equally probable. The velocity of a car, however, is far less stable and predictable as it is directly controlled by the user and indirectly influenced by environmental factors such as road traffic density, road signs and the weather. Especially abrupt speed changes are almost impossible to predict as they are often unexpected, even to the driver himself. The algorithm is sketched in Figure 5.2.

For speed prediction, we use a filter based approach that employs concepts of adaptive filters initially developed to adapt to varying channel conditions in wireless communications. Like the channel characteristics change depending on the environment, the speed change behavior of a car - or rather its driver - adapts to various environmental factors. This includes urban scenarios with steep velocity slopes and rural roads with fairly constant speeds. The character of the driver and the performance of the car also influence the prediction to a certain extent and are automatically taken into account by the adaptive filter. A self-adapting FIR filter approach based on a Least Mean Squares (LMS) algorithm with relatively low depth seems ideal to adapt to both the personal behavior of a driver and the current situation. Using past and current velocities, an ideal weight vector for the past situation is calculated. Due to the low

depth of the filter, the weight vector is rather unstable and consequently, it is combined with both the mean weight vector over the last iterations and a “boost” vector to improve reactivity at steep slopes. The resulting weight vector is then used to predict the future velocity, which is in turn used to calculate the distance covered in the desired interval.

The distance to cover, together with the current position and direction of movement, forms the input for the position predictor that outputs the predicted future location of the vehicle. In some cases, multiple positions are possible, for instance due to a crossroads between the current and the future position. In that case, the position that seems most probable to the algorithm is used as an output; however, internally a list of all possible locations is generated. In many situations, predominantly with cars traveling in sparsely populated areas or on highways, the prediction is rather reliable. In urban areas prediction reliability is reduced by intersections where a sudden change of direction can occur and a certain amount of past predictions may be invalidated. To make applications aware of such differences, an additional output variable was added to resemble the estimated reliability of the output.

Input Data

The algorithm requires a number of input data:

Position data: Obviously, the algorithm requires knowledge about the actual position of a vehicle and a timestamp. The position data used in the performance analysis has been downloaded from the “GPS Tracks” section of the OpenStreetMap online portal. Selected tracks were chosen that were provided by users around the globe and thus constitute a rather broad basis of real life data. Additionally, own traces have been used. The temporal resolution of the recorded tracks was or has been resampled to one second. A statement about the spatial resolution is not generally possible as different positioning hardware from various vendors has been used for the sample data. However, we shall assume a positioning accuracy of a few meters.

Map data: Also, the algorithm needs to be provided with map data of the area surrounding the actual position. This data, too, is provided by and downloaded from the open source OpenStreetMap project. It basically consists of an array of so-called nodes that are uniquely identified and reference a GPS position by latitude and longitude. A street is constructed by a list of subsequent nodes, forming a polyline that represents the shape of the street. Actual contiguous roads may be split apart, for instance if the name of a street changes or if two streets merge, on intersections etc.

Number of steps to predict: The major parameter influencing the algorithm. It is common in most parts of the algorithm and hence introduced in the high level diagram. Many parts of the algorithm also refer to it as n . Depending on the input data, the usual assumption is that one timestep equals one second. Most of the evaluations were done using a medium interval of prediction of 8 seconds - however results using different values are discussed in Section 5.3.5.

5.3.2. Speed Prediction

A car typically moves in different classes of environments: urban, suburban, peripheral and highway. Each of those has different characteristics concerning the speed change of a car. On a

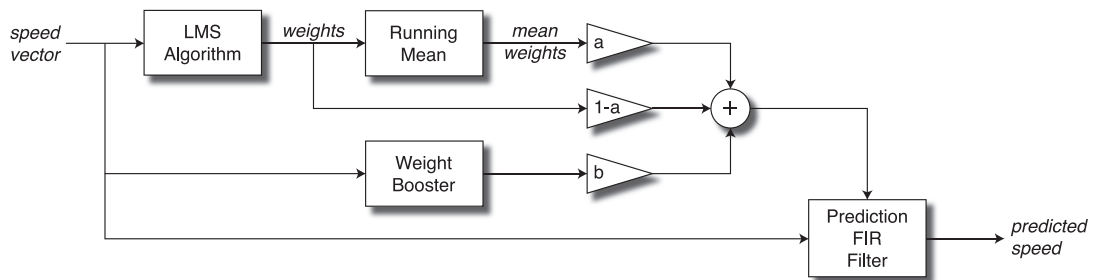


Figure 5.3.: Structure of the speed predictor.

highway speed changes are rare but usually with rather steep slopes whereas in urban areas, the speed is hardly ever constant for more than a few seconds. This allows for two different approaches in implementing a speed prediction algorithm. On the one hand, specialized algorithms could be engineered for all of the above scenarios and another algorithm that determines the algorithm that is most appropriate in an actual situation. In typical situations one would expect such an approach to give very accurate results, but clearly there are many situations where none of the implementations will be adequate. Furthermore, this approach involves increased efforts in development because multiple algorithms need to be designed and there is a high number of factors influencing the situation that are hard to quantize.

On the other hand, it seems more appropriate to design an algorithm that automatically adapts to changing situations and as such can also adapt to factors like driver attitude and others mentioned above. This introduces some delay caused by the responsiveness of the adaption algorithm, but works also in an environment that cannot be properly classified into one of the above scenarios. In some situations, especially with quickly varying conditions, this may result in weaker performance than the approach discussed above, but the overall performance is expected to be better with less development efforts. A solution for this approach is discussed in the next sections.

Structure

The signal flow graph of the speed prediction is shown in Figure 5.3. The input variables are the current speed of the car and the number of steps n to predict. The only output is the predicted speed for the given time frame.

Prediction FIR Filter: The actual prediction is done in an FIR filter on the right hand side of the signal flow plan. It uses the current speed and a weight vector to predict the velocity from the last speed values. The length of the weight vector is given by the depth of the FIR filter - in the evaluations performed here a depth of 12 was used.

LMS algorithm: The most important building block. It is the adaptive part of the algorithm and calculates an ideal weight vector from its two input values - the current velocity forms the desired signal, a delayed version forms the input for the algorithm. The weight vector is adapted with a fixed step size in the direction of steepest descent in order to achieve the minimum square error and, at the same time, limit the dynamics of the weight vector. The weight vector is recalculated each time step, for more details see [BC02, GKDA71].

parameter	example value	description
n	8	number of steps to predict
l	12	depth of FIR filters and dimension of weights vector
a	0.275	influence of the mean weights vector
b	2	influence of weight booster
c	0.2	boost limit
d	1	boost gain

Table 5.1.: Speed Prediction parameters with example values used during development.

Mean Weight: Because the weight vector generated by the LMS algorithm is very reactive to acceleration and deceleration processes, it is averaged by a running mean block that calculates the mean weight vector over the length of the situation. Both the mean and the LMS weight vector are combined into a slowed weight vector by multiplication with the parameter a or $1 - a$ respectively.

Weight Booster: The LMS algorithm adapts to new situations with a delay that is roughly its depth l plus the length of the prediction interval n , which equals the number of memory elements involved in the adaption. A change in velocity needs to pass through most of the memory elements before its effect becomes visible in the weight vector. For instance, for a car traveling in a city, the weight vector produces rather stable results while the car is traveling at a constant speed but it will react slowly to sharp braking or fast acceleration. The algorithm is designed to fix this problem by manipulating the weight vector in order to emphasize the most recent speed history elements to react more quickly to a spontaneous change in behavior: a length l base vector is multiplied with a scalar calculated from the slope of the velocity curve and is bounded above by the boost limit c . In order for the impact of the booster to remain present for a longer period, the generated “impulse” is broadened using a unity-weight FIR filter.

Parameters

The performance and precision of the speed predictor depends on some fundamental parameters that are summarized in Table 5.1. The given values are the result of some evaluations during the design phase based on few exemplary scenarios and should give a rough idea to start an implementation. However for a proper implementation a more thorough, numerical optimization is recommended but out of scope of this essay.

It is important to note that all of the below parameters influence the prediction in a way that usually makes adoptions to all parameters necessary if one parameter is changed. In many cases more than one possibility exists that can lead to a desired result for one scenario, but looking at multiple scenarios usually only one if any of the possibilities lead to an overall improvement of performance.

n – Number of steps to predict: This key parameter determines the number of steps to be predicted — $n = 8$ means the algorithm predicts the speed in 8 time steps. Obviously a higher value increases the prediction error, whereas lower values gives more precise predictions. The setting of this parameter is very important because its influence on the other parameters is tremendous, for instance a high value for n will on the one hand require a higher a and on the other hand require more influence of the weight booster,

b. Also, this parameter is common with all components of the algorithm, so its influence has to be regarded globally. Different settings and their impact, especially on position prediction, are discussed in Section 5.3.5.

l – **Depth of FIR filters:** The FIR filters' depth used in the speed predictor is a common value because all blocks share the weight vector. Also the parameter *l* is, unlike all other parameters mentioned here, a design time parameter that cannot be changed easily as it is hard-coded into the FIR filters and the constants. Nevertheless, its influence on the prediction should be discussed here.

For the fact that the depth of a filter resembles its amount of memory elements, higher values for *l* give more stable and less reactive prediction results. Changes in the situation need more time to propagate through the memory elements, hence it takes a longer time to adapt to changes. Smaller values for *l* improve reaction time but also result in less stable and more fluctuating predictions that often overshoot at slight changes.

a – **Influence of the Mean Weights Vector:** The weight vector in the standard case (disregarding the weight booster) is combined from the current weight vector produced by the LMS algorithm and its running average. Setting *a* to the maximal appropriate value $a = 1$ produces a very stable weight vector but also removes the direct influence of the LMS algorithm to the weight vector and thus the reactivity. This is caused by the fact that in this model, the mean weight vector is never reset and thus provides an "all time average".

b – **Influence of the Weight Booster:** This parameter determines the overall influence of the weight booster. Higher values tend to produce overshoots as a trade-off to slow response to a change in situation if lower values are used. Generally all three values influencing the weight booster should be tuned according to the length of the prediction *n*. With high *n*, *b* should be increased because a faster reaction is necessary due to the latency of the LMS algorithm.

c – **Boost Limit:** The "boost" vector, or more precisely its scalar values, are influenced by the slope of the velocity curve. The "boost limit" defines an upper bound to those scalar values.

d – **Boost Gain:** This parameter multiplies the influence of the slope difference before the broadening and limiting of the pulse. Thus a higher value generates very quick increase once a steep slope is detected - in other words, it pushes the boost weight vector more quickly to the limit. Lower values produce a smoother response to steep velocity slopes.

5.3.3. Distance Calculation

The speed predictor predicts the vehicle speed some time steps ahead. The position predictor in turn requires as an input the distance to cover in the next time steps to calculate the future position. The most precise approach is to predict a velocity value for each time step in the prediction period and sum up the difference. Because this requires a set of *n* speed predictors which increases the computational efforts by *n*, a simpler approach is chosen in this implementation. Our algorithm uses the current speed and the predicted speed and calculates a linear approximation between the two. The distance to cover *s* is then the area under the speed curve for a duration of *t* (*n* time steps):

$$s = \frac{t}{2}(v_{current} + v_{pred})$$

5.3.4. Position Prediction

The position predictor uses the current position and direction of movement, digital map data as well as the predicted distance to cover as inputs and outputs a predicted position and its reliability. It is invoked once per time step and tries to first find the current road segment of the vehicle, then determines a number of possible prediction paths and finally chooses the most probable path and returns its end point.

Determine current road segment

All known nearby road segments (taken from the digital map) are evaluated for the distance of the current position to the closest point on the respective road segment. Three criteria must be met in order for a road segment to be chosen:

1. The distance to the closest point is smaller than a threshold.
2. The absolute value of the difference between the direction of movement and the road segment's direction is not larger than $\pi/2$ because vehicles usually do not move perpendicular to streets.
3. It is the closest road segment satisfying both criteria 1 and 2.

In case no road segment is found that fulfills all of the above criteria, the algorithm returns the current position as prediction result with an estimated accuracy of 0%. Possible causes range from wrong GPS positions during the initialization phase of the GPS device and inexact map material to driving or parking on streets or private property that is not (yet) included in the map material.

Determine possible paths

First, the remaining distance from the current position to the respective end point of the road segment s_r is calculated. If the road segment's end point is further away than the distance to cover ($s_r \geq s$), the predicted position will be located between the current position and the road segment's end point. Therefore, the predicted position is determined along the road segment's polyline towards the end point, covering the given distance s .

In the case that the remaining distance s_r is smaller than the distance to cover ($s_r < s$), the predicted position is moved to the road segment's end point and that distance is subtracted from the remaining distance. Subsequently, the next road segment of the prediction path is determined. If the mission of the vehicle is known in advance, the next road segment is chosen according to that mission. Otherwise, in order to find the next road segment, the number of possibilities is determined from the digital map: at a junction, all connected street segments are considered possible candidates. The current road segment, however, is not considered as an alternative — in other words, the vehicle is not expected to u-turn. Three cases exist:

- (a) **No candidates** exist, so the current road segment ends in a node that has no other road segments referenced. In this case the relative probability of the current path is decreased in the relation to the amount of distance already covered.
- (b) **One candidate** means there is no choice and the vehicle is moving along a road without an intersection at the current node. Determining the next road segment and updating the path accordingly is trivial.

(c) Multiple candidates are available, so the predicted path hits some kind of intersection. Hence the process of determining the next road segment becomes a bit more complex: Initially, all candidates must be assumed to be equally probable.

The procedure is repeated recursively until all distance s is covered and all possible paths of length s have been determined (effectively yielding a tree of possible road segments, with leaves at all possible future locations).

Pick best path

It may be desirable for an application that the prediction comprises all possible future realizations. However, if the prediction routine should return the future position along only one predicted path, the best of the alternative paths found must be chosen. If the mission of an observed vehicle is unknown to the algorithm, it must more or less issue a guess as to what option the driver of a car will go for. The range of alternatives is narrowed down in three steps:

- (a) Estimated probability:** In the current implementation of the algorithm, this first step will only remove the paths that end in a *dead end* and hence have a reduced relative probability. All other paths are considered equally probable and hence cannot be classified by their probability. For instance, the car hits an intersection with three alternatives, one of which being a dead end street. The dead end would be removed from the candidates, whilst the other two possibilities are equally probable.
- (b) Way Changes:** The number of street changes is the primary decision criterion for the algorithm. It is assumed that in case multiple paths exist, the driver stays on the current street. Hence the path with the least number of street changes is favored for the prediction. It is furthermore assumed that if it is necessary to change the road at some stage in all paths, the driver still stays on the current road as long as possible.
- (c) Direction Difference:** Should the way change criteria be unable to choose one candidate, the total difference of direction along the path is considered. Assuming the driver to be lazy, the path encountering the least change in direction is chosen to be the best path.

Clearly, criteria (b) and (c) do not increase the probability of a certain path. These are merely decision criteria in order to choose one path from multiple options. Choosing a random path statistically produces the same error, but has a severe disadvantage in terms of continuity: as the algorithm is executed each time step, it should return consistent values from one step to the next; when using a random selection, it is most likely that the algorithm will return a completely different position each time it is invoked. From a statistical point of view, this does not change much but for another program or algorithm that is based on the results of the prediction it may very well change things depending on the application. For the very same reason, it is very important for the algorithm to return the estimated probability of a given prediction because another program can then classify the prediction accordingly.

5.3.5. Simulative Evaluation of Speed and Position Prediction Accuracy

Three representative scenarios were chosen for the performance evaluation of the developed algorithm. These scenarios are based on GPS tracks downloaded from the OSM portal that

were selected to provide maximum diversity in the results presented below: the chosen tracks were recorded in a city as well as in suburban and highway surroundings. We have evaluated the three scenarios concerning the accuracy of both the speed prediction and the resulting predicted position under the three different environmental settings.

City scenario

The first data set represents a typical city scenario. It has been recorded in the German city of Herne in the Ruhr area, with speeds of up to 50 kilometers per hour and a total length of about 20 minutes.

Figure 5.4(a) shows a section of the actual vehicle speed (solid line), the area of the filled curve reflects the velocity prediction error where the upper or lower edge of the area marks the predicted speed. For easy comparison, the predicted values are shifted by 8 seconds, so that the real value and the value that has been predicted for that instant are matched in time. The results show that especially at steep slopes, the algorithm overshoots significantly and predicts too low or too high velocity values. This could be tuned using the parameters of the speed prediction in order to achieve better performance in the particular scenario, but the impact on other scenarios is hard to estimate and thus requires significant research efforts.

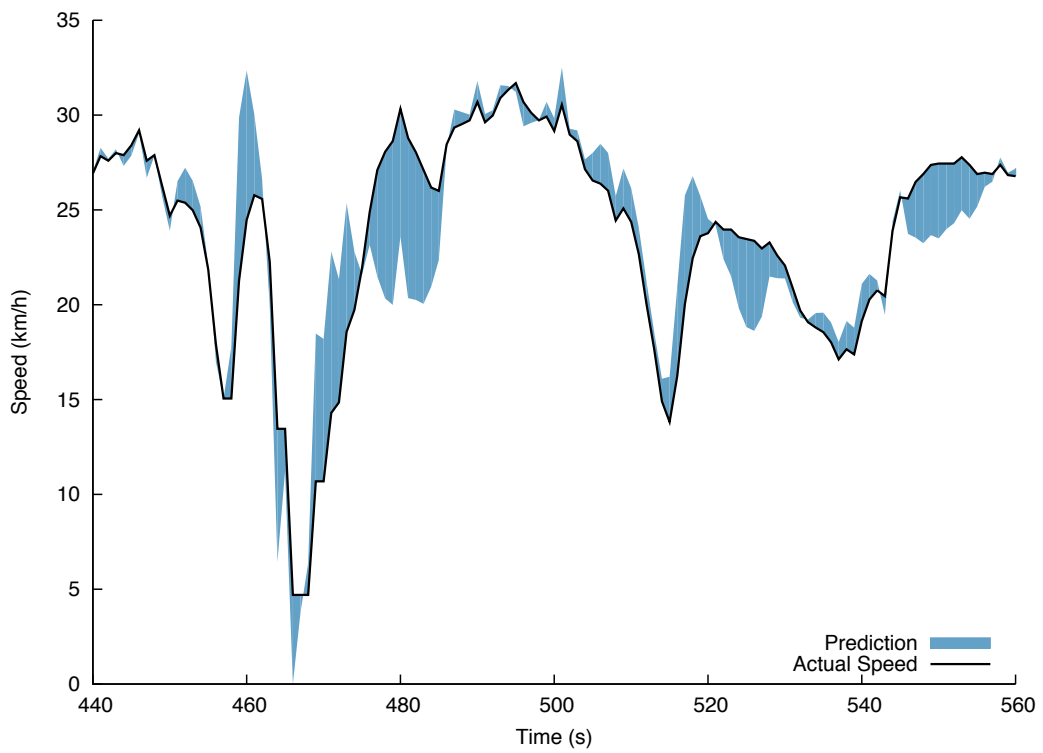
Figure 5.9(a) shows the distribution function of the position prediction error in meters (upper blue line). The mean error is 13.4 meters, the median amounts to 7.5 meters. Figure 5.4(b) shows a section of the prediction error over time; the filled curve represents the estimated probability (correctness) of the prediction. Note that the second Y axis has been reversed for better readability.

As explained in section 5.3.4, the estimated probability generally equals 1 if the position predictor identifies only one possible path for the vehicle, based on the map data. In the presented case that the mission or route of the car are unknown to the algorithm, the choice of the path used for prediction is arbitrary once it encounters p multiple possible paths. Hence the estimated probability drops to $1/p$. This, in turn, means that if a large error occurs while the estimated probability is 1, an error in the position predictor or the map material should be assumed, while high prediction errors with low estimated probability are most likely to be produced by the fact that the mission of the car is unclear.

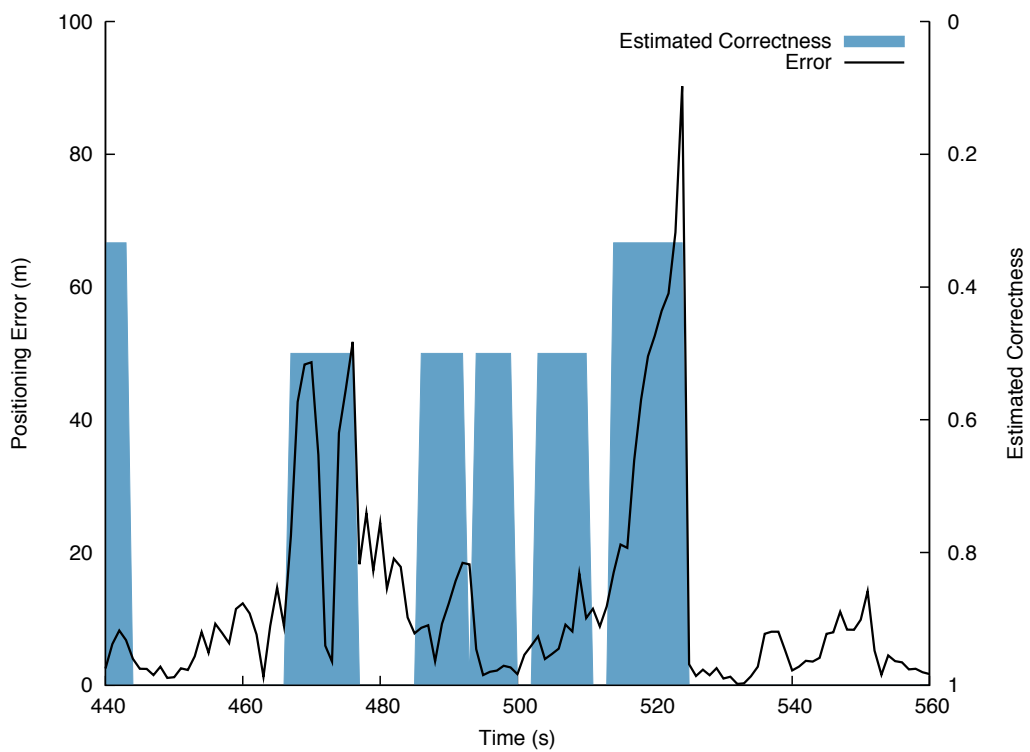
Should the position predictor be either unable to find the current segment or to find any path to continue, the estimated prediction probability drops to zero. This is the case at the beginning of the city scenario and is the result of pulling out of a private parking area in a sort of backyard. As there is no map material covering that area, the position predictor cannot give useful predictions based on the fact that it is unclear on which road the vehicle is driving. In such situations, the position predictor simply returns the current position.

To get an idea of the nature of an error, it is helpful to visualize the real and the predicted path as shown in Figure 5.5. The actual path is shown as a black solid line while the predicted path is shown as a dashed orange line.

Around time step 520, Figure 5.5(a) shows a typical situation in which the prediction algorithm encounters a crossroads. For the reasons explained in Section 5.3.4, the algorithm always prefers to choose the path that continues on the current road. This can be seen in the Figure where the predicted green dots continue straight on, while the real, blue trace turns onto the intersecting road. Once the car is on the new road, the prediction adapts to the new situation



(a) Velocity prediction



(b) Prediction error

Figure 5.4.: City scenario.

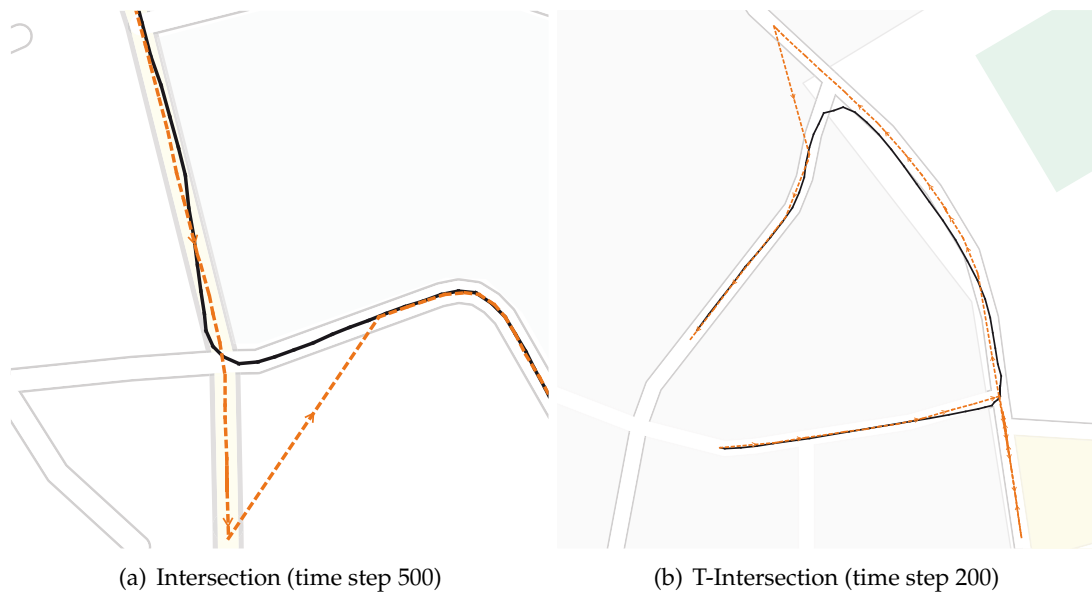


Figure 5.5.: City scenario - prediction error at crossroads.

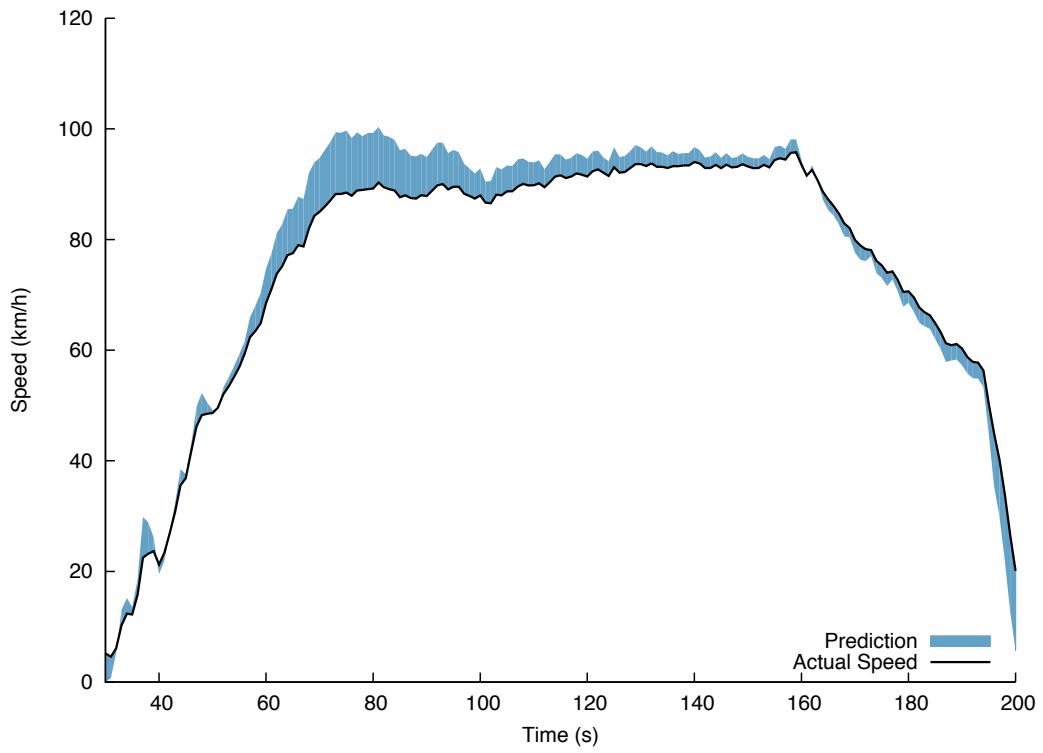
and continues its prediction along the new road. This can also be seen in Figure 5.4(b), where the error peaks due to the large discrepancy between the real and the predicted position. At the same time, the estimated probability drops to 0.33, due to the fact that the algorithm recognizes three alternative paths at the intersection. Figure 5.5(b) shows a similar example around time step 200 as the car moves towards a T-crossing. The algorithm chooses the path with the lowest total change in angle, which in this case is the wrong choice. This, again, results in a drop of the estimated probability and a peaking error.

As can be seen from the examples above, the high error in urban scenarios is widely based on the fact that usually many intersections lie along the path and high prediction errors are introduced if the algorithm chooses the wrong path. We have argued that this fact can be significantly improved if the cars mission is known to the position predictor and, consequently, the correct path can be used for the prediction. For the city scenario, Figure 5.9(b) shows the CDF of the error histogram, with and without a priori knowledge of the route. Clearly, the positioning is much more precise if the route is known.

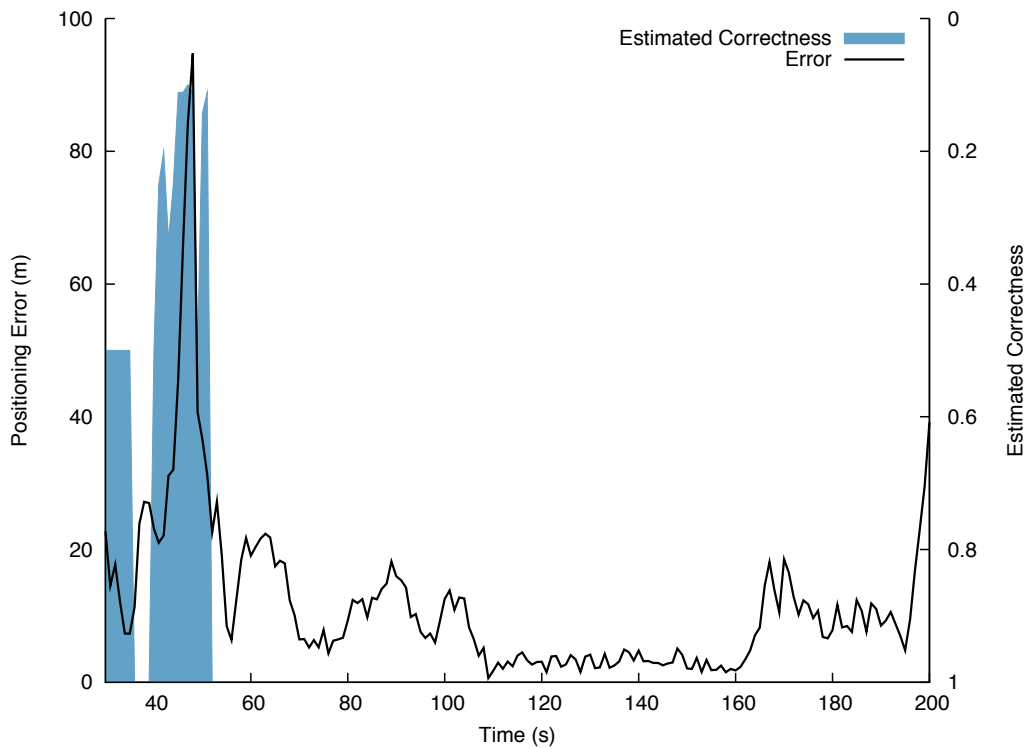
Suburban scenario

The second scenario covers the suburban area of Wiener Neustadt in Austria. The driver first hits the B17 road and afterwards enters the suburban area where the car is parked at a shopping center.

The section of the velocity graph in Figure 5.6(a) shows a short drive to the highway like state road. The speed prediction is rather stable whilst traveling at constant speeds between second 50 and second 200. This is accompanied by a rather small prediction error as shown in Figure 5.6(b). A peak in the prediction error at second 40 occurs due to a wrong choice of the next segment - again based on the fact that the cars mission is unknown. The fact that the algorithm had the choice of multiple directions is visualized by a significant drop of the



(a) Velocity prediction



(b) Prediction error

Figure 5.6.: Suburban scenario.

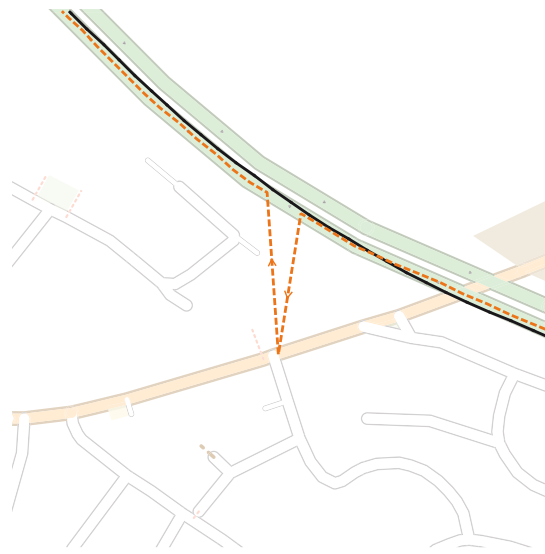


Figure 5.7.: Highway scenario - prediction error at highway bridge.

estimated correctness curve.

Due to a very sharp deceleration around second 200, Figure 5.6(b) shows another peak without a drop in probability for the fact that no other possible directions are identified. The reason for the braking is unclear, an explanation cannot be found in the map material nor the satellite image of the area. Figure 5.6(b) also shows a few more peaks based on decisions for the wrong directions and braking actions.

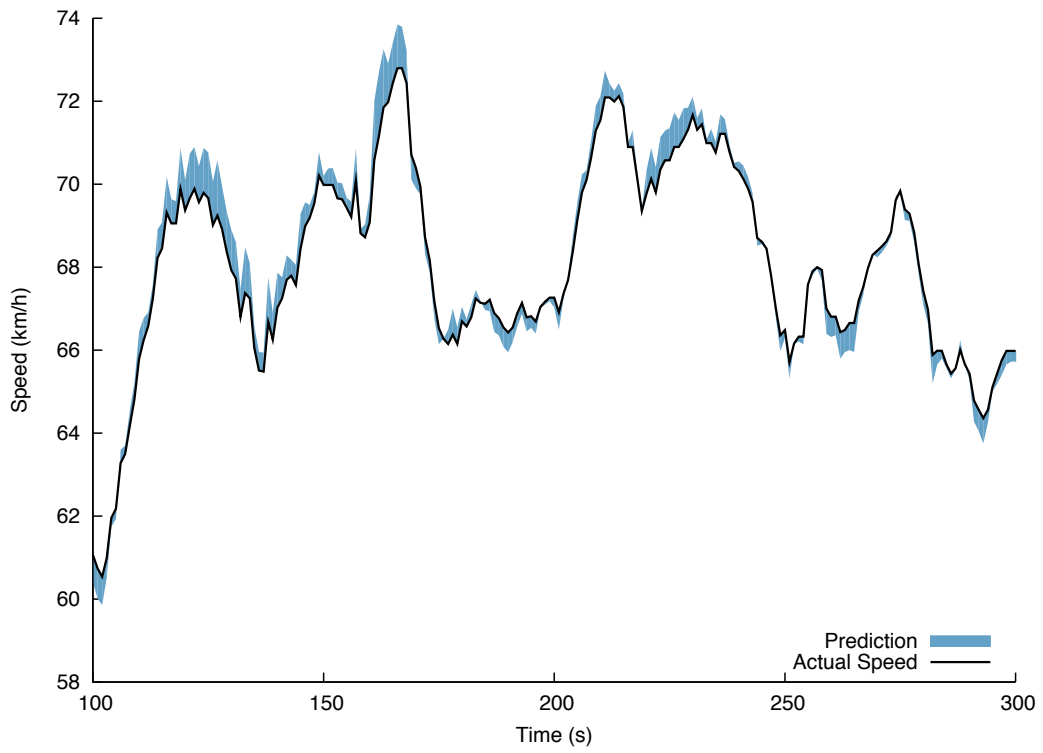
The distribution function shown in Figure 5.10(a) (upper blue line) is slightly flatter than the one from scenario 1. The median error (about 10 meters) is slightly higher than in the city, probably caused by the fact that either map material or the GPS device used to record the track are less precise than in the city scenario. The 90% percentile is significantly smaller (22 meters compared to 34 meters), which supports the before assumption and leads to the conclusion that the overall position prediction is better in the suburban scenario. The mean error of 13.5 meters, however, is almost identical to the city scenario.

Highway scenario

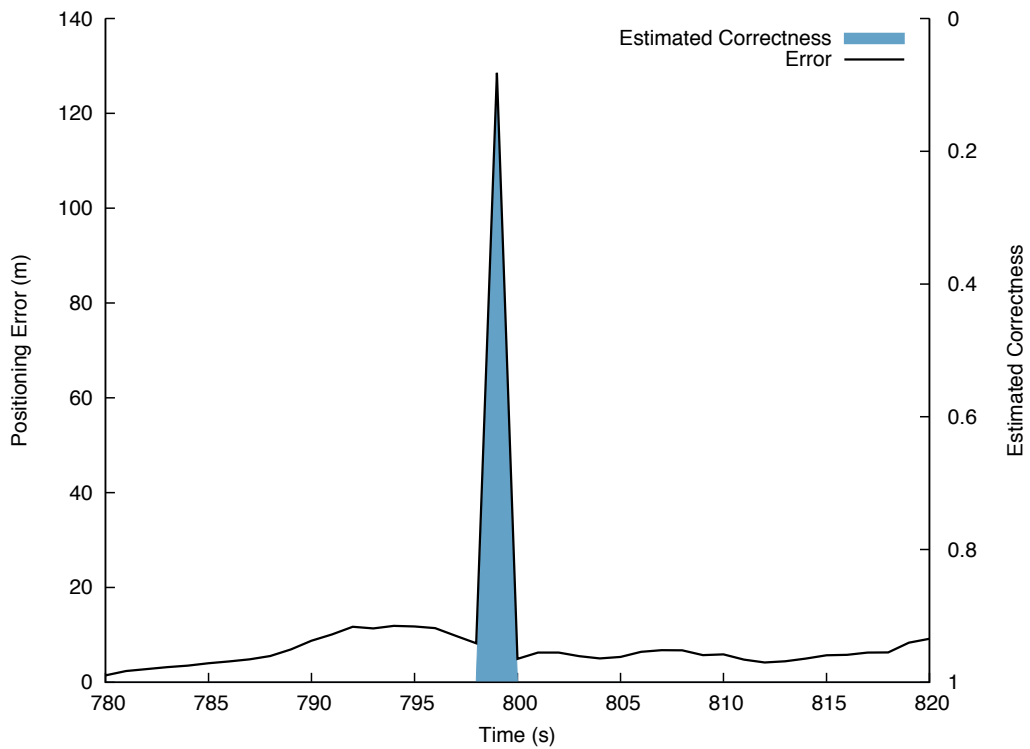
The third scenario covers a ride on a highway near the English town of Cambridge during rush hour traffic, which explains the unsteady velocity curve shown in Figure 5.8(a). Again, a representative section has been chosen for presentation.

The prediction error plotted in Figure 5.8(b) shows constantly low prediction errors. From the distribution function shown in Figure 5.10(b) (upper blue line) reveals a very steep slope, which means excellent performance of the algorithm as more than 95% of all errors are below 10 meters. The mean error amounts to only 4.6 meters and the median is 3.8 meters.

One notable peak of the error, accompanied by a drop in the estimated probability occurs around time step 800 (see Figure 5.8(b)). Figure 5.7 visualizes both the real trace (shown as blue arrows) and the predicted trace (shown as green dots). At the instant when the car is crossing a highway bridge — as highlighted in the screenshot — the algorithm wrongly



(a) Velocity prediction



(b) Prediction error

Figure 5.8.: Highway scenario.

chooses the current road segment to be part of the road below the bridge that shares a node with the highway. Consequently, the algorithm chooses the wrong road segment to continue prediction. This error is caused by an unfortunate combination of a small measuring error of the GPS device and an imprecision of the map material, where the highway shares a node with the intersecting road (although they are on different levels).

Another error source stems from the fact that in the used map material, a road is represented by a polyline, and all vehicles are assumed to be positioned on this line. In reality, highways consists of a number of parallel lanes that have a certain lateral displacement. Although a suitable representation of road lanes has been suggested, the data available today does not yet represent different lanes. We expect, however, that the error would be decreased if this information could be accounted for in the prediction.

Influence of Prediction Length

The results that we have discussed above were obtained through prediction with period lengths of eight seconds. This sections evaluates the same scenarios with longer prediction lengths of 16 and 32 seconds. The resulting position error distribution functions are shown in Figures 5.9 and 5.10.

The steepness of the distribution functions decrease as the prediction length increases, due to less prediction accuracy across a longer period of time, i.e., the tendency to produce greater errors. The maximum error also increases dramatically, because in case that a wrong path is chosen, the prediction continues along the wrong path for a much longer time before it is corrected as the car turns the other way. The mean error is also shifted towards higher values with increasing prediction intervals.

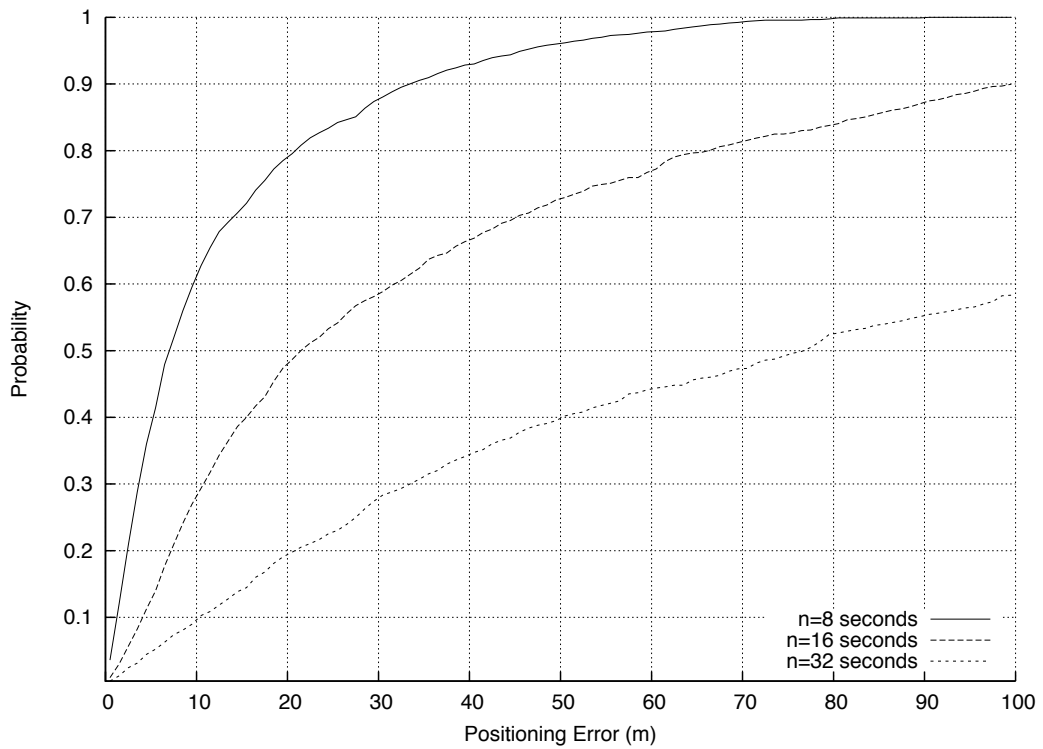
In the city and suburban scenarios, the prediction is already significantly less reliable with $n = 16$ time steps (i.e., seconds) as a prediction interval. It is rendered basically useless with a prediction interval of $n = 32$ and the majority of errors are out of scale of the histogram. The highway scenario, however, behaves much more stable as the prediction interval is increased and still returns useful results using a prediction horizon of 32 seconds. To a large extent, this is based on the relatively stable velocities and absent alternative paths along the way.

5.4. Channel Parameter Estimation and Prediction

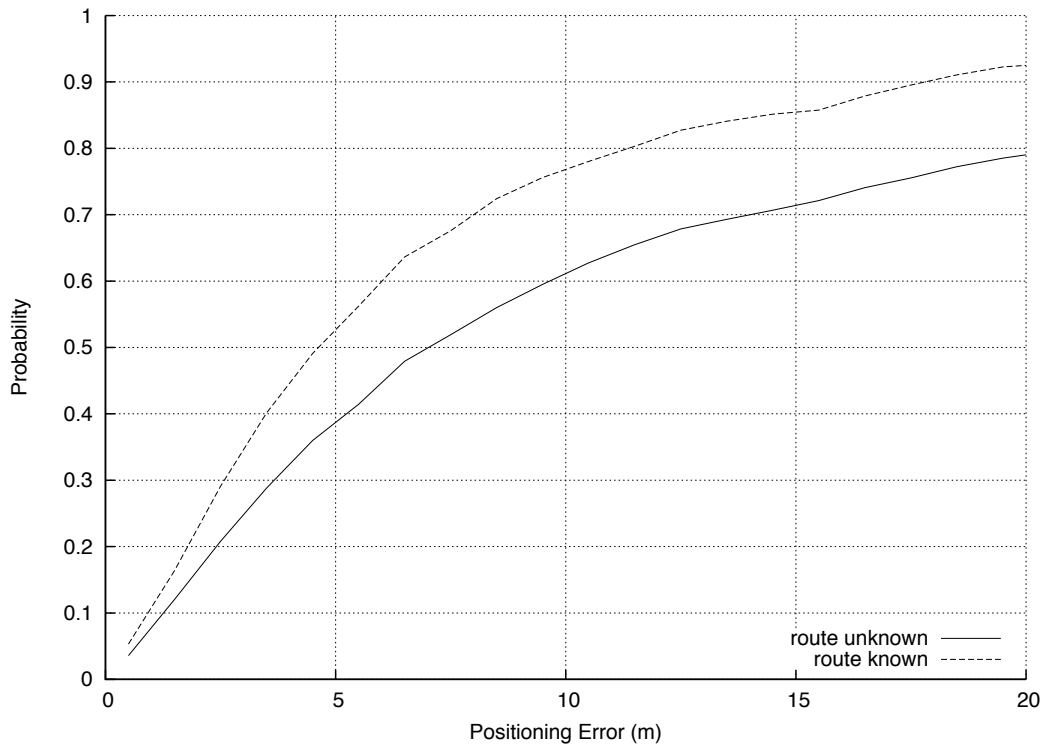
It is clear from Equation (5.5) that the network's future connectivity does not only depend on the future vehicles' positions. An adequate channel model has to be chosen and constantly updated to reflect the changing radio environment. In Equation (3.9), we have shown a simple channel function, the *disc model*. We shall call two nodes i and j connected if the path loss $\beta(d)$, a function of the distance between the two nodes, does not exceed a certain threshold β_{max} :

$$\beta_{max} \stackrel{!}{>} \beta(d) = 20 \log_{10} \frac{4\pi d_0}{\lambda} + 10\alpha \log_{10} \frac{d}{d_0} \quad (5.6)$$

The path loss consists of two components: a constant addend that reflects the loss related to the wavelength of the signal and a distance-dependent term that represents the propagation of the radio wave through space and the resulting diminishment of power due to the growth of

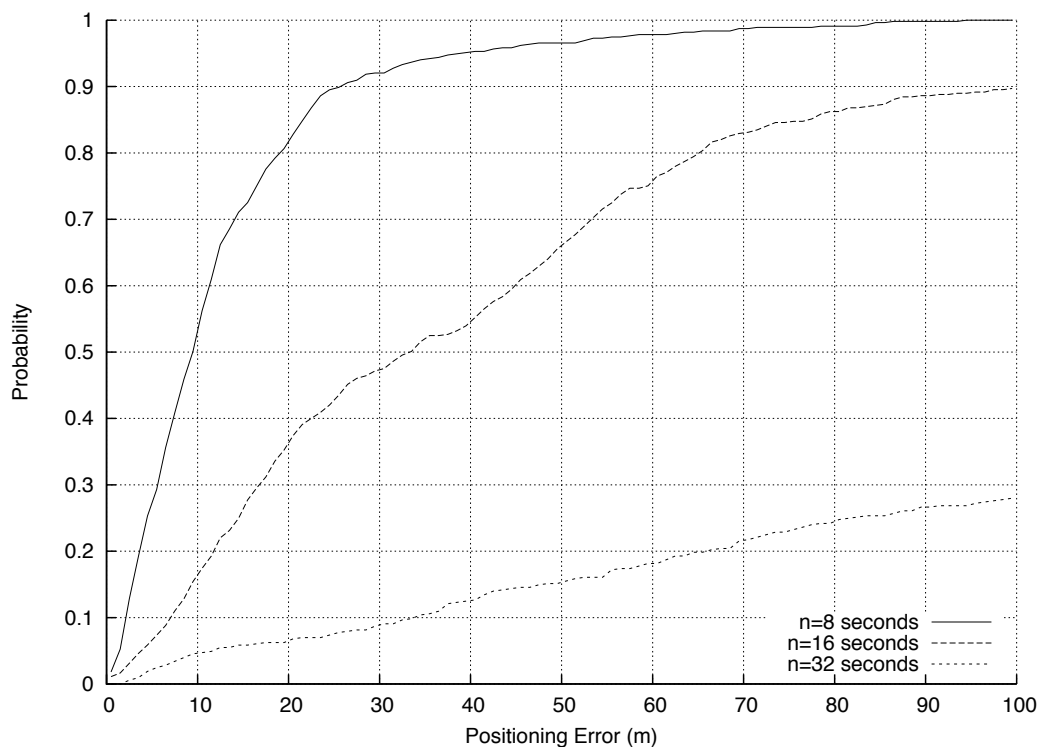


(a) City scenario

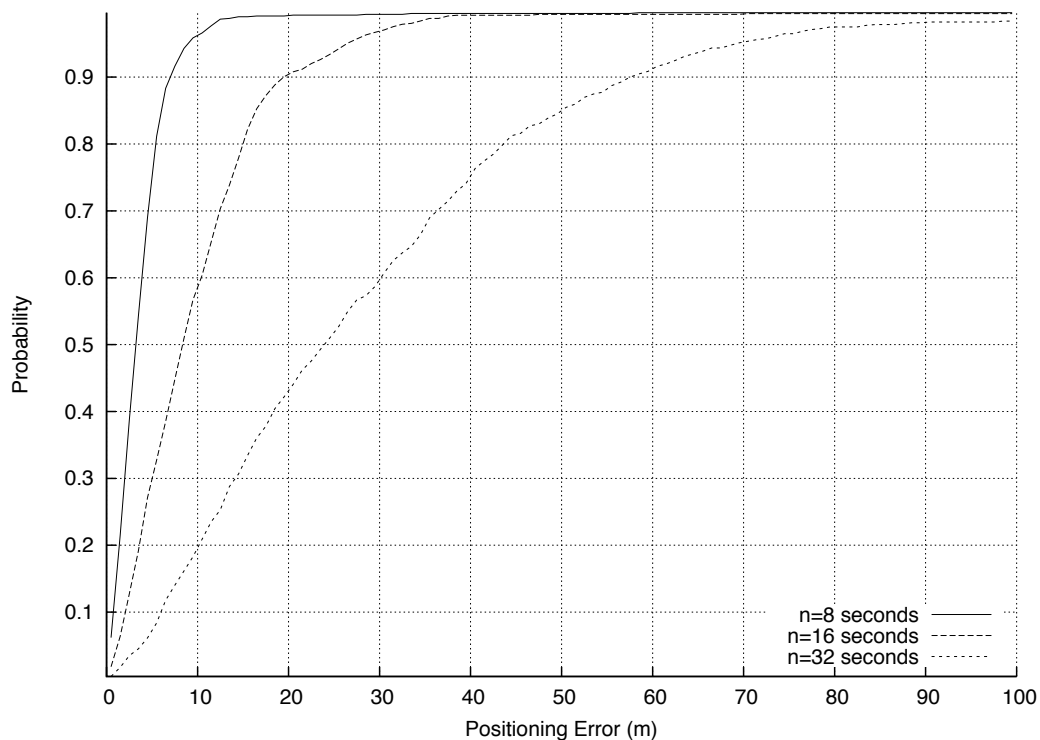


(b) City scenario - Route known

Figure 5.9.: Prediction error histogram - different prediction lengths for the city scenarios and the influence of known routes on prediction accuracy.



(a) Suburban scenario



(b) Highway scenario

Figure 5.10.: Prediction error histogram - different prediction lengths for the suburban and highway scenarios.

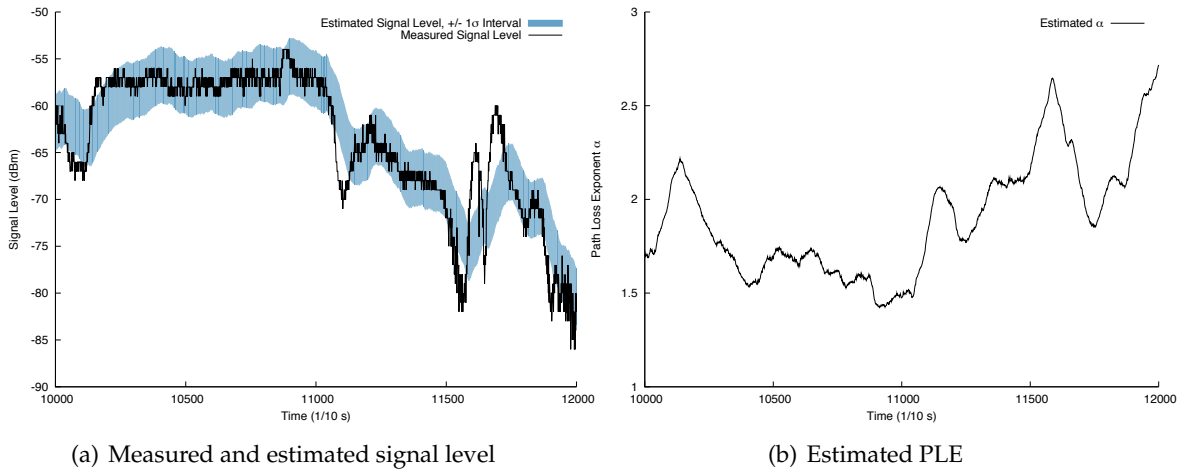


Figure 5.11.: Parameter estimation using particle filter: measured and estimated path loss, estimated PLE.

the wave sphere's surface. Due to various propagation effects, the PLE α is variable, to reflect various environments' radio properties (and usually ranges between 2 and 3). To account for reflections, scattering and shadowing, an additional stochastic variable β_s is introduced that is log-normally distributed with zero mean and variance σ^2 :

$$\underbrace{\beta(d)}_{\text{measured}} = C + \underbrace{10\alpha}_{\text{unknown}} \log_{10} \frac{\underbrace{d}_{\text{known}}}{\underbrace{d_0}_{\text{known}}} + \underbrace{\beta_s}_{\text{unknown}} \quad (5.7)$$

Through constant exchange of position messages, two nodes can determine their distance d and at the same time measure the path loss $\beta(d)$ between them (terms marked as "known"). Assuming that β_s is log-normally distributed and knowing the order of magnitude of the variance, we suggest to use a particle filter [CGM07] for online estimation of the PLE α and subsequent prediction, analogous to the work presented in [RC10]. To study the vehicular channel, we have recorded and evaluated several hours of measurements.

Figure 5.11(a) shows the path loss (solid line) measured in a real suburban scenario. These measurements consist of the positions of the vehicles and the signal level at the receiver and have been used to estimate the PLE using the particle filter method. From this estimation, the signal level has been computed again, it is shown as the filled curve including a β_s 's 68% (one standard deviation) confidence interval. The standard deviation of the measured SNR was estimated around 3 dB, the system constant C was -42 dB and the duration of the displayed dataset is 20 s. The estimated PLE is shown in Figure 5.11(b). Clearly, the PLE estimation works quite well and the results are very satisfying. However, the responsivity of the filter for the displayed data set was too low to cover the peaks between 1150 s and 1200 s. This issue, however, can easily be cured by a varied parametrization of the filter. Note how strong the PLE varies over the duration ($\Delta\alpha \approx 1.2$).

Furthermore, as we have discussed in the section on related work, it is very important to distinguish between LOS and NLOS conditions. In [NE08], we have introduced a method for V2V channel simulation in environments that include objects that possibly obstruct a direct

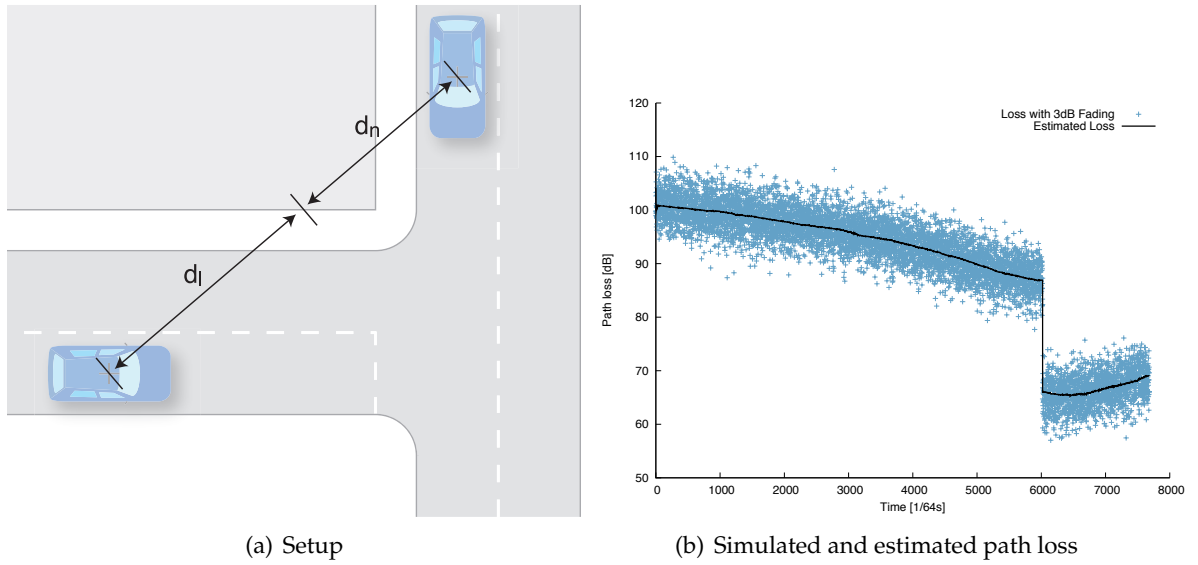


Figure 5.12.: Parameter estimation using 2D particle filter: setup and estimated pathloss.

LOS path and have discussed how a dual-slope channel model can be implemented to account for these objects. Consequently, we propose to complement the path loss formula in Equation (5.7) accordingly (see also Equation 3.12 and Figure 5.12(a)) and incorporate the information on buildings and other obstacles from the digital map material (that is already used in the position prediction) to determine if the path between the predicted future vehicle positions is LOS or not. The propagation breakpoint d_l derived from the map should then be accounted for in the PLE estimation:

$$d = d_l + d_n \quad (5.8)$$

$$\underbrace{\beta_p(d)}_{\text{measured}} = C + \underbrace{10\alpha_l}_{\text{unknown}} \log_{10} \underbrace{\frac{d_l}{d_0}}_{\text{known from map}} + \underbrace{10\alpha_n}_{\text{unknown}} \log_{10} \underbrace{\frac{d}{d_l}}_{\substack{\text{measured and} \\ \text{known from} \\ \text{map}}} \quad (5.9)$$

In simulations, we have obtained quite accurate channel parameter estimations using a two-dimensional particle filter that accounts for LOS and NLOS conditions, based on information about surrounding radio obstacles. The simulation scenario is shown in Figure 5.12(a): while the upper right vehicles is fixed in its position, the vehicle on the lower left moves towards the intersection. The simulated path loss, superimposed with a random process resembling fading with a variance of 3 dB, is depicted by the blue points in Figure 5.12(b). Clearly, as the total distance between the two vehicles decreases, the path loss also decreases. Initially, there exists no line-of-sight between the two vehicles until the lower vehicle moves out of the building's shadow. This causes the jump at around 6000/64 s. The solid line is the loss that results from the estimation of the two PLE exponents; obviously the 2D filter approach works rather good. Depending on the precision of the GPS devices and the quality of the digital map, which are crucial for determining the breakpoint distance, the quality of real-world estimations remains to be investigated.

The particle filter algorithm is outlined in Algorithm 3. It is parameterized through lower

Algorithm 3: Particle filter

Data: Lower and upper bounds of LOS PLE α_l^-, α_l^+ and NLOS PLE α_n^-, α_n^+ , system constant C , PLE variances $\sigma_{\alpha_l}, \sigma_{\alpha_n}$, noise variance σ_n , number of particles N .

Input: Continuous distance d and path loss $\beta_p(d)$ measurements, breakpoint d_l obtained from digital map.

Result: LOS PLE estimate $\alpha_l[t]$, NLOS PLE estimate $\alpha_n[t]$.

```

1 for  $i = 1, \dots, N$  do
2    $\tilde{w}^{(i)}[0] \leftarrow \frac{1}{N}$  ▷ Initialize weights
3    $\alpha_l^{(i)}[0] \leftarrow \mathcal{U}(\alpha_l^-, \alpha_l^+)$  ▷ Initialize LOS PLE
4    $\alpha_n^{(i)}[0] \leftarrow \mathcal{U}(\alpha_n^-, \alpha_n^+)$  ▷ Initialize NLOS PLE
5 end
6 while measurements available do
7   Measure distance  $d$  and path loss  $\beta_p(d)$ 
8   Obtain breakpoint  $d_l$  from digital map
9   for  $i = 1, \dots, N$  do
10     $\alpha_l^{(i)}[t] \leftarrow \alpha_l^{(i)}[t-1] + \frac{d_l}{d} \Delta \alpha_l, \Delta \alpha_l \sim \mathcal{N}(0, \sigma_{\alpha_l})$  ▷ Vary particle's LOS PLE
11     $\alpha_n^{(i)}[t] \leftarrow \alpha_n^{(i)}[t-1] + (1 - \frac{d_l}{d}) \Delta \alpha_n, \Delta \alpha_n \sim \mathcal{N}(0, \sigma_{\alpha_n})$  ▷ Vary particle's NLOS PLE
12     $\beta'_p(d) \leftarrow C + 10\alpha_l^{(i)}[t] \log_{10} \frac{d_l}{d_0} + 10\alpha_n^{(i)}[t] \log_{10} \frac{d}{d_l}$  ▷ Propagate
13     $\tilde{w}^{(i)}[t] \leftarrow \tilde{w}^{(i)}[t-1] \cdot \frac{1}{\sqrt{2\pi}\sigma_n} \exp\left(-\frac{(\beta_p(d) - \beta'_p(d))^2}{2\sigma_n^2}\right)$  ▷ Compute particle's weight
14  end
15   $w^{(i)}[t] \leftarrow \tilde{w}^{(i)}[t] / \sum_{j=0}^N \tilde{w}^{(j)}[t]$  ▷ Normalize weights
16   $\alpha_l[t] \leftarrow \sum_{i=1}^N w^{(i)}[t] \alpha_l^{(i)}[t]$  ▷ Compute estimated LOS PLE
17   $\alpha_n[t] \leftarrow \sum_{i=1}^N w^{(i)}[t] \alpha_n^{(i)}[t]$  ▷ Compute estimated NLOS PLE
18  Resample particles if necessary
19 end
    
```

and upper bounds α_l^-, α_l^+ and α_n^-, α_n^+ of two uniform distributions from which the particles' LOS and NLOS PLEs are drawn upon initialization. Also, the runtime variances $\sigma_{\alpha_l}, \sigma_{\alpha_n}$ need to be specified. Higher values means higher responsivity of the algorithm but also higher susceptibility to disturbances. Also, a rough (over-)estimate of the fading processes' variance σ_n should be specified. A number of $N = 256$ particles has yielded very good results. The particle filter is continuously updated with measurements of the path loss (or the signal level, respectively) and the distance between the vehicles plus the breakpoint as determined from the digital map. Using this information, it updates the particles and estimates the PLE. The novel approach is to increase the filter's accuracy by weighting the PLE variances with the LOS and NLOS fractions of the link, respectively (lines 10 and 11). This has the great advantage

that the algorithm can universally be used both in LOS and NLOS scenarios.

For the subsequent channel parameter prediction, we propose to employ the same concepts as used for position prediction to at least estimate the trend of the PLE. Also, it is clear that the effects of large-scale fading have a large impact on the future connectivity but are hard to account for. Small-scale fading effects can impossibly be accounted for due to positioning errors. Therefore, fading effects should be considered through an additional stochastic component. When evaluating the connectivity matrix computed from the predicted positions and the predicted channel, additional information about the reliability of the prediction should be provided and considered.

5.5. Connectivity Prediction

To determine the future connectivity of a network, a node has to predict the positions of all relevant vehicles (usually the one- or two-hop radio neighborhood) and determine the resulting path loss to decide whether it will be connected to this vehicle or not. The first error source of the path loss estimation is, of course, the error induced by inaccurate position prediction. Fortunately, this error term strongly depends on the distance d between the two involved vehicles. Let us assume that the estimating vehicle has perfect ego positioning and position prediction (the estimating vehicle also needs to know its future position) and let Δd denote the maximum positioning error. The resulting absolute estimation error range (peak-to-peak) is then:

$$\Delta\beta(d, \Delta d) = \beta(d + \Delta d) - \beta(d - \Delta d) = 10\alpha \log_{10} \left(\frac{d + \Delta d}{d - \Delta d} \right) \quad (5.10)$$

The second influence on path loss estimation is the accuracy of the predicted PLE. Let $\Delta\alpha$ denote the PLE's maximum estimation error. The resulting absolute path loss estimation error is:

$$\Delta\beta(d, \Delta\alpha) = \beta(d, \alpha + \Delta\alpha) - \beta(d, \alpha - \Delta\alpha) = 20\Delta\alpha \log_{10} \left(\frac{d}{d_0} \right) \quad (5.11)$$

Clearly, there exists a strong negative correlation between the path loss estimation error and the distance to the tracked vehicle, d . With increasing d , the implications of prediction errors become less important with respect to the path loss. The situation is contrary regarding the PLE estimation: because the relation is linear, a large path loss estimation error results if the distance d to the tracked vehicle increases. The problem is that Δd and $\Delta\alpha$ are not known at runtime; therefore, we suggest to keep the prediction results and constantly compare them against the predictions to obtain a statistic of the errors. This information should consequently be used to determine a prediction's reliability.

Let us assume that through constant observation the distribution of the estimated distance d , $f_D(d)$, is known, and that the distribution of the estimated PLE α , $f_\alpha(\alpha)$, is also known. We wish to determine the distribution of the path loss estimation, $f_\beta(\beta)$, as a function of $f_D(d)$ and $f_\alpha(\alpha)$:

$$\beta = 10\alpha \log_{10} d \quad (5.12)$$

To determine the probability distribution of β , we will use the method of conditioning. First, the PDF of β given d is fixed ($f_{\beta|D}(\beta|d)$), is obtained through transformation of $f_{\alpha}(\alpha)$:

$$\begin{aligned}\alpha(\beta, d) &= \frac{\beta}{10 \log_{10} d} \\ \frac{d\alpha(\beta, d)}{d\beta} &= \frac{1}{10 \log_{10} d} \\ f_{\beta|D}(\beta|d) &= f_{\alpha}(\alpha(\beta, d)) \frac{d}{d\beta} \alpha(\beta, d)\end{aligned}$$

The joint probability $f_{\beta,D}(\beta, d)$ is then:

$$\begin{aligned}f_{\beta,D}(\beta, d) &= f_{\beta|D}(\beta|d) f_D(d) \\ &= f_{\alpha}(\alpha(\beta, d)) \frac{d}{d\beta} \alpha(\beta, d) f_D(d) \\ &= f_{\alpha}\left(\frac{\beta}{10 \log_{10} d}\right) \frac{1}{10 \log_{10} d} f_D(d)\end{aligned}$$

Finally, integration over the joint probability and, thus, elimination of d , results in the distribution of the estimated path loss, $f_{\beta}(\beta)$:

$$f_{\beta}(\beta) = \int_{-\infty}^{\infty} f_{\beta,D}(\beta, d) dd \quad (5.13)$$

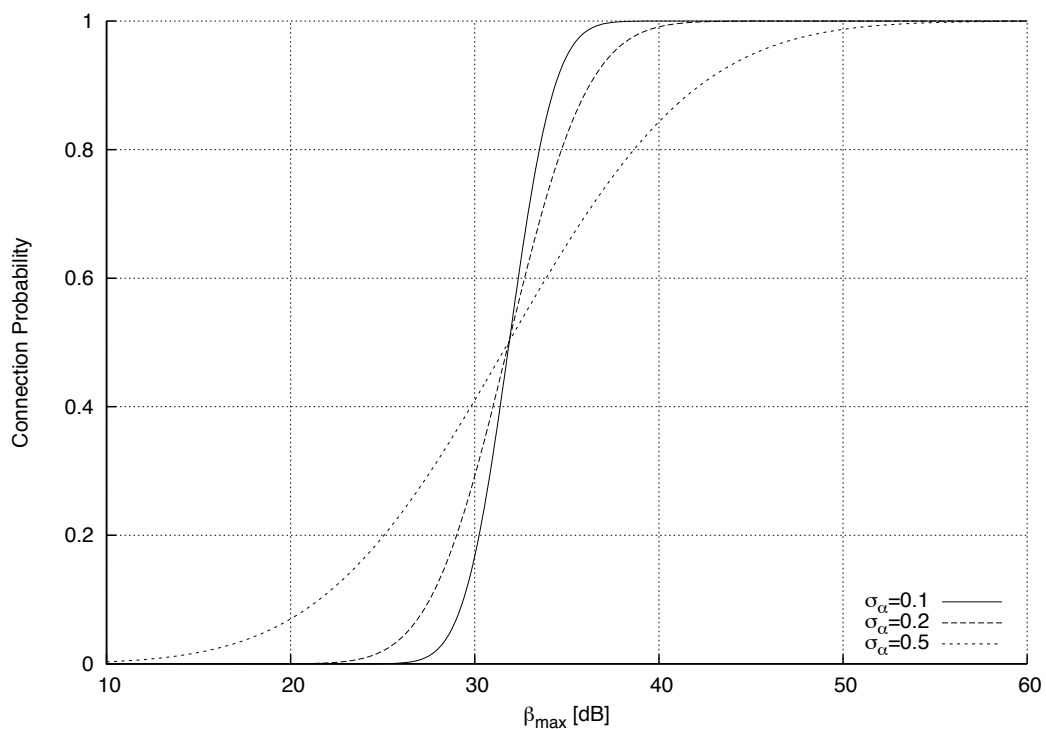
The probability that a node is connected (i.e., the path loss is below β_{max}), which corresponds to the channel function (see Equation 5.5), is then:

$$\chi(f_D(d), f_{\alpha}(\alpha)) = \int_0^{\beta_{max}} f_{\beta}(\beta) d\beta \quad (5.14)$$

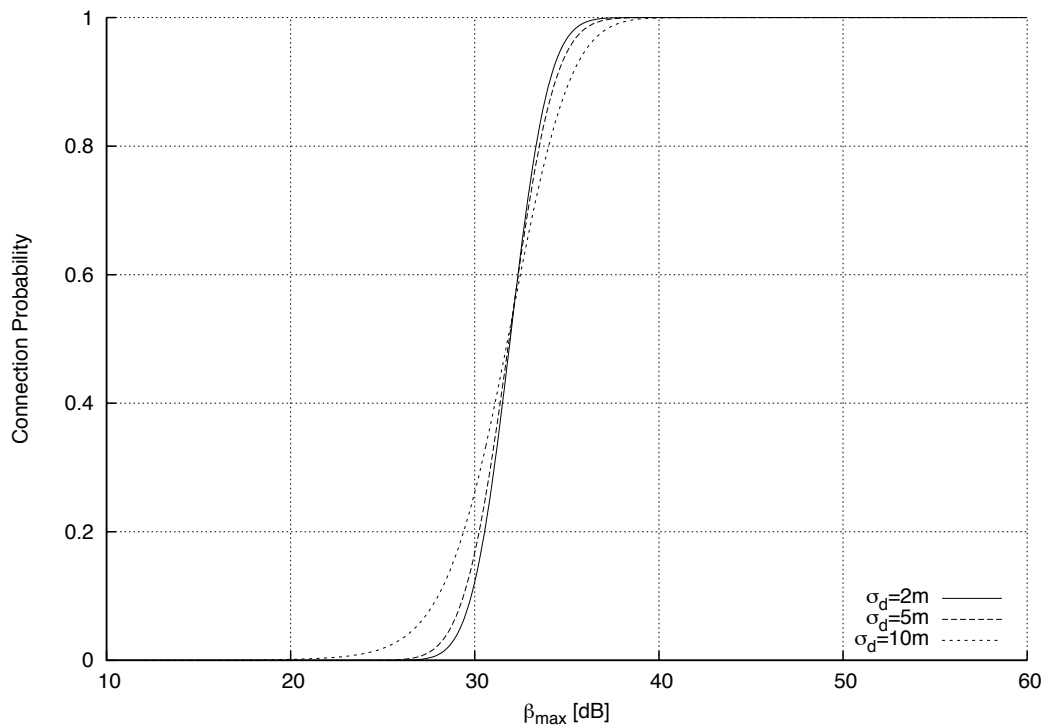
Figure 5.13 shows exemplary connection probabilities over the maximum allowable path loss β_{max} , computed under the assumption that both $f_D(d)$ and $f_{\alpha}(\alpha)$ are gaussian distributions. The parameters have been varied according to the numbers given in the figure. Clearly, the curves are much more susceptible for variations of the PLE.

5.6. Conclusions and Outlook

In this chapter, we have presented an algorithm for the self-adaptive prediction of mobile nodes' future positions. The algorithm is targeted at vehicular applications with nodes that move along the road grid, of which a digital map is available at runtime. We have introduced the necessary building blocks along with their parameterization, discussed some performance studies and pointed out individual strengths and shortcomings. Three exemplary scenarios have been studied: city, suburban, and highway. Given a prediction interval of eight seconds, the algorithm performed well in all of the scenarios, resulting in a mean prediction error of only about 14 meters. On a highway, the mean error is less than 5 meters. As the prediction interval increases, the performance of the algorithm degrades significantly in the city and



(a) $\bar{\alpha} = 2$, σ_α varied, $\bar{d} = 40$ m, $\sigma_d = 2$ m



(b) $\bar{\alpha} = 2$, $\sigma_\alpha = 0.1$, $\bar{d} = 40$ m, σ_d varied

Figure 5.13.: Connection probabilities for gaussian $f_D(d)$ and $f_\alpha(\alpha)$ with varying parameters over the maximum allowable path loss β_{max} .

suburban scenario. On a highway, however, the mean error is around 30 meters for an interval of 32 seconds which may still be acceptable, depending on the application.

We have already argued in the discussion that the position prediction accuracy in the city and suburban scenario is mainly degraded due to an incorrect path selection as the considered vehicle approaches an intersection. In our studies, the future path has been selected randomly from the set of possible paths. The necessary assumptions have been explained in Section 5.3.4. If the information is available, we strongly propose to consider vehicles' missions for path prediction. Considering the city scenario, if only those prediction errors are evaluated for which the path selection is correct (i.e., the predictor estimates the correctness as 1), the mean error can be decreased to about 8 meters, the median to about 5 meters. Taking the mission into account, these extremely low errors seem feasible.

The computation of the distance to cover is currently calculated using the area under a linear graph between the current velocity and the predicted velocity, thus assuming a linear acceleration. Some thoughts should be given to a substitution of this simple approximation with a more sophisticated implementation. One idea that is rather complex in terms of computational efforts is to use n velocity predictors to predict a velocity for each time instant and thus removing the interpolation. Another approach could be to model the acceleration and deceleration behavior of a typical driver. If the vehicle is autonomous, reproducing the design of the longitudinal controller could increase the prediction performance.

Velocity prediction, too, offers some optimizations opportunities. The key measure necessary here is a numerical optimization of the parameters a , b and c mentioned in Table 5.1 over a large number of scenarios of adequate length. Appropriate parameter sets could be computed beforehand (and even optimized online) and information about the current driving situation could be used to select the most suitable set. This selection, in turn, could be used to provide other applications with valuable information about the current environment. It is expected that an adoption of these parameters will lead to a somewhat significant improvement of the speed prediction. An urban scenario requires much quicker reactions to speed changes and thus needs more contributions and stronger influence of the weight booster than a highway scenario. The highway scenario, in turn, profits from a more stable prediction based to a large extent on the mean weight vector and requires virtually no influence of the weight booster.

We have proposed a particle-based method for the fast and efficient online-estimation of the Path Loss Exponent (PLE) using signal level measurements from the physical layer and exchanged positioning information and we have discussed the performance with actual data measured in a suburban environment. We have then demonstrated how the estimator could be extended to account also for NLOSs conditions and discussed results obtained from simulations. The mathematical foundation for a channel function that computes connection probabilities from the estimated parameters, distance between vehicles and PLE, has been laid and discussed. From the shown results, it is clear that the connectivity prediction is more susceptible to wrong estimations of the PLE, which gives raise to the need for development of effective channel estimation and — most importantly — further improved channel parameter prediction mechanism.

Longer-term prediction of the wireless channel still imposes the largest problem when it comes to evaluate the future connectivity from predicted positions. Further work is necessary to evaluate the dynamics of the radio channel and design an appropriate predictor. We propose to include further information about the environment (see above) in order to distinguish between different surroundings and consequently adjust the appropriate channel parameters (such as

the variance of the large-scale fading). An interesting idea in this context is to share and aggregate knowledge of the communication channel obtained from measurements between nearby vehicles. Another situation that requires attention is the channel prediction for vehicles that are actually outside of a node's communication range and channel parameter estimation is obviously not possible. In this case, the channel has to be estimated from measurements conducted with and from nearby vehicles.

6. A System Architecture for Cooperative Cognitive Technical Systems

In the following, we present a communication solution tailored to the communication needs of cooperative vehicles as seen from an application perspective. We describe how such a solution can integrate into and amend the software structure of cognitive vehicles. Without going into the technical details of the underlying PHY and MAC layers, we describe the *data object transfer* mechanism geared towards cooperative perception modules, its integration in the data flow, and discuss some protocol issues. The *channels* mechanism is elaborated, which is specifically designed for management and control of cooperative groups of vehicles.

Data transfer in networks is generally handled by the protocols of the network layer and above. The most commonly known network layer protocol is the Internet Protocol (IP) and its companion transport layer protocols, Transmission Control Protocol (TCP) for reliable end-to-end connections and User Datagram Protocol (UDP) for unreliable datagram communications. Today, these protocols are used throughout the internet and in almost all Local Area Networks (LANs). They offer various features, such as a hierarchical addressing scheme for routing, fragmentation, differentiated services and large packet sizes.

The applications that we have presented in Chapter 2, however, do not make use of these features. Connections are mostly local, point-to-multipoint and routing (if needed) is usually determined by geographical positions rather than network addresses. Adhering to the traditional IP network stack, the headers of UDP and IPv4 would sum up to a total length of 28 B, without being relevant. Due to the shortage of IPv4 addresses, many studies suggest to use IPv6 for future networks, and hence for vehicular networks, which would increase the total length of the headers to 48 B. Checksum are unnecessary because packet errors are already detected and handled at lower layers.

Consequently, the decision has been made to build a complete protocol that covers the networking layer up to the session layer. In this section, we will discuss the details of the protocol and show how a prototypical communication solution integrates seamlessly with the software architecture proposed in the KogniMobil project. Most of the material in this chapter has been published in [NEE07, TAB⁺08, GAB⁺08, Nag09].

6.1. A Lightweight Network Layer Protocol

In order to keep transmissions as short as possible to save valuable airtime, we have decided to drop the IP stack as the network layer of choice and replaced it with a proprietary protocol that better suits our needs. This significantly reduces the amount of overhead due to headers which are not used anyway and the amount of configuration effort, since no IP addresses need to be assigned. The computational complexity needed to process IP packets is also saved.

Every packet is assembled from information pieces (*Packet Elements (PEs)*, such as, for example, measurement PEs, object update PEs, etc.) that are retrieved either periodically or on-

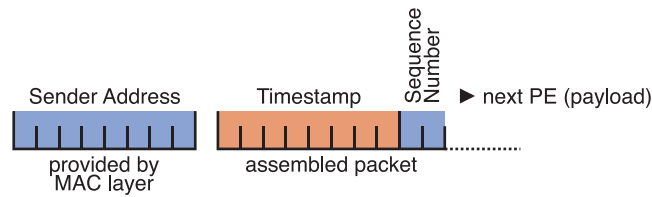


Figure 6.1.: Structure of a basic network layer packet.

demand from the transmit queue. The exact order and selection of these information pieces depends on the scheduler that tries to maximize the benefit while, at the same time, optimizing the amount of consumed air-time. A packet is headed by the senders address (which is actually provided by the MAC layer and does not consume any additional payload), a sequence number and a timestamp of when the packet was enqueued for transmission followed by an arbitrary number of PEs (see Figure 6.1). The number of PEs is bounded above by the Maximum Transmission Unit (MTU) determined by the MAC layer.

6.1.1. Radio As A Sensor

To allow a vehicle to become aware of its surrounding (one-hop neighborhood) vehicles, a mixed concept of beaconing and piggy-backing is used. If no PEs are waiting for transmission, a timer makes sure that an empty packet is periodically emitted (beaconing). The basic packet structure carries the important fields: the sender's address, timestamp and sequence number. Every node that receives a packet can immediately update its internal list of neighbors from these fields. Also, lost packets can be determined from the contained sequence number.

Two-hop neighborhood awareness is achieved through the measurement PEs. The structure is shown in Figure 6.2:

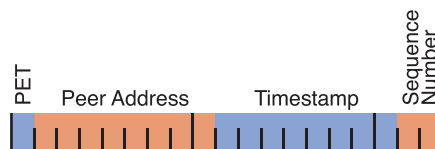


Figure 6.2.: Structure of a measurement PE.

Measurement PEs are constructed from the list of one-hop neighborhood vehicles by simply copying the content of the list into the PE. Therefore, a measurement PE, upon reception, contains information about the identities of a neighbor's neighbors and the timestamp when they were actively heard at last. This information is sufficient for the QoS algorithm presented in Chapter 4.

Note that no information about the actual geographical positions of vehicles is exchanged. In this very basic mode of operation, communication presents a way of knowing which vehicles are around, which may already be significant information for higher layers.

A careful trade-off has to be made when configuring the period at which beacons are transmitted and at which measurement PEs are included in packets. Clearly, every such beacon and measurement packet transmission comes at the price of increased bandwidth usage. On

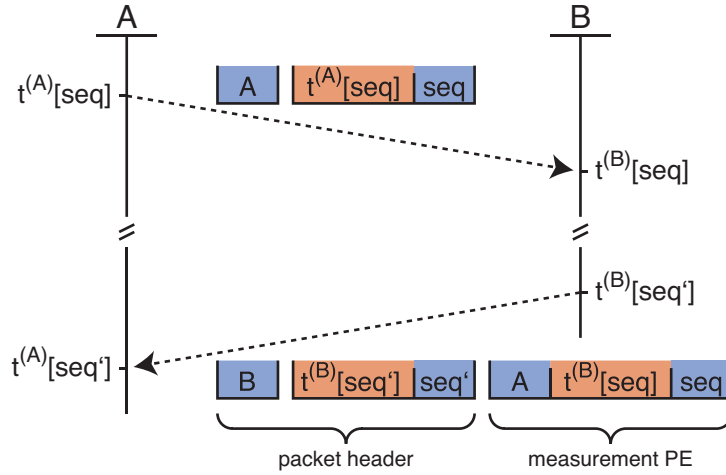


Figure 6.3.: Message flow diagram of the timing measurement.

the other hand, neighborhood information must be updated regularly, otherwise it will become invalid. Especially in highly mobile networks, mobility of nodes can be handled more correctly and efficiently if the frequency at which this information is updated is higher. The same care must be taken when evaluating if a node has timed out to avoid false positives.

6.1.2. Timing Measurement

As the name already suggest, measurements PEs are also used to measure the channel, the round-trip time of messages and the skew between vehicles' local clocks. This information can later be used for timestamp correction of exchanged data objects, if needed. The beaconing mechanism makes sure that packets are transmitted at least with the defined periodicity, which allows for continuous signal strength collection, if supported by the PHY layer.

The message flow used for timing measurement is shown in Figure 6.3: Every node (A) keeps a log of the timestamps of a number of messages that it has sent, indexed by the sequence number. As the packet is received by another node B, the sequence number along with the timestamp of when the message was received by B is repeated in a measurement PE and transmitted by B. When this measurement PE is received by A, A looks up the timestamp of when it originally sent the message that the PE references (via the sequence number) and can then compute the Round-Trip Time (RTT) t_{RTT} :

$$t_{RTT} = (t^{(A)}[seq'] - t^{(A)}[seq]) - (t^{(B)}[seq'] - t^{(B)}[seq]) = 2t_p + t_{QA} + t_{QB} \quad (6.1)$$

Due to time-variant queueing delays at A and B, t_{RTT} will vary over time. Note that the RTT t_{RTT} is the sum of twice the propagation delay between A and B and the queueing delays (the delay between the time when a packet has been added to the MAC transmit queue and its actual sending time) at A and B, respectively. The difference between the vehicles' clocks, Δ_{clock} can be estimated as:

$$\Delta_{clock} = \frac{(t^{(A)}[seq'] - t^{(B)}[seq']) + (t^{(A)}[seq] - t^{(B)}[seq])}{2} + \frac{t_{QA} - t_{QB}}{2} \quad (6.2)$$

Note that if the queueing delays t_{QA} and t_{QB} are equal, the last term of Equation (6.2) is zero and the clock skew estimation is correct. Clearly, if the packets contained the timestamps of when they were actually sent, the term would also be zero. However, since the statistics of $t_{QA} + t_{QB}$ is known, we can use deconvolution to retrieve the distributions of t_{QA} and t_{QB} and find the distribution of $t_{QA} - t_{QB}$. Under the assumption that t_{QA} and t_{QB} are equally distributed, averaging can be used to estimate the clock skew. See also the NTP protocol [MMBK10].

6.1.3. Identification

In many cases, it is desirable to transmit some information about the sender, such as a cleartext identifier, certificates, keys, etc. This information can be transmitted in every message or with a certain period, using an identification PE:

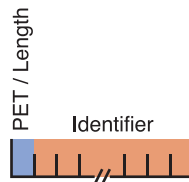


Figure 6.4.: Structure of an identification PE.

Note that the structure of the identification data itself is not specified and can be determined by higher-layer software.

6.2. The Communication Manager

The information flow (Figure 6.5 from top-left to bottom-right) within the vehicles software modules is based on a real-time database, which is basically a shared memory segment [GF08] that provides functions to create, update, retrieve and delete data objects as well as the possibility for software modules to subscribe to data objects and receive notifications upon updates of subscribed objects.

Following this paradigm, every sensor used in the vehicle has a corresponding data object. For instance, images taken by the onboard cameras or LIDAR data are stored as database objects, which are updated periodically as the sensor completes a cycle. These database objects are subscribed by instances of lane trackers, object detectors and classifiers which, in turn, have associated data objects that contain the outputs of these modules. The behavior control algorithms process these output contents and finally decide on a track that should be used for driving. Again, this track is routed through the database to the body control modules that control the vehicle's actors.

6.2.1. Network Topology Information

We have stated before that the information gathered by exchanging beacons, packets and measurement PEs can be seen as a kind of additional sensorial information. Consequently, the

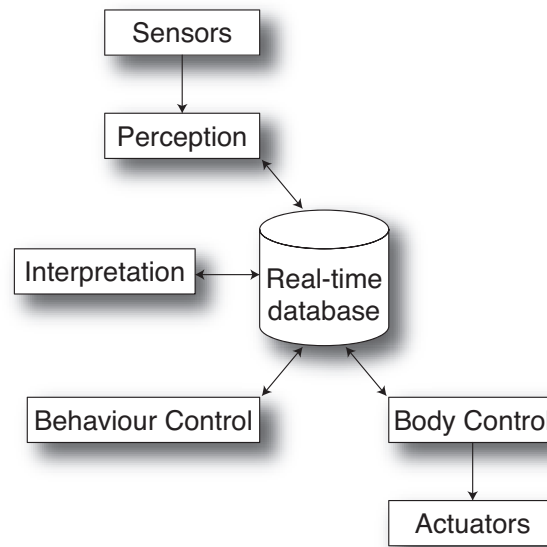


Figure 6.5.: Information flow through the real-time database

★ Peer Object

remote address	addr_t
round-trip time [s]	double
clock skew [s]	double
signal [dBm]	double
noise [dBm]	double
packet loss percentage [%]	double
packets total	u64

Table 6.1.: The Peer Object.

communication manager maintains a database object (the peer object, see Table 6.1) for each known neighboring node, that contains information about the address of the sender, the quality of the radio link (if available) and timing information as described above.

From a hierarchical standpoint, the peer object represents the topmost element under which all objects received from or related to that peer are organized. If no packet is received from a known sender for a certain time (timeout), the senders associated Peer Object and all subordinate received data objects are removed from the real-time database.

6.2.2. Time-triggered Communication

In order to allow vehicles to perceive and interpret their environment and to make decisions cooperatively, it is necessary to share the information needed by the involved modules between vehicles. To keep things simple in terms of module interface complexity, this is accomplished by mirroring the corresponding data objects between the individual real-time databases of vehicles participating in these tasks (see requirements Section 2.1.1). The design objective is to guarantee that data objects of same type (but from different sources, i.e. other

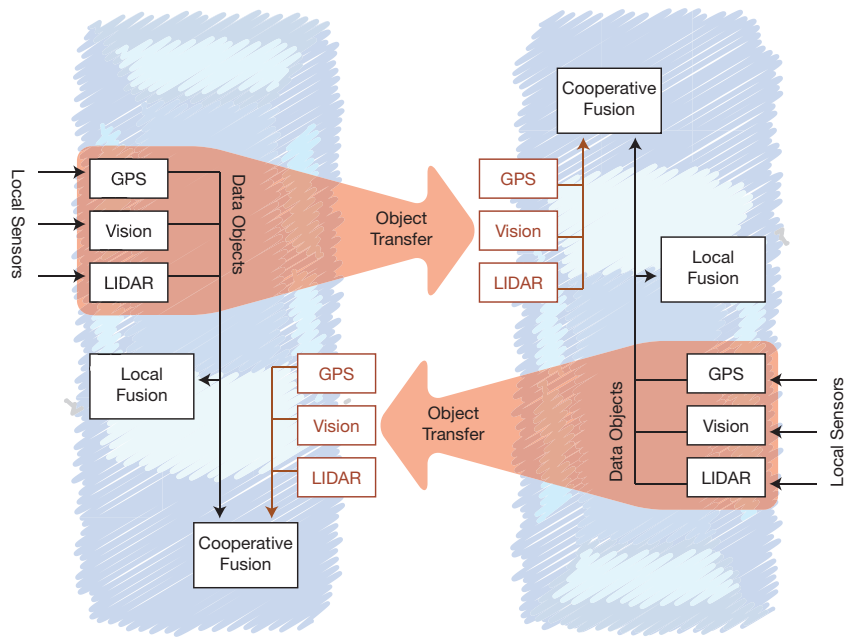


Figure 6.6.: Object transfer between two cooperative vehicles

★ Proxy Object

export-object id	id_t
divider	u16
priority	u16
maximum delay [ns]	time_t
flags	array[bool]

Table 6.2.: The Proxy Object.

vehicles) are stored locally and accessed by software modules as simple as if they originated from a local software module. Of course, it is necessary to additionally indicate the source which the data object originated from (the other vehicle).

This task of the communication solution is called *Object transfer*, which can be divided into two tasks as shown in Figure 6.6: *exporting* (sending, red arrow) and *importing* (receiving, red objects) data objects.

Exporting Data Objects

Vehicles that wish to share local information with other vehicles have to designate those data objects that they wish to be transmitted to other vehicles. This is done through so-called *proxy objects* (Table 6.2). For each designated export-object, one proxy object exists. This proxy object has a pointer to the export-object as well as additional information, such as a priority and a maximum tolerable delay, which is used internally by the communication manager to schedule the transmission of data objects. It also has a clock divider, that allows to export only every n-th object update, and a number of flags to indicate the internal status. Proxy objects may be handled directly by the communication manager, given a pre-defined configuration.

They may also be created by applications that wish to have their objects exported to other vehicles.

The communication manager itself has a connection to the real-time database and monitors the object hierarchy for the creation of proxy objects. As soon as a proxy object is created, it subscribes to the export-object and retrieves the necessary information from the proxy object. Upon notification of an update of the export-object, the updated content of the export-object is retrieved and an *object update PE* is generated, which is then sent to the transmit queue:

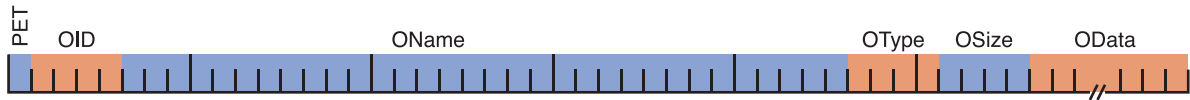


Figure 6.7.: Structure of an object update PE.

The object update PE contains all information that is necessary to create a new database object: the objects name, its type identifier and its size. The remote object identifier is also transmitted to allow for the correct assignment of the (sender address, remote object id) pair to the local object identifier. Although this additional information imposes an overhead of 40 B on the communication layer, it guarantees that received objects can always be added to the local database. The overhead can be reduced by using the *short object update PE*:

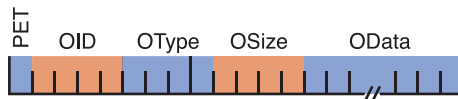


Figure 6.8.: Structure of a short object update PE.

The short object update PE consists of the same information as the object update PE, except for the objects name. Normally, short object update PEs do not carry the necessary information and are therefore not capable of adding an object to a local database. They may, however, be used to update objects that have previously been created by a full object update PE, at the tradeoff of lost information. However, an alternative mode allows for an exception: if a globally unique type-name relation exists for a certain object type, the name can be looked up from a pre-defined list and the object can then be created. The flags in the proxy objects handle the differentiation between regular and short object update PEs.

Due to the fact that most objects depend, either directly or through other data objects, on periodic information that originates from sensors, the resulting data traffic shows highly deterministic properties that can be exploited by the transmission scheduler and possibly also by the underlying medium access scheme.

If necessary, large data objects can also be fragmented. It is, however, not recommended to use this feature, as the broadcast operation does not easily allow for simple re-transmission mechanisms and consequently, updates may be lost if any fragments (that may spread over many packets) are lost.

Importing Data Objects

Assuming that every car desires to maximize its local knowledge about the environment, every receivable object is processed by every car. Therefore, as soon as an object update PE from

another car is received by the communication manager, it checks whether a peer object exists for the sender of the data object. The received data object is then unpacked and stored hierarchically under the peer object that represents the sender (imported).

If the imported data object has been received for the first time, a corresponding local object is created (with the possible exception of short object update PEs). After creation, or if the local object already exists, the content of the imported database object is updated. By doing so, the design objective mentioned above is fulfilled: To a software module connected to the real-time database, the imported object looks and feels like an ordinary local object — the module can subscribe to the data object and, upon reception of an updated data object, be notified to retrieve its content as if it originated from a local data source. Additionally, by looking at the object that is hierarchically above an imported object, the sender can be easily identified.

Removing Objects

Generally, if an application stops the export of a certain object through deletion of the proxy object or the export-object itself, vehicles that have previously imported this object into their local databases will recognize this after a certain timeout and consequently remove the corresponding local object. In some cases it may be desirable to make sure that the end of export is immediately signaled to the importing vehicles. This can be handled by using the *remove notification PE*:

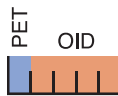


Figure 6.9.: Structure of an object remove notification PE.

The generation of remove notification PEs is triggered by setting the appropriate flags in the proxy object. If desired, sending can be repeated for several periods to ensure correct operation in the presence of lost packets.

6.2.3. Event-triggered Applications

Apart from the time-triggered data object transfer, it is desirable for many application to pass event-triggered, variable-length control messages. For instance, an application coordinating cooperative maneuvers needs to signalize the begin or end of such a maneuver (see requirements Section 2.1.2). In order to cope with this, we have introduced the concept of *Channels*, which can be compared to the channels available on walkie-talkies. Figure 6.10 shows how two channels for emergency messages and overtaking coordination are shared between three vehicles. Every vehicle that has subscribed a channel may transmit and receive on the channel (multiple-sources-to-multiple-sinks).

Access To Channels

While the data communication over the channel itself is routed through a standard local UNIX or UDP sockets that can be accessed in a generic way, channels are managed via the real-time database using *Channel Objects* (see table 6.3).

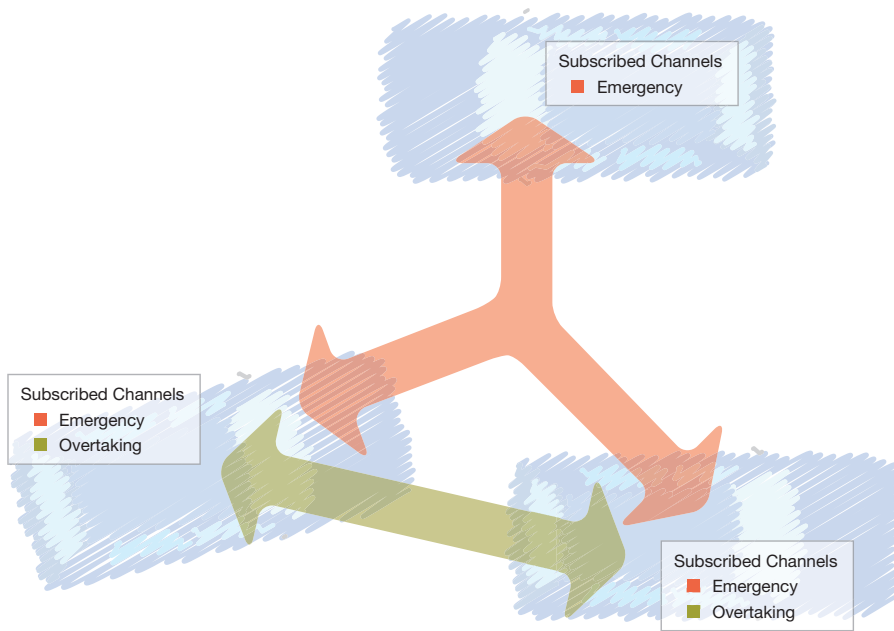


Figure 6.10.: Channels between three cooperative vehicles

★ Channel Object

local path	string
description	string
priority	u16
state	array[bool]

Table 6.3.: The Channel Object.

If an application needs to open a new channel, it simply generates an empty channel database object with only the description and priority field set. The communication manager subsequently generates a new socket and sets the local path field of the channel object accordingly. If the channel already exists and is known to the communication manager, the application only needs to look up the local path in the database. The application can then access this socket to write data to and receive data from the socket.

Channel objects are not associated with other peers because channels themselves are abstract of individual vehicles. Therefore, channel objects can exist at any hierarchical level in the database; for logical reasons, however, channel objects that are generated by the communication manager itself are child objects of the communication manager process. Applications should create new channel objects at the same place or as child objects of themselves.

Data that is written to the socket is encapsulated in *channel data PEs*:

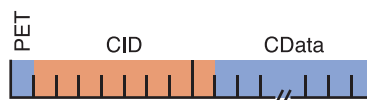


Figure 6.11.: Structure of a channel data PE.

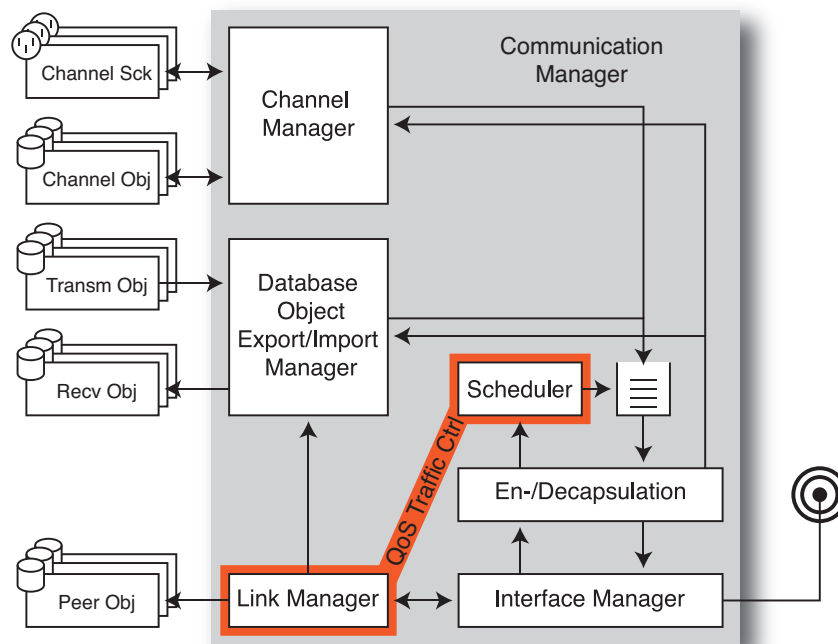


Figure 6.12.: Structure of the communication manager.

Channel data PEs are treated like other PEs by the queue and scheduler. However, to circumvent possible delays, channel data PEs, when enqueued in the PE queue, trigger the network layer to flush the pending PE queue and immediately start transmitting the waiting PEs (on-demand packet assembly).

If a channel data PE is received by the communication manager, it checks if the channel already exists locally. If it does not, a new local socket is set up and the associated channel object is inserted into the database. Then, the received channel data is forwarded to the appropriate socket where it can be received from by any application.

The communication manager constantly watches the state of the local channel sockets. If no data has been sent through a channel for a certain time, but applications are still connected, an empty channel data PE is sent so that other vehicles know about the channels existence. However, when the last application disconnects from the socket and no data has been received for a certain time, the channel is removed (timeout).

Membership of channels is not controlled by the communication manager. Every vehicle may subscribe to every channel and initiate as many new channels as it wants to. Also, encryption of messages, addressing and acknowledgement of point-to-point messages are not part of the channels functionality and need to be implemented in higher layers.

6.2.4. System Integration

The communication manager integrates seamlessly within the software architecture of the cognitive vehicle (Figure 6.12). The interfaces to the real-time database are shown to the left, the channel sockets that interface with applications on the top-left. The interface manager keeps track of the wireless link and configures the wireless interface.

The link manager keeps track of neighboring vehicles and the two-hop connectivity of the network. This information is stored in the database in the form of peer objects. The decapsulation block dispatches the received PEs to either the object import/export manager or to the channel manager. The object manager uses the data encapsulated in the object update PE by updating or — if necessary — creating the local database objects (aided by the link manager that provides the respective parent peer objects). The channel manager forwards the received data to the respective sockets.

In the other direction, the channel and object managers send their PEs, generated from the data received from the channel sockets or updated local objects, to the transmit queue. The queue is handled by the scheduler, which selects PEs for encapsulation. Completely encapsulated packets are then sent to the interface manager for transmission. The channel and object managers, however, maintain a handle to each PE they send to the transmit queue, which is valid until the PE has been selected for transmission. This way, they can replace queued but yet unsent PEs if updates become available that replace outdated PEs.

The scheduler itself selects PEs from the transmit queue according to their priority and their deadline (with respect to the worst RTT). In this way, we can guarantee that — if the necessary data rate is available — PEs are sent before their deadline expires and that higher-priority PEs are preferred in the selection process. The scheduler also makes sure that the MTU of the interface is not exceeded.

Following the proposed QoS framework presented in Chapter 4, the traffic control mechanism is implemented through the interaction of the link manager and the scheduler: the link manager provides the necessary network topology information needed for the QoS algorithm, i.e., the neighborhood information. The traffic limit for the node is computed and the determined admitted traffic is then used by the scheduler (highlighted section in Figure 6.12) to limit and smoothen the sourced traffic. To optimize the PE selection to yield the highest benefit for the network, the scheduler is parameterized with individual benefit functions through the proxy and channel objects (according to the content of the PEs).

The admitted traffic information is also stored in the database objects maintained by the link manager. If desired, it can be retrieved from there by the applications, which use the information to parametrize the pre-processing of the database objects they export. The benefit functions, as contained in the proxy objects, may be dynamically modified by the applications to account for varying traffic situations and to adapt their benefit accordingly.

The connectivity prediction module presented in Chapter 5 runs outside of the communication manager. It maintains connections to the peer objects, from which the current channel information is read, and monitors the positioning objects associated with the peer objects to obtain the peer's positioning information. With these informations, it can then run the channel estimation, channel and mobility prediction, and finally obtain an estimate of the future connectivity to a certain peer. This information is then written to the peer object, from where it can be retrieved by other applications.

6.3. Conclusion

In this chapter, we have elaborated on two communication primitives that support cooperative and cognitive behavior among autonomous vehicles. Real-time database objects can be transferred between several vehicles' databases using data object transfers. Event-triggered

control messages can be exchanged among groups of vehicles using the channels mechanism. We have also shown how these communication capabilities are integrated seamlessly into the existing software framework using a set of additional database objects, thus effectively hiding the underlying communication solution from the end user. Only in the case of channels, an additional interface to the application (standard UNIX or UDP sockets) is required.

The stringent cross-layer design could, if supported by the underlying communication hardware, allow for the control of modulation schemes and bit rates, error correction and other PHY layer parameters through additional fields appended to the controlling object.

We have shown how the QoS mechanism derived in Chapter 4 can be integrated in the communication manager and how the connectivity prediction module presented in Chapter 5 integrates in the system as an application.

To demonstrate the capabilities and seamless integration of our communication solution, some exemplary applications have been deployed:

- Exchange of GPS data objects: Using data object transfer, the position objects originating in the high-precision DGPS modules of vehicles have been exchanged. These position objects are then used to select the closest vehicle in view and to control a steerable tele camera to observe the selected vehicle, thus aiding visual object detection algorithms with an object hypothesis.
- Transmission of live video through channels: Using the channels concept, we have shown that it is possible to transmit streams of compressed live video from the onboard cameras between several vehicles and to roadside observers.
- Intercom: Using Data Channels, we have established walkie-talkie-like audio links between several vehicles and roadside observers.

7. Conclusion and Outlook

Vehicle-to-Vehicle (V2V) communication over wireless ad-hoc networks has been discussed for a long time as an approach to enable novel driver assistance systems, ultimately targeted at increasing safety. However, up to the current date, no such systems have actually been introduced in series-production vehicles. The reasons for this are manifold: first, common hard- and software standards have only recently been defined that assert the interoperability of devices from various manufacturers. Second, applications that actually make use of the possibilities offered by communications have rarely been proposed and until today it is not clear how cooperative driver assistance systems will look like. Third, it is not clear if the defined standards are actually capable of fulfilling the requirements of these new assistance systems.

The project KogniMobil, which sets the context of this thesis, researches cognitive autonomous vehicles. Ultimately, as we have argued in Chapter 2, a perfect autonomous vehicle can be understood as the superset of all possible driver assistance systems. Through means of communications, autonomous vehicles can extend their range of capabilities and become perfect cooperative, autonomous vehicles; and consequently, perfect cooperative autonomous vehicles can be seen as the superset of possible cooperative driver assistance systems. We have presented and discussed two specific classes of cooperative applications: cooperative perception, which allows vehicles to extend their view of the surrounding beyond the range of their onboard sensors, and cooperative behavior, which allows vehicles to form groups and act commonly to avoid collisions, improve traffic flow, etc. We have also discussed the applications' specific communication requirements and presented a survey of contemporary wireless communication standards.

7.1. Results and Contributions

The analytical framework presented in Chapter 3 and 4 give rise to new insights on the performance (in terms of throughput, delay, packet loss) of wireless communication. The main contribution lies in the interdisciplinary and holistic approach and in the open formulation: we combine aspects of traffic flow theory, connectivity as determined through the physical parameters of the communication channel, and medium access protocols to establish a statement about various networking parameters. We have presented a number of representative models for each individual aspect and have described how other models, if required, can be formulated to comply with our approach.

Consequently, the presented analytical framework can be used at design time by application designers that require a statement about the limits of the employed communication solution. Contrary to that, it can also be used by communication designers to find solutions that comply with the requirements of applications that should be enabled. The presented models are most suitable for the analysis of limiting scenarios and identifications of potential issues, for any given traffic scenario under any channel parameters using any communication technology.

Based on the previous analysis, we have contributed a suitable mechanism for achieving and guaranteeing sustainable Quality of Service (QoS) in a wireless network (Chapter 4), requiring only minimal knowledge of the network's topology. The proposed algorithm continuously controls the data rate of the traffic that is generated by the network nodes and is designed for decentralized deployment. The main design objectives of the algorithm, fairness and deterministic behavior, have been proven to be fulfilled. We have formulated an optimization problem that, based on the control decision of the QoS algorithm, describes how cooperative applications can be selected for channel access to yield the best possible benefit, given the current state of the network.

By means of prediction, we have contributed a concept of how a statistical QoS forecast can be achieved (Chapter 5) and how the future control decision can be estimated. This estimation can then be used to allow the proactive selection or rejection of cooperative applications on the basis of their longer-term QoS requirements. For instance, a cooperative maneuver may be refused if the required QoS cannot be asserted for the maneuver's duration.

Finally, we have outlined a novel lightweight network layer protocol that is specifically designed to support the communication requirements of cooperative cognitive applications. A communication manager entity has been specifically developed that integrates seamlessly into the existing software platform. To support cooperative perception, it allows for transparent access to data objects that have been received from surrounding vehicles. Cooperative behavior is enabled through the introduction of multipoint-to-multipoint communication channels.

The workflow to analyze connectivity and QoS, based on the contributions of this thesis, is outlined in Appendix C.

7.2. Outlook

As we have stated in the respective chapters, the formulation of the QoS criterium opens some interesting research opportunities. Especially the optimization of the network's connectivity matrix (or bounded local parts thereof) by means of power control or — more sophisticated — smart antennas on the basis of applications' concepts of their relevance to a group of nodes seems a promising approach. Today's topology control algorithms are mainly geared towards optimizing connectivity; our formulation could help to actually optimize connectivity to suit applications' demands.

Regarding QoS prediction, the algorithm for the forecast of vehicles' future positions appears very mature. The estimation and prediction of future channel state, however, seems to require further attention, since it has significant influence of the connectivity prediction's outcome. Especially the concept of radio maps (as proposed, for instance, in [LL07a]), combined with channel parameter estimation, machine learning and peer-to-peer data exchange could be a sensible approach to allow for a decentralized radio survey which may in turn be used for better channel predictions.

Our proposed communication architecture should at this point be regarded as a reference design for future cognitive vehicles. Although it has been successfully demonstrated at various events, it is still tailored to integrate with the software structure specific to the KogniMobil project. Further research will definitely see additional functionality at the communication layer and advances regarding the software architecture.

A. A Spline-Shaped Road Model

Cubic splines are widely used in the design of (free-form) curves and surfaces in computer-aided design applications, especially in the construction of ships, airplanes and cars. They are also being used in the process of laying railroad tracks. Their adequacy can be justified by the fact that for every curve section, boundary conditions can be defined in the terms of points and values for the first and second derivative (i.e, gradient and curvature). By doing so, it can be ensured that the curvature along a route, which may consist of many individual segments, is always continuous. Consequently, the resulting lateral acceleration when traveling along the route is also continuous; a prerequisite for the planning of roads. For this reason, cubic splines are very well suited as road models.

A.1. Definition of a Spline

The basis function for cubic splines is shown in Figure A.1. It is defined as:

$$\gamma(t) = \frac{1}{6} \begin{cases} (2+t)^3 & \text{if } -2 < t \leq -1 \\ 4 - 6t^2 - 3t^3 & \text{if } -1 < t \leq 0 \\ 4 - 6t^2 + 3t^3 & \text{if } 0 < t \leq 1 \\ (2-t)^3 & \text{if } 1 < t \leq 2 \\ 0 & \text{otherwise} \end{cases} \quad (\text{A.1})$$

A segment n of the spline is defined as a parametric curve $\underline{x}_n(t)$, $t \in [0 \dots 1]$ as the weighted sum of the positions of its so-called *knots*. Every segment is defined by four knots \underline{k}_{n+i} , $i \in \{0, 1, 2, 3\}$. The weights γ_i result from the four highlighted sections of the basis function (see Figure A.1) and are dependent of the parameter t :

$$\begin{aligned} \gamma_0(t) &= \frac{1}{6} (-t^3 + 3t^2 - 3t + 1) \\ \gamma_1(t) &= \frac{1}{6} (3t^3 - 6t^2 + 4) \\ \gamma_2(t) &= \frac{1}{6} (-3t^3 + 3t^2 + 3t + 1) \\ \gamma_3(t) &= \frac{1}{6} t^3 \end{aligned}$$

The position $\underline{x}_n(t)$ of a point on the spline segment n at time t is then:

$$\begin{aligned} \underline{x}_n(t) &= \underline{k}_n \gamma_0(t) + \underline{k}_{n+1} \gamma_1(t) + \underline{k}_{n+2} \gamma_2(t) + \underline{k}_{n+3} \gamma_3(t) \\ &= [t^3 \quad t^2 \quad t \quad 1] \underline{\mathbf{M}} \begin{bmatrix} \underline{k}_n \\ \underline{k}_{n+1} \\ \underline{k}_{n+2} \\ \underline{k}_{n+3} \end{bmatrix} \end{aligned} \quad (\text{A.2})$$

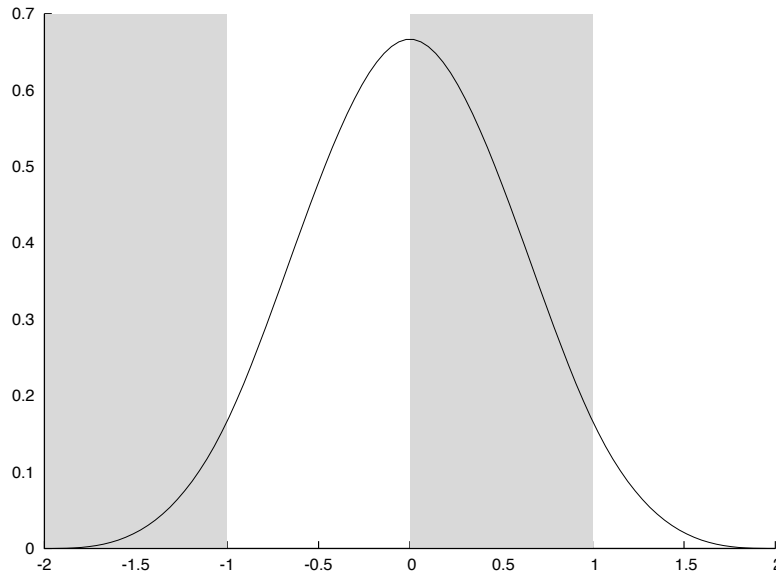


Figure A.1.: Basis function for cubic splines.

If there are j knots $\{\mathbf{k}_0 \dots \mathbf{k}_{j-1}\}$, the spline has $j - 3$ segments. The matrix $\underline{\mathbf{M}}$ corresponds to the $\gamma_n(t)$ functions defined above:

$$\underline{\mathbf{M}} = \frac{1}{6} \begin{bmatrix} -1 & 3 & -3 & 1 \\ 3 & -6 & 3 & 0 \\ -3 & 0 & 3 & 0 \\ 1 & 4 & 1 & 0 \end{bmatrix} \quad (\text{A.3})$$

A.2. Shape Generation

In our simulations, we use splines to model the shape of streets. Depending on the complexity of the street's shape, these splines have a varying number of knots j , therefore the exact position of a vehicle on the shape can only be computed if both the parameter $t \in [0 \dots 1]$ as well as the segment $n \in [0 \dots j - 3]$ is known. Furthermore, the spline can be understood as a "guiding shape", the particular lanes, however, follow the same shape but with a certain offset o .

How t and n are computed is discussed later, let us assume that they are known at this time. To get the exact position of a point $\underline{\mathbf{x}}_n(t, o)$ with offset o , we first determine the tangent vector of the spline, i.e., its first derivative:

$$\underline{\mathbf{x}}'_n(t) = \frac{\partial}{\partial t} \underline{\mathbf{x}}_n(t) = [t^2 \quad t \quad 1] \underline{\mathbf{M}}' \begin{bmatrix} \mathbf{k}_n \\ \mathbf{k}_{n+1} \\ \mathbf{k}_{n+2} \\ \mathbf{k}_{n+3} \end{bmatrix}$$

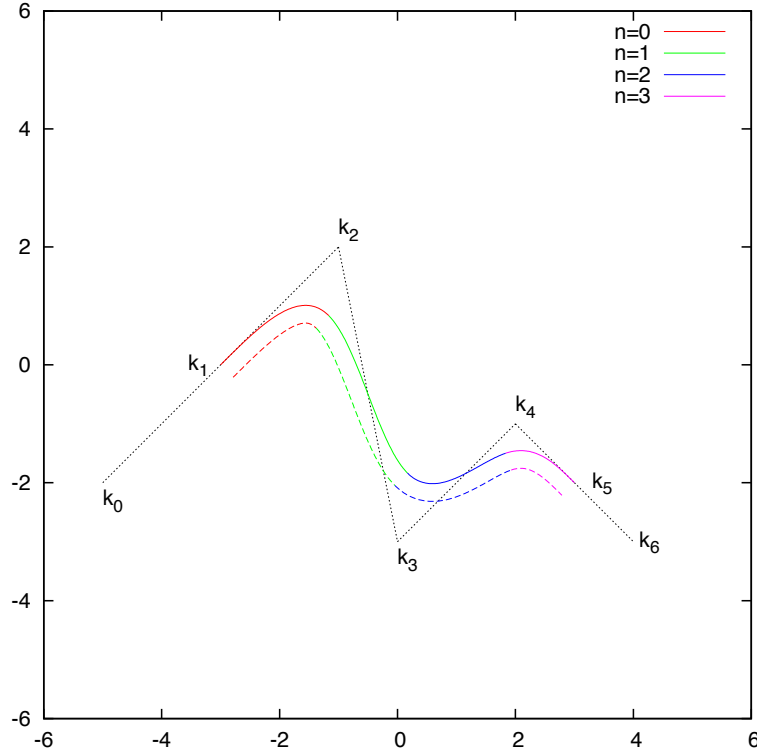


Figure A.2.: A spline consisting of four segments, its knot vector and its offset spline (dashed line).

where $\underline{\underline{\mathbf{M}'}}$ is the matrix of the basis functions' first derivative:

$$\underline{\underline{\mathbf{M}'}} = \frac{1}{2} \begin{bmatrix} -1 & 3 & -3 & 1 \\ 2 & -4 & 2 & 0 \\ -1 & 0 & 1 & 0 \end{bmatrix} \quad (\text{A.4})$$

We can then take the normal vector (perpendicular to the tangent), scale it to length o and compute:

$$\underline{\underline{\mathbf{x}}}_n(t, o) = \underline{\underline{\mathbf{x}}}_n(t) + \frac{o}{|\underline{\underline{\mathbf{x}}}'_n(t)|} \begin{bmatrix} 0 & 1 \\ -1 & 0 \end{bmatrix} \underline{\underline{\mathbf{x}}}'_n(t) \quad (\text{A.5})$$

The situation is depicted in Figure A.2: The spline consists of $n = 4$ segments, defined through the knots $\underline{\underline{\mathbf{k}}}_0 \dots \underline{\underline{\mathbf{k}}}_6$. The offset spline at $o = 0.1$ is represented by the dashed line.

A.3. Length of a Spline

As mentioned above, practical simulations make it necessary to determine the coordinates of a vehicle on a lane based on its distance l_v from the origin of the lane (arc length). Therefore, we need to determine the spline parameters t and n from l_v . The total arc length l_n of a spline segment can be determined by integrating the length of the tangent vector over the spline segment:

$$l_n = \int_0^1 |\underline{\underline{\mathbf{x}}}'_n(t)| dt \quad (\text{A.6})$$

The total length of the spline l can then be computed by summing up all l_n of the $j - 3$ segments:

$$l = \sum_{n=0}^{j-3} l_n \quad (\text{A.7})$$

The section above has introduced the idea of a guiding spline and resulting parallel lanes. The arc length of the spline computation as demonstrated in Equation (A.6) can not be used unmodified as the arc length of a lane is a function of the knot vector and the offset o . As a consequence, we have to integrate:

$$l_n^*(o) = \int_0^1 \left| \frac{\partial}{\partial t} \underline{\mathbf{x}}_n(t, o) \right| dt \quad (\text{A.8})$$

Differentiating Equation (A.5) yields:

$$\underline{\mathbf{x}}_n'(t, o) = \underline{\mathbf{x}}_n'(t) + \frac{o}{|\underline{\mathbf{x}}_n'(t)|} \begin{bmatrix} 0 & 1 \\ -1 & 0 \end{bmatrix} \left(\underline{\mathbf{x}}_n''(t) - \frac{\underline{\mathbf{x}}_n'(t)\underline{\mathbf{x}}_n''(t)}{|\underline{\mathbf{x}}_n'(t)|^2} \underline{\mathbf{x}}_n'(t) \right) \quad (\text{A.9})$$

Integration over the length of the offset-splines' tangent vector $\underline{\mathbf{x}}_n'(t, o)$ gives the correct arc length. The second derivative $\underline{\mathbf{x}}_n''(t)$ is defined as:

$$\underline{\mathbf{x}}_n''(t) = \frac{\partial^2}{\partial t^2} \underline{\mathbf{x}}_n(t) = [t \quad 1] \underline{\mathbf{M}}'' \begin{bmatrix} \underline{\mathbf{k}}_n \\ \underline{\mathbf{k}}_{n+1} \\ \underline{\mathbf{k}}_{n+2} \\ \underline{\mathbf{k}}_{n+3} \end{bmatrix}$$

where $\underline{\mathbf{M}}''$ is the matrix of the basis functions' second derivative:

$$\underline{\mathbf{M}}'' = \frac{1}{2} \begin{bmatrix} -1 & 3 & 3 & 1 \\ 1 & -2 & 1 & 0 \end{bmatrix} \quad (\text{A.10})$$

A.3.1. Numerical Integration

In our implementation, the arc length is computed through numerical integration according to Kepler's Fassregel [Kep15], sometimes also called Simpson's rule:

$$\int_a^b f(x) dx \approx S(a, b) = \frac{b-a}{6} \left(f(a) + 4f\left(\frac{a+b}{2}\right) + f(b) \right) \quad (\text{A.11})$$

For improved precision and performance, an adaptive algorithm [McK62] is used that recursively divides the integration interval in halves (midpoint c) if an error estimate exceeds a pre-defined relative error ϵ :

$$\frac{|S(a, c) + S(c, b) - S(a, b)|}{15} > \epsilon \quad (\text{A.12})$$

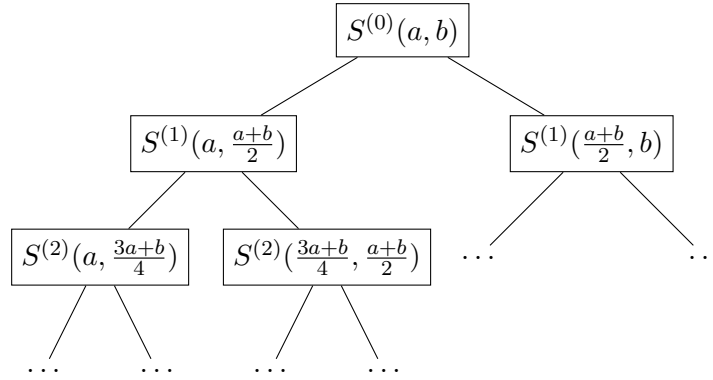


Figure A.3.: Representation of the Recursive Integration Calling Sequence as a Binary Tree

A.3.2. Parameter lookup

The advantage of this integration algorithm is the fact that the calling sequence of the recursive integration interval partitioning can be represented as a binary tree (Figure A.3):

- The initial invocation $S^{(0)}(a, b)$ corresponds to the root node.
- Recursively, at every parent node $S^{(i)}(a, b)$ two child nodes are added, corresponding to the function calls for the two sub-intervals $S^{(i+1)}(a, \frac{a+b}{2})$ and $S^{(i+1)}(\frac{a+b}{2}, b)$ until the desired precision (Equation (A.12)) of the sub-integral is reached.
- As the functions return, their result is stored in the child nodes. The arc length stored at a node $S^{(i)}(a, b)$ corresponds to the sum of the arc lengths stored at the child nodes. Ultimately, the root node stores the arc length of the integral.

Along with the arc length, we store the spline parameters t and n in the child nodes and build the tree during arc length computation. Given an arbitrary arc length l' , we can now use the tree as a search tree and thus easily find the lower and upper bound nodes that correspond to the desired spline parameters.

A.4. Fitting

When planning streets, it is generally more intuitive to provide a set of geometric knots and fit the spline so that it goes through these knots. Given n geometric knots, we need to determine $j = n + 2$ parametric knots. To get a definite equation set and make sure that the spline is continuous at its ends, we introduce the ingress and egress gradient vectors g_i and g_e and get:

$$\begin{bmatrix} -\frac{N}{2} & 0 & \frac{N}{2} & \dots & 0 & 0 & 0 \\ \gamma_0(0) & \gamma_1(0) & \gamma_2(0) & \dots & 0 & 0 & 0 \\ 0 & \gamma_0(0) & \gamma_1(0) & \dots & 0 & 0 & 0 \\ \vdots & \vdots & \vdots & \ddots & \vdots & \vdots & \vdots \\ 0 & 0 & 0 & \dots & \gamma_1(0) & \gamma_2(0) & 0 \\ 0 & 0 & 0 & \dots & \gamma_0(0) & \gamma_1(0) & \gamma_2(0) \\ 0 & 0 & 0 & \dots & -\frac{N}{2} & 0 & \frac{N}{2} \end{bmatrix} \begin{bmatrix} \underline{\mathbf{k}}_{-1} \\ \underline{\mathbf{k}}_0 \\ \underline{\mathbf{k}}_1 \\ \vdots \\ \underline{\mathbf{k}}_{n-2} \\ \underline{\mathbf{k}}_{n-1} \\ \underline{\mathbf{k}}_n \end{bmatrix} = \begin{bmatrix} \underline{\mathbf{g}}_i \\ \underline{\mathbf{x}}_0 \\ \underline{\mathbf{x}}_1 \\ \vdots \\ \underline{\mathbf{x}}_{n-2} \\ \underline{\mathbf{x}}_{n-1} \\ \underline{\mathbf{g}}_e \end{bmatrix} \quad (\text{A.13})$$

Through matrix inversion, we can then determine the set of parametric knots $\{\underline{\mathbf{k}}_{-1} \dots \underline{\mathbf{k}}_n\}$.

Another possibility to achieve intuitive behavior of splines is to use “clamped” splines, that pass through defined start and end points. To achieve this, we need to add two parametric knots $\underline{\mathbf{k}}_{-1}$ and $\underline{\mathbf{k}}_j$, so that

$$\underline{\mathbf{k}}_{-1} = 2\underline{\mathbf{k}}_0 - \underline{\mathbf{k}}_1 \tag{A.14}$$

$$\underline{\mathbf{k}}_j = 2\underline{\mathbf{k}}_{j-1} - \underline{\mathbf{k}}_{j-2} \tag{A.15}$$

Clamping has been used to generate the spline in Figure A.2: Its knots $\underline{\mathbf{k}}_0$ and $\underline{\mathbf{k}}_6$ have been determined using the above equations.

B. Physical Layer Parameters

Table B.1 shows the relevant modulation parameters as specified in the IEEE 802.11a OFDM PHY layer standard ([IEEE07a], chapter 17). For the minimum sensitivity numbers, the packet error rate was claimed to be less than 10 % at a packet length of 1000B. A noise factor of 10 dB and 5 dB implementation margins are assumed.

The thermal noise floor's power can be computed through

$$P_t^{(\text{lin})} = k_B T B \quad (\text{B.1})$$

where $k_B \approx 1.38 \cdot 10^{-23}$ J/K is Boltmann's constant, $T = 300$ K the room temperature and B the bandwidth in Hz. The noise power in a 10 MHz channel is 41.4 fW, or -104 dBm. In a 5 MHz or 20 MHz channel, the noise power is -107 dBm or -101 dBm, respectively.

OFDM Parameter	5 MHz		10 MHz		20 MHz	
	Channel Spacing	Channel Spacing	Channel Spacing	Channel Spacing	Channel Spacing	Channel Spacing
Data subcarriers N_{SD}	48	48	48	48	48	48
Pilot subcarriers N_{SP}	4	4	4	4	4	4
Subcarrier frequency spacing ΔF	78.125 kHz	156.25 kHz	156.25 kHz	312.5 kHz	312.5 kHz	312.5 kHz
FFT/IFFT period $T_F = 1/\Delta F$	12.8 μ s	6.4 μ s	6.4 μ s	3.2 μ s	3.2 μ s	3.2 μ s
Guard interval $T_G = T_F/4$	3.2 μ s	1.6 μ s	1.6 μ s	0.8 μ s	0.8 μ s	0.8 μ s
Symbol duration $T_S = T_F + T_G$	16.0 μ s	8.0 μ s	8.0 μ s	4.0 μ s	4.0 μ s	4.0 μ s
Preamble duration T_P	64 μ s	32 μ s	32 μ s	16 μ s	16 μ s	16 μ s
Modulation [Coding Rate, Data Bits / Symbol]	Minimum Sensitivity (dBm)	Data Rate (Mbit/s)	Minimum Sensitivity (dBm)	Data Rate (Mbit/s)	Minimum Sensitivity (dBm)	Data Rate (Mbit/s)
BPSK [1/2, 24]	-88	1.5	-85	3	-82	6
BPSK [3/4, 36]	-87	2.25	-84	4.5	-81	9
QPSK [1/2, 48]	-85	3	-82	6	-79	12
QPSK [3/4, 72]	-83	4.5	-80	9	-77	18
16-QAM [1/2, 96]	-80	6	-77	12	-74	24
16-QAM [3/4, 144]	-76	9	-73	18	-70	36
64-QAM [2/3, 192]	-72	12	-69	24	-66	48
64-QAM [3/4, 216]	-71	13.5	-68	27	-65	54

Table B.1.: IEEE 802.11a OFDM Physical Layer Specifications

C. Analysis Workflow

In this thesis, we have contributed means of analyzing the connectivity of vehicular networks and the QoS that can be attained in these networks. This chapter gives a brief summary of the workflow of such an analysis and should be regarded as a guideline for application and networking designers. It may be used iteratively in the design process, to tune parameters to obtain an optimal conformance of applications when deployed.

The workflow is illustrated in Figure C.1.

C.1. Networking Parameters

At the beginning of the connectivity analysis process as described in Chapter 3, the user needs an appropriate formulation of the channel model $\chi(\cdot, \cdot)$ and to determine the maximum tolerable attenuation β_{max} (see, for instance, Table B.1).

The formulation of the physical layout of the traffic scenario is accomplished by using a road model as the projection function $\Phi(\cdot)$. We suggest splines as road model, see Appendix A. The properties of the traffic flow itself are represented through the traffic density ρ and the choice of a fundamental diagram $Q(\rho)$ or $v(\rho)$, respectively (see Equation (3.37)).

Using these input parameters, the user can then determine:

- the distribution of node degrees $f_D[d]$, through Equation (3.54)
- the distribution of link durations $f_T(t)$, through Equation (3.76), (3.98)
- the expected link generation and break rate Λ , through Equation (3.116)

C.2. QoS Analysis

As a prerequisite for QoS analysis as described in Chapter 4, the user needs statistical information about the node degree. For instance, the degree distribution $f_D[d]$ as obtained above can be used here. Alternatively, one can model the degree distribution to represent a desired scenario. It is also possible to use the channel model and a spatial distribution as input parameters. It is also necessary to know the throughput function of the MAC protocol $v(u)$. Subsequently, the requirements from the application (see Chapter 2) are used to determine the maximum allowable load \hat{u} .

By using either Algorithm 1 (centralized) or Algorithm 2 (decentralized), the traffic limits s_i for the individual network nodes v_i can be determined. This figure can then be used in the design phase to determine if the traffic limits are sufficient for the application or be used to decide if the analyzed MAC protocol is suitable for the application. Given the benefit functions, the output from the traffic limits algorithms can also be used to determine which applications would be selected in a certain situation and how they would be parameterized.

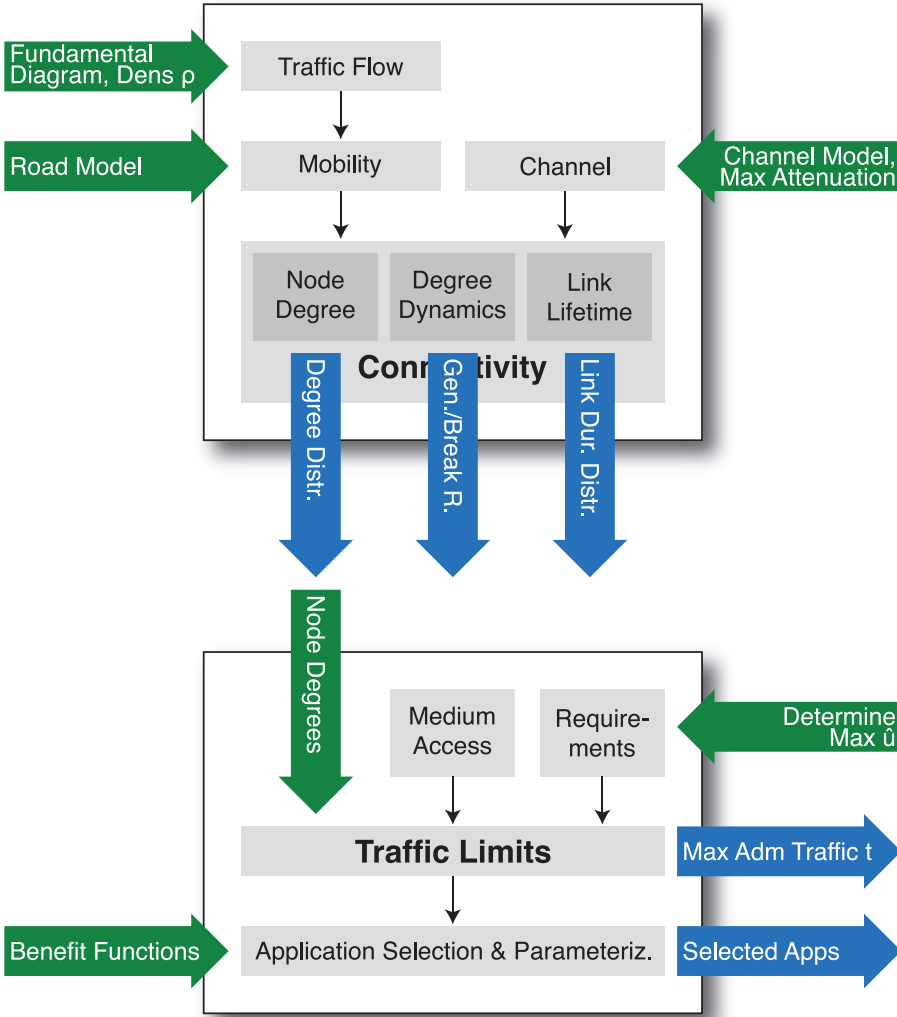


Figure C.1.: Analysis Workflow

List of Figures

1.1. Traffic-related fatalities in Germany [Bun09].	2
1.2. The thematic organization of this thesis	6
2.1. Internal structure of a cognitive vehicle.	8
2.2. Cooperation of vehicles: Platooning (1) and perception (2) “around the corner”.	9
2.3. Cycle times of sensors, controllers and cooperative tasks.	10
2.4. The WAVE communication stack.	15
2.5. The WAVE frequency assignment.	15
3.1. The fundamental relations between number of vehicles, distance, and time in terms of traffic flow theory (outer text) and networking parameters (inner text).	20
3.2. Classification of attenuation effects (red) and their distributions (blue).	21
3.3. Attenuation for Log-Distance (non-obstructed part) and Dual-Slope path loss models ($\alpha_l = 2$, $\alpha_n = 3$). The obstacle (grey box) significantly influences the attenuation.	24
3.4. Received power P_r over distance d for Log-distance and Dual-slope path loss models.	25
3.5. Position and velocity of communication nodes	31
3.6. Border strategies for random direction mobility.	32
3.7. Traffic flow continuity in fundamental road scenarios.	34
3.8. Fundamental diagrams of (a) highway and (b) city traffic flow.	36
3.9. Reference setup for node degree analysis.	39
3.10. Typical highway traffic patterns.	41
3.11. Disconnection probabilities over traffic density.	45
3.12. Leafnode probabilities over traffic density.	46
3.13. Average node degree over velocity.	48
3.14. CDFs of free-flow and congested traffic headway distributions for a traffic density of $\rho = 40 \text{ km}^{-1}$	49
3.15. Dispersion of node degree probabilities over traffic density for (a) freeflow and (b) congested traffic. Radio range is $r = 100 \text{ m}$	50
3.16. Reference setup for link lifetime analysis.	52
3.17. PDF (a), (c) and CDF (b), (d) of communication duration with oncoming and same-direction fast lane vehicles. PDFs shown for a communication range of $r = 100 \text{ m}$	56
3.18. Minimum required radio ranges for communication times t (a) and fractions of shorter times, ϵ (b).	59
3.19. CDF (b) and PDF (a) of communication duration with roadside infrastructure. PDFs shown for a communication range of $r = 100 \text{ m}$	62
3.20. Median connection duration \tilde{t} over traffic densities ρ_A, ρ_B for two lanes.	63
3.21. Median connection duration \tilde{t} over traffic density ρ in the V2I scenario.	64
3.22. Reference setup for link generation analysis, V2I scenario.	65

3.23. Reference setup for link generation analysis, V2V scenario.	66
3.24. Link generation rates Λ_b over traffic densities ρ_A, ρ_B for two lanes.	67
4.1. Exemplary network. The radio ranges are indicated for nodes B, C, and F. . . .	75
4.2. Throughput over offered traffic.	77
4.3. Packet loss probability and number of transmissions.	78
4.4. The 802.11 DCF mechanism	81
4.5. The 802.11 EDCA mechanism	82
4.6. Average admitted traffic per node \bar{s} (in units of \hat{u}) over average node degree \bar{d} . Upper and lower bounds are also shown (dashed lines).	89
4.7. Average load \bar{u} (in units of \hat{u}) over average node degree \bar{d} . Upper and lower bounds are also shown (dashed lines).	91
4.8. Node degrees for the intersection scenario.	93
4.9. Admitted traffic (a) and cumulated load (b) for the intersection scenario.	94
4.10. An example for a stub configuration	95
4.11. Average load and per-node traffic fairness over degree dispersion (a) and alge- braic connectivity (b).	96
4.12. The proposed mechanism for application selection and parameterization	97
5.1. Structure of the connectivity predictor.	104
5.2. Structure of the mobility predictor.	105
5.3. Structure of the speed predictor.	107
5.4. City scenario.	113
5.5. City scenario - prediction error at crossroads.	114
5.6. Suburban scenario.	115
5.7. Highway scenario - prediction error at highway bridge.	116
5.8. Highway scenario.	117
5.9. Prediction error histogram - different prediction lengths for the city scenarios and the influence of known routes on prediction accuracy.	119
5.10. Prediction error histogram - different prediction lengths for the suburban and highway scenarios.	120
5.11. Parameter estimation using particle filter: measured and estimated path loss, estimated PLE.	121
5.12. Parameter estimation using 2D particle filter: setup and estimated pathloss. . . .	122
5.13. Connection probabilities for gaussian $f_D(d)$ and $f_\alpha(\alpha)$ with varying parameters over the maximum allowable path loss β_{max}	126
6.1. Structure of a basic network layer packet.	130
6.2. Structure of a measurement PE.	130
6.3. Message flow diagram of the timing measurement.	131
6.4. Structure of an identification PE.	132
6.5. Information flow through the real-time database	133
6.6. Object transfer between two cooperative vehicles	134
6.7. Structure of an object update PE.	135
6.8. Structure of a short object update PE.	135
6.9. Structure of an object remove notification PE.	136
6.10. Channels between three cooperative vehicles	137
6.11. Structure of a channel data PE.	137

6.12. Structure of the communication manager.	138
A.1. Basis function for cubic splines.	144
A.2. A spline consisting of four segments, its knot vector and its offset spline (dashed line).	145
A.3. Representation of the Recursive Integration Calling Sequence as a Binary Tree .	147
C.1. Analysis Workflow	152

List of Tables

2.1. Typical requirements of cooperative applications.	18
3.1. Parameters of the section-based traffic model.	37
3.2. Vehicle-to-Vehicle on straight, parallel lanes. Scenarios and parameters used for computation.	57
3.3. Some values of κ as a function of ϵ	60
3.4. Relevant formulas derived in this chapter.	70
4.1. Some characteristics of MAC protocol families.	84
4.2. Average admitted traffic per node \bar{s} and average node degree \bar{d} for some representative network topologies.	90
4.3. Per-node traffic gains for various network sizes	92
4.4. Relevant formulas derived in this chapter.	100
5.1. Speed Prediction parameters with example values used during development.	108
6.1. The Peer Object.	133
6.2. The Proxy Object.	134
6.3. The Channel Object.	137
B.1. IEEE 802.11a OFDM Physical Layer Specifications	150

Abbreviations

AP	Access Point
C2CCC	Car-to-Car Communication Consortium
CDF	Cumulated Density Function
CSMA	Carrier Sense Multiple Access
CSMA/CA	Carrier Sense Multiple Access with Collision Avoidance
CW	Contention Window
DCF	Distributed Coordination Function
DSRC	Dedicated Short Range Communication
EDCA	Enhanced Distributed Channel Access
FCC	Federal Communications Commission
FIR	Finite Impulse Response
GPS	Global Positioning System
ICT	Information and Communication Technologies
IP	Internet Protocol
IVC	Inter-Vehicle Communication
LAN	Local Area Network
LMS	Least Mean Squares
LOS	Line-Of-Sight
LWR	Lighthill-Williams-Richards
MAC	Medium Access Control
MPC	Multi-Path Component
MTU	Maximum Transmission Unit
NLOS	Non-Line-Of-Sight
OFDM	Orthogonal Frequency Division Multiplex
PCF	Point Coordination Function
PDF	Probability Density Function
PE	Packet Element
PLE	Path Loss Exponent
PMF	Probability Mass Function
QoS	Quality of Service

RD Random Direction
RMS Root Mean Square
RTT Round-Trip Time
RWP Random Waypoint
SNR Signal-to-Noise-Ratio
TCP Transmission Control Protocol
TDMA Time Division Multiple Access
UDP User Datagram Protocol
V2I Vehicle-to-Infrastructure
V2V Vehicle-to-Vehicle
WAVE Wireless Access in Vehicular Environments
WLAN Wireless Local Area Network
WME Wireless Multimedia Extensions
WMM Wi-Fi Multimedia
PHY Physical Layer

Mathematical Notations

General

\mathbf{a}	A Vector
$\mathbf{1}$	“Ones” Vector
\mathbf{A}	A Matrix
\mathbf{I}	Identity Matrix
\mathcal{A}	A Set
$E\{\cdot\}$	Expected Value
$\text{Var}\{\cdot\}$	Variance
$\mathcal{L}(\cdot)$	Laplace Transform

Connectivity: Channel Models

α	Path Loss Exponent
α_l, α_n	(Non) Line-Of-Sight Path Loss Exponent
β	Attenuation (in dB, also indicated as ^(dB) ; linear scale indicated as ^(lin))
$\beta_p(d)$	Path Loss
β_s	Statistic Path Loss Component
d	Distance between Transmitter and Receiver [m]
d_0	Reference Distance [m] (usually 1 m)
d_l, d_n	(Non) Line-Of-Sight Distance between Transmitter and Receiver [m]
$f_{\beta_s}(\beta_s)$	Distribution of the Statistic Path Loss Component
λ	Wavelength [m]
P_r	Received Power [W, dBW]
P_s	Receiver Sensitivity (may also depend on data rate) [W, dBW]
P_t	Transmitted Power [W, dBW]
r	Radio Range [m]
$\chi(\cdot, \cdot)$	Channel Model Function

Connectivity: Spatial Node Distribution, Node Degree, Link Lifetime, Link Generation Rate

\mathbf{a}	Acceleration of a Vehicle (World Coordinates)
C	Lane Capacity [h^{-1}]
d	Node Degree
η	Equipment Ratio
$f_D(d)$	Node Degree Distribution
$f_H(h)$	Headway Distribution
$f_H^{(n)}(h)$	n-fold Convolution of the Headway Distribution
$f_T(t)$	Connection Duration Distribution
$f_V(v)$	Velocity Distribution
$f_{\mathbf{v}}(\mathbf{v})$	Velocity Distribution
$f_{\mathbf{x}}(\mathbf{x})$	Spatial Distribution
h_0	Minimum Vehicle Distance [m]
$I(x)$	Number of Lanes

l	Vehicle Length [m]
l_e	Effective Vehicle Length [m]
Λ	Link Generation Rate [s^{-1}]
φ	Direction of Velocity [$^\circ$]
$\underline{\Phi}(\cdot)$	Projection Function
$\rho(x, t)$	Average Density of Vehicles [kmlane $^{-1}$]
$\rho_t(x, t)$	Total Density of Vehicles [km $^{-1}$]
$\rho_i(x, t)$	Density of Vehicles on lane i [km $^{-1}$]
ρ_j	Traffic Jam Density [km $^{-1}$]
ρ_c	Critical Density [km $^{-1}$]
s_i	Longitudinal Position of Vehicle i on a Lane [m]
s_r	Effective Radio Range [m]
s_\perp	Lateral Lane Offset [m]
σv	Velocity Standard Deviation [m/s]
t	Time [s]
T	Average Time Headway [s]
\tilde{t}	Median Connection Duration [s]
v	Magnitude of Velocity [m/s]
\bar{v}	Average Velocity [m/s]
$v(x, t)$	Average Velocity [m/s]
v_0	Average Free Velocity [m/s]
$V_e(\rho)$	Equilibrium Velocity [m/s]
$v_i(x, t)$	Velocity of Vehicles on lane i [m/s]
\underline{v}	Velocity of a Vehicle (World Coordinates)
$Q(x, t)$	Average Flow of Vehicles [hlane $^{-1}$]
$Q_i(x, t)$	Flow of Vehicles on lane i [h $^{-1}$]
$Q_t(x, t)$	Total Flow of Vehicles [h $^{-1}$]
$Q_e(\rho)$	Fundamental Diagram [h $^{-1}$]
\underline{x}	Position of a Vehicle (World Coordinates)

QoS Analysis and Provisioning

\mathcal{A}	Set of Send Hyperarcs
\mathcal{A}'	Set of Receive Hyperarcs
$\underline{\mathcal{C}}$	Connectivity Matrix
c_{ij}	Connectivity of Nodes v_i and v_j
Δ	Maximum Node Degree
$\delta(u)$	Average Normalized Packet Delay at Offered Traffic u [s]
\mathcal{E}	Set of Edges
G	A Network Graph
l	Message Length [bit, B]
λ	Message Generation Rate [s^{-1}]
\underline{L}	Laplacian Matrix
n	Number of Nodes
n_s	Number of Stub Nodes
\mathcal{P}	Set of Applications
$p_l(u)$	Packet Loss Probability at Offered Traffic u
Φ	Global Fairness
ϕ	Local Fairness

\hat{R}	Channel Data Rate [bit/s]
\mathcal{R}_i	Set of Receivers from Node v_i
\mathcal{S}_j	Set of Transmitters to Node v_j
\underline{s}	Source Traffic Vector
s_b	Baseline Sourced Traffic [Erl]
s_i	Sourced Traffic (Offered Traffic) of Node v_i [Erl]
s_p	Traffic Admitted to Application p [Erl]
\underline{u}	Load Vector
\hat{u}	QoS Condition [Erl]
u_j	Load (Cumulated Offered Traffic) at Node v_j [Erl]
$U_p(s_p)$	Benefit of Application p at s_p
\mathcal{V}	Set of Nodes
v_i	Vertex (Node) i
$v(u)$	Throughput of a MAC Protocol at Offered Traffic u [Erl]
χ'	Chromatic Index

Predictive QoS Provisioning

a	Influence of Mean Weights Vector
b	Influence of Weight Booster
c	Boost Limit
$\mathcal{C} _{t_0+\Delta t}$	Predicted Connectivity Matrix, Δt ahead
d	Boost Gain
$f_\alpha(\alpha)$	Path Loss Exponent Distribution
$f_{\beta D}(\beta d)$	Attenuation Distribution, given the Distance d
$f_D(d)$	Distance Distribution
l	Depth of FIR filters
n	Number of Prediction Steps
s	Distance to Cover
$v_{current}$	Current Velocity [m/s]
v_{pred}	Predicted Velocity [m/s]
$\underline{x}_i _{t_0+\Delta t}$	Predicted Position of Node v_i , Δt ahead
$\chi(\cdot, \cdot) _{t_0+\Delta t}$	Predicted Channel, Δt ahead

Bibliography

Publications by the author

- [EEH⁺07] J. Eberspächer, S. Eichler, C. Hartmann, S. Meister, R. Nagel, R. Vilzmann, and H.-M. Zimmermann, *Wireless Multi-hop Networks: Classification, Paradigms and Constraints*, Tech. Report LKN-TR-4, Lehrstuhl für Kommunikationsnetze, Technische Universität München, October 2007.
- [GAB⁺08] M. Goebel, M. Althoff, M. Buss, G. Färber, F. Hecker, B. Heißing, S. Kraus, R. Nagel, F. Puente-Leon, F. Rattei, M. Russ, M. Schweitzer, M. Thuy, C. Wang, and H.-J. Wünsche, *Design and capabilities of the Munich Cognitive Automobile*, IEEE Intelligent Vehicles Symposium (IV), June 2008, pp. 1101–1107.
- [Nag09] R. Nagel, *A Communication Framework for Cognitive Autonomous Vehicles*, IEEE Intelligent Vehicles Symposium (IV), June 2009, pp. 1121–1124.
- [Nag10a] ———, *Altruistic Traffic Limits Computation in Wireless Broadcast Networks*, Proceedings of the Third International Conference on Advances in Mesh Networks (MESH), July 2010, pp. 23–27.
- [Nag10b] ———, *The Effect of Vehicular Distance Distributions and Mobility on VANET Communications*, IEEE Intelligent Vehicles Symposium (IV), June 2010, pp. 1190–1194.
- [NE08] R. Nagel and S. Eichler, *Efficient and realistic mobility and channel modeling for VANET scenarios using OMNeT++ and INET-framework*, Simutools '08: Proc. of the 1st international conference on Simulation tools and techniques for communications, networks and systems & workshops, ICST (Institute for Computer Sciences, Social-Informatics and Telecommunications Engineering), March 2008, pp. 1–8.
- [NEE07] R. Nagel, S. Eichler, and J. Eberspächer, *Intelligent Wireless Communication for Future Autonomous and Cognitive Automobiles*, IEEE Intelligent Vehicles Symposium (IV), June 2007, pp. 716–721.
- [NM11] R. Nagel and S. Morscher, *Wireless Communication*, ch. Connectivity Prediction in Mobile Vehicular Environments Backed By Digital Maps, INTECH Open Access Publisher, 2011.
- [TAB⁺08] M. Thuy, M. Althoff, M. Buss, K. Diepold, J. Eberspächer, G. Färber, M. Goebel, B. Heißing, S. Kraus, R. Nagel, Y. Naous, F. Obermeier, F. Puente-Leon, F. Rattei, C. Wang, M. Schweitzer, and H.-J. Wünsche, *Kognitive Automobile - Neue Konzepte und Ideen des Sonderforschungsbereichs/TR-28*, 3. Tagung Aktive Sicherheit durch Fahrerassistenz, April 2008.
- [VNBM07] S. Vacek, R. Nagel, T. Batz, and F. Moosmann, *An integrated simulation framework for cognitive automobiles*, IEEE Intelligent Vehicles Symposium (IV), June 2007, pp. 221–226.

General publications

- [Abr70] N. Abramson, *THE ALOHA SYSTEM: another alternative for computer communications*, AFIPS '70 (Fall): Proceedings of the November 17-19, 1970, fall joint computer conference (New York, NY, USA), ACM, 1970, pp. 281–285.
- [Abr77] ———, *The Throughput of Packet Broadcasting Channels*, IEEE Transactions on Communications **25** (1977), no. 1, 117–128.
- [AF96] M. Aoki and H. Fujii, *Inter-vehicle communication: technical issues on vehicle control application*, IEEE Communications Magazine **34** (1996), no. 10, 90–93.
- [AI06] G. Acosta and M.A. Ingram, *Doubly Selective Vehicle-to-Vehicle Channel Measurements and Modeling at 5.9 GHz*, Proceedings 2006 Wireless Personal Multimedia Communications Conference (WPMC'06) (San Diego, CA), July 2006.
- [AL10] A. Agarwal and T.D.C. Little, *Role of directional wireless communication in vehicular networks*, IEEE Intelligent Vehicles Symposium (IV), June 2010, pp. 688–693.
- [AM07] A. Y. Abul-Magd, *Modeling highway-traffic headway distributions using superstatistics*, Phys. Rev. E **76** (2007), no. 5, 057101.
- [APR05] M.M. Artimy, W.J. Phillips, and W. Robertson, *Connectivity with static transmission range in vehicular ad hoc networks*, Proceedings of the 3rd Annual Communication Networks and Services Research Conference, May 2005, pp. 237–242.
- [ARP04] M.M. Artimy, W. Robertson, and W.J. Phillips, *Connectivity in inter-vehicle ad hoc networks*, Canadian Conference on Electrical and Computer Engineering, vol. 1, May 2004, pp. 293–298.
- [AS64] M. Abramowitz and I. A. Stegun, *Handbook of Mathematical Functions with Formulas, Graphs, and Mathematical Tables*, 9th dover printing ed., Dover, 1964.
- [ASB10] M. Althoff, O. Stursberg, and M. Buss, *Computing reachable sets of hybrid systems using a combination of zonotopes and polytopes*, Nonlinear Analysis: Hybrid Systems **4** (2010), no. 2, 233–249.
- [ATI04] G. Acosta, K. Tokuda, and M.A. Ingram, *Measured joint Doppler-delay power profiles for vehicle-to-vehicle communications at 2.4 GHz*, Global Telecommunications Conference, 2004. GLOBECOM '04. IEEE, vol. 6, November 2004, pp. 3813–3817.
- [BC02] N. Benvenuto and G. Cherubini, *Algorithms for Communications Systems and Their Applications*, Wiley, New York, 2002.
- [BC03] C. Beck and E. G. D. Cohen, *Superstatistics*, Physica A: Statistical Mechanics and its Applications **322** (2003), 267–275.
- [BCCF03] F. Borgonovo, A. Capone, M. Cesana, and L. Fratta, *ADHOC: a new, flexible and reliable MAC architecture for ad-hoc networks*, IEEE Wireless Communications and Networking (WCNC), vol. 2, 2003, pp. 965–970.
- [Bet04] C. Bettstetter, *Mobility Modeling, Connectivity, and Adaptive Clustering in Ad Hoc Networks*, Ph.D. thesis, Technische Universität München, 2004.
- [BFO96] G. Bianchi, L. Fratta, and M. Oliveri, *Performance evaluation and enhancement of the CSMA/CA MAC protocol for 802.11 wireless LANs*, Seventh IEEE International Symposium on Personal, Indoor and Mobile Radio Communications, PIMRC'96, vol. 2, October 1996, pp. 392–396.

-
- [BH05] C. Bettstetter and C. Hartmann, *Connectivity of wireless multihop networks in a shadow fading environment*, *Wireless Networks* **11** (2005), no. 5, 571–579.
- [BHPC02] C. Bettstetter, H. Hartenstein, and X. Pérez-Costa, *Stochastic properties of the random waypoint mobility model: epoch length, direction distribution, and cell change rate*, *MSWiM '02: Proceedings of the 5th ACM international workshop on Modeling analysis and simulation of wireless and mobile systems* (New York, NY, USA), ACM, 2002, pp. 7–14.
- [Bia00] G. Bianchi, *Performance analysis of the IEEE 802.11 distributed coordination function*, *IEEE Journal on Selected Areas in Communications* **18** (2000), no. 3, 535–547.
- [BKK⁺03] R. Bogenberger, W. Kellerer, T. Kosch, T. Reicher, P. Sties, and M. Wagner, *Virtual city portal - a multi-network personal information system for automobile users*, In *Proceedings of Workshop on Multiradio Multimedia Communications, Communication Technology for Vehicles*, 2003.
- [BKSM06] L.L. Bello, G.A. Kaczynski, F. Sgro, and O. Mirabella, *A wireless traffic smoother for soft real-time communications over IEEE 802.11 industrial networks*, *IEEE Conference on Emerging Technologies and Factory Automation, ETFA '06*, September 2006, pp. 1073–1079.
- [Bre63] L. Breiman, *The Poisson Tendency in Traffic Distribution*, *The Annals of Mathematical Statistics* **34** (1963), 308–311.
- [BRG05] W. Brilon, M. Regler, and J. Geistefeldt, *Zufallscharakter der Kapazität von Autobahnen und praktische Konsequenzen*, *Strassenverkehrstechnik* **3 (part 1) and 4 (part 2)** (2005).
- [BRP09] A. Boukerche, C. Rezende, and R.W. Pazzi, *Improving Neighbor Localization in Vehicular Ad Hoc Networks to Avoid Overhead from Periodic Messages*, *IEEE Global Telecommunications Conference (GLOBECOM)*, November 2009, pp. 1–6.
- [BS09] M.S. Bouassida and M. Shawky, *A cooperative and fully-distributed congestion control approach within VANETs*, *9th International Conference on Intelligent Transport Systems Telecommunications (ITST)*, October 2009, pp. 526–531.
- [Bun09] Statistisches Bundesamt, *Verkehrsunfälle – Unfallentwicklung im Straßenverkehr*, Wiesbaden, 2009.
- [BUSB08] K. Bilstrup, E. Uhlemann, E.G. Strom, and U. Bilstrup, *Evaluation of the IEEE 802.11p MAC Method for Vehicle-to-Vehicle Communication*, *IEEE 68th Vehicular Technology Conference (VTC)*, September 2008, pp. 1–5.
- [BUSB09] K. Bilstrup, E. Uhlemann, E. G. Ström, and U. Bilstrup, *On the ability of the 802.11p MAC method and STDMA to support real-time vehicle-to-vehicle communication*, *EURASIP J. Wirel. Commun. Netw.* **2009** (2009), 5:1–5:13.
- [BVP⁺10] P. Belanovic, D. Valerio, A. Paier, T. Zemen, F. Ricciato, and C.F. Mecklenbrauker, *On Wireless Links for Vehicle-to-Infrastructure Communications*, *IEEE Transactions on Vehicular Technology* **59** (2010), no. 1, 269–282.
- [BWM09] M. Brackstone, B. Waterson, and M. McDonald, *Determinants of following headway in congested traffic*, *Transportation Research Part F: Traffic Psychology and Behaviour* **12** (2009), no. 2, 131–142.
-

-
- [CBS09] L. Cheng, F. Bai, and D.D. Stancil, *A new geometrical channel model for vehicle-to-vehicle communications*, IEEE Antennas and Propagation Society International Symposium (APSURSI), June 2009, pp. 1–4.
- [CGM07] O. Cappe, S.J. Godsill, and E. Moulines, *An Overview of Existing Methods and Recent Advances in Sequential Monte Carlo*, Proceedings of the IEEE **95** (2007), no. 5, 899–924.
- [CHBS08a] L. Cheng, B. Henty, F. Bai, and D.D. Stancil, *Doppler Spread and Coherence Time of Rural and Highway Vehicle-to-Vehicle Channels at 5.9 GHz*, IEEE Global Telecommunications Conference (GLOBECOM), December 2008, pp. 1–6.
- [CHBS08b] L. Cheng, B.E. Henty, F. Bai, and D.D. Stancil, *Highway and rural propagation channel modeling for vehicle-to-vehicle communications at 5.9 GHz*, IEEE Antennas and Propagation Society International Symposium (AP-S), July 2008, pp. 1–4.
- [CHC⁺08] L. Cheng, B. Henty, R. Cooper, D.D. Stancil, and F. Bai, *Multi-Path Propagation Measurements for Vehicular Networks at 5.9 GHz*, IEEE Wireless Communications and Networking Conference (WCNC), April 2008, pp. 1239–1244.
- [CHS⁺07] L. Cheng, B.E. Henty, D.D. Stancil, F. Bai, and P. Mudalige, *Mobile Vehicle-to-Vehicle Narrow-Band Channel Measurement and Characterization of the 5.9 GHz Dedicated Short Range Communication (DSRC) Frequency Band*, IEEE Journal on Selected Areas in Communications **25** (2007), no. 8, 1501–1516.
- [CLD⁺91] K.S. Chang, W. Li, P. Devlin, A. Shaikhbahai, P. Varaiya, J.K. Hedrick, D. McMahon, V. Narendran, D. Swaroop, and J. Olds, *Experimentation with a vehicle platoon control system*, Vehicle Navigation and Information Systems Conference, vol. 2, October 1991, pp. 1117–1124.
- [Com03] Commission of the European Communities, *Communication from the Commission to the Council and the European Parliament COM(2003) 542*, September 2003.
- [Cow75] Richard J. Cowan, *Useful headway models*, Transportation Research **9** (1975), no. 6, 371–375.
- [Cox83] D. Cox, *Antenna Diversity Performance in Mitigating the Effects of Portable Radiotelephone Orientation and Multipath Propagation*, IEEE Transactions on Communications **31** (1983), no. 5, 620–628.
- [Cox95] D.C. Cox, *Wireless personal communications: what is it?*, IEEE Personal Communications **2** (1995), no. 2, 20–35.
- [CRW⁺73] W. Crowther, R. Rettberg, D. Walden, S. Ornstein, and F. Heart, *A system for broadcast communication: Reservation-ALOHA*, Proc. 6th HICSS (Honolulu, Hawaii), jan 1973.
- [CS92] S.T.S. Chia and P. Snow, *Characterising radio-wave propagation behaviour at 1700 MHz for urban and highway microcells*, IEEE Colloquium on Micro-Cellular Propagation Modelling, November 1992.
- [CW94] W.C. Collier and R.J. Weiland, *Smart cars, smart highways*, IEEE Spectrum **31** (1994), no. 4, 27–33.
- [CWM02] D. Cassioli, M.Z. Win, and A.F. Molisch, *The ultra-wide bandwidth indoor channel: from statistical model to simulations*, IEEE Journal on Selected Areas in Communications **20** (2002), no. 6, 1247–1257.

-
- [DAA⁺04] M. Dohler, B. Allen, A. Armogida, S. McGregor, M. Ghavami, and H. Aghvami, *A new twist on UWB pathloss modelling*, IEEE 59th Vehicular Technology Conference (VTC), vol. 1, May 2004, pp. 199–203.
- [DTH02] O. Dousse, P. Thiran, and M. Hasler, *Connectivity in ad-hoc and hybrid networks*, Proceedings of 21st Annual Joint Conference of the IEEE Computer and Communications Societies (INFOCOM), vol. 2, 2002, pp. 1079–1088.
- [Eic07] S. Eichler, *Performance Evaluation of the IEEE 802.11p WAVE Communication Standard*, 66th Vehicular Technology Conference (VTC), oct 2007, pp. 2199–2203.
- [EMS06] S. Eichler, C. Merkle, and M. Strassberger, *Data Aggregation System for Distributing Inter-Vehicle Warning Messages*, 31st IEEE Conference on Local Computer Networks, November 2006, pp. 543–544.
- [ESKS06] S. Eichler, C. Schroth, T. Kosch, and M. Strassberger, *Strategies for Context-Adaptive Message Dissemination in Vehicular Ad Hoc Networks*, 3rd Annual International Conference on Mobile and Ubiquitous Systems - Workshops, July 2006, pp. 1–9.
- [ET90] A. Ephremides and T.V. Truong, *Scheduling broadcasts in multihop radio networks*, IEEE Transactions on Communications **38** (1990), no. 4, 456–460.
- [ETS09] ETSI, *C2C-CC Demonstrator 2008, Use Cases and Technical Specifications*, Tech. Report TR 102 698, ETSI, June 2009.
- [FBB08] C. Frese, T. Batz, and J. Beyerer, *Kooperative Verhaltensentscheidung für Gruppen kognitiver Automobile auf Grundlage des gemeinsamen Lagebilds*, at - Automatisierungstechnik **56** (2008), no. 12, 644–652.
- [FBR⁺94] M.J. Feuerstein, K.L. Blackard, T.S. Rappaport, S.Y. Seidel, and H.H. Xia, *Path loss, delay spread, and outage models as functions of antenna height for microcellular system design*, IEEE Transactions on Vehicular Technology **43** (1994), no. 3, 487–498.
- [FC05] M. Fazel and M. Chiang, *Network Utility Maximization With Nonconcave Utilities Using Sum-of-Squares Method*, 44th IEEE Conference on Decision and Control and 2005 European Control Conference (CDC-ECC '05), December 2005, pp. 1867–1874.
- [Fie73] M. Fiedler, *Algebraic connectivity of graphs*, Czechoslovak Mathematical Journal **23** (1973), no. 2, 298–305.
- [Fri46] H.T. Friis, *A Note on a Simple Transmission Formula*, Proceedings of the IRE **34** (1946), no. 5, 254–256.
- [GF08] M. Goebel and G. Färber, *Interfaces for integrating cognitive functions into Intelligent Vehicles*, IEEE Intelligent Vehicles Symposium (IV), June 2008, pp. 1093–1100.
- [GH08] W. Guan and S. He, *Statistical features of traffic flow on urban freeways*, Physica A: Statistical Mechanics and its Applications **387** (2008), no. 4, 944–954.
- [GKDA71] Ernst A. Guillemin, R. E. Kalman, N. DeClaric, and Jonny Andersen, *Aspects of network and system theory*, Holt Rinehart and Winston, New York, 1971.
- [GL00] A. C. V. Gummalla and J. O. Limb, *Wireless medium access control protocols*, IEEE Communications Surveys & Tutorials **3** (2000), no. 2, 2–15.
-

-
- [GMM09] J.R. Gallardo, D. Makrakis, and H.T. Mouftah, *Performance Analysis of the EDCA Medium Access Mechanism over the Control Channel of an IEEE 802.11p WAVE Vehicular Network*, IEEE International Conference on Communications (ICC), June 2009, pp. 1–6.
- [Gue87] R.A. Guerin, *Channel occupancy time distribution in a cellular radio system*, IEEE Transactions on Vehicular Technology **36** (1987), no. 3, 89–99.
- [GW98] N. Geng and W. Wiesbeck, *Planungsmethoden für die Mobilkommunikation*, Springer, 1998.
- [HC96] T.-S. Ho and K.-C. Chen, *Performance analysis of IEEE 802.11 CSMA/CA medium access control protocol*, Seventh IEEE International Symposium on Personal, Indoor and Mobile Radio Communications (PIMRC), vol. 2, October 1996, pp. 407–411.
- [HCY⁺08] C.-J. Huang, Y.-T. Chuang, D.-X. Yang, I.-F. Chen, Y.-J. Chen, and K.-W. Hu, *A mobility-aware link enhancement mechanism for vehicular ad hoc networks*, EURASIP J. Wirel. Commun. Netw. **2008** (2008), 1–10.
- [HD05] J. Hui and M. Devetsikiotis, *A unified model for the performance analysis of IEEE 802.11e EDCA*, IEEE Transactions on Communications **53** (2005), no. 9, 1498–1510.
- [Hel95] D. Helbing, *Improved fluid-dynamic model for vehicular traffic*, Phys. Rev. E **51** (1995), no. 4, 3164–3169.
- [Hel96] ———, *Gas-kinetic derivation of Navier-Stokes-like traffic equations*, Phys. Rev. E **53** (1996), no. 3, 2366–2381.
- [Hel01a] ———, *Traffic and related self-driven many-particle systems*, Rev. Mod. Phys. **73** (2001), no. 4, 1067–1141.
- [Hel01b] ———, *Verkehrsdynamik. Neue physikalische Modellierungskonzepte*, Springer, 2001.
- [Hel03] ———, *A section-based queueing-theoretical traffic model for congestion and travel time analysis in networks*, Journal of Physics A: Mathematical and General **36** (2003), no. 46, L593.
- [HFB09] J. Harri, F. Filali, and C. Bonnet, *Mobility models for vehicular ad hoc networks: a survey and taxonomy*, IEEE Communications Surveys & Tutorials **11** (2009), no. 4, 19–41.
- [HHM⁺03] G.R. Hiertz, J. Habetha, P. May, E. Weib, R. Bagul, and S. Mangold, *A decentralized reservation scheme for IEEE 802.11 ad hoc networks*, 14th IEEE Proceedings on Personal, Indoor and Mobile Radio Communications (PIMRC), vol. 3, September 2003, pp. 2576–2580.
- [HHST02] D. Helbing, A. Hennecke, V. Shvetsov, and M. Treiber, *Micro- and macro-simulation of freeway traffic*, Mathematical and Computer Modelling **35** (2002), no. 5-6, 517–547.
- [HVS02] Z. Hadzi-Velkov and B. Spasenovski, *On the Capacity of IEEE 802.11 DCF with Capture in Multipath-Faded Channels*, International Journal of Wireless Information Networks **9** (2002), 191–199, 10.1023/A:1016037711861.

-
- [IEE06a] IEEE, *IEEE Trial-Use Standard for Wireless Access in Vehicular Environments (WAVE) - Multi-Channel Operation*, IEEE Std 1609.4-2006 (2006).
- [IEE06b] ———, *IEEE Trial-Use Standard for Wireless Access in Vehicular Environments (WAVE) - Resource Manager*, IEEE Std 1609.1-2006 (2006).
- [IEE06c] ———, *IEEE Trial-Use Standard for Wireless Access in Vehicular Environments (WAVE) - Security Services for Applications and Management Messages*, IEEE Std 1609.2-2006 (2006).
- [IEE07a] ———, *IEEE Standard for Information Technology-Telecommunications and Information Exchange Between Systems-Local and Metropolitan Area Networks-Specific Requirements - Part 11: Wireless LAN Medium Access Control (MAC) and Physical Layer (PHY) Specifications*, IEEE Std 802.11-2007 (Revision of IEEE Std 802.11-1999) (2007).
- [IEE07b] ———, *IEEE Trial-Use Standard for Wireless Access in Vehicular Environments (WAVE) - Networking Services*, IEEE Std 1609.3-2007 (2007).
- [IEE10] ———, *IEEE Draft Standard for Information Technology - Telecommunications and information exchange between systems - Local and metropolitan area networks - Specific requirements - Part 11: Wireless LAN Medium Access Control (MAC) and Physical Layer (PHY) specifications Amendment : Wireless Access in Vehicular Environments*, IEEE Unapproved Draft Std P802.11p /D11.0, Mar 2010 (2010).
- [Inz04] T. Inzerilli, *Design and performance modeling for traffic control in wireless links*, IEEE International Conference on Communications, vol. 4, June 2004, pp. 2307–2311.
- [JCH84] R. Jain, D. Chiu, and W. Hawe, *A Quantitative Measure of Fairness and Discrimination for Resource Allocation in Shared Computer System*, Tech. Report TR-301, DEC Research Report, 1984.
- [JLB10] R. Jurdak, C.V. Lopes, and P. Baldi, *Performance analysis of IEEE 802.11e enhanced distributed channel access*, IEEE Communications Surveys & Tutorials **4** (2010), no. 6, 728–738.
- [JM96] David B. Johnson and David A. Maltz, *Dynamic Source Routing in Ad Hoc Wireless Networks*, Mobile Computing, Kluwer Academic Publishers, 1996, pp. 153–181.
- [Kah54] L. Kahn, *Ratio Squarer*, Proceedings of the IRE (Correspondence) **42** (1954), 1074.
- [KBSS01] W. Kellerer, C. Bettstetter, C. Schwingenschlogl, and P. Sties, *(Auto) mobile communication in a heterogeneous and converged world*, IEEE Personal Communications **8** (2001), no. 6, 41–47.
- [Kep15] Johannes Kepler, *Novia Stereometria Doliorum (Stereometrie der Fässer)*, 1615.
- [Ker04] B. S. Kerner, *The Physics of Traffic*, Springer, 2004.
- [KHB09] M. Kuehn, T. Hummel, and J. Bende, *Benefit estimation of advanced driver assistance systems for cars derived from real-life accidents*, Tech. Report 09-0317, German Insurers Accident Research, 2009.
- [KJ08] M. Kaynia and N. Jindal, *Performance of ALOHA and CSMA in Spatially Distributed Wireless Networks*, IEEE International Conference on Communications (ICC), May 2008, pp. 1108–1112.
-

-
- [KK93] B. S. Kerner and P. Konhäuser, *Cluster effect in initially homogeneous traffic flow*, Phys. Rev. E **48** (1993), no. 4, R2335–R2338.
- [KK10] H. Kaaniche and F. Kamoun, *Mobility Prediction in Wireless Ad Hoc Networks using Neural Networks*, Journal of Telecommunications **2** (2010), no. 1, 95–101.
- [KKH07] B. S. Kerner, S. Klenov, and A. Hiller, *Empirical test of a microscopic three-phase traffic theory*, Nonlinear Dynamics **49** (2007), 525–553.
- [KKHR06] Boris S. Kerner, Sergey L. Klenov, Andreas Hiller, and Hubert Rehborn, *Microscopic features of moving traffic jams*, Phys. Rev. E **73** (2006), no. 4, 046107.
- [KKJ98] S. Khurana, A. Kahol, and A.P. Jayasumana, *Effect of hidden terminals on the performance of IEEE 802.11 MAC protocol*, 23rd Annual Conference on Local Computer Networks (LCN), October 1998, pp. 12–20.
- [KL75] L. Kleinrock and S. Lam, *Packet Switching in a Multiaccess Broadcast Channel: Performance Evaluation*, IEEE Transactions on Communications **23** (1975), no. 4, 410–423.
- [Krb07] M. Krbálek, *Equilibrium distributions in a thermodynamical traffic gas*, Journal of Physics A: Mathematical and Theoretical **40** (2007), no. 22, 5813.
- [KS00] M. Krbalek and P. Seba, *The statistical properties of the city transport in Cuernavaca (Mexico) and random matrix ensembles*, Journal of Physics A **33** (2000), 229–234.
- [KT75] L. Kleinrock and F. Tobagi, *Packet Switching in Radio Channels: Part I—Carrier Sense Multiple-Access Modes and Their Throughput-Delay Characteristics*, IEEE Transactions on Communications **23** (1975), no. 12, 1400–1416.
- [KTH07] A. Kesting, M. Treiber, and D. Helbing, *General lane-changing model MOBIL for car-following models*, Journal of the Transportation Research Board **1999** (2007), 86–94.
- [KTH10] A. Kesting, M. Treiber, and D. Helbing, *Connectivity Statistics of Store-and-Forward Intervehicle Communication*, IEEE Transactions on Intelligent Transportation Systems **11** (2010), no. 1, 172–181.
- [KUH03] A. Kanzaki, T. Uemukai, T. Hara, and S. Nishio, *Dynamic TDMA slot assignment in ad hoc networks*, 17th International Conference on Advanced Information Networking and Applications (AINA), March 2003, pp. 330–335.
- [Kv03] M. Krbalek and P. Šeba, *Headway statistics of public transport in Mexican cities*, Journal of Physics A: Mathematical and General **36** (2003), no. 1, L7.
- [KvW01] M. Krbalek, P. Šeba, and P. Wagner, *Headways in traffic flow: Remarks from a physical perspective*, Phys. Rev. E **64** (2001), no. 6, 066119.
- [KWG96] S. Krauss, P. Wagner, and C. Gawron, *Continuous limit of the Nagel-Schreckenberg model*, Phys. Rev. E **54** (1996), no. 4, 3707–3712.
- [Lam80] S. S. Lam, *Packet Broadcast Networks A Performance Analysis of the R-ALOHA Protocol*, IEEE Trans. Comput. **29** (1980), no. 7, 596–603.
- [LHSR01] M. Lott, R. Halfmann, E. Schultz, and M. Radimirsch, *Medium access and radio resource management for ad hoc networks based on UTRA TDD*, Proceedings of the 2nd ACM international symposium on Mobile ad hoc networking & computing (New York, NY, USA), MobiHoc '01, ACM, 2001, pp. 76–86.

-
- [Lit61] J. D. C. Little, *A Proof for the Queueing Formula: $L=\lambda W$* , *Operations Research* **9** (1961), no. 3, 383–387.
- [LK75] S. Lam and L. Kleinrock, *Packet Switching in a Multiaccess Broadcast Channel: Dynamic Control Procedures*, *IEEE Transactions on Communications* **23** (1975), no. 9, 891–904.
- [LL07a] K. Lidstrom and T. Larsson, *Cooperative Communication Disturbance Detection in Vehicle Safety Systems*, *IEEE Intelligent Transportation Systems Conference (ITSC)*, October 2007, pp. 522–527.
- [LL07b] Y.-C. Lin and W.K. Lai, *Adaptive bandwidth sharing mechanism for quality of service administration in infrastructure wireless networks*, *Communications, IET* **1** (2007), no. 5, 846–857.
- [LPvA09] F. Liu, R. Pueboobpaphan, and B. van Arem, *Assessment of traffic impact on future cooperative driving systems: Challenges and considerations*, *International Conference on Ultra Modern Telecommunications Workshops (ICUMT)*, October 2009, pp. 1–5.
- [LW55a] M.J. Lighthill and G. B. Whitham, *On Kinematic Waves. I. Flood Movement in Long Rivers*, *Proceedings of the Royal Society of London. Series A. Mathematical and Physical Sciences* **229** (1955), no. 1178, 281–316.
- [LW55b] ———, *On Kinematic Waves. II. A Theory of Traffic Flow on Long Crowded Roads*, *Proceedings of the Royal Society of London. Series A. Mathematical and Physical Sciences* **229** (1955), no. 1178, 317–345.
- [MA06] D. Miorandi and E. Altman, *Connectivity in one-dimensional ad hoc networks: a queueing theoretical approach*, *Wirel. Netw.* **12** (2006), no. 5, 573–587.
- [Mau05] J. Maurer, *Strahlenoptisches Kanalmodell für die Fahrzeug-Fahrzeug-Funkkommunikation*, Ph.D. thesis, Universität Karlsruhe, 2005.
- [MC08] X. Ma and X. Chen, *Performance Analysis of IEEE 802.11 Broadcast Scheme in Ad Hoc Wireless LANs*, *IEEE Transactions on Vehicular Technology* **57** (2008), no. 6, 3757–3768.
- [McK62] W. M. McKeeman, *Algorithm 145: Adaptive numerical integration by Simpson’s rule*, *Commun. ACM* **5** (1962), no. 12, 604.
- [MFL06] H. Menouar, F. Filali, and M. Lenardi, *A survey and qualitative analysis of mac protocols for vehicular ad hoc networks*, *IEEE Transactions on Wireless Communications* **13** (2006), no. 5, 30–35.
- [MFSW04] J. Maurer, T. Fügen, T. Schäfer, and W. Wiesbeck, *A new inter-vehicle communications (IVC) channel model*, *IEEE 60th Vehicular Technology Conference (VTC)*, vol. 1, September 2004, pp. 9–13.
- [MFW02] J. Maurer, T. Fügen, and W. Wiesbeck, *Narrow-band measurement and analysis of the inter-vehicle transmission channel at 5.2 GHz*, *IEEE 55th Vehicular Technology Conference (VTC)*, vol. 3, 2002, pp. 1274–1278.
- [Mio08] D. Miorandi, *The Impact of Channel Randomness on Coverage and Connectivity of Ad Hoc and Sensor Networks*, *IEEE Transactions on Wireless Communications* **7** (2008), no. 3, 1062–1072.
-

-
- [MK09] Q. Meng and H. L. Khoo, *Self-Similar Characteristics of Vehicle Arrival Pattern on Highways*, *Journal of Transportation Engineering* **135** (2009), no. 11, 864–872.
- [MLD00] P. G. Michael, F. C. Leeming, and W. O. Dwyer, *Headway on urban streets: observational data and an intervention to decrease tailgating*, *Transportation Research Part F: Traffic Psychology and Behaviour* **3** (2000), no. 2, 55–64.
- [MSQT04] P. Mühlethaler, M. Salaun, A. Qayyum, and Y. Toor, *Comparison between Aloha and CSMA in multiple hop ad hoc networks*, Research Report RR-5129, INRIA, 2004.
- [MSX06] D. W. Matolak, I. Sen, and W. Xiong, *Channel Modeling for V2V Communications*, 3rd Annual International Conference on Mobile and Ubiquitous Systems - Workshops, July 2006, pp. 1–7.
- [MSXY05] D.W. Matolak, I. Sen, Wenhui Xiong, and N.T. Yaskoff, *5 GHz wireless channel characterization for vehicle to vehicle communications*, *IEEE Military Communications Conference (MILCOM)*, vol. 5, October 2005, pp. 3016–3022.
- [MTKM09] A. Molisch, F. Tufvesson, J. Karedal, and C. Mecklenbräuker, *A survey on vehicle-to-vehicle propagation channels*, *IEEE Transactions on Wireless Communications* **16** (2009), no. 6, 12–22.
- [Nak60] N. Nakagami, *The m -distribution, a general formula for intensity distribution of rapid fading*, *Statistical Methods in Radio Wave Propagation* (W. G. Hoffman, ed.), Oxford, England: Pergamon, 1960.
- [NHB05] T. Nolte, H. Hansson, and L. L. Bello, *Wireless Automotive Networks*, Proceedings of the 4th International Workshop on Real-Time Networks (RTN) in conjunction with the 17th Euromicro International Conference on Real-Time Systems (ECRTS) (Jörg Kaiser, ed.), ISBN 3-929757-90-7, July 2005, pp. 35–38.
- [NL03] C.Y. Ngo and V.O.K. Li, *Centralized broadcast scheduling in packet radio networks via genetic-fix algorithms*, *IEEE Transactions on Communications* **51** (2003), no. 9, 1439–1441.
- [NTH03] K. Nishinari, M. Treiber, and D. Helbing, *Interpreting the wide scattering of synchronized traffic data by time gap statistics*, *Phys. Rev. E* **68** (2003), no. 6, 067101.
- [PKC⁺07] A. Paier, J. Karedal, N. Czink, H. Hofstetter, C. Dumard, T. Zemen, F. Tufvesson, A.F. Molisch, and C.F. Mecklenbrauker, *Car-to-car radio channel measurements at 5 GHz: Pathloss, power-delay profile, and delay-Doppler spectrum*, 4th International Symposium on Wireless Communication Systems (ISWCS), October 2007, pp. 224–228.
- [PKC⁺09] A. Paier, J. Karedal, N. Czink, C. Dumard, T. Zemen, F. Tufvesson, A. F. Molisch, and C. F. Mecklenbräuker, *Characterization of Vehicle-to-Vehicle Radio Channels from Measurements at 5.2 GHz*, *Wirel. Pers. Commun.* **50** (2009), no. 1, 19–32.
- [PPQ10] F. Peng, B. Peng, and D. Qian, *Performance analysis of IEEE 802.11e enhanced distributed channel access*, *Communications, IET* **4** (2010), no. 6, 728–738.
- [PWR99] S.C.M. Perera, A.G. Williamson, and G.B. Rowe, *Prediction of breakpoint distance in microcellular environments*, *Electronics Letters* **35** (1999), no. 14, 1135–1136.
- [Rap96] T. S. Rappaport, *Wireless Communications: Principles and Practice*, Prentice Hall, 1996.

-
- [RC10] J. Rodas and C. J. Escudero Cascon, *Dynamic Path-Loss Estimation Using A Particle Filter*, International Journal of Computer Science Issues 7 (2010), no. 3, 1–5.
- [Ric56] P. I. Richards, *Shock Waves on the Highway*, Operations Research 4 (1956), no. 1, 42–51.
- [RML02] M. Rudack, M. Meincke, and M. Lott, *On the Dynamics of Ad Hoc Networks for Inter Vehicle Communications*, ICWN, 2002.
- [Rob75] L. G. Roberts, *ALOHA packet system with and without slots and capture*, SIGCOMM Comput. Commun. Rev. 5 (1975), no. 2, 28–42.
- [RPB09] C. G. Rezende, R. W. Pazzi, and A. Boukerche, *An efficient neighborhood prediction protocol to estimate link availability in VANETs*, Proceedings of the 7th ACM international symposium on Mobility management and wireless access (MobiWAC) (New York, NY, USA), ACM, 2009, pp. 83–90.
- [SD05] A. Sugiura and C. Dermawan, *In traffic jam IVC-RVC system for ITS using Bluetooth*, IEEE Transactions on Intelligent Transportation Systems 6 (2005), no. 3, 302–313.
- [SFK07] C. Stiller, G. Farber, and S. Kammel, *Cooperative Cognitive Automobiles*, IEEE Intelligent Vehicles Symposium (IV), June 2007, pp. 215–220.
- [SGSSA08] J. Santa, A. F. Gómez-Skarmeta, and M. Sánchez-Artigas, *Architecture and evaluation of a unified V2V and V2I communication system based on cellular networks*, Comput. Commun. 31 (2008), 2850–2861.
- [SH09] M. Schönhof and D. Helbing, *Criticism of three-phase traffic theory*, Transportation Research Part B: Methodological 43 (2009), no. 7, 784–797.
- [Shl07] S.E. Shladover, *PATH at 20 – History and Major Milestones*, IEEE Transactions on Intelligent Transportation Systems 8 (2007), no. 4, 584–592.
- [SJK⁺03] T.K. Sarkar, Z. Ji, K. Kim, A. Medouri, and M. Salazar-Palma, *A survey of various propagation models for mobile communication*, IEEE Antennas and Propagation Magazine 45 (2003), no. 3, 51–82.
- [SK05] N. Samaan and A. Karmouch, *A mobility prediction architecture based on contextual knowledge and spatial conceptual maps*, IEEE Transactions on Mobile Computing 4 (2005), no. 6, 537–551.
- [SK08] M.L. Sichitiu and M. Kihl, *Inter-vehicle communication systems: a survey*, IEEE Communications Surveys & Tutorials 10 (2008), no. 2, 88–105.
- [SM08] I. Sen and D.W. Matolak, *Vehicle–Vehicle Channel Models for the 5-GHz Band*, IEEE Transactions on Intelligent Transportation Systems 9 (2008), no. 2, 235–245.
- [SN09] T. Sukuvaara and P. Nurmi, *Wireless traffic service platform for combined vehicle-to-vehicle and vehicle-to-infrastructure communications*, IEEE Wireless Communications 16 (2009), no. 6, 54–61.
- [Ste87] S. Stein, *Fading Channel Issues in System Engineering*, IEEE Journal on Selected Areas in Communications 5 (1987), no. 2, 68–89.
- [SZW09] C. Sturm, T. Zwick, and W. Wiesbeck, *An OFDM System Concept for Joint Radar and Communications Operations*, IEEE 69th Vehicular Technology Conference (VTC), April 2009, pp. 1–5.
-

-
- [TAK03] V. Thamizh Arasan and R. Z. Koshy, *Headway Distribution of Heterogeneous Traffic on Urban Arterials*, Journal of the Institution of Engineers, India. Civil Engineering Division **84** (2003), 210–215.
- [Ter07] P. Terren, *The Big Picture: Step Away from the Vehicle!*, IEEE Spectrum **44** (2007), no. 5, 18–19.
- [TFM05] J.W. Tantra, Chuan Heng Foh, and A.B. Mnaouer, *Throughput and delay analysis of the IEEE 802.11e EDCA saturation*, IEEE International Conference on Communications (ICC), vol. 5, May 2005, pp. 3450–3454.
- [TH99] M. Treiber and D. Helbing, *Macroscopic simulation of widely scattered synchronized traffic states*, Journal of Physics A: Mathematical and General **32** (1999), no. 1, L17.
- [The64] T. Thedeen, *A note on the Poisson tendency in traffic distribution.*, Ann. Math. Stat. **35** (1964), 1823–1824 (English).
- [THH99] M. Treiber, A. Hennecke, and D. Helbing, *Derivation, properties, and simulation of a gas-kinetic-based, nonlocal traffic model*, Phys. Rev. E **59** (1999), no. 1, 239–253.
- [THH00] ———, *Congested traffic states in empirical observations and microscopic simulations*, Phys. Rev. E **62** (2000), no. 2, 1805–1824.
- [Tho93] J. Thoma, *Geschwindigkeitsverhalten und Risiken bei verschiedenen Strassenzuständen, Wochentagen und Tageszeiten*, bfu-Report 20, Bern, Schweiz, 1993.
- [TJM⁺04] V. Taliwal, D. Jiang, H. Mangold, C. Chen, and R. Sengupta, *Empirical determination of channel characteristics for DSRC vehicle-to-vehicle communication*, Proceedings of the 1st ACM international workshop on Vehicular ad hoc networks (VANET) (New York, NY, USA), ACM, 2004, pp. 88–88.
- [TK75] F. Tobagi and L. Kleinrock, *Packet Switching in Radio Channels: Part II—The Hidden Terminal Problem in Carrier Sense Multiple-Access and the Busy-Tone Solution*, IEEE Transactions on Communications **23** (1975), no. 12, 1417–1433.
- [TK76] ———, *Packet Switching in Radio Channels: Part III—Polling and (Dynamic) Split-Channel Reservation Multiple Access*, IEEE Transactions on Communications **24** (1976), no. 8, 832–845.
- [TK77] ———, *Packet Switching in Radio Channels: Part IV—Stability Considerations and Dynamic Control in Carrier Sense Multiple Access*, IEEE Transactions on Communications **25** (1977), no. 10, 1103–1119.
- [TKH07] M. Treiber, A. Kesting, and D. Helbing, *Variance-Driven Traffic Dynamics*, Traffic and Granular Flow '05 (A. Schadschneider, T. Pöschel, R. Kühne, M. Schreckenberg, and D. E. Wolf, eds.), Springer Berlin Heidelberg, 2007, pp. 551–557.
- [TKH10] ———, *Three-phase traffic theory and two-phase models with a fundamental diagram in the light of empirical stylized facts*, Transportation Research Part B: Methodological **44** (2010), no. 8-9, 983–1000.
- [TMJH04] M. Torrent-Moreno, D. Jiang, and H. Hartenstein, *Broadcast reception rates and effects of priority access in 802.11-based vehicular ad-hoc networks*, Proceedings of the 1st ACM international workshop on Vehicular ad hoc networks (New York, NY, USA), VANET '04, ACM, 2004, pp. 10–18.

-
- [TMMSH09] M. Torrent-Moreno, J. Mittag, P. Santi, and H. Hartenstein, *Vehicle-to-Vehicle Communication: Fair Transmit Power Control for Safety-Critical Information*, IEEE Transactions on Vehicular Technology **58** (2009), no. 7, 3684–3703.
- [Tob74] F. Tobagi, *Random Access Techniques For Data Transmission Over Packet Switched Radio Networks*, Ph.D. thesis, University of California, Los Angeles, 1974.
- [TTIF89] K. Takada, Y. Tanaka, A. Igarashi, and D. Fujita, *Road/Automobile Communication System (RACS) and its economic effect*, Conference Record Vehicle Navigation and Information Systems Conference, vol. A, September 1989, pp. 15–21.
- [vAvDV06] B. van Arem, C.J.G. van Driel, and R. Visser, *The Impact of Cooperative Adaptive Cruise Control on Traffic-Flow Characteristics*, IEEE Transactions on Intelligent Transportation Systems **7** (2006), no. 4, 429–436.
- [vEKH10] M. van Eenennaam, G. Karagiannis, and G. J. Heijenk, *Towards Scalable Beaconing in VANETs*, Fourth ERCIM workshop on eMobility, Luleå University of Technology, Sweden, May 2010, pp. 103–108.
- [vEWKH09] M. van Eenennaam, W.K. Wolterink, G. Karagiannis, and G. Heijenk, *Exploring the solution space of beaconing in VANETs*, IEEE Vehicular Networking Conference (VNC), October 2009, pp. 1–8.
- [Viz64] V. G. Vizing, *On an estimate of the chromatic class of a p -graph*, Diskret. Analiz (1964), no. 3, 25–30.
- [WAFS09] J. C.-P. Wang, M. Abolhasan, D. R. Franklin, and F. Safaei, *Characterising the behaviour of IEEE 802.11 broadcast transmissions in ad hoc wireless LANs*, Proceedings of the 2009 IEEE international conference on Communications (Piscataway, NJ, USA), ICC'09, IEEE Press, 2009, pp. 4934–4938.
- [Wan04] S.Y. Wang, *Predicting the lifetime of repairable unicast routing paths in vehicle-formed mobile ad hoc networks on highways*, 15th IEEE International Symposium on Personal, Indoor and Mobile Radio Communications (PIMRC), vol. 4, September 2004, pp. 2815–2819.
- [WCL⁺08] S.-Y. Wang, H.-L. Chao, K.-C. Liu, T.-W. He, C.-C. Lin, and C.-L. Chou, *Evaluating and improving the TCP/UDP performances of IEEE 802.11(p)/1609 networks*, IEEE Symposium on Computers and Communications (ISCC), July 2008, pp. 163–168.
- [Wol99] D. E. Wolf, *Cellular automata for traffic simulations*, Physica A: Statistical Mechanics and its Applications **263** (1999), no. 1-4, 438–451, Proceedings of the 20th IUPAP International Conference on Statistical Physics.
- [WR05] L. Wischhof and H. Rohling, *Congestion control in vehicular ad hoc networks*, IEEE International Conference on Vehicular Electronics and Safety, October 2005, pp. 58–63.
- [WTM09] T.L. Willke, P. Tientrakool, and N.F. Maxemchuk, *A survey of inter-vehicle communication protocols and their applications*, IEEE Communications Surveys & Tutorials **11** (2009), no. 2, 3–20.
- [YAEAF08] S. Yousefi, E. Altman, R. El-Azouzi, and M. Fathy, *Analytical Model for Connectivity in Vehicular Ad Hoc Networks*, IEEE Transactions on Vehicular Technology **57** (2008), no. 6, 3341–3356.
-

-
- [YLZ⁺09] S. Yin, Z. Li, Y. Zhang, D. Yao, Y. Su, and L. Li, *Headway distribution modeling with regard to traffic status*, IEEE Intelligent Vehicles Symposium (IV), June 2009, pp. 1057–1062.
- [You99] C.D. Young, *USAP multiple access: dynamic resource allocation for mobile multihop multichannel wireless networking*, IEEE Military Communications Conference Proceedings (MILCOM), vol. 1, 1999, pp. 271–275.
- [YY03] Y. Yang and T.-S.P. Yum, *Delay distributions of slotted ALOHA and CSMA*, IEEE Transactions on Communications **51** (2003), no. 11, 1846–1857.
- [ZDJ08] X. Zhou, S. Durrani, and H.M. Jones, *Connectivity of ad hoc networks: Is fading good or bad?*, 2nd International Conference on Signal Processing and Communication Systems (ICSPCS), December 2008, pp. 1–5.
- [ZGZC09] L. Zhou, B. Geller, B. Zhengi, and J. Cui, *Cross-layer design for scheduling in cooperative VANETs*, 9th International Conference on Intelligent Transport Systems Telecommunications (ITST), October 2009, pp. 505–509.
- [ZHZ⁺07] X. Zhang, J. Hong, L. Zhang, X. Shan, and V.O.K. Li, *CC-TDMA: Coloring- and Coding-Based Multi-Channel TDMA Scheduling for Wireless Ad Hoc Networks*, IEEE Wireless Communications and Networking Conference (WCNC), 2007, pp. 133–137.

Cited websites

- [c2c] *Car 2 Car Communication Consortium*, URL: <http://www.car-to-car.org>.
- [gst] *Global System for Telematics*, URL: <http://www.gstforum.org>.
- [MMBK10] D. Mills, J. Martin, J. Burbank, and W. Kasch, *Network Time Protocol Version 4: Protocol and Algorithms Specification*, RFC 5905 (Proposed Standard), June 2010.
- [now] *NOW: Network on Wheels*, URL: <http://www.network-on-wheels.de>.
- [Rys09] P. Rysavy, *HSPA to LTE-Advanced. 3GPP Broadband Evolution to IMT-Advanced (4G)*, URL: http://www.3gamericas.org/documents/3G_Americas_RysavyResearch_HSPA-LTE_Advanced_Sept2009.pdf, sept 2009.
- [The02] The eSafety Working Group on Road Safety, *Final Report*, URL: http://ec.europa.eu/information_society/activities/esafety/doc/wg/esafety_wg_final_report_nov02_final.pdf, nov 2002.